MASS IN AND AROUND GALAXIES AS INFERRED FROM OBSERVATIONS OF NEUTRAL HYDROGEN

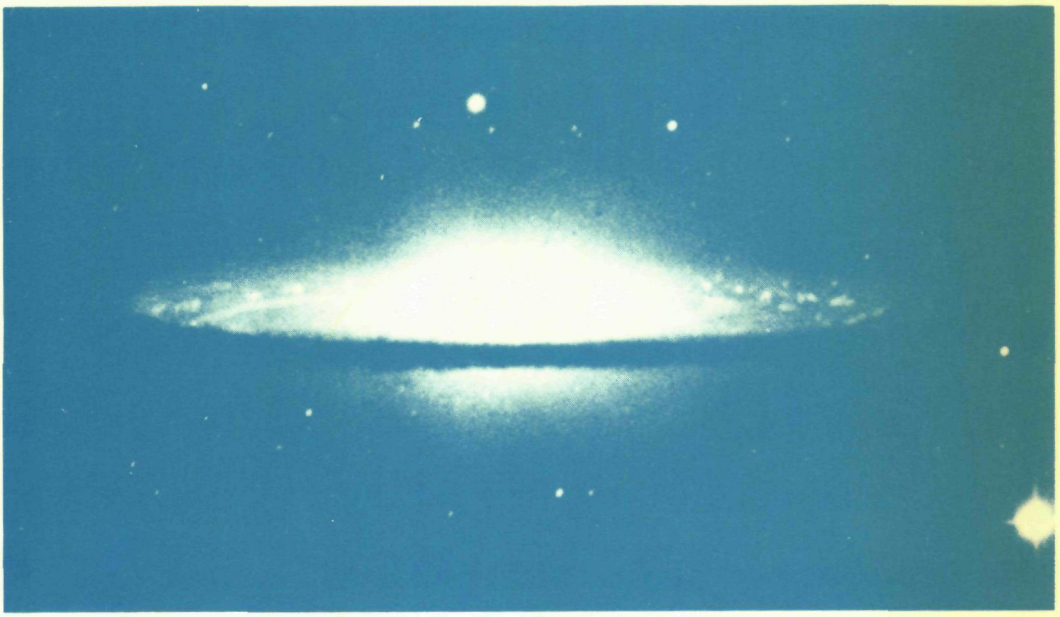

G. VAN DER BURG

MASS IN AND AROUND GALAXIES
AS INFERRED FROM
OBSERVATIONS OF NEUTRAL HYDROGEN

MASS IN AND AROUND GALAXIES AS INFERRED FROM OBSERVATIONS OF NEUTRAL HYDROGEN

PROEFSCHRIFT

TER VERKRIJGING VAN DE GRAAD VAN DOCTOR IN DE
WISKUNDE EN NATUURWETENSCHAPPEN
AAN DE KATHOLIEKE UNIVERSITEIT TE NIJMEGEN
OP GEZAG VAN DE RECTOR MAGNIFICUS
PROF. DR. B.M.F. van IERSEL,
VOLGENS BESLUIT VAN HET COLLEGE VAN DECANEN
IN HET OPENBAAR TE VERDEDIGEN
OP DONDERDAG 17 SEPTEMBER 1987
DES NAMIDDAGS TE 3.30 UUR

door

Gerrit van der Burg

geboren te De Steeg

druk: Krips Repro, Meppel
1987

Promotor: Prof. Dr. W.W. Shane

Cover: Photograph of the Sombrero galaxy in ultraviolet light made by W. Baade with the 200-inch Hale Telescope

aan mijn ouders,
aan Coby en Wilger

Graag wil ik iedereen die aan het voltooien van dit proefschrift heeft bijgedragen bedanken, in het bijzonder:

- mijn ouders voor de gelegenheid die ze mij hebben geboden een academische opleiding te volgen;
- Coby voor de steun die ze heeft gegeven en de opofferingen die ze zich heeft moeten getroosten, met name tijdens het afronden van dit proefschrift;
- alle (oud-)medewerkers van het Sterrenkundig Instituut Nijmegen, met name Yvonne Balster voor haar hulp ten aanzien van URC en IVV zaken;
- Jos van Maarseveen en Henk Hoevers voor hun medewerking aan hoofdstuk 4 resp. 6;
- Steve Bajaja, Sandy Faber and Gill Knapp for their cooperation, and Ilya Kazes for his hospitality during my stay at Nançay;
- de programmeurs van de sterrewacht Leiden voor hun advies ten aanzien van het onderhoud van het software pakket voor de reductie van Westerbork metingen;
- de medewerkers van het Universitair Reken Centrum, in het bijzonder de operators voor het talloze malen opspannen van magneetbanden;
- Mieke Thijssen-Boerrigter en Lieke Bochem-Becks voor het verrichten van typewerk;
- Annie Martens, Helma Uyen-de Vaan en Jo Beerens voor hun hulp bij het verwerken van het manuscript op de linotron fotozetter;
- de medewerkers van illustratie en fotografie;

Ten slotte dank ik Wilger die door zijn nadrukkelijke aanwezigheid mijn aandacht wist af te leiden naar niet-sterrenkundige zaken.

Contents

Chapter 4 Search for neutral hydrogen in two early-type galaxies, NGC 3593 and NGC 4281

G. van der Burg and J. van Maarseveen
(to be published)

Chapter 5 HI observations of some galaxies and their faint companions

G. van der Burg
published in 1985, *Astron. Astrophys. Suppl. Ser.* **62**, 147

Chapter 6 The mass of the early-type galaxy NGC 2859 inferred from HI observations of its companions

G. van der Burg, H.F.C. Hoevers and W.W. Shane
(to be published)

Chapter 7 The mass of the early-type galaxy NGC 4111 inferred from HI observations of its companions

G. van der Burg
(to be published)

For more than fifty years it has been known that dynamical estimates of masses in clusters of galaxies exceed the sums of the masses of the individual cluster members by large factors. This was first demonstrated by Zwicky (1933) who showed that if the Virgo cluster of galaxies is bound, there must be a considerable amount of unidentified mass associated with it. Various explanations have been offered for this discrepancy, however the hypothesis that many galaxies are embedded in larger concentrations of (nearly) invisible matter has attracted particular attention. From a theoretical point of view Ostriker and Peebles (1973) argued that massive envelopes might stabilize stellar disks which would otherwise be unstable against bar-like modes. Observational evidence for the presence of massive envelopes is mostly obtained from rotation curve measurements. These measurements show that for most galaxies the rotation curve is flat (Bosma, 1978; Rubin et al., 1980, 1982 and 1985). Observations of neutral hydrogen, which, in many galaxies, extend well beyond the optically visible system, show that even at these galactocentric radii the rotational velocities are constant. This indicates that considerable amounts of mass are present, even at the outermost measured points. This additional mass outside the optically visible system is generally attributed to the presence of a massive dark halo. Whether or not dark matter is present in the inner regions of galaxies is uncertain. The present observations show that at these small radii dark matter is not required, although its presence cannot be excluded. If it is there, a considerable amount must be located outside the disk (Freeman, 1987). If the rotation curve of a galaxy is known it is possible to construct models for the distribution of mass. These models are generally composed of a thin disk (Toomre, 1963; Freeman, 1970; Nordsieck, 1973), sometimes with additional spheroids to account for the bulge (Shu et al., 1971; Bosma, 1978; Visser, 1980a and b). Aside from the fact that these models are not unique, they do not provide for the presence of invisible mass in the outer regions of galaxies. In order to obtain a mass model of a galaxy it is more realistic first to calculate the distribution of

mass in the disk by assuming that M/L is constant (Wevers, 1984). The distribution of mass in the halo can then be inferred from the observed rotation curve from which the contribution of the disk is subtracted. As noted by Sancisi and van Albada (1987), in this approach the halo is the additional component necessary to explain the observed rotation curve. In this way the halo mass can be obtained without having to make ad hoc assumptions regarding its mass distribution. However, the resulting halo contribution is strongly dependent upon the adopted M/L-value for the disk, which is known only to within about a factor two from a small sample of spirals (van der Kruit and Freeman, 1986). Moreover, the unknown M/L-value leads to speculations as to whether galaxies possess a dominating or an insignificant disk or a disk with a mass between these two possibilities (for a discussion of this so-called disk-halo dilemma see Sancisi and van Albada, 1987). In case of an insignificant disk it would be difficult to explain why so many galaxies with flat rotation curves show a well developed spiral structure in their disks, since the presence of a massive halo would inhibit the formation of spiral structure in such a disk. As already noted by Sancisi and van Albada (1987) this is a strong argument against the insignificant disk case. Therefore, if spiral structure is observed, it might be useful first to examine the conditions under which a spiral of a given form can exist. Obviously, we have to specify a mass model for the disk which can sustain the observed spiral pattern and which is in agreement with a constant M/L. (The latter was well established by Wevers, 1984, for a sample of 21 spiral galaxies). The distribution of mass in the halo can then be inferred from the observed rotation curve after the contribution of the resulting disk model is subtracted. Because this procedure allows one to calculate the mass of the disk without having to assume its M/L, it provides a way out of the disk-halo dilemma. Moreover, it guarantees that we will obtain a model for the distribution of mass in a spiral galaxy which is consistent with both the observed rotation curve and the observed shape of the spiral pattern. This method for calculating a mass model by using the observed shape of the spiral pattern is the inverse of the procedure proposed by Shu et al. (1971) for calculating theoretical spiral patterns from mass models based on the observed rotation curves.

In the following two chapters of this thesis the shape of the spiral pattern in the disk of NGC 4594 (the "Sombrero") will be determined and used to derive a mass model. In chapter 2 high resolution observations in the 21-cm line of neutral hydrogen, made with the Westerbork Synthesis Radio Telescope (WSRT), are discussed. Model calculations presented in this chapter show that the observed distribution of neutral hydrogen can be represented by two partially overlapping rings of gas in which the rotational velocity is constant with radius.

In chapter 3 it will be shown that this ring-like distribution of gas can be interpreted as a tightly wound, two-armed spiral pattern. The local surface density in the disk is then derived from the dispersion relation for tightly wound spiral density waves (Lin and Shu, 1964). Combined with published surface photometry, the radial surface density distribution of the disk is calculated along with its M/L. Subtracting the contribution of the disk from the observed rotation curve the distribution of mass in the spheroid is derived.

In chapter 4 WSRT observations of NGC 3593 and NGC 4281 are discussed. Optically both galaxies show a strong resemblance to the Sombrero, although the disk in each of the galaxies is slightly less pronounced. A detailed analysis of the distribution of mass in these galaxies, as carried out for NGC 4594, was not possible. It appears that NGC 3593, like NGC 4594, contains a small amount of HI. However, within the uncertainties imposed by the observational circumstances, it is concluded that the distribution of this gas differs greatly from that observed in the Sombrero. In NGC 4281 no detectable HI was found, in contradiction with single dish measurements. The presence of an HI-rich companion close to NGC 4281 might account for these discordant results.

The region within which we can obtain the distribution of mass using the method discussed above is restricted to the radius of the visible or HI disk. For only a few galaxies can the HI rotation curve be measured out to very large galactocentric radii (e.g. NGC 3198, van Albada et al., 1985). However, at these extreme radii the rotation curves are sometimes irregular so that the assumption of circular motion may no longer be valid (Sancisi and van Albada, 1987). In that case we have to rely on other methods. An alternative way to acquire information out to very large galactocentric radii is to observe binary galaxies. Several studies have been undertaken (see van Moorsel, 1982) and in many cases there are clear indications for the presence of dark matter outside the optically visible galaxies. However, due to projection effects one needs a large sample of binaries to make a reliable estimate of the average amount of dark matter in these systems. The data on binaries obtained thus far are difficult to interpret in this respect (Faber and Gallagher, 1979; Blackman and van Moorsel, 1984).

In the following chapters of this thesis a study of some representatives of the class of single bright galaxies accompanied by several much less massive companions is presented. These companions can serve as test-particles moving in the potential field of the central galaxy. Radial velocity observations can then provide important new data regarding the distribution of mass in and around the central galaxy, including the possible presence of a dark halo (Bahcall and Tremaine, 1981; Gottesman and Hunter, 1982; Gottesman et al., 1983). Although these data pertain to about the same region as do binary galaxy observations, they offer several advantages. If the companions are much less massive than the primary galaxy, then their individual masses do not enter the

problem, thus eliminating an important source of uncertainty. Moreover the presence of several test-particles will greatly increase the statistical significance of a single mass determination. However, the limited detectability of the faint companions might severely limit the usefulness of this method. Therefore a feasibility study was made using the Nançay Decimetric Radio Telescope. The results of this study are given in chapter 5.

In chapters 6 and 7 we discuss WSRT observations of the NGC 2859 and NGC 4111 groups respectively. The central galaxies of these groups are classified as lenticular and they are surrounded by several HI-rich companions. The calculated masses and M/L ratios of these galaxies are of particular interest for at least two reasons. First of all, mass determinations over regions much greater than the optical radii are scarce, particularly for S0's. Second, they provide an M/L which is relatively free from the model dependent uncertainties which are present in mass determinations based on measurements of the stellar velocity dispersion (Tonry and Davis, 1981) or on the rotation velocity of HI in (polar) rings (Schechter et al., 1984).

In chapter 8 we discuss HI observations of NGC 5899, a late type spiral accompanied by three faint galaxies, one of which (NGC 5900) appeared to be rich in HI. The minimum mass required to bind the latter system to NGC 5899 is derived and compared with the sum of the individual masses. In addition, the distribution and kinematics of the neutral hydrogen in these galaxies is studied.

Finally, in chapter 9 we summarize the main results and make some suggestions for future work.

Bahcall, J.N., Tremaine, S.: 1981, Astrophys. J. 244, 805

Blackman, C.P., van Moorsel, G.A.: 1984, Mon. Not. R. Astron. Soc. 208, 91

Bosma, A.: 1978, The Distribution and Kinematics of Neutral Hydrogen in Spiral Galaxies of various morphological Types, Dissertation, University of Groningen

Faber, S.M., Gallagher, J.S.,: 1979, Ann. Rev. Astron. Astrophys. 17, 135

Freeman, K.C.: 1970, Astrophys. J. 160, 811

Freeman, K.C.: 1987, Dark Matter in the Universe, eds. J. Kormendy and G.R. Knapp, IAU Symp. 117, 119

Gottesman, S.T., Hunter, J.H.: 1982, Astrophys. J. 260, 65

Gottesman, S.T., Hunter, J.H., Shostak, G.S.: 1983, Mon. Not. R. Astron. Soc. 202, 21p

Lin, C.C., Shu, F.H.: 1964, Astrophys. J. 140, 646

Nordsieck, K.H.: 1973, Astrophys. J. 184, 719

Ostriker, J.P., Peebles, P.J.E.: 1973, Astrophys. J. 186, 467

Rubin, V.C., Ford, W.K., Thonnard, N.: 1980, Astrophys. J. 238, 471

Rubin, V.C., Ford, W.K., Thonnard, N., Burstein, D.: 1982, Astrophys. J. 261, 439

Rubin, V.C., Burstein, D., Ford, W.K., Thonnard, N.: 1985, Astrophys. J. 289, 81

Sancisi, R., van Albada, T.S.: 1987, Dark Matter in the Universe, eds. J. Kormendy and G.R. Knapp, IAU Symp. 117, 67

Schechter, P.L., Sancisi, R., van Woerden, H., Lynds, C.R.: 1984, Mon. Not. R. Astron. Soc. 208, 111

Shu, F.H., Stachnik, R.V., Yost, J.C.: 1971, Astrophys. J. 166, 465

Tonry, J.L., Davis, M.: 1981, Astrophys. J. 246, 666

Toomre, A.: 1963, Astrophys. J. 138, 385

van Albada, T.S., Bahcall, J.N., Begeman, K., Sancisi, R.: 1985, Astrophys. J. 295, 305

van der Kruit, P.C., Freeman, K.C.: 1986, Astrophys. J. 303, 556

van Moorsel, G.A.: 1982, Neutral Hydrogen Observations of Binary Galaxies, Dissertation, University of Groningen

Visser, H.C.D.: 1980a, Astron. Astrophys. 88, 149

Visser, H.C.D.: 1980b, Astron. Astrophys. 88, 159

Wevers, B.M.H.R.: 1984, A Study of Spiral Galaxies, using HI synthesis observations and photographic surface photometry, Dissertation, University of Groningen

Zwicky, F.: 1933, Helv. Phys. Acta 6, 110

CHAPTER 2 THE DISTRIBUTION OF NEUTRAL HYDROGEN IN THE SOMBRERO GALAXY, NGC 4594

Summary

Fan beam observations with an E-W resolution of 11'4 of NGC 4594 (the Sombrero galaxy) in the 21-cm line, made with the Westerbork Synthesis Radio Telescope, are reported The results are presented in the form of a position-velocity contour map Global properties of the galaxy are $M_{HI} = 1.3\ 10^9\ M_\odot$ (distance 18 6 Mpc), $[M_{HI}/L_B] = 0.010$ and $V_{sys} = 1100$ km s^{-1} (heliocentric) A model is proposed which reproduces the gross properties of the HI distribution The gas appears to be confined to an annulus between radii 12 and 19 kpc, coincident with the distribution of dust in the galaxy, and to be concentrated within this annulus into two concentric rings The rotation velocity in this region is about 370 km s^{-1} and either constant or slightly decreasing with radius The velocity distribution in the annulus shows that radial motions in the gas are less than about 15 km s^{-1}, arguing against recent explosive or accretion phenomena

The relative HI content $[M_{HI}/L_B]$ is very much lower for this galaxy than for other Sa galaxies and is lower than for HI-rich ellipticals The HI distribution suggests that only gas outside the optical bulge has been able to survive Mechanisms causing the removal of gas from the spheroid of the galaxy are briefly discussed

1 Introduction

In this paper, we present aperture synthesis observations of the HI distribution in NGC 4594 (M 104), the "Sombrero" galaxy, classified Sa to Sb. The galaxy has a well-developed stellar disk with an approximately exponential brightness distribution (van Houten, 1961); however the optical structure of the bulge resembles that of a giant elliptical galaxy (cf. Faber et al., 1977, hereafter FBGK). The bulge is very large, with a diameter of 285 kpc at the assumed distance of 18.6 Mpc (Burkhead, 1979); its surface brightness distribution follows a de Vaucouleurs law, and its velocity dispersion is large ($\sigma_* = 210$ km s^{-1}: Williams, 1977; Kormendy and Illingworth, 1982). The galaxy also contains a compact nuclear radio continuum source with an inverted spectrum (de Bruyn, 1978; Shaffer and Marsher, 1979). While HI emission has been detected from the galaxy (FBGK), the relative HI content [M_{HI}/L_B] is much lower than the values typical for early-type spirals (e.g. Bottinelli et al., 1980), is lower than values for gas-rich ellipticals, and is lower than the sensitive upper limits set for many normal ellipticals. The galaxy is isolated, with no known companions, and the photometry of van Houten (1961) suggests that the disk has the peculiar property that the radial distributions of the light and of the dust are quite different, with the dust lying in an annulus outside the bright part of the stellar disk.

Observations of the distribution of the interstellar HI in this galaxy are therefore of interest for at least two reasons. As discussed by FBGK, the motions of the gas disk provide a probe of the mass distribution of an elliptical like system that is relatively free of the model-dependent uncertainties which are present in mass estimates from stellar velocity dispersions. In addition, the properties of the gas disk might be useful for understanding the state of the interstellar matter in early-type galaxies.

Despite its southerly declination (-11°), NGC 4594 is a good candidate for observation with the Westerbork Synthesis Radio Telescope (WSRT) because of its east-west orientation and edge-on aspect. At this declination the telescope is a fan-beam instrument with resolution only in the east-west direction.

The first WSRT observations of NGC 4594 were made in 1972 using the provisional line receiver. A marginal detection was achieved (Bajaja and Shane, 1981) which, despite the very weak signal, pointed toward some of the results discussed here.

In section 2 we describe the observations and the reduction procedure and in sections 3 and 4 the results and their interpretation. In section 5 we discuss the global properties of the galaxy and of its interstellar medium, and in section 6 we present some conclusions.

2 Observations and reductions

NGC 4594 was observed with the WSRT during two nine-hour periods in 1981, on 27 and 28 February and 19 and 20 March. The baselines ranged from 54 m to 2754 m in steps of 36 m; the synthesized beam has half power dimensions of 11.″4 × 81.″6 ($\alpha \times \delta$). The system temperature was 55 K. The digital line back-end (Bos et al., 1981) was used to observe a single polarization in 63 channels over a total bandwidth of 5 MHz; the resulting channel separation is 16.6 km s^{-1}. The data were Hanning smoothed to give a half-power channel width of 33 km s^{-1}. (All velocities in this paper are heliocentric). Both observations appeared to be of good quality and it was not necessary to delete any data. The two observations were combined and reduced as a single unit.

The continuum data were Fourier-transformed to a map and examined for the presence of continuum sources in the field. A list of the detected sources and their 1.4 GHz fluxes can be found in Table 1. The positions and fluxes of the point sources were determined by fitting the antenna pattern to the data. Extended sources, however, were resolved into components with the aid of a "clean" algorithm (sometimes after subtraction of an initial point source) and the fluxes and positions are the sums and flux-weighted averages of these components. Among the continuum sources in Table 1 is the nuclear point source of NGC 4594; the flux of this source for the epoch of observation is 72.1 ± 1.1 mJy, showing no significant change from published values.

The strongest point sources in the field were subtracted from the data which were then Fourier-transformed to produce a sky map at each velocity. For two extended sources some residual grating rings appeared close to the position of NGC 4594. These residual grating rings were removed from all channel maps using the resolution into components on the continuum map and the "clean" procedure described by Högbom (1974).

Because the galaxy is essentially edge-on and east-west (i = 85°, van Houten, 1961) and the instrumental resolution perpendicular to the equator is 82″, there is no information in the observations about the distribution of gas perpendicular to the major axis of the image. We therefore constructed a one-dimensional map of the HI distribution by taking a cross-cut along the major axis (p.a. = 90°). This map, a position-velocity (or l-v) map, consisted of 60 rows each of 512 points, spaced at intervals of 4.″5. Three channels, one at the lowest velocity and two at the highest velocities, were deleted because of band-edge effects. All further data reduction was done in this l-v plane.

Table 1. Radio continuum sources in the field

α_{1950} h m s	δ_{1950} ° ′ ″	S_{1415} mJy	Notes
12 35 31.46 ±0.07	-11 42 53.4 ±4.7	90.8 ±11.5	
12 35 48.59	-11 20 02.3	102.9 ±02.6	E
12 36 08.82 ±0.04	-11 20 02.1 ±1.2	76.8 ±03.3	
12 36 46.06 ±0.05	-11 12 38.7 ±1.9	18.1 ±00.7	
12 37 22.27 ±0.06	-11 42 22.9 ±3.4	24.5 ±02.3	N
12 37 23.39 ±0.04	-11 20 54.7 ±1.1	72.1 ±01.1	C
12 37 36.03 ±0.05	-11 47 36.7 ±2.1	86.8 ±08.5	
12 37 47.76 ±0.06	-11 31 41.4 ±3.8	10.4 ±00.9	N,D
12 37 50.19 ±0.05	-11 31 29.4 ±2.7	15.6 ±01.0	N,D
12 37 55.76	-11 10 16.0	70.4 ±02.7	E
12 38 01.32 ±0.04	-11 04 57.8 ±1.1	115.3 ±04.9	
12 38 29.40	-11 39 47.7	183.4 ±10.5	E
12 38 34.98 ±0.06	-11 27 56.3 ±3.1	20.8 ±01.7	
12 39 23.92 ±0.07	-11 23 23.7 ±4.2	51.5 ±06.5	N

Notes: C = central continuum source of NGC 4594; D = both sources marked with a D comprise possibly one double source; E = extended source; N = not subtracted from the data

The initial continuum correction map was made by averaging at each right ascension point over all velocities outside a widely chosen mask whose velocity limits varied with right ascension, leaving only grid points without line emission. This continuum map was then subtracted from the l-v map.

Due to the finite (though small) width of the galaxy in declination compared with the synthesized antenna pattern in this direction, a slight attenuation is introduced by using only one declination from each channel map. This has been evaluated by comparing this map with a map made by averaging three successive rows in declination, properly normalized by the antenna pattern. We found a small systematic residual, close to the noise level, suggesting an attenuation of about 5%, independent of position and velocity. We have continued to use the original single-declination strip scan because of its slightly better signal-to-noise ratio, but all fluxes have been corrected for this small effect.

The negative declination of NGC 4594 makes it impossible to achieve complete spatial coverage with the interferometers of the WSRT. The available coverage produces a synthesized antenna pattern with pronounced negative side-lobes in the E-W direction, as illustrated in Figure 1 (curve a), where the maximum negative amplitude is 31% of the central peak. The effect of these side-lobes overlapping the central peak is to make

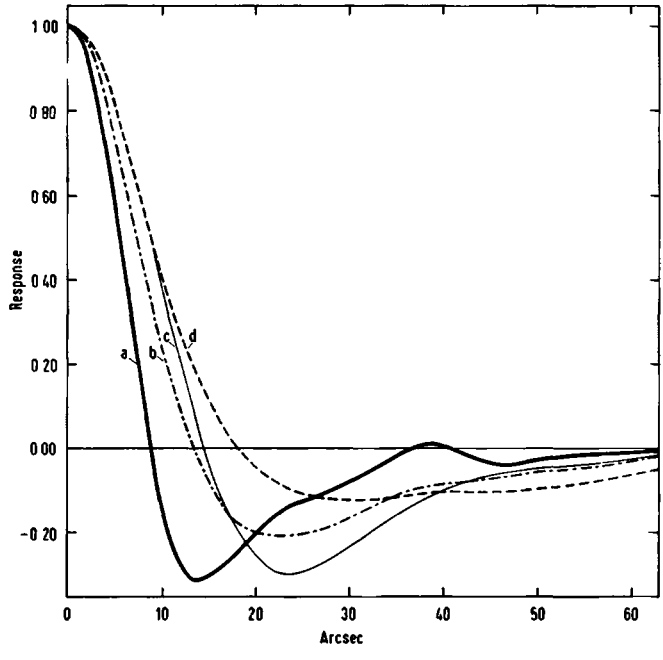

Figure 1: Curve a: east-west crosscut of the synthesized antenna pattern expressed as a function of the distance, x, from the central peak, in grid points; Curves b and d: antenna pattern convolved with an exponential function, (exp(-|x|/2) and exp(-|x|/4) respectively); Curve c: antenna pattern convolved with a Gauss function, $exp(-x^2/8)$.

extended features, even well above the theoretical detection level, unidentifiable on the original maps. This applies not only to visual inspection but also to the cleaning algorithm, which fails to find these peaks amongst the noise. Clearly these side-lobes must be removed by cleaning, but first the peaks must be made visible by suppressing the side-lobes. Convolution with the gaussian function (Figure 1, curve c) does not suffice, but an exponential function (Figure 1, curves b and d) substantially reduces the amplitude of the side-lobes while only slightly broadening the central peak.

In order to retain the maximum resolution, the cleaning was done in an iterative way. The original map was cleaned to a conservative level (about 2.5σ), the components which were found were subtracted and the resultant map and the antenna pattern convolved as shown in Figure 1, curve b. This map was then cleaned and the components found in this step were also subtracted from the resultant map described above, giving a full-resolution map from which both sets of components had been subtracted. A broader convolution was applied and the process repeated. The fourth (and last) cleaning step, now carried to a level of 1σ, was applied to the map as convolved to the antenna pattern shown in Figure 1, curve d. Finally all of the delta-function components found in the above iterations were subtracted from the original map and restored (i.e. added to the residual map using only the central maximum of the unconvolved antenna pattern).

In the original continuum subtraction, the far side-lobes of the line radiation were subtracted along with the continuum. In order to compensate for this, an additional continuum correction map was made in the same way as the first correction map, but using a mask with smaller dimensions and applying it to the cleaned map. This second correction map was subtracted from the same cleaned l-v map, and the result, after primary beam correction, is shown in Figure 2a. This map is used in the subsequent analysis. The r.m.s. noise is about 0.07 mJy arcsec^{-1}; the lowest positive contour is 0.10 mJy arcsec^{-1}, and the other contours are integral multiples of this number.

3 Global results

Examination of Figure 2a shows that the gas distribution is quite symmetric and that there is a linear run of velocity with position along the major axis. This could indicate a disk of HI rotating as a solid body or a ring of HI in circular rotation. The optical rotation curve data (see Figure 3) and the observed distribution of gas along the major axis (Figure 4) are inconsistent with the first possibility. Figure 3 shows the stellar rotation curves of FBGK and Schweizer (1978, which included HII velocities) superimposed on the HI l-v map, which has been symmetrized by rotating it about its position and velocity center and averaging. It is evident that the upper envelope of the HI distribution falls well below the optically determined rotation velocity out to about 120″ from the center, indicating the absence of HI from this part of the galaxy. The behaviour of the upper envelope between 120″ and 210″ suggests an approximately constant rotation velocity of about 370 km s^{-1} in this region. More accurate results can be derived from model fitting, as discussed in the following section. It appears that the optical rotation velocities, at least at all radii where HI is present, are contaminated by light from the slowly rotating bulge.

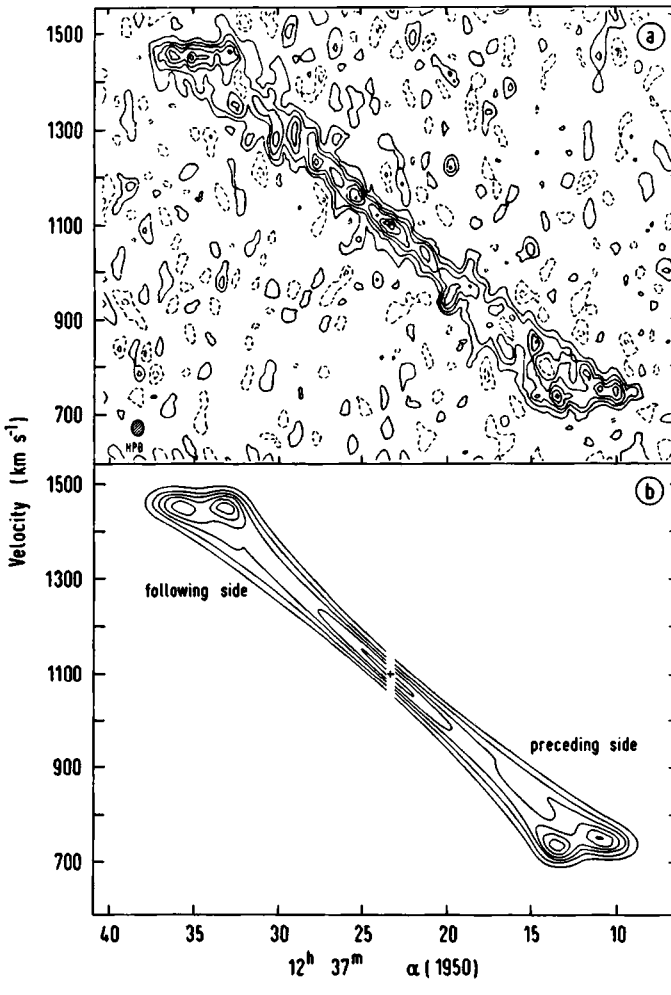

Figures 2a and b: *Map of the HI line flux from NGC 4594 plotted as a function of right ascension and velocity at the declination of the center of the galaxy. The position of the central continuum source has been marked with a cross at a velocity of 1100 km s^{-1}.*
a. *The observed l-v diagram; the lowest positive contour and the contour interval are 0.10 mJy arcsec^{-1}; the zero-level contour is not shown. Broken contours enclose regions whose flux level is lower than that of the surroundings (including regions of negative flux).*
b. *The calculated l-v diagram. Parameters used to calculate the model for the preceding and following sides of the galaxy can be found in Table 3. The model calculation is described in Section 4.*

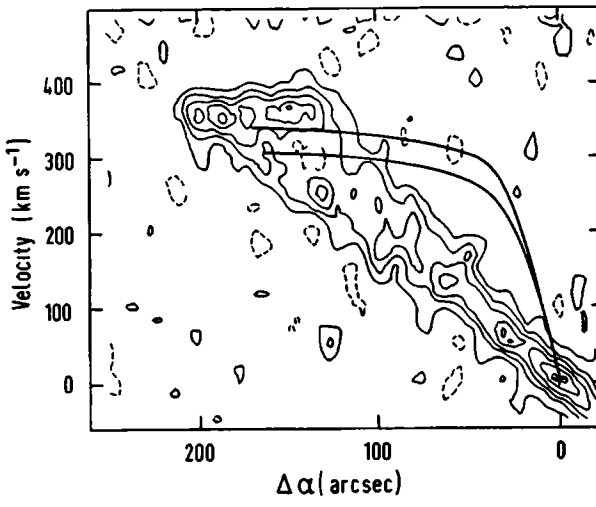

Figure 3 Symmetrized HI distribution of NGC 4594 as a function of velocity and projected distance from the center (see text) with contours as in Figure 2 The solid curves are the stellar rotation curve from FBGK (lower curve) and the emission line/stellar curve of Schweizer (1978) (upper curve)

Figure 2a shows that the HI line at the projected center of the galaxy is narrow, with a full width at half power of 48 km s^{-1} Subtracting quadratically the instrumental bandwidth (33 km s^{-1}) and the spread due to the velocity gradient across the 11"4 beam (25 km s^{-1}) we derive an intrinsic line width of 25 km s^{-1} This could be accounted for by the turbulent motions in the gas together with larger-scale effects like velocity gradients associated with density waves (postulating that NGC 4594 is in fact a spiral galaxy) Even without these effects it sets an upper limit to systematic radial motions in the gas of about 15 km s^{-1}, arguing against a recent origin of the gas either by accretion or by ejection from the nucleus The peak at the projected center of the galaxy can be explained to a large extent by velocity crowding

The regions of depressed flux level (regions surrounded by dashed contours) which show up within the maxima near both ends of the l-v diagram suggest that the HI forms two separate linear structures in the l-v plane, indicating the presence of two approximately concentric rings

The projected HI column density distribution along the major axis has been obtained by integrating the masked l-v map over all velocities. The result is shown in Figure 4. The position of the central continuum source has been taken as the point of symmetry and the data are smoothed in right ascension with a three-point running mean. The HI distribution shown in Figure 4 is also consistent with the assumption that the gas is distributed in two concentric rings, where the maximum at $\Delta\alpha$ = 140″ can be attributed to the inner ring and the broad shoulder at $\Delta\alpha$ = 180″ to the outer. The peaks inward of $\Delta\alpha$ = 120″ cannot be explained in the same way because of their lower projected velocities and must be due to individual HI concentrations in the rings, with typical HI masses of 2 10^7 $M_\odot$ Their

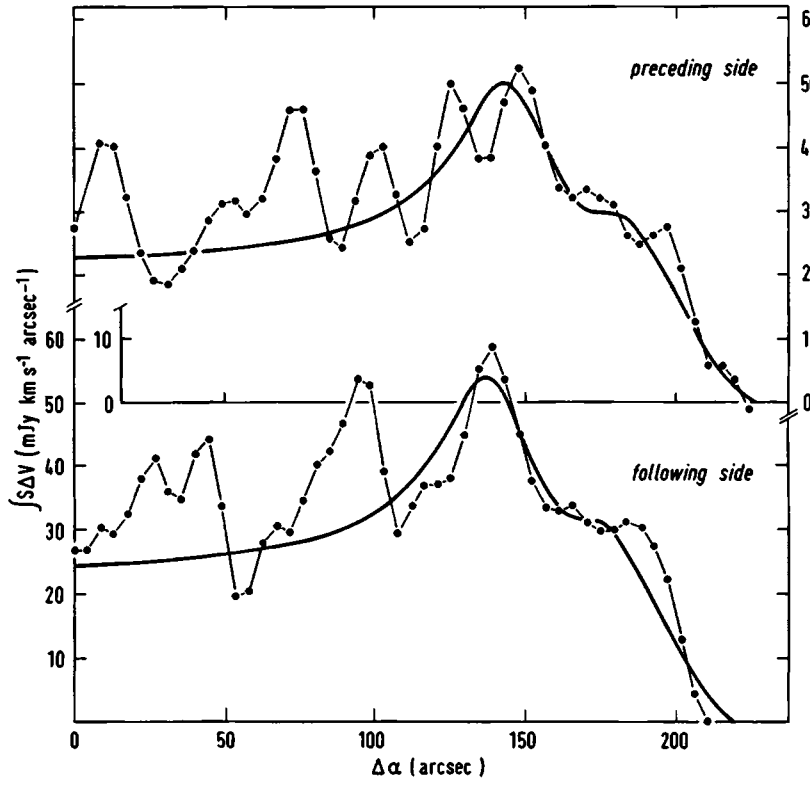

Figure 4: Plot of the integrated HI flux along the long axis of NGC 4594. The observations are represented by connected dots, the model by a solid curve.

amplitudes are considerably in excess of the expected instrumental noise level of about 5 mJy km s^{-1} $arcsec^{-1}$. Similar concentrations in the region $\Delta\alpha > 120''$, where the rings are seen tangentially, may influence the shapes of the terminal peaks and shoulders but will be crowded too closely to be seen individually. In these regions the behaviour of the HI column density is therefore orderly and quite similar on both sides. We note, however, that the curves are systematically displaced with respect to one another in the sense that the HI extends further on the preceding than on the following side. With the aid of the model described in section 4, we find that, at least for the regions in which such a determination is possible, the center of the HI distribution lies about 300 pc westward of the coincident optical and radio continuum nuclei. This asymmetry is smaller than that which we are accustomed to find in spiral galaxies.

The global HI line profile has been obtained by integrating the l-v map over all positions after masking as above and is shown in Figure 5; it has the characteristic two-horned shape which arises from gas in an annulus or a disk with a flat rotation curve. The line profile agrees well with that measured with the NRAO 43-meter telescope (FBGK); likewise, the two measurements of the total flux of the line are in satisfactory agreement. From the WSRT profile we find $\int Sdv$ = 14.2 Jy km s^{-1}, while the value found by FBGK is 11.1 Jy km s^{-1}. Since the two types of observation lose sensitivity for quite different types of extended structures, this agreement suggests that the WSRT observations have detected essentially all of the line flux and that little if any HI has been deleted by the side-lobe correction and masking procedures or is concealed in structures larger than a few minutes of arc.

The apparent mass of HI in the galaxy is $M_{HI} = 1.15\ 10^9\ M_\odot$ at the assumed distance of 18.6 Mpc. Saturation effects in various forms will cause this to be an underestimate. In edge-on galaxies shadowing by superposition of clouds (as opposed to HI self-absorption within clouds, which is independent of inclination) is of particular importance. We will derive in the next section a shadowing correction of 12%, leading to a corrected mass estimate $M_{HI} = 1.3\ 10^9\ M_\odot$ and an HI to blue luminosity ratio of $[M_{HI}/L_B] = 0.010$ (cf. FBGK). This is much smaller than the mean value of $[M_{HI}/L_B]$ of 0.05 - 0.15 for Sa galaxies (Bottinelli et al., 1980) and smaller than the mean value of 0.04 for HI-rich ellipticals (Knapp, 1983). It is also close to the low end of the range of upper limits for ellipticals with no detected HI (0.003 - 0.05, Knapp et al., 1979).

The peaks in the line profile (Figure 5) are at 735 and 1449 km s^{-1}, giving an approximate systemic radial velocity of 1092 km s^{-1}. A better estimate of the systemic velocity was made as follows: The l-v map was rotated through 180° about a point whose right ascension is that of the central continuum source; the velocity coordinate of the rotation center was varied until the difference between the rotated and non-rotated maps

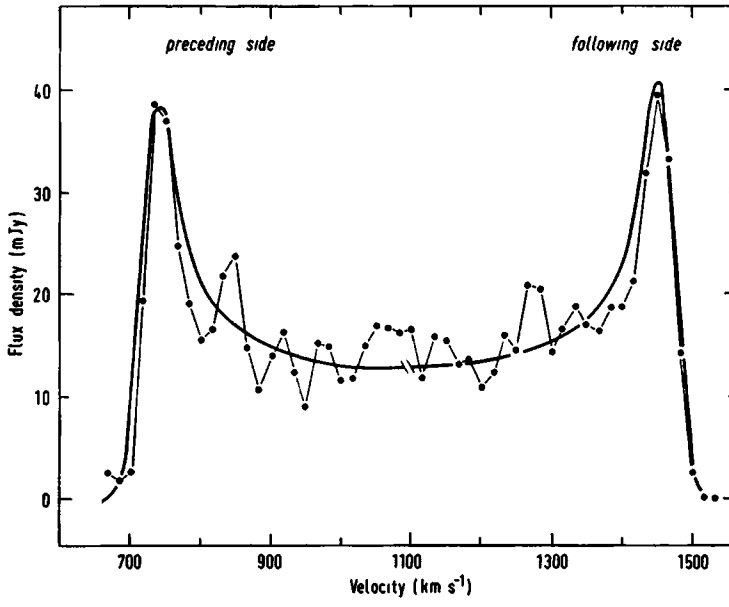

Figure 5: Global HI line profile for NGC 4594. The observations are represented by connected dots, the model by a solid curve.

showed no systematic variation with velocity. In this way an accurate determination of the systemic radial velocity, 1100 ± 3 km s^{-1}, was made. This value has been used throughout the remainder of this paper. It agrees well with the mean velocity of the peaks of the smoothed global profile (1100 km s^{-1}), with the flux weighted mean velocity (1102 km s^{-1}) and with the value found by FBGK. However, it is slightly higher than the optically-measured value given by Schweizer (1978). In deriving the systemic velocity of 1100 km s^{-1}, it has been assumed that the continuum point source coincides with the dynamical center of the galaxy. However, as has been pointed out, the slight asymmetry of the HI distribution (Figure 4) suggests a slightly different center. Adopting this center results in a systemic velocity of about 1093 km s^{-1}. Various rules of thumb may be used for estimating the rotation velocity, assuming a flat rotation curve. Identifying the rotation velocity with the peaks in Figure 5 leads to a value of 360 km s^{-1}; using the half-

maximum points on the outer flanks gives 380 km s^{-1} The best value may be expected to lie in this range

The global properties assumed or derived from these observations are summarized in Table 2

Table 2 Global properties of NGC 4594

Position (1950) (Gallouet et al , 1975)
$\alpha = 12^h37^m22^s8, \delta = -11°21\ 00$
Distance, D = 18 6 Mpc (assuming $H_0 = 50$ km s^{-1} Mpc^{-1})
Inclination, i = 85° (van Houten, 1961)
Systemic velocity, V = 1100 ±3 km s^{-1} (heliocentric)
Maximum rotation velocity, V_c(max) = 370 ±10 km s^{-1}
21 cm line flux, $\int Sdv$ = 14 2 Jy km s^{-1}
Hydrogen mass, M_{HI} = 1 15 10^9 $M_\odot$ (observed)[a]
Blue luminosity, L_B = 1 12 10^{11} $L_\odot$ (FBGK)

[a] This value is calculated directly from the total flux Including shadowing corrections (section 4) the best estimate is M_{HI} = 1 3 10^9 $M_\odot$

4 Model calculations

The large scale distribution and kinematics of the neutral hydrogen in NGC 4594 may be described with the aid of a simple model In constructing the model an effort has been made to include the minimum number of free parameters required to produce the main features of the l-v diagram The adopted model has the following properties

1) The HI is confined to a flat disk whose inclination and orientation are determined from optical observations (see section 2) and is assumed to be optically thin

2) Within this disk the HI is assumed to be distributed uniformly in azimuth, so that it can be represented as a series of concentric rings Detailed departures from uniformity, such as clumpiness in the HI distribution or the possibility that the rings in fact approximate sections of spiral arms, have not been included The position of the radio continuum source, which coincides closely with the optical center (de Bruyn et al , 1976), was chosen as the center of symmetry Since the HI is not quite symmetrically distributed

with respect to this position, slightly different parameters were derived for the preceding and the following halves of the galaxy.

3) Each HI ring was described by a radius R, a central surface density σ at radius R, and a radial extent W between half-density points. Various forms of the radial density distribution were allowed, but in practically all models a Gaussian form was used. The maximum number of rings used in any model was two.

4) All HI was assumed to describe circular orbits. The circular velocity Θ was assumed to be a constant within each ring.

5) A constant isotropic velocity dispersion was introduced as a free parameter. After the line profiles had been calculated, they were further convolved with the instrumental profile. The model calculations yielded only an upper limit to the intrinsic velocity dispersion.

The model l-v diagrams were produced by integrating along lines in the plane of the galaxy and perpendicular to the line of nodes. Attenuation by the declination profile of the synthesized beam was included. The integration was carried out by summing the contributions from consecutive 50 pc intervals in the plane of the galaxy, including only those where the density was above 10% of the maximum. The 50 pc interval is sufficiently small that velocity and density gradients can be neglected. The lines of sight were spaced at 4'.5 intervals, as were the observational grid points. The resulting map was smoothed in right ascension by the central maximum of the synthesized beam.

The choice of parameter values was determined by matching the calculated and observed l-v diagrams, where subjective criteria were used to decide upon a suitable fit. In addition to the l-v diagrams it was useful to compare the observed and calculated global line profiles (Figure 5) and the integrated right ascension distributions (Figure 4).

The requirement that the HI be distributed in (at least) two rings is evident from the right-ascension distribution shown in Figure 4. The pronounced shoulder, which is practically identical on both sides, can be reproduced in no other way. The broad flat top, with one or two depressions, seen at both ends of the l-v diagram, indicates the same; a single-ring model always leads to a distribution which is sharply peaked in those directions where the ring is seen tangentially. The integrated right-ascension distribution can be used to determine all positional parameters unambiguously. When appropriate rotational velocities and velocity dispersions are introduced, minor adjustments in the other parameters are made, and account is taken of the observed asymmetry, an adequate fit with the observed l-v diagram is obtained, as shown in Figure 2b.

This global model does not reproduce the observed clumpiness of the HI distribution in the rings. In the tangential region, $\Delta\alpha > 120''$, the clumps tend to overlap and average out, so that here the large-scale HI distribution is most clearly revealed. For this reason, and because the l-v diagram is here most sensitive to the choice of model parameters (except for the velocity dispersion), the parameters were adjusted so as to give a good fit to the observations in this region (see Figures 2 and 4).

It is evident from Figure 4 that the model which fits the observations at $\Delta\alpha > 120''$ predicts too little flux at $\Delta\alpha < 120''$. The most plausible explanation for this discrepancy is cloud-cloud shadowing in the tangential region, where the highest brightness temperatures will be encountered. Since the influence of shadowing will be least in directions close to the center of the galaxy, it is here that the model flux should be fitted to the observations. This requires a 30% increase in the model HI surface density. The total flux predicted by the model then increases to 15.9 Jy km s^{-1}, which is 12% more than the observed value reported in Table 2.

We note in Figure 4 that the model does not reproduce the steepness of the outer flanks of the shoulders. Replacing the Gaussian distribution with a rectangular one improves the fit only marginally, and introducing a more extreme assumption seems unduly artificial. A more plausible explanation is that the sharpness is due to the clumpiness of the HI in the tangential region. In view of this possibility, no further effort has been made to model the steepness of the flank with greater accuracy.

Figures 2a and 4 indicate a remarkable degree of symmetry between the preceding and following sides of the galaxy, except for the apparent displacement of about 3″ in the preceding direction with respect to the adopted center. In calculating the models, both sides were initially represented by the same parameters. Finally, the radii were adjusted to introduce the observed asymmetry. The surface densities were scaled accordingly so as to retain equally high peaks on both sides in the model l-v plot. The resulting differences in surface density are not significant relative to other sources of uncertainty.

The rotational velocities were determined by matching the high velocity peaks in the l-v diagram on both sides of the center and by reproducing the run of flux-weighted mean velocity with right ascension (Figure 6). On the following side, both rings show practically the same velocity; on the preceding side, the innermost ring shows a higher velocity than the outermost.

The parameters of the final model (before the 30% increase due to shadowing) are summarized in Table 3 and were used to produce the calculated curves in Figures 2b, 4, 5 and 6. The radial extent of the HI (12-19 kpc, see Figure 7) agrees well with the distribution of dust found by van Houten (1961). If we assume the thickness of the disk to be 100 pc then the inferred average HI space density, after correction for shadowing,

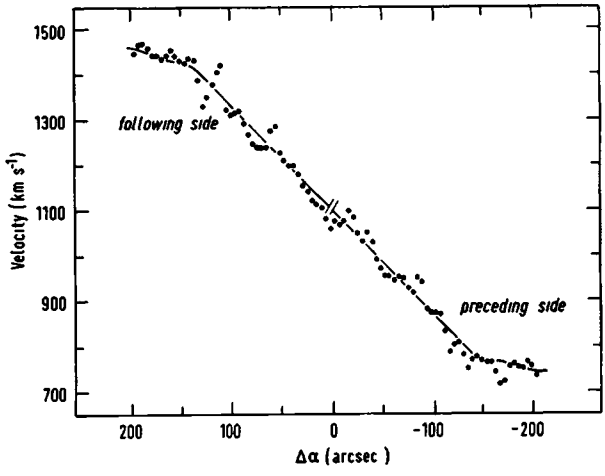

Figure 6: The flux-weighted mean velocity as a function of distance along the long axis to the center of NGC 4594 The dots represent the observations, the solid curve is derived from the model

Table 3. Model parameters

	Preceding side		*Following side*	
	Inner ring	Outer ring	Inner ring	Outer ring
R (kpc)	13.6	17.3	13.0	16.7
W (kpc)	2.3	3.2	2.3	3.2
σ_H ($M_\odot$ pc^{-2})	2.23	1.48	2.40	1 60
Θ (km s^{-1})	380	367	365	365
$\langle v^2 \rangle^{1/2}$ (km s^{-1})	33	33	33	33

σ_H is the value used in calculating the model fits. The true value will be about 30% larger as a consequence of shadowing

is 0.8 cm^{-3}.

From the model velocities of the rings (Figure 7), we conclude that the rotation velocity of the gas (370 km s^{-1} at R = 15 kpc) is constant or slightly decreasing with radius over the region where the HI is present. Examination of Figure 3 suggests that, at all radii, the optically-measured absorption-line rotation curves are strongly affected by contamination by light from the more slowly rotating bulge. This is indicated by the flatness of the HI rotation curve compared to the slow rise seen in the optical rotation curves, and by the differences in shape between the curve of NGC 4594 and those seen for many other galaxies (e.g. the compilations by Bosma, 1978 and Rubin et al., 1980 a, b). For most galaxies, especially those of early type, the solid-body rise of the rotation curve occurs over a much shorter radial distance than it appears to do in NGC 4594, and the velocity is thereafter roughly constant. Preliminary results from new observations on

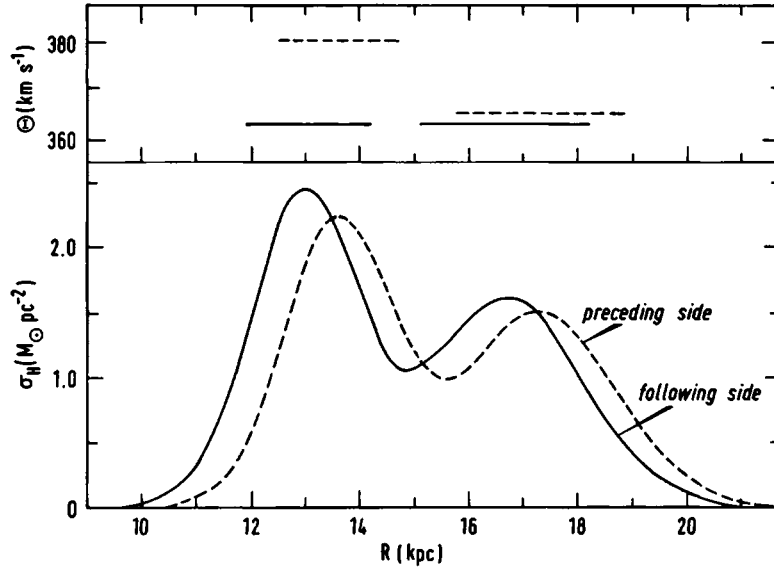

Figure 7: Lower panel: plot of the radial HI surface density derived from the model parameters in Table 3, using a Gaussian density profile in each ring. The parameters have not been corrected for shadowing (see text). Upper panel: rotational velocities of the individual rings.

which only emission lines have been measured have been communicated to us by V. Rubin (private communication). These are consistent with a rotation curve which rises rapidly to an extended flat maximum, in agreement with observations of other early-type galaxies and with the HI observations reported here.

Van Houten's (1961) deconvolution of the surface photometry of NGC 4594 suggests the presence of an exponential disk of stars which begins at a radius of about 30", at the same location as the bend in the optical rotation curves shown in Figure 3. This and the gradual rise of the optical curves toward the HI terminal velocity suggests that the disk spectrum is always contaminated by bulge light, with the contamination becoming less important with increasing radius. The rotation curve by Schweizer (1978) is made using both absorption and emission lines. Despite the fact that this rotation curve lies significantly below the HI velocities, Schweizer finds no systematic difference between absorption and emission velocities. The kinematics of the HII regions evidently require further study.

5 Discussion

5.1 The mass and mass-to-light ratio of NGC 4594

This subject was discussed extensively by FBGK, and the present observations add little to that discussion except to better define the range of radii over which the circular velocity is measured. The HI observations described in the preceding sections give the circular velocity, V_c, at R = 215" (19 kpc) as 370 km s^{-1}, so that the mass within this radius (assuming a spherical distribution) is:

$$M(R) = V_c^2 R/G \ , \qquad (1)$$

or 6 10^{11} $M_\odot$ corresponding to $[M/L_B] = 5.3$. This value provides a measurement of M/L at roughly the Holmberg radius for an elliptical-like stellar population which is in reasonable agreement with the average central values in elliptical galaxies (Faber and Gallagher, 1979).

The one-dimensional velocity dispersion, σ_*, of the bulge is 210 km s^{-1} and is roughly constant with radius, except very near the center of the galaxy (Kormendy and Illingworth, 1982). The bulge light falls with radius as roughly r^{-3} (van Houten, 1961; Burkhead, 1979). The equation of motion of the bulge stars is:

$$\frac{d}{dr}\left[\varrho_*(r)\sigma_*^2(r)\right] = \frac{-GM(r)\varrho_*(r)}{r^2} \quad . \tag{2}$$

If we assume the mass-to-light ratio of the bulge stars to be constant, so that $\varrho_*(r) \propto \varrho^{-3}$, then equations (1) and (2) give $V_c = \sigma_* \sqrt{3}$. With $V_c = 370$ km s^{-1}, we observe $V_c/\sigma_* = 1.76$, in good agreement with the above prediction. This value of V_c/σ_* and the approximate constancy of V_c within the HI annulus shows that the mass in this galaxy, as in all other large galaxies observed to date, increases roughly linearly with radius in the outer regions.

5.2 The interstellar medium in NGC 4594

The observations described above show that the HI is confined to an annulus with inner and outer radii of about 130″ and 210″ within which the HI distribution is fairly smooth over a large scale. The mean surface density of the annulus projected on the plane is then $1.8 \pm 0.4\ 10^{20}$ cm^{-2}. The half-density limits in radius of the dust distribution (van Houten, 1961) agree rather well with the measured extent of the HI. The mean value of the visual extinction perpendicular to the plane, A_V, in the annulus is $0^m.17$ (this may be a lower limit because of the high inclination of the galaxy), giving $N(HI)/A_v \leqslant 10^{21}$ atom cm^{-2} mag^{-1}, which is about half of the value in the local solar neighbourhood for the ratio of total H (HI + H_2) column density to visual extinction. Schweizer (1978) finds that there are at least two HII regions in the HI annulus of luminosity comparable to the luminosities of the brighter HII regions in the Galaxy. Thus, on the average, the interstellar matter in NGC 4594 resembles that in a spiral galaxy in its overall physical properties, as opposed to that in an elliptical or S0 galaxy.

Searches for CO emission from NGC 4594 have so far yielded only upper limits, $T_A^* \lesssim 0.03$ K using the NRAO 11 m antenna, whose half-power beam width is 65″ (Balick and Gallagher, unpublished). Suppose that the mass of molecular gas in the galaxy equals the mass of atomic gas and that the molecular gas has a similar radial distribution. If we assume that all of the molecular gas is in clouds like those seen in the solar neighbourhood (T = 8 K, $\Delta V = 5$ km s^{-1}, r = 5 pc, M = 2000 $M_\odot$) then the expected value of T_A^* (CO) is about 0.01 K, as long as the telescope used to make the observations has a beamwidth less than the radius of the galactic disk.

The observations described herein show that the HI distribution in NGC 4594 is confined to an annulus whose radial distribution is about the same as that of the dust. The symmetrized map of the distribution (Figure 3) shows that the HI intensity integrated

over ± 15 km s^{-1} at V = 335 km s^{-1} is at least ten times smaller at a radius of < 100″ than in the HI annulus. While other early-type spirals frequently show a ring-type distribution, HI emission is still detectable at 20% of the peak value almost to the center of the galaxy (e.g. the Sa galaxy NGC 7814, van der Kruit and Searle, 1982; NGC 891, Sancisi and Allen, 1979). At the present time, molecular observations have not been made to great enough sensitivity to show whether or not the hole in the HI distribution in NGC 4594 is due to molecule formation, but this is somewhat unlikely because of the close correspondence between the dust, HI and HII radial distributions.

When similar holes exist in the HI distributions in other spirals (Bosma, 1978), they roughly correspond in radius to the radius of the bulge. In our own galaxy and in M 31 (the only cases for which sufficient information exists at present) this hole is also present in molecular gas (Gordon and Burton, 1976; Stark, 1984). Several mechanisms have been considered for clearing spiral bulges of gas, including the presence of a hot, outflowing wind (Faber and Gallagher, 1976). Here we consider another mechanism, suggested by Gunn (1979), namely the loss of angular momentum of the disk gas due to collisions with gas shed by dying stars in the bulge. Assuming the latter to have zero net angular momentum, the net flux of mass inwards, for a galaxy with a flat rotation curve, is:

$$\dot{M} = 2\pi r^2 \dot{\mu}, \tag{3}$$

where $\dot{\mu}$ is the mass flux onto the disk.

Suppose that the original gas disk in NGC 4594 followed the distribution of the stellar disk. Then, if the gas in the annulus is assumed to be unperturbed at the present epoch, the original gas surface density of the disk will have been:

$$\Sigma(r) = 6\ 10^{21} \exp(-0.2(r-3.3))\ \mathrm{cm}^{-2} \tag{4}$$

where r is in kpc. If the stellar density in the bulge decreases as r^{-3}, the total blue luminosity of the bulge is 1.2 10^{11} $L_\odot$ and the rate of mass loss from dying bulge stars is 1.5 10^{-11} $M_\odot\ yr^{-1}\ L_\odot^{-1}$ (Faber and Gallagher, 1976), then the time scale for removal of the gas is:

$$T(r) = 1.7\ 10^9\ (r/3.3)^3 \exp(-0.2(r-3.3))\ \mathrm{yr}. \tag{5}$$

The dependence of T on r is shown in Figure 8, where it can be seen that the radii over which the gas has sufficiently long lifetime against this effect agree with those of the gas annulus in the galaxy. Some small amount of gas continues to be transferred to the central regions of the galaxy, where it could be responsible for the continued fuelling of the central radio continuum point source.

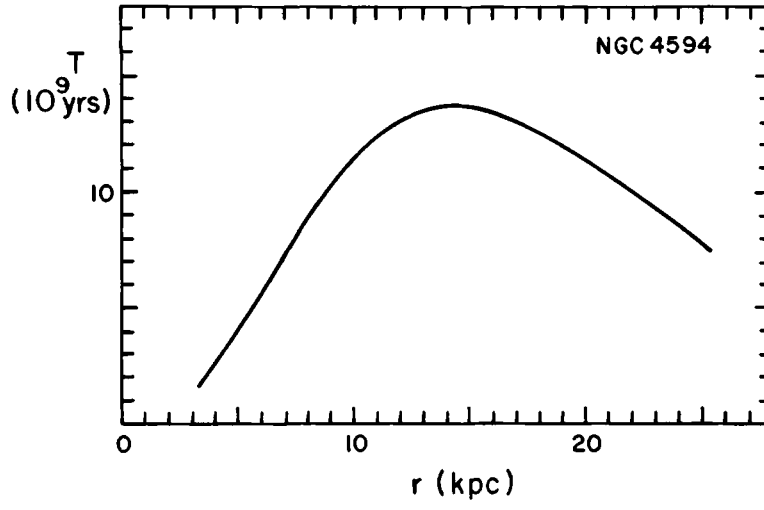

Figure 8: Lifetime of cold gas as a function of radius in the disk of NGC 4594 against removal by angular momentum transfer with bulge stars.

6 Conclusions

From aperture synthesis observations of HI in the luminous Sa galaxy NGC 4594, we have shown that:

(1) The HI lies in an annulus between 12 and 19 kpc from the center of the galaxy, with the density at radii within 12 kpc at least a factor of ten lower than in the annulus. The radial extent of HI is coextensive with that of the dust found by van Houten (1961).

(2) At the radii where HI is detected, the rotation curve is flat at 370 ± 10 km s^{-1}. The mass of the galaxy within 19 kpc is 6.0 10^{11} $M_\odot$ and the correspondig mass-to-light ratio is 5.3 $M_\odot/L_\odot$. There is no bulk radial motion of the gas greater than about 15 km s^{-1}. Comparison of the velocity fields measured by stellar absorption lines and by HI suggests that the former are contaminated by light from the more slowly-rotating spheroid.

(3) The interstellar matter in NGC 4594 resembles in its properties that in the solar neighbourhood, while star formation as revealed by the presence of HII regions, is confined to the HI annulus. The relative HI content, $[M_H/L_B]$, is lower by a factor of order ten than values found for other Sa galaxies, and is lower than the fractional HI content of detected ellipticals. It is likely that this is due to gas having been removed from most of the disk by interaction with the large spheroid of the galaxy.

Acknowledgements

We are grateful to Dr. R. Sancisi for his enthusiastic and valuable help and advice, to Drs J.E. Gunn, U.J. Schwarz and W. van Driel for many valuable discussions, to Dr. V. Icke for suggestions based on a critical reading of the manuscript and to an anonymous referee for several useful comments. The initial data reduction was carried out using the Groningen Image Processing System (GIPSY). G.R.K. acknowledges financial support from the Netherlands Organisation for the Advancement of Pure Research (ZWO) for research at the Kapteyn Laboratory of the University of Groningen and is grateful to Dr. H. van Woerden and other members of the staff for their hospitality. Support was also provided through NSF grants AST-80009252 and AST-8213292 to Princeton University. E.B. acknowledges fellowship support provided by the Consejo Nacional de Investigaciones Científicas y Técnicas of Argentina and the Netherlands Foundation for Radio Astronomy (SRZM). S.M.F. acknowledges financial support from ZWO, from the Leiden Kerkhoven-Bosscha Fund and from NSF grant AST-8211551 to the University of California. The Westerbork Synthesis Radio Telescope is operated by SRZM with financial support from ZWO.

References

Bajaja, E., Shane, W.W.: 1981, Bol. Asoc. Argentina Astron., No.26, p. 123

Bos, A., Raimond, E., van Someren Greve, H.W.: 1981, Astron. Astrophys. 98, 251

Bosma, A.: 1978, The Distribution and Kinematics of Neutral Hydrogen in Spiral Galaxies of Various Morphological Types, Dissertation, University of Groningen

Bottinelli, L., Gouguenheim, L., Paturel, G.: 1980, Astron. Astrophys. 88, 32

de Bruyn, A.G.: 1978, in Structure and Properties of Nearby Galaxies, IAU Symp. No. 77, eds E.M. Berkhuijsen and R. Wielebinski, Reidel, Dordrecht, p. 205

de Bruyn, A.G., Crane, P.C., Price, R.M., Carlson, J.B.: 1976, Astron. Astrophys. 46, 243

Burkhead, M.S.: 1979, in Photometry, Kinematics an Dynamics of Galaxies, ed. D.S. Evans, University of Texas, Austin, p. 143

Faber, S.M., Gallagher, J.S.: 1976, Astrophys. J. 204, 365

Faber, S.M., Gallagher, J.S.: 1979, Ann. Rev. Astron. Astrophys. 17, 135

Faber, S.M., Balick, B., Gallagher, J.S., Knapp, G.R.: 1977, Astrophys. J. 214, 383 (FBGK)

Gallouët, L., Heidmann, N., Dampierre, F.: 1975, Astron. Astrophys. Suppl. 19, 1

Gordon, M.A., Burton, W.B.: 1976, Astrophys. J. 208, 346

Gunn, J.E.: 1979, in Active Galactic Nuclei, eds. C. Hazard and S. Mitton, Cambridge University Press, p. 213

Högbom, J.A.: 1974, Astron. Astrophys. Suppl. 15, 417

van Houten, C.J.: 1961, Bull. Astron. Inst. Netherland 16, 1

Knapp, G.R.: 1983, in Internal Kinematics and Dynamics of Galaxies, IAU Symp. No. 100, ed. E. Athanassoula, Reidel, Dordrecht, p. 297

Knapp, G.R., Kerr, F.J., Henderson, A.P.,: 1979, Astrophys. J. 234, 448

Kormendy, J., Illingworth, G.: Astrophys. J. 256, 460

van der Kruit, P.C., Searle, L.: 1982, Astron. Astrophys. 110, 79

Rubin, V.C., Ford, W.K., Thonnard, N.: 1980a, Astrophys. J. 238, 471

Rubin, V.C., Burnstein, D., Thonnard, N.: 1980b, Astrophys. J. Letters 242, L149

Sancisi, R., Allen, R.J.: 1979, Astron. Astrophys. 74, 73

Schweizer, F.: 1978, Astrophys. J. 220, 98

Shaffer, D.B., Marscher, A.P.: 1979, Astrophys. J. Letters 233, L105

Stark, A.A.: 1984, IAU Symp. No. 106, ed. H. van Woerden (in press)
Williams, T.B.: 1977, Astrophys. J. 214, 685

Summary

The mass distribution in the stellar disk of the early-type, highly inclined galaxy NGC 4594 is inferred by interpreting the observed ring-like distribution of HI as tightly wound spiral arms. Starting with the dispersion relation for tightly wound spirals and using published surface photometry, we show that the local surface density in the stellar disk at a galactocentric distance r = 15 kpc is about 40 to 50 $M_\odot pc^{-2}$ (for Toomre's stability factor Q = 2). Assuming that M/L_B is constant we derive a disk mass (for r < 20 kpc) of $1.14\ 10^{11}\ M_\odot$ and an upper limit of 10 for $[M/L_B]$ in the disk (for $H_0 = 50$ km s^{-1} Mpc^{-1}). Subtracting the contribution of the stellar disk from the observed rotation curve of the HI, we derive the distribution of mass in the spheroid. It is shown that, in the range of radii where the HI is observed, $[M/L_B]$ for the spheroid increases only slightly with radius from about 5 at r = 10 kpc to about 6 at r = 20 kpc. Of the total mass out to a galactocentric distance of 20 kpc, at least 20% resides is the disk. It is concluded that the stellar disk of this early type spiral resembles in most of its properties those of later type galaxies.

1 Introduction

Recent 21-cm line observations of NGC 4594 made by Bajaja et al. (1984, hereafter Paper I) with the Westerbork Synthesis Radio Telescope (WSRT) have shown that the large-scale distribution of neutral hydrogen in the disk of this galaxy can be represented by two partially overlapping rings of gas. The radial extent of the observed HI appeared to agree well with the distribution of dust in the disk of the galaxy. It was noted that the two overlapping annuli may in fact be sections of tightly wound spiral arms in the well-developed stellar disk. The presence of spiral arms in the disk of this galaxy, classified as Sa to Sb, was already noted by Lindblad (1951) who published a photograph in ultraviolet light, taken by Baade. From this photograph Lindblad tried to reconstruct the spiral structure of this galaxy by tracing the "luminous spots" in the disk. The resulting picture, after correction for foreshortening, is that of a very tight leading spiral of which the outer part seems to be associated with the band of obscuring matter. Although the way in which Lindblad connected the spiral arm indicators is certainly controversial, the presence of the arms and their locations, where seen tangentially, seem well established. In the Hubble Atlas of Galaxies (Sandage, 1961) the spiral pattern of NGC 4594 is compared with the nearly circular arms observed in the more face-on Sb galaxy NGC 488. Because the gas in the disk of NGC 4594 shows only small random motions (Paper I), its response to a gravitational disturbance associated with a density wave will be strong. If the observed HI in the disk of NGC 4594 outlines spiral arms, then, through application of the density wave theory for tightly wound spirals, an estimate of the local surface density in the disk can be made.

In section 2 we describe the spiral pattern inferred from the model presented in Paper I. Based on the linear density wave theory of Lin et al. (1969) we estimate the local surface density and the thickness of the stellar disk (section 3). Using the surface photometry of van Houten (1961) we derive in section 4 the mass distribution and an upper limit to $[M/L_B]$ in the stellar disk. In section 5 the distribution of mass in the spheroid is inferred, and in section 6 we present some conclusions.

The assumed distance to NGC 4594, 18.6 Mpc, is based on a Hubble constant of 50 km s^{-1} Mpc^{-1} and will be used throughout this paper in order to be consistent with Paper I.

2 Determination of the spiral structure in NGC 4594

The model calculations presented in Paper I have shown that the observed distribution of HI in the disk of NGC 4594 can be represented by two partially overlapping annuli of gas, both rotating with the same circular velocity. Due to small asymmetries in the distribution of the gas on the preceding and following side of the galaxy the final model parameters on the two sides were slightly different, but, as argued in Paper I, this asymmetry is smaller than that which we are accustomed to find in spiral galaxies. Therefore, for the purpose of fitting a spiral pattern to the model data, the two sides were averaged. The central radii of the two rings which constitute the symmetrized model are 13.6 and 17.3 kpc.

The apparent double ring structure of the HI can be interpreted as a two-armed spiral pattern (m = 2) as follows. Assume that the apparent radii of the inner and outer rings correspond to the galactocentric distances at which the lines of sight tangent to the (almost circular) arms pass closest to the center. Then, if the arms wind outward with increasing phase angle, the radial wave number k and the pitch angle i of a pattern which takes the form of a logarithmic spiral can be calculated from the spacing λ between the rings. For λ = 3.7 kpc and r = 15 kpc we find k = 1.7 kpc^{-1} and i = 4°.4. (The same values for λ and k follow for any even number of arms). This small value of i is slightly less than the minimum pitch angle of 6°.1, given by Schlosser and Musculus (1984) for galaxies of morphological type Sa to Sb and it reflects the high rotational velocity (see Paper I). It makes NGC 4594 one of the most tightly wound spiral galaxies known and confirms the remark in the Hubble Atlas that its spiral pattern is almost circular. Note that this value of i combined with the maximum rotation velocity of 370 km s^{-1} (see Paper I) is consistent with the fairly strong correlation between these quantities noted by Kennicutt (1981) from a sample of 113 spiral galaxies. In Figure 1 the symmetrized annular model and the two-armed spiral pattern fitted to this model are shown. The spacing at r = 15 kpc agrees with Lindblads tracings of the outer spiral branches associated with the band of obscuring matter.

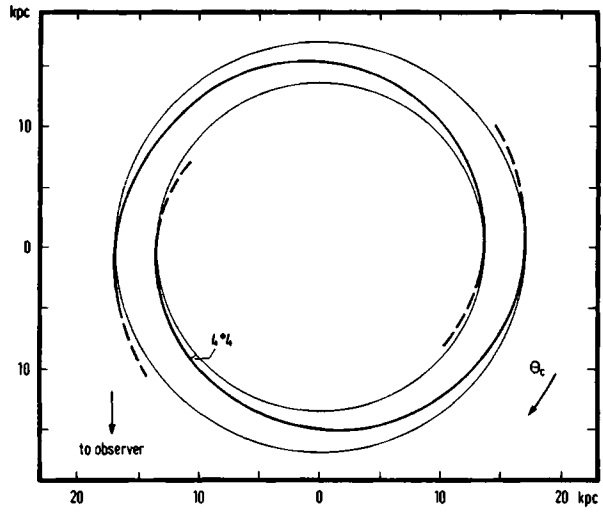

Figure 1: Face-on view of the two-armed spiral pattern in NGC 4594 with a pitch angle of 4°4, fitted to the symmetrized model of the HI distribution described in Paper I. The circles (with radii 13.6 and 17.3 kpc) represent the ring model as discussed in Paper I.

3 The local surface density in the disk

3.1 Discussion of the method

In Paper I and in the preceding section we have established values for the rotational velocity Θ_c and for the radial wave number k for radii around 15 kpc. We will now employ the linear density wave theory for tightly wound spirals (Lin and Shu, 1964; Lin, 1966; Lin et al., 1969) to estimate, from these and other data (see below), the local surface density σ_{tot} in the disk. This theory is valid when the disk is self-gravitating and thus not stabilized by a massive spheroid. The presence of spiral arms indicates in itself that the disk of NGC 4594 is not stabilized by the spheroid and thus, in a first approximation, may be considered as self-gravitating. This is confirmed by the photometry of the disk (described in section 4.2) which indicates that, for any plausible mass-to-light ratio for the disk population, the volume density in the disk greatly exceeds that expected from matter associated with the spheroid alone.

The dispersion relation for tightly wound spirals (see equations 2 and 4) can be expressed in simplified form as:

$$\sigma_{tot} = \frac{\varkappa^2}{\pi G k \chi}, \qquad (1)$$

where $\varkappa$ is the local epicyclic frequency, G the gravitational constant and χ a dimensionless parameter of order one which depends upon the radial velocity dispersion[1] of the stars $\langle v_R^2 \rangle^{1/2}$, the thickness of the stellar disk z_0 and the pattern speed Ω_p. In sub-section 3.2 we will determine the range of χ values for the admissible range of values of these three quantities. In addition to the dispersion relation we will use the Camm (1950) relation between the perpendicular velocity dispersion $\langle v_z^2 \rangle^{1/2}$ in a self-gravitating locally isothermal stellar sheet and the disk thickness z_0 (equation 5).

If, for a spiral galaxy, the rotation curve and the radial wave number are known, then four undetermined variables remain, z_0, σ_{tot}, Ω_p and $\langle v_R^2 \rangle^{1/2}$ (or $\langle v_z^2 \rangle^{1/2}$ assuming a constant ratio for $\langle v_z^2 \rangle^{1/2} / \langle v_R^2 \rangle^{1/2}$, see equation 6). For NGC 4594, for which no further information is available, we will proceed by expressing simultaneous solutions of both equations in the (σ_{tot}, z_0)-plane. Using the constraints on Ω_p set by the rotation curve data and the extent of the spiral pattern and adopting acceptable values for the perpendicular velocity dispersion, we can restrict the range of solutions in the (σ_{tot}, z_0)-plane. If we also include the relation which defines the critical radial velocity dispersion required for stability (equation 7) and adopt a value for Toomre's stability factor Q, we can further restrict the range of solutions for σ_{tot} and z_0 and thus we arrive at our final estimate of the local surface density at r = 15 kpc.

This method of estimating σ_{tot} is based upon the procedure outlined by Shu et al. (1971) and used to calculate the expected radial wave numbers in M33, M51 and M81 from mass models constructed from the observed rotation curves (see also Roberts et al., 1975, and Visser, 1980a, b). However, we have reversed the procedure and now calculate σ_{tot} from the observed rotation curve and spiral pattern. Using published surface photometry we then derive a mass model for the disk, assuming M/L_B to be constant. We subtract the contribution of this disk model from the observed rotation curve in order to determine the distribution of mass in the spheroid (see section 5). For those spirals for which the pattern speed Ω_p can be determined (e.g. Roberts et al., 1975) and the radial velocity dispersion can be measured (e.g. van der Kruit and Freeman, 1986; Kormendy, 1984) the three basic equations described above can be solved. This offers, for instance,

---

[1] By "radial velocity dispersion" here and elsewhere in this paper we mean velocity dispersion along the galaxian radius rather than along the line of sight.

the possibility of calculating Q without having to assume, as has previously been done by Kormendy (1984) and van der Kruit and Freeman (1986), a value for M/L_B for the disk. Finally, the resulting value of σ_{tot} allows one to determine the contribution of a (possibly dark) spheroid to the observed rotation curve without adopting a value for the total mass in the disk (or, equivalently, a value for M/L_B for the disk; Sancisi and van Albada, 1985).

3.2 Application of the method

The local surface density σ_{tot} in the stellar disk of NGC 4594 can be calculated from the dispersion relation for tightly wound spirals, which relates the dimensionless frequency ν to the radial wave number k. The general form of this relation, accounting for the presence of gas and the finite thickness of the stellar and gaseous disks, is (Lin ,1970):

$$\frac{k_T}{k}(1-\nu^2) = \frac{\sigma_*}{\sigma_{tot}} F_* T_* + \frac{\sigma_g}{\sigma_{tot}} F_g T_g . \qquad (2)$$

Here σ_* and σ_g are the surface densities of the stellar and the gaseous components of the disk, respectively, k_T is the Toomre wave number, defined as

$$k_T = \frac{\varkappa^2}{2\pi G\, \sigma_{tot}}, \qquad (3)$$

and ν is the frequency (expressed in units of $\varkappa$) with which a star or gas cloud encounters the periodic gravitational perturbation associated with the density wave. F_* and F_g are reduction factors associated with the radial velocity dispersions of the stars and the gas respectively (Lin, 1970), and T_* and T_g are reduction factors for the finite thicknesses of the stellar and gaseous disks (Vandervoort, 1970; Lin, 1970).

In Paper I it was shown that the radial velocity dispersion of the gas in the disk of NGC 4594 is smaller than about 15 km s^{-1}. Because of the smallness of these random motions, the gas reacts strongly to a gravitational potential disturbance and can be used as a tracer of the density wave. On the other hand, the gas content is low (see Paper I) so that the total surface density in the disk (σ_{tot}) is determined almost entirely by the stars. Therefore, the second term on the right hand side of equation (2) may be neglected and σ_{tot} can be expressed as :

$$\sigma_{tot} \approx \Theta_c^2 \frac{(1-\nu^2)}{\pi G k r^2 F_* T_*}, \qquad (4)$$

where the epicyclic frequency $\varkappa$ for a flat rotation curve is approximated by $\varkappa = \sqrt{2}\Theta_c/r$

with the rotation velocity Θ_c = 370 km s^{-1} (Paper I; Rubin et al., 1985). It is shown by Lin et al. (1969) that, once k and $\varkappa$ are fixed, $F_\bullet$ is a function of ν and the velocity dispersion $\langle v_R^2 \rangle^{1/2}$, while $T_\bullet$ depends only upon the thickness of the disk. The surface density σ_{tot} can therefore be expressed in terms of the three parameters, ν (or the pattern speed Ω_p), the velocity dispersion $\langle v_R^2 \rangle^{1/2}$ and the thickness of the stellar disk, hereafter expressed as z_0, the scale-height of a self-gravitating locally isothermal stellar disk with a perpendicular density distribution $\varrho(z) = \varrho_0 \mathrm{sech}^2(z/z_0)$. For a flat rotation curve it can be shown that α, the ratio of the perpendicular to the radial velocity dispersion, is 0.6 (see Visser, 1980a,b, quoting relations suggested by Kuzmin, 1961, Wielen, 1977 and Lindblad, 1959; see also Shu et al., 1971). If we combine this value of α with the Camm (1950) relation for the perpendicular velocity dispersion:

$$\langle v_z^2 \rangle = \pi G \sigma_{tot} z_0, \tag{5}$$

then the radial velocity dispersion can be written as a function of z_0 and σ_{tot}:

$$\langle v_R^2 \rangle = \frac{\pi G}{\alpha^2} \sigma_{tot} z_0. \tag{6}$$

Using equation (6) we can calculate solutions of the dispersion relation in the (σ_{tot}, z_0)-plane for each $|\nu|$ between 0 (corotation) and 1 (the Lindblad resonances). In Figure 2 we show solutions of the dispersion relation for various values of $|\nu|$ as relations between the local surface density σ_{tot} (at r = 15 kpc) and the scale height z_0 (solid curves); curves of constant velocity dispersion (which are seen from equation (6) to be hyperbolae) are represented by broken curves in this figure. It appears that for $|\nu|$ less than about 0.70, z_0 must be less than about 325 pc. For values of $|\nu|$ greater than 0.70 there is a rapid increase in the maximum permitted z_0. In the neighbourhood of the Lindblad resonances, $|\nu| = 1$, the solutions of the dispersion relation become unreliable.

Once the location of the corotation radius R_c has been determined, the value of ν (at r = 15 kpc) is fixed (provided the rotational velocity $\Theta_c(R_c)$ is known). From the constraints on Ω_p set by the rotation curve data and the radial extent of the spiral pattern it will next be shown that the admissible range of ν-values is restricted to $-0.90 < \nu < +0.31$. It is argued by Roberts et al. (1975) that the location of corotation can be determined from the maximum radial extent of three observable tracers, viz. the prominent spiral structure, the easily visible disk and the distribution of HII regions. Lindblad (1951) showed that the maximum radial extent of the outermost luminous spots agrees with that of the dust. According to the WSRT observations presented in Paper I, the HI, in which the arms were observed, is coextensive with the band of dust and is limited to radii less than about 20 kpc. From photometric observations carried out by van

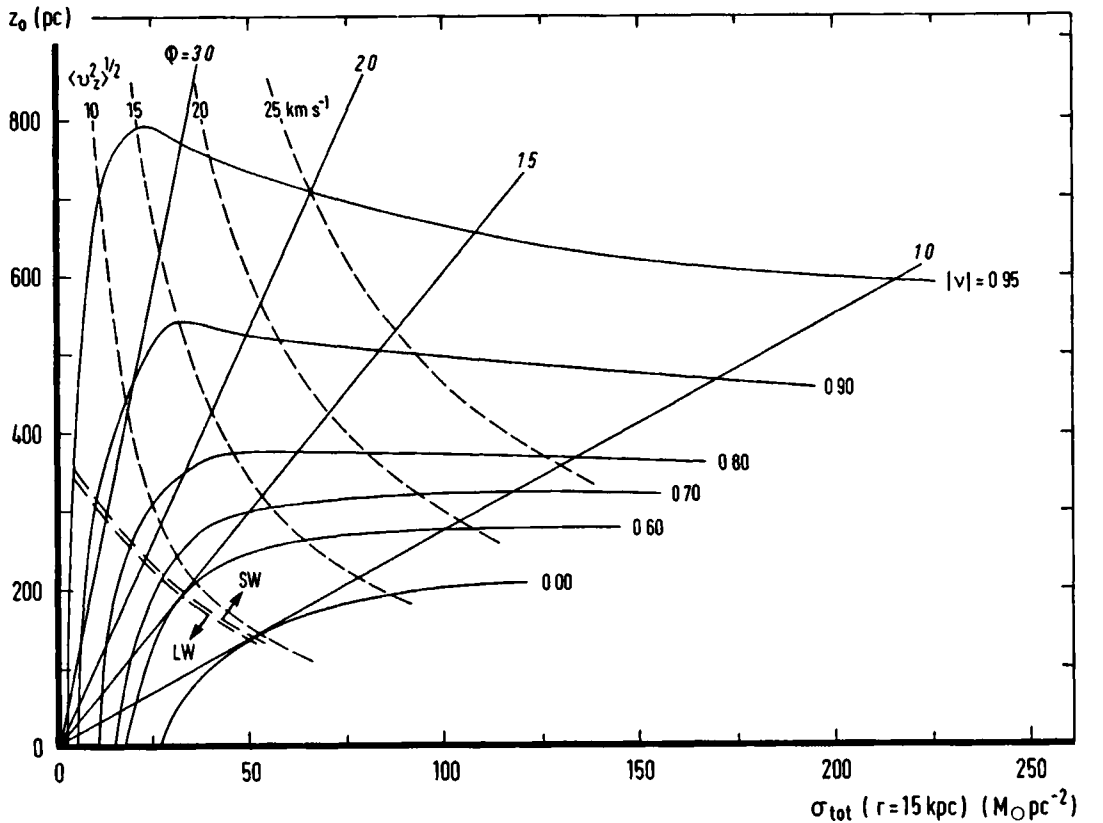

Figure 2: Plot of the assumed thickness z_0 (in pc) of the stellar disk of NGC 4594 versus the local surface density σ_{tot} (in $M_\odot$ pc^{-2}) at a galactocentric distance of 15 kpc The solid curves, for various values of $|\nu|$, represent solutions of the dispersion relation for tightly wound spirals Curves of constant radial and perpendicular velocity dispersion are represented by broken lines Loci of constant Q in this (σ_{tot}, z_0)-plane are straight lines The regions with long wave solutions (LW) and short wave solutions (SW) are indicated The plot is based on a distance of 18 6 Mpc and $\alpha = 0\,6$

Houten (1961) and by Burkhead (1979) it appears that the radius of the bright stellar disk, which has an exponential distribution of the light, is at least 18 kpc. This is slightly greater than the maximum radius of about 15 kpc to which Schweizer (1978) detected NII line emission from HII regions in the plane of the galaxy. If we adopt a minimum corotation radius of about 20 kpc, we obtain $\nu < -0.36$ or $\Omega_p < 18.5$ km s^{-1} kpc^{-1}. However, numerical calculations by Lin and Bertin (1983) and recent WSRT observations of UGC 2885 made by Roelfsema and Allen (1985) have shown that spiral structure may penetrate beyond the corotation radius, extending from the inner to the outer Lindblad resonance. In fact, if we demand only that the outer Lindblad resonance not lie within the observed HI, then we obtain $\nu < +0.31$ and $R_c > 11$ kpc, slightly inside or within the observed HI and the obscuring matter. A lower limit to ν is obtained by requiring that the inner Lindblad resonance be located inside the inner edges of the optical and HI spiral arms. The inner radius of the HI arms lies at about 12 kpc, but in view of the luminous spots traced by Lindblad (1951) to radii well within that of the inner edge of the dust, it seems plausible that the inner Lindblad resonance be located well inward of 12 kpc. Although it is not entirely clear how far inward the spiral structure extends it is certainly still present at galactocentric distance 9 kpc. From the rotation curve data published by Rubin et al. (1985) we then derive $\nu > -0.90$. Thus the extent of the spiral pattern restricts the admissible values of ν to the range -0.90 to +0.31. According to Figure 2 this leaves open a wide range of values for σ_{tot} and z_0.

This range of values can be further restricted if we consider Toomre's stability factor Q. Toomre (1964) showed that rotation and random motions stabilize a disk against axisymmetric (Jeans) instabilities. For a thin disk he showed that the critical radial velocity dispersion $\langle v_R^2 \rangle_{crit}^{1/2}$ required for stability is given by:

$$\langle v_R^2 \rangle_{crit}^{1/2} = \frac{cG}{\varkappa} \sigma_{tot} \ , \qquad (7)$$

so that Q, defined as the ratio of the actual to the critical radial velocity dispersion, should exceed one. The factor c depends upon the value of the parameter α. For an infinitely thin disk, for which $\alpha = 0$, c takes the value 3.36 (Toomre, 1964). For finite thickness, c must be reduced (Toomre, 1974). According to Kormendy (1984), c takes the value 2.6 for $\alpha = 0.6$, in the absence of gas. From equations (6) and (7) we then derive a relation between σ_{tot} and z_0 with Q as a free parameter:

$$z_0 = \frac{(\alpha c Q)^2 G}{\varkappa^2 \pi} \sigma_{tot} , \qquad (8)$$

i.e. each value of Q specifies a straight line in the (σ_{tot}, z_0)-plane. In Figure 2 solutions of

equation (8) are shown for values of Q between one and three.

Recently Illingworth and Kormendy (quoted by van der Kruit and Freeman, 1986) measured the velocity dispersion in the disk of the Sb galaxy NGC 488 which, according to the Hubble Atlas, bears a close resemblance to NGC 4594 (see section 1). Based on an $[M/L_B]$-value of 6 for an old disk population with (B-V) = 0.8, van der Kruit and Freeman (1986) argue that these measurements indicate $Q \approx 2$, in agreement with the modest amount of spiral structure that is observed in NGC 488. If we adopt $Q = 2$ for the disk of NGC 4594 (for which (B-V) is roughly 0.7, Faber et al., 1977) then, according to Figure 2, the upper limits to σ_{tot} and z_0 are about 50 $M_\odot\,pc^{-2}$ and 525 pc respectively (for $\nu = -0.90$). However, it should be emphasized that the value of Q in the disk of NGC 4594 is not measured and that a different value for Q would significantly alter the admissible values of σ_{tot}. For instance, if we had adopted $Q = 3$, as might be plausible in this fairly stable galaxy, the upper limit to σ_{tot} (for $\nu = -0.90$) would be only about 20 $M_\odot\,pc^{-2}$.

A lower limit to σ_{tot} and z_0 might be obtained if we reject, as usual (see Shu, 1970, and Shu et al., 1971), the long-wave solutions of the dispersion relation, indicated by LW in Figure 2, in which case $|\nu| > 0.75$ (for $Q = 2$), so that with $\nu < +0.31$, there remains only $\nu < -0.75$. Moreover, it will be argued in section 4.1 that in order to arrive at acceptable values for the perpendicular velocity dispersion, $\langle v_z^2 \rangle^{1/2} > 15$ km s^{-1}, ν must be smaller than about -0.85, so that the long-wave solution is eliminated on this account as well. Therefore, the final range of possible ν-values is limited to $-0.90 < \nu < -0.85$, leading to a corotation radius $R_c > 37$ kpc (assuming Θ_c constant), which is well beyond the observable spiral tracers, and a radius for the inner Lindblad resonance between 8 and 9 kpc. In summary, the lower limit to the final range of ν is set by locating the inner Lindblad resonance at $r < 9$ kpc, while the upper limit is fixed by the constraints to the perpendicular velocity dispersion. The corresponding range for the pattern speed is $9.0 < \Omega_p < 10.0$ km s^{-1} kpc^{-1}.

One of the main uncertainties in the derived values of σ_{tot} and z_0 arises from the assumed distance to NGC 4594. According to de Vaucouleurs and de Vaucouleurs (1973), NGC 4594 is a member of a sub-cloud of galaxies in the Virgo II cluster. Its position is at the outer edge of sub-cloud Y, opposite the center of the Virgo I cluster. De Vaucouleurs and de Vaucouleurs conclude, however, that this sub-cloud is probably not a physical member of a single cluster and that the approximate equality of the mean velocity of galaxies in this sub-cloud and in Virgo I is accidental. The angular distance of NGC 4594 from the center of Virgo I is less than 25°, so that the correction for the velocity field of the Local Super Cluster, as suggested by Aaronson et al. (1982), does not apply. Therefore, our assumed distance of D = 18.6 Mpc is based on the systemic velocity of NGC 4594 corrected for solar motion in the Local Group, assuming $H_0 =$

50 km s^{-1} Mpc^{-1} (Schweizer, 1978) Using the mean velocity of the (X,Y) sub-cloud in Virgo II (V_0 = 1434 km s^{-1}, de Vaucouleurs and de Vaucouleurs, 1973) yields D = 28 7 Mpc assuming H_0 = 50 km s^{-1} Mpc^{-1}, or 19 1 Mpc assuming H_0 = 75 km s^{-1} Mpc^{-1} In view of these uncertainties, and in order to be consistent with previous papers, we continue to use D = 18 6 Mpc throughout this paper The curves of constant radial and perpendicular velocity dispersion in Figure 2 are independent of D, in contrast to the solutions of equation (4) and (8) The effect of decreasing D is to reduce the slope of lines of constant Q while the solutions of the dispersion relation level off at lower values of z_0 The net result is to shift the range of possible z_0 and σ_{tot} to lower and higher values respectively For instance, for H_0 = 75 km s^{-1} Mpc^{-1} (D = 12 4 Mpc) and $\nu > -0\,90$ the maximum values of z_0 and σ_{tot} are 350 pc and 70 $M_\odot$ pc^{-2} respectively

4 Properties of the stellar disk of NGC 4594

4 1 The thickness of the stellar disk

It was shown in the previous section that $\nu > -0\,90$ leads to an upper limit to z_0 of about 525 pc (for Q = 2 and D = 18 6 Mpc) The lower limit of z_0 which would result from the constraint $\nu < -0\,75$, is 250 pc but at the end of this section a higher limit will be suggested Note that z_0 is calculated at a galactocentric distance of about three disk scale lengths (see sub-section 4 2) and that its upper limit is almost independent of the value of Q as long as Q is less than about 2 5 (see Figure 2) The z_0 values given by van der Kruit and Searle (1982a,b), largely for later type galaxies, are about a factor two larger than the presently calculated z_0 range for NGC 4594, if we account for the different values of H_0 This might be the result of an intrinsic difference between the thicknesses of stellar disks in early and late type galaxies However, the only Sab galaxy in their sample (NGC 7814, a bulge dominated galaxy) has a z_0 of about 1 kpc (H_0 = 75 km s^{-1} Mpc^{-1}) But the apparent difference may also be due to the quite different methods used to arrive at the values of z_0 and reflect the difference in the perpendicular distribution of the stellar populations used for the two determinations The scale heights reported by van der Kruit and Searle are based upon a fit of the perpendicular distribution of the light at high values of z, and are thus measures of the thickness of the old stellar population, reaching large distances from the plane The dispersion relation, however, which forms the basis of the present calculation, is more sensitive to the distribution of mass close to the equatorial plane of the galaxy Note in this regard the agreement of the range of z_0 values in NGC

4594 with the characteristic perpendicular dimensions of the intermediate and old stellar populations in the solar neighbourhood of the galactic disk (see Blaauw, 1965).

Van der Kruit and Freeman (1984,1986) have measured the perpendicular velocity dispersion $\langle v_z^2 \rangle^{1/2}$ in three Sc galaxies, viz. NGC 628, NGC 1566 and NGC 5247. Their observations of NGC 628 and NGC 1566 pertain to only a single radial scale length from the center. In the face-on spiral NGC 5247 they measured an exponential decrease of the perpendicular velocity dispersion as a function of galactocentric distance. At the maximum observed distance of about two disk scale lengths the value of $\langle v_z^2 \rangle^{1/2}$ is found to be about 22 km s^{-1}. The values for the perpendicular velocity dispersion in several other spiral galaxies (including the Milky Way, NGC 891, NGC 4565 and NGC 5907) have been predicted by Bahcall and Casertano (1984). These predictions are based on mass models of these four galaxies in which the disk is not described by an isothermal, self-gravitating component. They show that at a galactocentric distance of about three scale lengths the expected perpendicular velocity dispersion for the old disk population in these galaxies lies in the interval 15 to 20 km s^{-1} which, according to van der Kruit and Freeman (1986), is only 4% lower than the values calculated directly from equation (5). Because of the lack of observations of $\langle v_z^2 \rangle^{1/2}$ in early type disk galaxies we will adopt the range 15 to 20 km s^{-1} for the perpendicular velocity dispersion at about three radial scale lengths in the disk of NGC 4594. According to Figure 2 this leads to $415 < z_0 < 585$ pc for $Q = 2$. However, Bahcall and Casertano (1984) showed that the effect of an extra gravitational field due to the presence of a halo would be to decrease z_0. As already stated in sub-section 3.2, the requirement $\langle v_z^2 \rangle^{1/2} > 15$ km s^{-1} leads to $\nu < -0.85$ (see Figure 2). The upper limit of z_0 which would result from $\langle v_z^2 \rangle^{1/2} < 20$ km s^{-1} is slightly greater than the corresponding limit of 525 pc imposed by the constraint $\nu > -0.90$. Therefore, the final range of z_0 is $415 < z_0 < 525$ pc.

4.2 The mass and light distribution in the disk

In the previous sub-section it was shown that, under certain assumptions, the range of admissible z_0 values is restricted to about 415 to 525 pc. According to Figure 2 we then arrive at values for the total column density σ_{tot} in the disk of NGC 4594 of about 40 to 50 $M_\odot\,pc^{-2}$ at r = 15 kpc. (Henceforth we will write $\sigma_{tot} = 45 \pm 5\ M_\odot\,pc^{-2}$ and a similar form will be used for quantities inferred from σ_{tot}). These values for σ_{tot} are slightly lower than the dynamical surface density of $80 \pm 20\ M_\odot\,pc^{-2}$ quoted by van der Kruit and Freeman (1986) for the surface density in the solar neighbourhood. Using the surface photometry of van Houten (1961), we are now able to construct a crude mass model of the disk of

NGC 4594. Van Houten resolved the light distribution along the major axis into components due to the spheroid and to the disk. The latter shows an approximately exponential decrease in intensity out to at least 200″ (18 kpc), with a central hole at $r < 40''$ (3.6 kpc). The scale length h of the disk is about 4.8 kpc, as confirmed by Burkhead (1979). Assuming that the disk mass is distributed in the same way as the disk light (M/L_B is constant), we derive a total disk mass in the annulus between 3.6 and 20 kpc of $M_D = (1.14 \pm 0.13)\ 10^{11}\ M_\odot$ for the stellar disk whose surface density distribution is given by:

$$\sigma_{tot}(r) = (1051 \pm 118)\ e^{(-0.21\,r)}\ M_\odot\,pc^{-2}. \qquad (9)$$

This value of M_D is comparable to the values listed by van der Kruit and Searle (1982a, see their Table III) for galaxies with morphological type Sb or later (accounting for the different values of H_0). In the annulus where the HI is observed ($10 < r < 20$ kpc) the fractional HI mass (M_{HI}/M_D) is about 6%; only 1% of the mass of the disk out to 20 kpc consists of HI.

Once the total luminosity of the disk is known we can calculate its M/L. However, as noted by Faber et al. (1977), the surface brightness of the disk is probably strongly affected by the presence of dust. In order to obtain at least an upper limit to M/L_B we have integrated the uncorrected surface brightness, given by van Houten, out to 20 kpc (assuming a galactic extinction $A_B = 0.21$; see Faber et al., 1977). We find $L_B > 1.13\ 10^{10}\ L_\odot$ (for $3.6 < r < 20$ kpc), leading to $[M/L_B]_{disk} < 10 \pm 1$. This upper limit is in agreement with the mean value of 4 for stellar disks suggested by van der Kruit and Freeman (1986) for a sample of five spiral galaxies, adjusting H_0 to 50 km s^{-1} Mpc^{-1}.

5 Properties of the spheroid of NGC 4594

Using the rotation curve of the HI in the disk of NGC 4594 (Paper I) and the surface photometry of van Houten (1961), we can now construct a mass model for the spheroid and calculate its M/L_B in the range $10 < r < 20$ kpc. The distribution of mass in the spheroid can be inferred from the observed rotation curve if we subtract the contribution of the exponential disk (following Freeman, 1970). In order to exclude the central hole (see sub-section 4.2) we fit the disk with a surface mass distribution specified by:

$$\sigma_{tot}(r) = \sigma_0\,[e^{-r/h_1} - e^{-r/h_2}], \qquad (10)$$

where the surface density scale factor $\sigma_0 = 1051 \pm 118\ M_\odot\,pc^{-2}$. A similar form has been

used by Ostriker and Caldwell (1978) for the surface density distribution of the galactic disk. The first term between brackets on the right hand side represents the exponential light distribution outside $r = 3.6$ kpc by a disk with scale length $h_1 = 4.8$ kpc. The scale length $h_2 = 1.99$ kpc in the second term is chosen so as to subtract a luminosity equal to that contributed by the first term in the region $r < 3.6$ kpc. The rotation curve calculated for the disk specified by equation (10), is almost flat at about 200 km s^{-1} for r between 10 and 15 kpc; outside 15 kpc it starts to decline to about 180 km s^{-1} at $r = 20$ kpc. These calculated velocities are consistently less than the observed rotational velocities at the corresponding radii, so that the disk described by equation (10) is less massive than the "dominating disk" as discussed by Sancisi et al. (1985). The mass distribution of the additional spheroid required to reproduce the observed rotation curve corresponds to a rotational velocity of 310 to 320 km s^{-1} between 10 and 20 kpc.

The mass density for a spheroid with a flat rotation curve is proportional to r^{-2} where r is the galactocentric distance in kpc along the major axis (see Schmidt, 1965; see also van der Kruit and Searle, 1982b, in their discussion of NGC 7814). For NGC 4594 we find (applying the sign convention introduced in section 4.2):

$$\varrho_m(r) = (2.54 \mp 0.08)\, r^{-2}\ M_\odot\, pc^{-3}\,. \qquad (11)$$

Here it is assumed that the axial ratio of the spheroids of equal density is 0.63, as determined by van Houten (1961) from the photometry. Combining equation (11) with the spatial distribution of light in the spheroid specified by van Houten:

$$\varrho_l(r) = 0.81\, r^{-2.19}\ L_\odot\, pc^{-3}\,, \qquad (12)$$

we conclude that the local M/L_B is only weakly dependent on r: $[M/L_B]$ varies from 4.8 ∓ 0.2 at $r = 10$ kpc to 5.6 ∓ 0.2 at $r = 20$ kpc, in agreement with Faber et al. (1977), who noted that "no discernible increase in M/L is measured over the easily visible halo". Note that according to the (preliminary) analysis of Burkhead's (1979) surface photometry, $\varrho_l(r)$ decreases as $r^{-2.78}$ for $r > 18$ kpc. This would result in a slightly steeper increase of M/L_B than that indicated by the photometry of van Houten at these radii. The total mass within a spheroid with a major axis of 20 kpc and an axial ratio b/a = 0.63, is $M_{sph} = (4.02 \mp 0.12)\ 10^{11}\ M_\odot$.

6 Discussion

In the previous section we derived some properties of the disk and the spheroid of NGC 4594 by assuming that the observed rings of HI are in fact sections of tightly wound spiral arms. Starting with the dispersion relation and using the surface photometry of van Houten (1961) we derived the mass distribution in the disk and, within a limited range of radii, in the spheroid

In Table 1 the final range of values for the relevant properties of the disk as derived from Figure 2, assuming Q = 2, are summarized.

Table 1. Inferred properties of the stellar disk of NGC 4594

Final range of values
frequency ν -0 90 to -0.85
pattern speed Ω_p 9 0 to 10 0 km s^{-1} kpc^{-1}
corotation radius R_c 37.0 to 41.4 kpc
location inner Lindblad resonance. 8 to 9 kpc
surface density σ_{tot} (r = 15 kpc) 40 to 50 $M_\odot pc^{-2}$
thickness z_0 415 to 525 pc
disk mass M_D (3 6 < r < 20 kpc). (1 14 ± 0 13) 10^{11} $M_\odot$
$[M/L_B]$: < 10

Note Values are based on D = 18.6 Mpc, α = 0 6 and Q = 2

The fraction of mass in the disk appears to be about 20 to 25% of the total mass within 20 kpc of the center. This value of M_D/M_{tot} is slightly smaller than the values listed by van der Kruit and Searle (1982a, see their Table 3) largely for later type galaxies with no appreciable visible bulge In the only bulge dominated galaxy in their sample, NGC 7814 (classified Sab), they find that about 2% of the total mass resides in the disk. Thus we may conclude that in this respect the situation in the early type disk galaxy NGC 4594 resembles that in later type disk galaxies which lack a prominent, visible halo. (Note that the ratio M_D/M_{tot} is independent of the assumed distance). Moreover, the ratio R_e/h (with $R_e \approx 20$ kpc the extreme radius of the disk and h the scale length) is about 4, which agrees with the values found in later type galaxies. At a galactocentric radius of 15 kpc the density of the disk in the equatorial plane is about 0.047 ± 0 005 $M_\odot pc^{-3}$ (assuming z_0 = 475 pc). This exceeds the density of the spheroid at a corresponding distance along

the major axis by about a factor of 5. It is in agreement with the assumption that the disk, in a first approximation, may be considered as self-gravitating, as equation (5) in section 3.2 demands. (At the outer edge of the disk, $R_e \approx 20$ kpc, this factor is about 2.5).

The effect of the potential of the disk on the structure of the bulge is likely to be considerable if the disk is as massive as it appears. Kormendy and Illingworth (1982) have found a slight excess flattening of the bulge with respect to a model supported exclusively by rotation and isotropic residual velocities, and they attribute this excess to the presence of a disk. This was confirmed by Jarvis and Freeman (1985) who constructed dynamical models of the bulge of NGC 4594 in the presence of a fairly prominent disk. Assuming M/L to be constant, $M_D/M_{sph} = 0.25$ and $z_0/h = 0.1$, they were able to fit accurately the observed two-dimensional surface brightness distribution in the bulge. However, they note that the values of M_D/M_{sph} and z_0/h have only a second order effect on the quality of the fit which is mainly determined by the central bulge potential and the amount of bulge rotation. Nevertheless, their assumptions as listed above are confirmed by the present calculations which show that a considerable fraction of the mass resides in the disk ($M_D/M_{sph} = 0.24$ to 0.33), that $z_0/h \approx 0.1$, and that M/L_B is almost independent of r over the range of radii where the HI is observed. The presence of a massive disk may also explain the relatively large value of z at which the increase of the axial ratio b/a of the bulge isophotes sets in (approaching unity only at 600" : Burkhead, 1979) compared with the value z = 70" above which no significant halo rotation is observed (Kormendy and Illingworth, 1982).

As noted in section 4.2, the upper limit of about 10 for $[M/L_B]$ of the disk (assuming that the mass is distributed as the light) is at the upper end of the range of $[M/L_B]$ values published for later type disk galaxies. A rough estimate of the actual $[M/L_B]$ of the stellar disk can be obtained if we assume that the extinction is restricted to a thin central layer. This is not unrealistic because much of the disk light comes from stellar populations with larger scale-heights than that of the dust (see below). Then, if the intrinsic luminosity of the stellar disk of NGC 4594 is twice the observed luminosity, we find $[M/L_B] = 5\ d^{-1}$ for D = 18.6 d Mpc. It is interesting to note that, within the uncertainties, the range of $[M/L_B]$-values for the disk of this early type galaxy resembles the corresponding values for later type disk galaxies.

In Paper I it was noted that the HI mass to blue luminosity ratio, $[M_{HI}/L_B]$, in NGC 4594 (0.010) is very much lower than the average value of 0.092 found by Huchtmeier (1982) for early type spiral galaxies. Omitting the light from the bulge we find for the disk $[M_{HI}/L_B] < 0.13$; in the annulus where the HI is observed the upper limit is 0.28. If we assume as above that in this part of the disk the intrinsic luminosity is twice the observed luminosity then $[M_{HI}/L_B] = 0.14$. Therefore we may conclude that in the annulus where

HI is detected the gas content resembles that in later type spiral galaxies.

That the thickness of the dust layer can actually be small may be inferred from the measurements of Hacke et al. (1982). These authors measured, for a sample of 80 edge-on galaxies, the apparent width of the dust layer on the blue prints of the Palomar Observatory Sky Survey. They show that, accounting for the internal extinction, the measured widths of 500 to 1600 pc are consistent with a characteristic perpendicular dimension of about 150 pc, as is found for the dust layer in the galactic plane. However, the apparent width of the dust layer of NGC 4594 given by Hacke et al. (1982), 725 ± 25 pc (adjusting D to 18.6 Mpc), is also not corrected for projection due to the tilt angle of 5° of the plane of the disk to the line of sight. It appears that the projection of the dust ring alone can almost completely explain the width of the dust layer as reported by Hacke et al. (1982). This suggests that the z-thickness of the dust layer must be very small, consistent with the assumption made above.

As shown by Efstathiou et al. (1982), the halo mass plays an important role in stabilizing stellar disks against global bar-like modes. They show that the parameter $Y = [h/(M_D G)]^{\frac{1}{2}}$ should exceed 1.1 in order to ensure stability. An alternative form of this condition is given by van der Kruit and Freeman (1986) who showed that the criterion may be written :

$$M_{sph}/M_D \geq 0.87 \frac{e\ R_e}{h\ \arcsin\ e} . \qquad (13)$$

For NGC 4594 the right hand side of this equation takes the value 3.1 if the eccentricity e is 0.78 (taking b/a = 0.63) and R_e (the extreme radius of the disk) is 20 kpc. Efstathiou et al. have discussed several problems in applying this criterion to early type galaxies like NGC 4594. Nevertheless, the value $M_{sph}/M_D = 3.6 \mp 0.6$ for NGC 4594 is consistent with this criterion.

In Paper I is was argued that, on the average, the interstellar matter in the disk of NGC 4594 strongly resembles that in later type spiral galaxies. In the present paper it is shown that this conclusion is valid for the large scale mass distribution as well. We conclude that the disk of the early type spiral NGC 4594 resembles that of later type spirals but is embedded in a much more luminous spheroid. The mass of this spheroid is slightly greater than those in most later type spirals (e.g. van der Kruit and Searle, 1982a) while the maximum radius, at least of the disk, is slightly less than average, together accounting for the relatively high rotational velocity and the low pitch angle of the spiral arms. The striking difference in appearance between NGC 4594 and later type spirals is thus due not so much to an exceptionally massive spheroid as to the exceptionally low value of M/L.

Acknowledgements

We would like to thank Drs. F.H. Shu and S.M. Faber for stimulating suggestions which encouraged us to undertake this problem, and we acknowledge valuable discussions with Drs. C.C. Lin and A. Toomre. We are grateful to Dr. P. C. van der Kruit for reading the manuscript carefully and suggesting several important improvements.

References

Aaronson, M., Huchra, J., Mould, J., Schechter, P.L., Tully, R.B.: 1982, Astrophys. J. 258, 64

Bahcall, J.N., Casertano, S.: 1984, Astrophys. J. Letters 284, L35

Bajaja, E., Burg, G. van der, Faber, S.M., Gallagher, J.S., Knapp, G.R., Shane, W.W.: 1984, Astron. Astrophys. 141, 309 (Paper I)

Blaauw, A.: 1965, Galactic Structure, Stars and Stellar Systems Vol. V, eds. A. Blaauw and M. Schmidt, Univ. Chicago Press, p. 435

Burkhead, M.S.: 1979, in Photometry, Kinematics and Dynamics of Galaxies, ed. D.S. Evans, University of Texas, Austin, p.143

Camm, G.L.: 1950, Monthly Notices Roy. Astron. Soc. 110, 305

Efstathiou, G., Lake, G., Negroponte, J.: 1982, Monthly Notices Roy. Astron. Soc. 199, 1069

Faber, S.M., Balick, B., Gallagher, J.S., Knapp, G.R.: 1977, Astrophys. J. 214, 383

Freeman, K.C.: 1970, Astrophys. J. 160, 811

Hacke, G., Schielicke, R., Schmidt, K.H.: 1982, Astron. Nachr. 303, 245

Houten, C.J. van: 1961, Bull. Astron. Inst. Netherland 16, 1

Huchtmeier, W.K.: 1982, Astron. Astrophys. 110, 121

Jarvis, B.J., Freeman, K.C.: 1985, Astrophys. J. 295, 324

Kennicutt, R.C.: 1981, Astron. J. 86, 1847

Kormendy, J., Illingworth, G.: 1982, Astrophys. J. 256, 460

Kormendy, J.: 1984, Astrophys. J. 286, 116

Kuzmin, G.G.: 1961, Publ. Tartu Astron. Obs. 33, 351

Lin, C.C., Shu, F.H.: 1964, Astrophys. J. 140, 646

Lin, C.C.: 1966, SIAM J. Appl. Math. 14, 876

Lin, C.C.: 1967, Ann. Rev. Astron. Astrophys. 5, 453

Lin, C.C., Yuan, C., Shu, F.H.: 1969, Astrophys. J. 155, 721

Lin, C.C.: 1970, in Galactic Astronomy, Vol. 2, ed. H.Y. Chiu and A. Muriel, p.1

Lin, C.C., Bertin, G.: 1981, in Proceedings of an International School and Workshop on Plasma Astrophysics at Varenna, Italy, ed. Guyenne and Levy (ESA SP-161)

Lindblad, B.: 1951, Publ. Astron. Soc. Pacific 63, 133

Lindblad, B.: 1959, Handbuch der Physik 53, 21

Ostriker, J.P., Caldwell, J.A.R.: 1978, in The large-scale Characteristics of the Galaxy, ed. W.B. Burton, I.A.U. Symp. No. 84, p.441

Roberts, W.W., Roberts, M.S., Shu, F.H.: 1975, Astrophys. J. 196, 381

Roelfsema, P.R., Allen, R.J.: 1985, Astron. Astrophys. 146, 213

Rubin, V.C., Burstein, D., Ford Jr., W.K., Thonnard, N.: 1985, Astrophys. J. 289, 81

Sancisi, R., van Albada, T.S.: 1985, to be published in IAU Symposium No. 117, "Dark Matter in the Universe", Princeton

Sandage, A.: 1961, The Hubble Atlas of Galaxies, Carnegie Institution of Washington, Publication 618

Schlosser, W., Musculus, D.: 1984, Astron. Astrophys 131, 367

Schmidt, M.: 1965, Galactic Structure, Stars and Stellar Systems Vol. V, eds. A. Blaauw and M. Schmidt, Univ. Chicago Press, p. 513

Schweizer, F.: 1978, Astrophys. J. 220, 98

Shu, F.H.,: 1970, Astrophys. J. 160, 99

Shu, F.H., Stachnik, R.V., Yost, J.C.: 1971, Astrophys. J. 166, 465

Toomre, A.: 1964, Astrophys. J. 139, 1217

Toomre, A.: 1974, Highlights of Astronomy, ed. Contopoulos, p.457

van der Kruit, P.C., Freeman, K.C.: 1984a, Astrophys. J. 278, 81

van der Kruit, P.C., Freeman, K.C.: 1986, Astrophys. J. 303, 556

van der Kruit, P.C., Searle, L.: 1981, Astron. Astrophys. 95, 105

van der Kruit, P.C., Searle, L.: 1981, Astron. Astrophys. 95, 116

van der Kruit, P.C., Searle, L.: 1982a, Astron. Astrophys. 110, 61

van der Kruit, P.C., Searle, L.: 1982b, Astron. Astrophys. 110, 79

Vandervoort, P.O.: 1970, Astrophys. J. 161, 87

de Vaucouleurs, G., de Vaucouleurs, A.: 1973, Astron. Astrophys. 28, 109

Visser, H.C.D.: 1980a, Astron. Astrophys. 88, 149

Visser, H.C.D.: 1980b, Astron. Astrophys. 88, 159

Wielen, R.: 1977, Astron. Astrophys. 60, 263

CHAPTER 4 SEARCH FOR NEUTRAL HYDROGEN IN TWO EARLY-TYPE GALAXIES, NGC 3593 AND NGC 4281

Summary

High resolution HI observations with the Westerbork Synthesis Radio Telescope of two lenticular galaxies, NGC 3593 and NGC 4281, are presented and discussed. Only one of the two, NGC 3593, was detected, with $[M_{HI}/L_B] = 0.02$. The HI found in this galaxy appears to be restricted to the central region. The radial velocities of the gas are in agreement with those measured for the stars (Demoulin, 1969). Aside from an upper limit to $[M_{HI}/L_B]$ of NGC 4281, HI data for NGC 4273, an SB(s)c galaxy located 6.8 arcmin from NGC 4281 and detected in the same observation, are reported.

1 Introduction

In this paper we describe high resolution HI observations of NGC 3593 and NGC 4281. Both galaxies are classified as early type (SA(s)0/a: and $S0^+$:sp respectively; de Vaucouleurs et al., 1976, hereafter 2RCBG). Optically the galaxies bear some resemblance to the Sombrero galaxy, NGC 4594. On the Palomar Observatory Sky Survey each galaxy shows a pronounced bulge intersected by a weak band of dust which is visible only where it lies in front of the central part of the bulge. NGC 3593 was studied by Demoulin (1969), who published photographs taken with the 120-inch telescope at the Lick Observatory. Demoulin noted that the galaxy is a disk-shaped system seen almost edge-on and that it contains a large amount of dust. Moreover, she noted that "a very poorly defined spiral arm can be seen in front of the bulge". From rotation curve measurements Demoulin concluded that the mass of NGC 3593 is smaller than generally measured in spiral galaxies. The galaxy was observed in HI by several observers using different single-dish radio telescopes. The resulting total 21-cm line fluxes, systemic velocities and velocity widths show considerable spread. Except for the optical properties listed in 2RCBG and in the Uppsala General Catalogue of Galaxies (Nilson, 1973), very little is known about NGC 4281. An HI observation made with the Arecibo radio telescope suggested that the galaxy contained a detectable amount of HI (Krumm, private communication). A summary of the relevant optical data for these galaxies is given in Table 1. According to de Vaucouleurs (1975), NGC 3593 is probably a member of the M66 cluster of galaxies. This group consists of a triplet of spirals (NGC 3623, NGC 3627 and NGC 3628) along with several outlying systems among which is NGC 3593, located about 1° south west of the triplet. Materne (1978) defined a sub-group (called the GEa cluster) which consists only of the triplet and NGC 3593. According to de Vaucouleurs (1975) NGC 4281 is member of the G46 (Virgo W) group. This group consists of five galaxies, and NGC 4281 is located at its eastern edge.

High resolution HI observations of NGC 3593 and NGC 4281 are of interest for at least two reasons. Firstly, as noted above, these galaxies resemble in their global optical properties the Sa-Sb galaxy NGC 4594. Based on high resolution HI observations made by Bajaja et al. (1984), van der Burg and Shane (1986) showed that the distribution of HI in NGC 4594 is probably associated with tightly wound spiral arms in the disk. Through application of the density wave theory they derived a mass model for the disk and for the inner parts of the halo. If the present high resolution observations of NGC 3593 and NGC 4281 should show that the HI in these galaxies were also associated with spiral arms, we could use the method outlined by van der Burg and Shane to obtain mass models for these galaxies as well. This method allows one to derive the contribution of the disk and

Table 1. Optical properties of NGC 3593, NGC 4273 and NGC 4281

	NGC 3593	NGC 4273	NGC 4281	Ref.
α_{1950}	$11^h11^m59\overset{s}{.}7$	$12^h17^m23\overset{s}{.}0$	$12^h17^m48\overset{s}{.}4$	a
δ_{1950}	13°05′22″	5°37′18″	5°39′52″	a
type	SA(s)0/a:	SB(s)c	S0$^+$sp:	b
velocity (km s^{-1})	660	2302	2602	b
B_T^0	11.24	11.96	11.78	b
blue dimensions	5′.2 × 2′.1	2′.5 × 1′.2	2′.5 × 1′.2	c
D_0	4′.9	2′.2	2′.8	b
D_{25}	5′.8	2′.3	3′.1	b
position angle	92°	10°:	88°	c
inclination	68°	48°	69°	d,e,f

a: Gallouët and Heidmann (1971)
b: 2RCBG
c: Nilson (1973)
d: Krumm and Salpeter (1979b)
e: Shostak (1978)
f: computed using the formulae in Fisher and Tully (1981)

of the halo to the total mass without having to assume an M/L_B for the disk or having to make ad hoc assumptions regarding the mass distribution in the halo (Sancisi and van Albada, 1987).

A second reason for making high resolution HI observations of these galaxies is related with their classification as early-type galaxies. It has been known for some time that the HI content of galaxies of this morphological class shows a considerable spread (van Woerden et al., 1983). In order to understand this spread it is necessary to investigate mechanisms for acquiring and removing gas in this kind of galaxy. Whether external mechanisms (e.g. interaction with nearby galaxies or with an intracluster gas) play an important role can be investigated by comparing the HI content and distribution in field galaxies and in cluster members. As discussed above, NGC 3593 and NGC 4281 are both member of groups. Therefore they seem to be good candidates for the study of the possible influence of the environment on the evolution of gas in an early-type galaxy.

In section 2 of this paper we describe the observations and reduction procedures, in sections 3, 4 and 5 we present the results, and the conclusions are given in section 6.

2 Observations and reductions

NGC 3593 and NGC 4281 were observed with the Westerbork Synthesis Radio Telescope (WSRT) on 5 and 12 September 1983 respectively. For each observation the four movable telescopes were linked with the ten fixed to give forty interferometers whose baselines extended in steps of 72 m from 90 to 2754 m. At the low declinations of the galaxies (see Table 1) the half-power dimensions of the synthesized antenna patterns were greatly elongated in declination, 12.″6 × 55.″4 and 12.″6 × 131.″3 ($\alpha \times \delta$) respectively. The lack of high spatial resolution in the north south direction along with the edge-on aspect and east-west orientation of these galaxies (see Table 1) implies that there will be almost no information on the distribution of gas perpendicular to the planes; for NGC 3593 about two beams will fit along the optical minor axis and for NGC 4281 only one. This situation in analogous to that encountered in NGC 4594 (Bajaja et al., 1984). Also because of the low declination, complete UV-plane coverage could not be obtained. For NGC 4281 this resulted in a synthesized antenna pattern with maximum negative sidelobes of approximately 25% of the central peak; for NGC 3593 these sidelobes attained a negative amplitude of 10%. For both observations the digital line backend was used (Bos et al., 1981). In case of the NGC 3593 observation a total bandwidth of 2.5 MHz was used; for NGC 4281 a bandwidth of 5 MHz was chosen in order to be able to detect other group members in the same primary beam. The observational parameters are summarized in Table 2.

For each galaxy the following reduction procedure was used. As a first step the observations were inspected for the presence of interference, and it appeared necessary to reject substantial parts of the U-V data. For the NGC 3593 observation it was necessary to reject all data from the interferometers with baselines of 90 and 162 m. The remaining data in each of the observations were Fourier-transformed to give a map of the distribution of the 21-cm radiation in the field. This map was searched for the presence of continuum sources. The positions and fluxes of the identified point sources were determined by fitting the synthesized antenna pattern to the data, provided that the maximum flux exceeded a specified threshold value (about 3σ). The results, after correction for attenuation by the primary beam, are listed in Tables 3a and b. The fluxes of the extended regions of emission were determined by summing the components of a clean procedure (Högbom, 1974). The corresponding positions are the flux-weighted averages of the positions of the clean components. The strongest sources were subtracted from the data before transformation to the individual channel maps. The channel maps were then made and inspected for the presence of HI emission. It appeared that line emission from NGC 3593 was present in the velocity interval 500 to 700 km s^{-1}.

Table 2. Parameters of the observations

	NGC 3593	NGC 4281
Date of observation	5 September 1983	12 September 1983
length of observation	11.8 hours	10.6 hours
$\alpha(1950)$ field center	$11^h 11^m 53^s$	$12^h 17^m 18^s$
$\delta(1950)$ field center	+13°7′	+5°41′
baselines		
(min, max, increment)	90, 2754, 72 m	90, 2754, 72 m
synthesized beam ($\alpha \times \delta$)	12″.6 × 55″.4	12″.6 × 131″.3
FWHP primary beam	36′	36′
bandwidth	2.5 MHz	5 MHz
number of		
frequency channels	32	32
central velocity	+620 km s^{-1}	+2250 km s^{-1}
channel spacing	16.6 km s^{-1}	33.6 km s^{-1}

(All velocities in this paper are heliocentric). However, no line emission associated with NGC 4281 was found. Only emission from NGC 4273, an SB(s)c galaxy located 6.8 arcmin from NGC 4281, was detected. The channel maps of NGC 3593 were corrected for residual continuum radiation by subtracting the average of 11 channel maps free from any line emission (six on the low velocity and five on the high velocity side; because of increasing noise near the band edges, channels 1, 30 and 31 were not used). In order to remove the sidelobes, the channel maps were cleaned (to a level of about 1σ), and restored using the positive central part of the antenna pattern. After correction for attenuation by the primary beam this resulted in the set of channel maps shown in Figure 1.

3 Continuum sources

Among the continuum sources listed in Table 3a is an extended source associated with NGC 3593. The angular size of this source in the east west direction is about 0.5 arcmin. The flux-weighted position is in very good agreement with the position of the optical center listed in Table 1. The flux, corrected for the presence of line emission, is slightly less than the flux given by Bieging and Biermann (1977) as measured with the Arecibo telescope (82 mJy). However, Bieging and Biermann report an error in telescope

Table 3a Positions and fluxes of continuum sources in the NGC 3593 field

α_{1950} h m s	δ_{1950} °	flux mJy	Notes
11 10 27 5	13 02 07	10 9	
11 10 28 2	12 59 35	24 7	
11 10 37 6	13 06 02	6 2	
11 10 39 0	13 16 53	7 3	
11 10 54 5	13 10 49	7 5	
11 10 56	12 53 24	33 1	a
11 10 57 1	13 10 26	7 2	
11 11 06 7	13 28 42	15 0	
11 11 09	13 04 00	20 6	a b
11 11 18 4	13 12 43	6 3	
11 11 40 3	13 17 02	14 8	
11 11 55 7	13 14 23	9 3	
11 11 59 3	13 00 04	28 8	
11 11 59	13 08 41	11 7	a c
11 12 00	13 05 20	73 6	a,d
11 12 10	12 54 39	32 6	a
11 12 16 0	12 57 23	5 6	
11 12 20	13 11 14	10 6	a
11 12 21 3	13 09 34	6 7	
11 12 23	13 14 44	87 5	a
11 12 37 4	13 27 49	21 1	
11 12 58 5	13 10 22	11 7	
11 13 04	12 57 52	37 6	a
11 13 13 3	13 28 27	26 6	
11 13 48 3	13 09 05	34 3	

Notes

a extended source

b this source was also reported by Bieging and Biermann (1977)

c source just north of NGC 3593 (see section 3)

d central continuum source of NGC 3593

Table 3b Positions and fluxes of continuum sources in the NGC 4281 field

α_{1950} h m s	δ_{1950} °	flux mJy	Notes
12 15 54 2	5 35 52	23	
12 16 19	5 31 26	532	a
12 16 34 0	5 55 33	17	
12 16 35 6	5 30 48	21	
12 16 40 1	5 38 24	21	
12 16 41	6 06 32	872	a b
12 16 47 3	5 13 44	25	
12 16 58 6	5 43 15	11	
12 17 10 4	5 46 40	5	
12 17 12 0	5 41 21	9	
12 17 20 6	5 44 59	11	
12 17 23	5 37 14	67	a,c
12 17 37 7	5 50 32	9	
12 17 46 0	5 40 30	8	d
12 18 13 5	5 17 22	30	
12 19 19 2	5 26 58	305	

Notes

a extended source

b 3C270

c central continuum source of NGC 4273

d source close to the position of NGC 4281

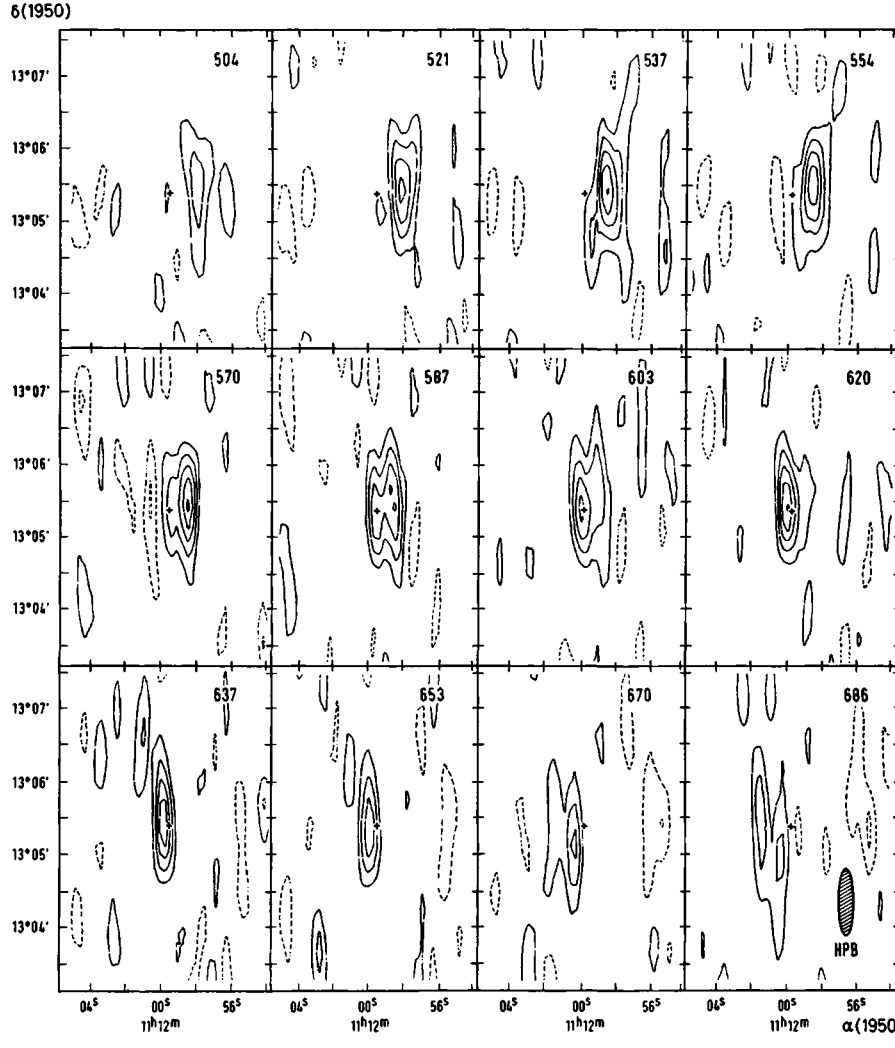

Figure 1. *Full resolution channel maps of NGC 3593. Crosses mark the position of the optical nucleus. The heliocentric radial velocity (in km* s^{-1}*) is indicated in the upper right hand corner of each map. The first contour is plotted at a level of 1.7 K; negative contours are plotted as broken curves. The zero level contour has been omitted.*

pointing during their measurements; the telescope was pointed less than 1 arcmin north of NGC 3593. Together with the existence of a continuum source approximately 3 arcmin north of NGC 3593 (see Table 3a) this pointing error may account for the larger value they report. The continuum source at $\alpha = 11^h\ 11^m\ 09^s$, $\delta = 13°\ 04'\ 00''$ has also been reported by Bieging and Biermann. The flux they measured, 16 mJy, is some 20% less than our value. Note that Table 3b includes a very weak continuum source which falls within the optical image of NGC 4281. The distance of this source from the optical center of NGC 4281 (listed in Table 1) is only 52".

4 HI results for NGC 4281 and NGC 4273

In section 2 it was noted that no HI was found associated with NGC 4281. However, a neighbouring galaxy, NGC 4273, located 6.8 arcmin from NGC 4281, was clearly detected. The upper limit to $[M_{HI}/L_B]$ for NGC 4281, calculated from the 3σ level in the line profile, assuming a velocity width of 250 km s^{-1}, and with L_B the blue luminosity calculated from the total blue magnitude listed in Table 1, is 0.01. The line profile was obtained by integration of the channel maps (corrected for attenuation by the primary beam) over an ellipse centered on the optical position of NGC 4281 and with major and minor axes three times the corresponding optical axes. The flux of NGC 4273 was determined in a similar way, but integrating over an ellipse with axes of five times the corresponding optical axes. Integration of the line profile of NGC 4273, which is shown in Figure 2, resulted in $\int Sdv$ = 8.0 Jy km s^{-1}. The systemic velocity V_{20}, defined as the velocity midway between the points at 20% of the maximum flux in the line profile, is 2376 km s^{-1}. The profile width W_{20}, which is the velocity difference between these 20% points, is 345 km s^{-1}. The HI properties are summarized in Table 4. The WSRT flux is 45% of the value given by Shostak (1978), as measured with the 91-m NRAO telescope. It was suggested by Shostak that in the NRAO observation a flux contribution from NGC 4277, located 2 arcmin east of NGC 4273, might be present. However, the WSRT observation shows no flux associated with NGC 4277 in this velocity interval. The systemic velocity and the profile width derived from the WSRT observation are in adequate agreement with the corresponding values given by Shostak (2375 and 299 km s^{-1} respectively). Moreover, they resemble the corresponding values derived from the line profile of NGC 4281 as measured with the Arecibo telescope (Krumm, private communication). This would suggest confusion with NGC 4273. However, after accounting for the beam attenuation, the estimated flux contribution of NGC 4273 to an Arecibo observation centered on NGC 4281 is much less than that actually measured by Krumm.

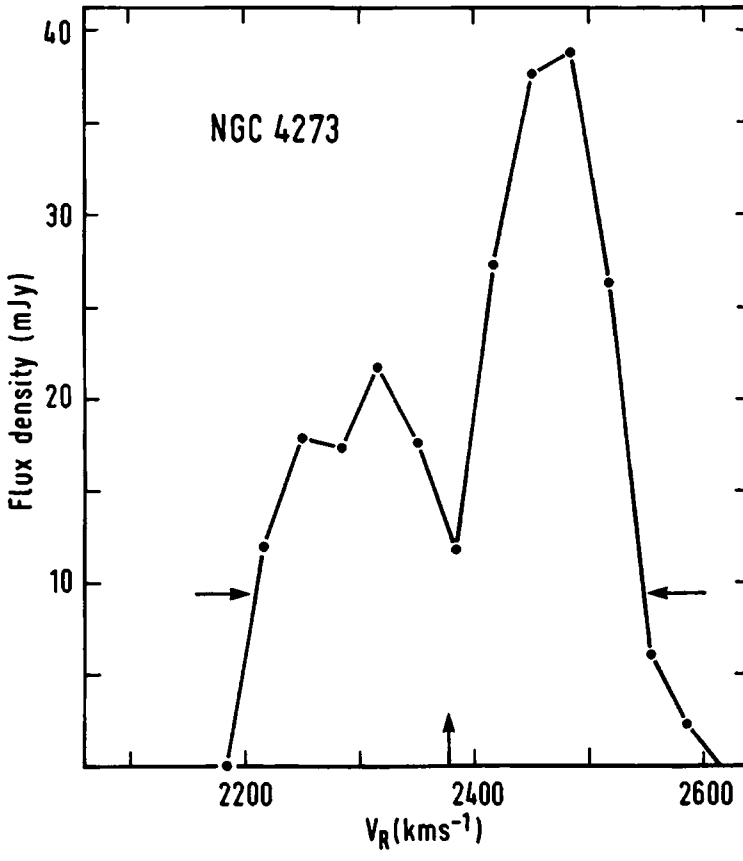

Figure 2. Global HI line profile of NGC 4273 The horizontal arrows indicate the points at 20% of the maximum flux, the vertical arrow marks the systemic velocity

Table 4. HI properties of NGC 3593, NGC 4273 and NGC 4281, obtained with the WSRT

	NGC 3593	NGC 4273	NGC 4281
$\int$SdV (Jy km s^{-1})	4 2	8.0	< 0.5
V_{20} (km s^{-1})	587	2376	
W_{20} (km s^{-1})	216	345	

5.1 Global HI line profile

In order to obtain the 21-cm line profile of NGC 3593 the following procedure was carried out. The individual channel maps were convolved to a resolution of about 1 arcmin in right ascension and declination. These convolved maps were used to define masks, i.e. polygons which enclose the 1.5σ contour in the region of the line emission. In order to obtain at each grid point a single continuous series of velocities minor extensions were made to these masks. The total flux in each channel was then determined in two steps. First the clean components (see section 2) within the mask were summed after correction for primary beam attenuation. This sum was then added to the remnant flux within the mask, determined by integration of the cleaned channel map over the corresponding region, normalized by the sum of the antenna pattern over the same area and after correction for attenuation by the primary beam. The resulting HI line profile is shown in Figure 3. Integration of the line profile yields a total HI flux of 4.2 Jy km s^{-1}. The corresponding HI-mass to blue-luminosity ratio, $[M_{HI}/L_B]$, is 0.02, where L_B was calculated from the total blue magnitude listed in Table 1. Despite the edge-on aspect of the galaxy, the profile plotted in Figure 3 shows almost no central depression. This indicates that, if the gas follows circular orbits, the HI distribution must be strongly concentrated to the center (Thonnard, 1982). The systemic velocity V_{20} and the velocity width W_{20} are listed in Table 4. In Table 5 we give a summary of published results of HI observations of NGC 3593, made with different single dish radio telescopes, along with the results of optical measurements. The rotational velocity derived from W_{20} and corrected for inclination is 116 km s^{-1}. This is in agreement with the rotational velocity quoted by Faber and Gallagher (1979). The WSRT flux is only 60% of the minimum flux listed in Table 5. Since no source of confusion seems to be present, this apparent flux deficiency in the WSRT observation might be attributed to the missing short spacings. For a shortest baseline of 234 m (see section 2) the visibility of a source with a circular Gaussian intensity distribution with a FWHM of 1'.5 drops to 0.5. Because the observed extent in right ascension of the HI features on every channel map is 0'.5 at most (in declination the structures are not resolved), this can only partly explain the small WSRT flux. At the low velocities there appears to be a good resemblance between the shape of the line profile measured with the WSRT and those published in the literature (see Table 5). However, at velocities between about 700 and 750 km s^{-1}, where no emission was found in the WSRT observation, some published profiles show a relatively small bump.

This is most clearly illustrated in the line profile measured by Huchtmeier (1982) with the 91-m NRAO radio telescope. The absence of this high velocity bump in the WSRT observation explains to a large extent why the systemic velocity and the velocity width are at the low end of the range of published values, but it is not sufficient to account for the flux deficiency. The apparent flux deficiency in the WSRT observation might indicate the presence of extended low-level emission lying outside the masks which were used to derive the HI line profile. Note in this respect that Hunter et al. (1982) measured a signal in

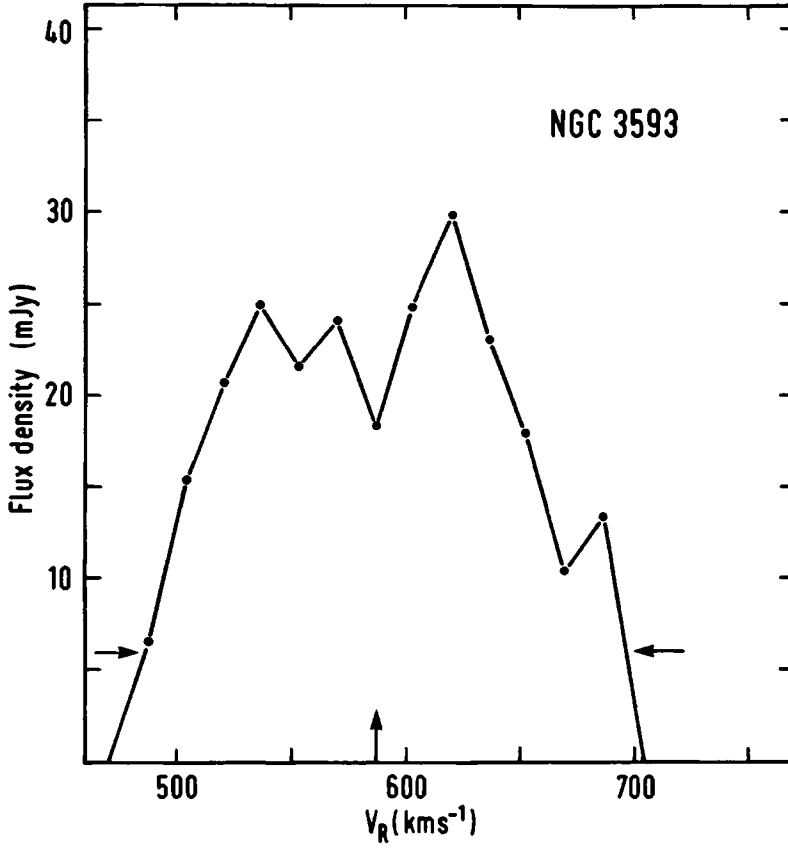

Figure 3. Global HI line profile of NGC 3593. The horizontal arrows indicate the points at 20% of the maximum flux; the vertical arrow marks the systemic velocity.

the velocity range 500 to 750 km s^{-1} when pointing the 91-m NRAO telescope 10 arcmin north of NGC 3593 These authors attributed this 21-cm line emission to hydrogen extending beyond the optical boundary of the galaxy Their line profile, measured in this direction, shows a pronounced peak at velocities between 700 and 750 km s^{-1} where no HI emission is found in the WSRT observation.

Table 5. Published optical and HI properties of NGC 3593

systemic velocity (km s^{-1})	profile width (km s^{-1})	$\int$SdV (Jy km s^{-1})	Telescope	Ref
547*				a
429*				b
660*				c
627	300		NRAO (91 m)	d
500	270†	7 01	Arecibo (300-m)	e
628*				f
		7 11	Arecibo (300-m)	g
621	232†		Arecibo (300-m)	h
550	387	8 9	Nançay	i
641	248‡	8 1	NRAO (91-m)	j
641	227‡	8 6	Effelsberg (100-m)	j
631	252*	18 9	NRAO (91-m)	k
693				l
621	223†	8 1	Arecibo (300-m)	m

References

a Nilson (1973)
b de Vaucouleurs (1975)
c 2RCBG
d Rood and Dickel (1976)
e Bieging and Biermann (1977)
f Materne (1978)
g Krumm and Salpeter (1979a)
h Krumm and Salpeter (1979b)
i Balkowski (1979)
j Huchtmeier (1982)
k Hunter et al (1982)
l Huchra et al (1983)
m Giovanardi et al (1983)

Notes.

* optically derived velocity
†, ‡ and * velocity width of the line profile measured between 50, 25 or 20% points respectively

5.2 HI surface density distribution

In order to obtain the integrated HI surface density distribution the full resolution channel maps plotted in Figure 1 were integrated over the relevant velocity interval. To prevent unnecessary noise being added all intensities outside the masks were set to zero before the integration was carried out. In the upper panel of Figure 4 the resulting HI surface density map is shown. In the lower panel a reproduction of a 45 minute blue exposure of NGC 3593 made with the Lick 120-inch telescope by Demoulin (1969) is shown. Superposed are some contours from the plot in the upper panel of this figure. As is clear from Figure 4, the distribution of HI in NGC 3593 is restricted to the central part of the galaxy and appears to be concentrated mainly in two clumps. The western clump coincides with a small bright knot (possibly an HII region) in the band of dust. The other clump is apparently located slightly east of the optical center and may actually originate on the far side of the galaxy. The location of the outermost fragments of gas on the eastern side (at r = 0.'3) suggests that not all of the gas is located in the principal plane of the galaxy. On the western side, at r = 0.'8, a small amount of gas is seen on or slightly north of the major axis. Due to the limited resolution in declination this plot will not contain much information regarding the distribution of gas perpendicular to the plane.

5.3 Kinematics

Because of the high inclination of NGC 3593 and the limited resolution perpendicular to the major axis, it is inappropriate to calculate a velocity field for NGC 3593. More useful is a plot of the distribution of HI as a function of velocity and position along the major axis. This position-velocity map, shown in Figure 5, is made through the optical position listed by Gallouët and Heidmann (1971) with a position angle of 92° (Nilson, 1973). The maximum radius at which HI is found is, on both sides, about 30″. The extreme observed radial velocities are 500 km s^{-1} (on the western side) and 730 km s^{-1} (on the eastern side). On the west side this velocity is in agreement with the optically measured radial velocity (Demoulin, 1969). However, on the east side the maximum radial extent of the observations of Demoulin is about 13 arcsec where a velocity of about 780 km s^{-1} is measured. Note that on this side, at radii greater than 13 arcsec, the HI emission along the major axis is fairly weak.

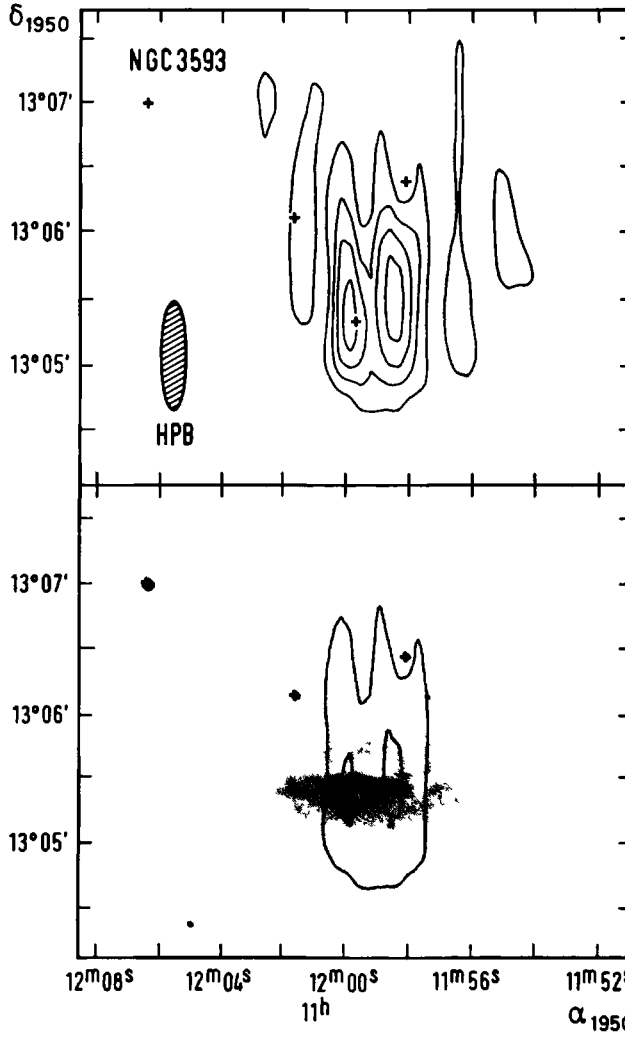

Figure 4. *HI column density map of NGC 3593 (upper panel). The first contour is plotted at a level of* 1.7 10^{20} *atoms* cm^{-2}*; the contour interval is* 3.4 10^{20} *atoms* cm^{-2}*. Aside from a cross at the optical nucleus of NGC 3593 some crosses indicating reference stars are shown. In the lower panel a reproduction is shown of a photograph made by Demoulin (1969) using the Lick 120-inch telescope. Superposed are some contours from the HI surface density map shown in the upper panel.*

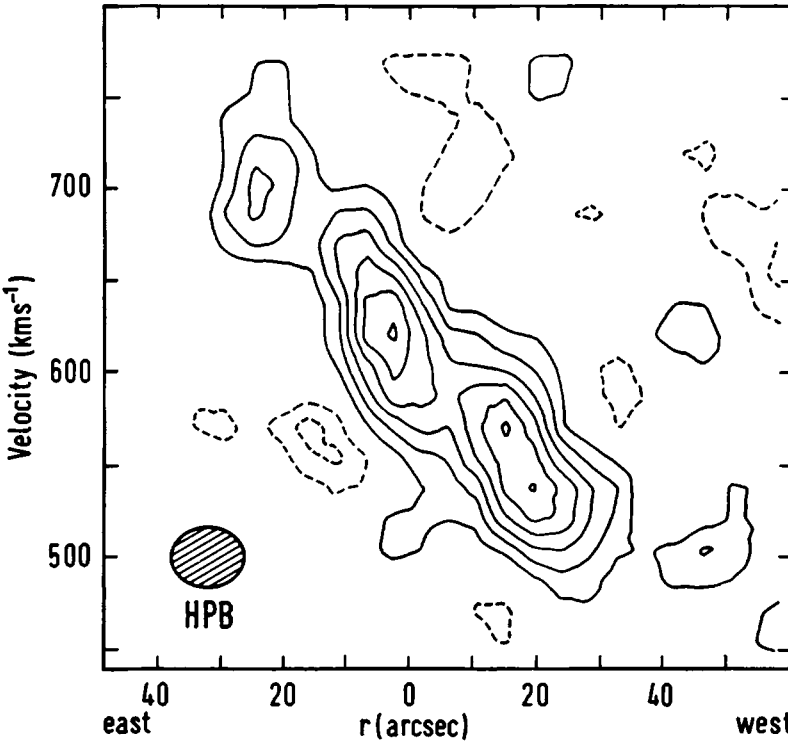

Figure 5. Map of the HI brightness distribution in NGC 3593 along the major axis as a function of radial velocity and distance r from the center. The first contour and contour interval are 1 4 K, negative contours are plotted as broken curves. The zero level contour has been omitted.

6 Discussion

In the previous section it was shown that NGC 3593 contains only a very small amount of neutral hydrogen. The corresponding HI-mass to blue-luminosity ratio of 0.02 falls in the range of values for HI-rich ellipticals listed by Gouguenheim (1979) and is at the low end of the range of values for S0 galaxies with a detectable HI content (Wardle and Knapp, 1986). As noted by van Woerden et al. (1983), the distribution of HI in lenticular galaxies may take a variety of forms including filled disks, inner HI rings with radii about 0.4 times the optical radius, and annular configurations (sometimes highly

inclined) with diameters roughly two times the optical diameter. In NGC 3593 the HI appears to be restricted to very small galactocentric radii. Assuming a distance of 7.5 h^{-1} Mpc (based on the velocity of the GEa group given by Materne, 1978, and a Hubble constant H_0 = 100 h km s^{-1} Mpc^{-1}), the maximum galactocentric radius of the gas is about 1 h^{-1} kpc, corresponding with 0.2 Holmberg radius, although on the western side some weak emission might be present at greater radii (see Figure 4). Moreover, the distribution of HI is asymmetric with respect to the center and seems to be shifted slightly towards the north-west side. If the two peaks are associated with a slightly acentric inner HI ring, its diameter of 0.2 D_{25} (with D_{25} taken from 2RCBG) is only slightly smaller than the average value of 0.4 D_{25} quoted by van Woerden et al. (1983) for a sample of lenticular galaxies. As Figure 4 shows, the radial extent of the HI is smaller than that of the dust. A close correlation between the radial distributions of the gas and the dust, as observed in NGC 4594, seems not to be present in NGC 3593. No information regarding the shape of the spiral pattern, if present, can be obtained from the observed distribution of HI in NGC 3593. This means that a calculation of a mass model, as carried out for NGC 4594 (van der Burg and Shane, 1986), is ruled out. The question arises why the HI size and content in NGC 3593 are exceptionally small. If one thinks of an accretion event of which the two clumps are the remnants (such events have been suggested for other early-type galaxies, e.g. NGC 1023, Sancisi et al., 1984), it must have occurred recently; otherwise the clumps would have been smeared out by differential rotation (Baldwin et al., 1980). However, in case of a recent accretion event one would not expect the observed velocities of the gas to agree with those of the stars. Note that in NGC 4569, an SAB(rs)ab galaxy located not far from the center of the Virgo cluster, the HI is also confined to the center (Warmels, 1986). From the data listed by Warmels, we compute for the ratio of the HI diameter (3') to optical diameter (using D_0 = 7'.9; 2RCBG) a value of 0.4 (compared with 0.2 - 0.3 for NGC 3593, depending on whether the outer weak features in the HI distribution are included). Since all galaxies in the Virgo cluster observed by Warmels and showing a small HI content and size also have velocities quite different from the cluster average, Warmels concludes that ram-pressure stripping by a hot intracluster gas is probably the cause of these HI properties. Whether or not HI can be stripped from NGC 3593 depends upon the presence of intracluster gas in the GEa group. This can be revealed by X-ray observations. However, no such observations of the GEa group have been reported.

If we assume that the gas is in circular motion, the rotational velocity of 116 km s^{-1} yields a total mass of 3.1 10^9 h^{-1} $M_\odot$ (for a spherical mass distribution). The corresponding mass-to-light ratio [M/L_B] is 1.1 h. Note that these values are valid within about 1 h^{-1} kpc or 0.2 Holmberg radius from the center. The [M/L_B]-value measured

within a corresponding radius from the center of NGC 4594 is about 4 h, as derived from optical rotation curve measurements made by Schweizer (1978). Accounting for the large uncertainty in L_B due to corrections for absorption of light in the band of dust, and the fact that the assumption that the gas and the stars move in circular orbits might not be valid at small radii (Schweizer, 1978), the $[M/L_B]$-values of NGC 3593 and NGC 4594 are roughly in agreement.

Acknowledgements

The Westerbork Synthesis Radio Telescope is operated by the Netherlands Foundation for Radio Astronomy (SRZM), with the financial support of the Netherlands Organization for the Advancement of Pure Research (Z.W.O.).

Bajaja, E., van der Burg, G., Faber, S.M., Gallagher, J.S., Knapp, G.R., Shane, W.W.: 1984, Astron. Astrophys. 141, 309

Baldwin, J.E., Lynden-Bell, D., Sancisi, R.: 1980, Mon. Not. R. Astron. Soc. 193, 313

Balkowski, C.: 1979, Astron. Astrophys. 78, 190

Bieging, J.H., Biermann, P.: 1977, Astron. Astrophys. 60, 361

Bos, A., Raimond, E., van Someren Greve, H.W.: 1981, Astron. Astrophys. 98, 251

Demoulin, M.-H.: 1969, Astrophys. J. 157, 75

de Vaucouleurs, G.: 1975, in Stars and Stellar Systems, Vol. 9, ed. A. Sandage, M. Sandage, J. Kristian (University of Chicago Press), p. 557

de Vaucouleurs, G., de Vaucouleurs, A., Corwin, H.G.: 1976, Second Reference Catalogue of Bright Galaxies (University of Texas press) (2RCBG)

Faber, S.M., Gallagher, J.S.: 1979, Ann. Rev. Astron. Astrophys. 17, 135

Fisher, J.R., Tully, R.B.: 1981, Astrophys. J. Suppl. Ser. 47, 139

Gallouët, L., Heidmann, N.: 1971, Astron. Astrophys. Suppl. Ser. 3, 325

Giovanardi, C., Krumm, N., Salpeter, E.E.: 1983, Astron. J. 88, 1719

Gouguenheim, L.: 1979, in Photometry, Kinematics and Dynamics of Galaxies, ed. D.S. Evans (University of Texas Press), p. 201

Högbom, J.A.: 1974, Astron. Astrophys. Suppl. 15, 417

Huchra, J., Davis, M., Latham, D., Tonry, J.: 1983, Astrophys. J. Suppl. Ser. 52, 89

Huchtmeier, W.K.: 1982, Astron. Astrophys. 110, 121

Hunter, D.A., Gallagher, J.S., Rautenkranz, D.: 1982, Astrophys. J. Suppl. Ser. 49, 53

Krumm, N., Salpeter, E.E.: 1979a, Astrophys. J. 227, 776

Krumm, N., Salpeter, E.E.: 1979b, Astrophys. J. 228, 64

Materne, J.: 1978, Astron. Astrophys. 63, 401

Nilson, P.: 1973, Uppsala General Catalogue of Galaxies, Ann. Uppsala Astron. Obs. 6

Rood, H.J., Dickel, J.R.: 1976, Astrophys. J. 205, 346

Sancisi, R., van Woerden, H., Davies, R.D., Hart, L.: 1984, Mon. Not. R. Astron. Soc. 210, 497

Sancisi, R., van Albada, T.S.: 1987, in Dark Matter in the Universe, eds. J. Kormendy and G.R. Knapp, IAU Symp. 117, 67

Schweizer, F.: 1978, Astrophys. J. 220, 98

Shostak, G.S.: 1978, Astron. Astrophys. 68, 321

Thonnard, N.: 1982, in Proceedings of the Workshop: The Comparative HI content of Normal Galaxies, Green Bank, West Virginia

van der Burg, G., Shane, W.W.: 1986, Astron. Astrophys. 168, 49

van Woerden, H., van Driel, W., Schwarz, U.J.: 1983, in Internal Kinematics and Dynamics of Galaxies, IAU Symp. No. 100, ed. E. Athanassoula, p. 99

Wardle, M., Knapp, G.R.: 1986, Astron. J. 91, 23

Warmels, R.H.: 1986, HI Properties of Spiral Galaxies in the Virgo Cluster, Dissertation, University of Groningen

CHAPTER 5 HI OBSERVATIONS OF SOME GALAXIES AND THEIR FAINT COMPANIONS

Summary

21-cm line observations of single galaxies with multiple faint companions have been carried out with the Nançay Decimetric Radio Telescope 12 galaxies have been detected including 6 companion galaxies Three new detections in HI are reported Flux density upper limits are given for the undetected galaxies

1 Introduction

In recent years many galaxies have been observed in the 21 cm line of neutral hydrogen and accurate determinations of radial velocities and HI masses are now available for a large sample However, a class of objects which seems to have received less attention than it deserves is that of single galaxies accompanied by several much less massive companions Redshift observations of these small companions can provide important data on the distribution of mass in and around galaxies (e g Bahcall and Tremaine, 1981) The physical properties of these companions may also be of interest

The usefulness of this method depends upon the detectability of the faint companions An estimate of the expected signal strength of these objects can be made, based on the mean $[M_{HI}/L]$ value of 0 60 for late type dwarf galaxies with $M_{pg} = -18$ (Fisher and Tully, 1975) If we assume this ratio for the companions, then the expected flux density (taking an HI line profile width of 150 km s^{-1} and an apparent magnitude m = 15) is about 25 mJy This would mean that a large sample of candidates is available for this kind of investigation For most of these candidates, in particular in the more crowded groups, the angular resolution of a synthesis telescope is required However, before making these synthesis observations a feasibility study was carried out to evaluate the detectability of these companions In order to acquire rapidly observations with the required accuracy the filled aperture radio telescope at Nançay was employed

Groups north of declination +30° were given preference because of the likelihood that additional observations with the Westerbork Synthesis Radio Telescope (WSRT) would be required The groups were selected from the Catalogue of Galaxies and Clusters of Galaxies (Zwicky et al , 1961 - 1968, hereafter CGCG), the Uppsala General Catalogue of Galaxies (Nilson, 1973, hereafter UGC) and the Palomar Observatory Sky Survey (POSS) No strict selection criteria have been applied, but the following factors were considered Each primary galaxy, for which the velocity must be approximately known, should be accompanied by at least three faint companions, preferably of late morphological type The diameter of the group should be about one half power primary Westerbork beam (0°6) or less The brightest companions must be at least one magnitude fainter than the primary and there should be no bright galaxies with comparable velocities within a few group radii Several dozen possible groups which satisfy these requirements were noted

This paper describes 21-cm line observations of 43 galaxies distributed over 12 of these groups The results are presented in the following section, where each group is discussed briefly The HI line profiles of all detected galaxies are shown and optical and 21-cm line parameters are given Three new detections are reported (one of which is doubtful) For some other galaxies the new observations yield improved HI parameters

For galaxies with no detected HI in the observed velocity range, upper limits to the HI fluxes are listed The results of HI observations of three isolated galaxies, made during the same period, are also reported For one of these isolated galaxies, discordant velocities have probably been resolved

2 Observations and results

The observations were carried out with the Nançay Decimetric Radio Telescope during the period May 26 to June 5, 1982 The halfpower beamwidth of the instrument is 3 6 in right ascension and 22 in declination (larger at high declination, Foy et al , 1968) The system temperature of the 21-cm receiver was about 50 K The autocorrelation spectrometer sampled the spectrum in two orthogonal polarizations each in 256 frequency channels, covering a total bandwidth of 6 4 MHz The resulting velocity coverage of 1350 km s^{-1} was usually centered on the systemic velocity of the primary galaxy of the group The Nançay radio telescope is a meridian instrument with which a maximum tracking time on a source of about one hour may be achieved, depending upon the declination The observations were made in the position switching mode each track was divided into cycles of 5 minutes useful integration time, 2 5 minutes on the source and 2 5 minutes off the source for comparison on the same part of the track The total on source observing time per galaxy during the whole observing run ranged between about 20 and 120 minutes The efficiency of the Nançay telescope and receiver for declinations up to +30° is about 1 25 K Jy^{-1} and decreases at higher declinations The limiting sensitivity for a one hour observation, after averaging orthogonal polarizations, corresponds to a neutral hydrogen mass of about 10^6 $M_\odot$ Mpc^{-2} for a line width of 150 km s^{-1} The observations were made on the positions given in the UGC For one anonymous galaxy, a member of the NGC 3656 group, the coordinates were measured from the POSS

Much of the available observing time was devoted to relatively bright, late type companions The remaining candidates were used to fill in gaps in right ascension in order to form a continuous observing sequence In this way a total of 46 galaxies (including three isolated galaxies) were observed, 32 of which are companions After deleting interference spikes and measurements in which the spectrum showed evidence of extensive interference or other disturbances, a baseline was fitted to the data Usually a linear baseline was satisfactory However, in a few cases (UGC 3937, NGC 2798, UGC 5841 and NGC 4111) a quadratic baseline has been removed An example is shown in Figure 1, along with the quadratic baseline which was fitted to the data after excluding the part indicated by dots along the horizontal axis

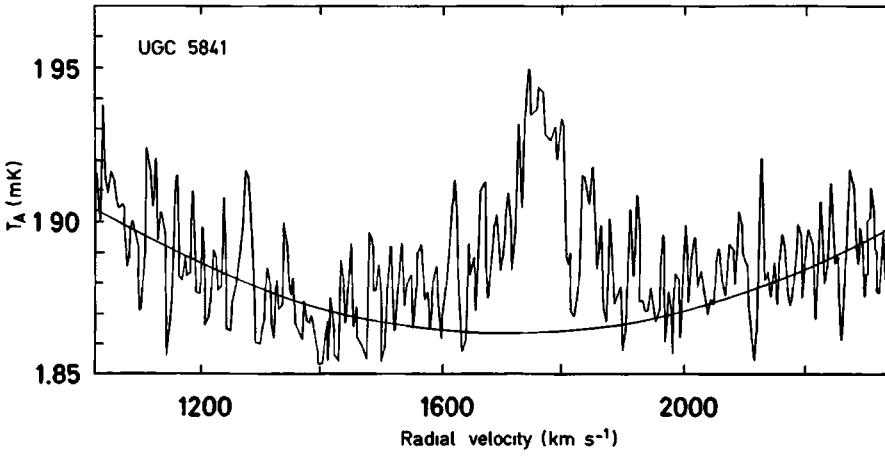

Figure 1. *The observed line profile of UGC 5841 (heliocentric radial velocity in km s^{-1} versus antenna temperature in mK) This plot is an example of one of the four observed line profiles to which a quadratic baseline has been fitted (the other cases are UGC 3937, NGC 2798 and NGC 4111) The resulting fit is drawn as a solid curve the part which is excluded from the fit is indicated by dots*

After removal of the baseline, the profiles were smoothed to give a velocity resolution of 16 km s^{-1} In Figure 2 the resulting line profiles of the detected galaxies are presented, members of each group are shown together All velocities are heliocentric and computed according to the conventional optical definition

In Table I the following information has been listed for each of the detected galaxies

Column (1) *Line a* Identification of a galaxy by its NGC or UGC number,

Column (2) *Lines a, b* The α, δ coordinates of the pointing center,

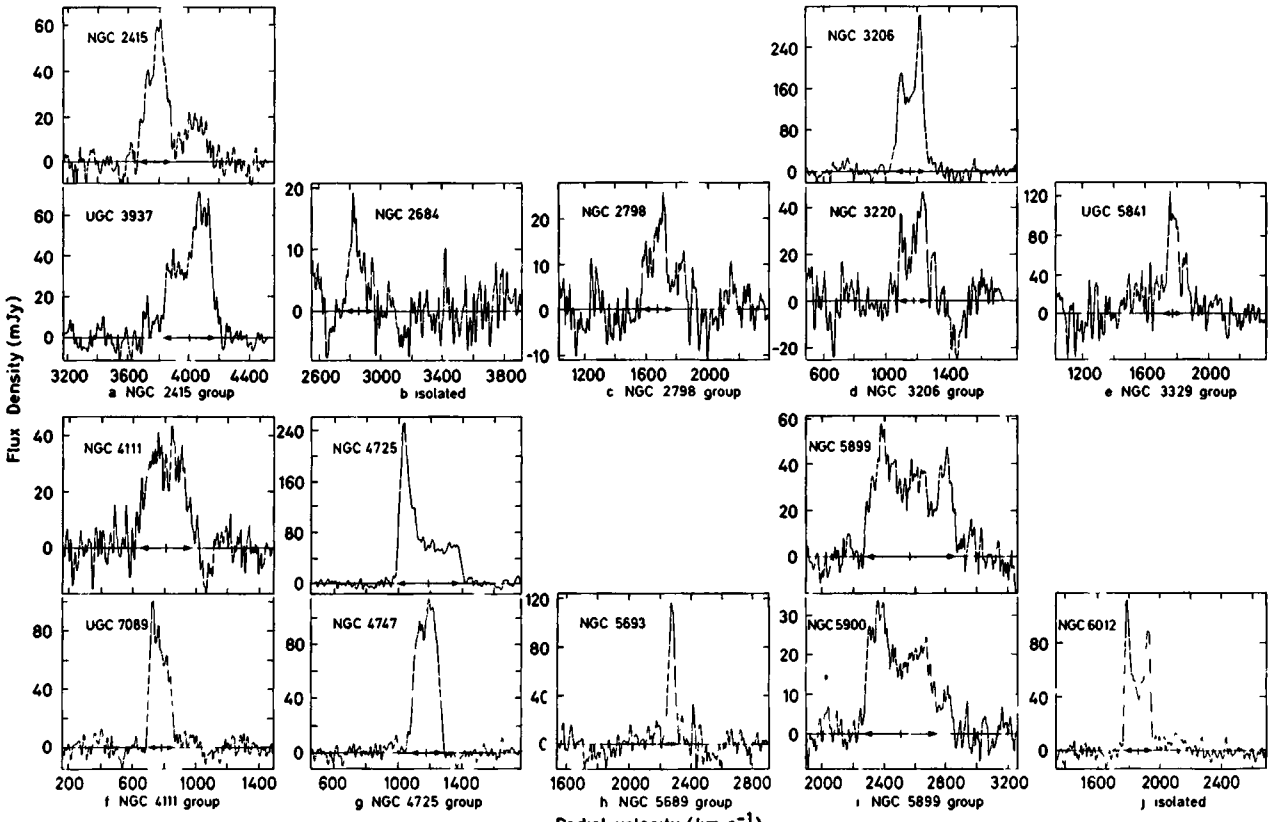

Figure 2: *HI line profiles of detected galaxies. The horizontal axes are the heliocentric radial velocities; the vertical axes are the observed flux densities. For each galaxy the profile width and the systemic velocity are indicated.*

Table I Optical and 21 cm data on detected galaxies

(1)	(2)	(3)	(4)	(5)	(6)	(7)	(8)	(9)	(10)	(11)	(12)
name	α_{1950} (h m s)	type	m_p	B_T	V (km s^{-1})	F_H (Jy km s^{-1})	F_H^C (Jy km s^{-1})	publ flux (Jy km s^{-1})	publ vel (km s^{-1})	refs	V_{opt} (km s^{-1})
	δ_{1950} (^{o})		diameters (arcmin)	B_T^0	W_{20} (km s^{-1})	f	$[M_{HI}/L_B]$				
NGC 2415 group											
NGC 2415	07 33 36	Im?	12 5	12 7	3773	8 1	10 8	9 7[a]	3782	a	
	+35 21		1 0x1 0	12 7	205	1 33	0 20	5 3	3786	b	
								10 2[a]	3797	c	
UGC 3937	07 34 18	SB?	14 2	14 1	3999	15 1	15 1	11 6[a]	3990	a	
	+35 43		2 1x0 5	12 9	323	1 00	0 34				
Isolated galaxy											
NGC 2684	08 51 18	S	13 4	13 4	2860	1 4	1 6	10 5[a]	3522	d	2858
	+49 20		0 9x0 8	13 3	180	1 13	0 32	< 8 5	-400 +3000	e	
NGC 2798 group											
NGC 2798	09 14 06	SB(s)aP	12 9	12 9	1669	3 2	3 8	8 5	1744	f	1733
	+42 12		2 8x0 9	12 3	175	1 20	0 04	10 9	1740	g	
								11 4	1726	h	
NGC 3206 group											
NGC 3206	10 18 30	SBcd	12 7	12 4	1158	34 9	42 2	35 7[a]	1158	i	1161
	+57 12		3 0x2 0	12 3	189	1 21	0 48	36 1[a]	1161	e	
NGC 3220	10 20 24	Sb sp	13 7	13 7	1192	6 0	6 8				1226
	+57 17		1 3x0 5	13 2	154	1 13	0 20				
NGC 3329 group											
UGC 5841	10 40 48	SAB(s)c	15 1	14 8	1766	11 7	12 9				
	+76 58		1 7x0 9	14 6	102	1 10	1 23:				
NGC 4111 group											
NGC 4111	12 04 30	SA(r)0$^+$ sp	11 4	11 6	807	9 2	11 6	< 29 4	-400 +3000	e	794
	+43 20		4 3x0 8	11 6	327	1 26	0 08				
UGC 7089	12 03 24	dm m	14 8	13 7	775	11 2	13 8	17 7[a]	778	e	
	+43 25		3 5x0 9	13 0	161	1 23	0 36				
NGC 4725 group											
NGC 4725	12 48 00	SAB(r)abP	10 2	10 8	1189	36 7	>36 7	107	1205	j	1207
	+25 46		12 x9	10 8	394		> 0 11				
NGC 4747	12 49 18	SBcd?spP	13 2	12 7	1181	16 4	>16 4	33	1185	j	1189
	+26 02		3 5x1 5	12 4	194		> 0 23				
NGC 5689 group											
NGC 5693	14 34 24	SB(rs)d	14 5	13 9	2283	8 0	9 9	7 3	2276	a	2276
	+48 47		1 7x1 7	13 9	75	1 25	0 55	6 2	2282	k	
NGC 5899 group											
NGC 5899	15 13 12	SAB(rs)c	12 6	12 4	2560	18 9	21 5	20 1	2549	l	2554
	+42 14		2 8x1 2	12 0	579	1 14	0 20	16 5	2554	a	
								21 4	2496	k	
NGC 5900	15 13 12	Sb sp	15 0	14 7	2498	8 9	10 6	26 6	2551	k	
	+42 24		1 5x0 4	14 0	457	1 19	0 63				
Isolated galaxy											
NGC 6012	15 51 54	SB(rs)ab	13 1	12 7	1851	12 1	14 5	22 9	1846	h	1848
	+14 44		2 1x1 6	12 5	177	1 20	0 22	20 2[a]	1847	d	
								22 1[a]	1855	m	

References for column (9) and (10)

a Peterson (1979)
b Bottinelli et al (1973)
c Gordon and Gottesman (1981)
d Balkowski and Chamaraux (1981)
e Fisher and Tully (1981)
f Huchtmeier (1982)
g Peterson and Shostak (1974)
h Bottinelli et al (1980)
i Shostak (1975)
j Wevers et al (1984)
k Bottinelli et al (1981 and 1982a,b)
l McCutcheon and Davies (1970)
m Hewitt et al (1983)

Column (3) *Line a* Morphological type taken from the Second Reference Catalogue of Bright Galaxies (de Vaucouleurs et al , 1976, hereafter 2RCBG) or the UGC,

Column (4) *Line a* Apparent photographic magnitude from the CGCG or the UGC,
Line b Blue diameters as reported in the UGC,

Column (5) *Line a* CGCG or UGC magnitude transformed to the total blue apparent magnitude, B_T, as defined in 2RCBG The transformations have been performed according to the precepts given by Fisher and Tully (1981, hereafter FT),
Line b Total blue apparent magnitude, B_T^0, corrected for internal and galactic absorption, as described by FT,

Column (6) *Line a* Heliocentric radial velocity (in km s^{-1}) defined as the midpoint between the points at 20% of the maximum flux,
Line b The HI line profile width at 20% of the peak (uncorrected for instrumental resolution),

Column (7) *Line a* The total observed flux, F_H, in the HI line (in Jy km s^{-1}) uncorrected for attenuation,
Line b A correction factor, f, applied to the observed flux in line a This factor accounts for resolution effects of the finite observing beam and for attenuation of the beam due to any offset of the beam center with respect to the optical center of the galaxy (taken, in order of preference, from Dressel and Condon, 1976, or from Gallouet et al , 1973) Using the same assumptions as Chamaraux et al (1980), taking into account the finite width of a galaxy and the large extension of the Nançay beam in the NS direction, leads to

$$f = \left[1+(\Gamma_H/\theta)^2\right]^{1/2} \exp[(\frac{\Delta\alpha\cos\delta}{0\,6\,\theta})^2 \frac{1}{1+(\Gamma_H/\theta)^2}],$$

where θ is the halfpower beamwidth in the EW direction (3 6) and $\Delta\alpha$ is the difference in right ascension (in arcmin) between the pointing center (column 2, line a) and the adopted optical center of the galaxy Γ_H is the projection of the apparent HI ellipse of the galaxy in the EW direction and was computed using the relation between the ratio of the HI to the optical (Holmberg) diameter and the morphological type (Bottinelli, 1971) This relation is valid

for late type galaxies For galaxies of type SO^+ to Sab a mean value of 1 4 for the effective HI to isophotal optical diameter, determined by Fouque (1983), was used The transformation of the UGC diameters to diameters in the Holmberg system (corrected for inclination and galactic absorption) was carried out using the formulae given by FT and in 2RCBG

Column (8) *Line a* The total corrected flux, F_H^C, in the HI line (in Jy km s ^{1}), assuming that the observed flux originated in the galaxy which was being observed,
Line b The ratio of HI mass to blue luminosity, $[M_{HI}/L_B]$, in solar units, taking M_B (Sun) = +5 48,

Column (9) *Line a* Published HI fluxes as given by Huchtmeier et al (1983, hereafter HRBH) The fluxes are given in Jy km s ^{1} or reduced to these units using the relevant data given by the authors Values corrected by the authors for beam filling are marked with an asterisk,

Column (10) *Line a* Published velocities (in km s^{-1}) as quoted by HRBH,

Column (11) *Line a* References for the data quoted in columns (9) and (10),

Column (12) *Line a* Optical velocities as quoted by Huchra et al (1983, hereafter HDLT)

The galaxies listed in Table II were not detected In this table flux density upper limits are given and reference is made to previous observations of some of these galaxies For each galaxy the following information is given

Column (1) Identification of the galaxy by its NGC or UGC number, when listed,

Column (2) The α, δ coordinates of the pointing center,

Column (3) Apparent photographic magnitude from the CGCG or the UGC,

Column (4) Total on-source integration time (minutes),

Table II List of non-detected and possibly detected galaxies

(1)	(2)		(3)	(4)	(5)	(6)	(7)		(8)
name	α_{1950} (h m s)	δ_{1950} (° ′)	m_p	integration time (min)	3σ flux limit (mJy)	velocity range (km s^{-1})	publ. vel. HRBH (km s^{-1})	HDLT	notes
NGC 2415 group									
anon	07 33 54	+35 46	15.3	80.0	18	3195-4445			
NGC 2798 group									
anon.	09 12 30	+42 28	14.8	65.0	23	1052-2284			
anon.	09 15 42	+42 13	15.6	47.5	"	"			
NGC 3158 group									
NGC 3158	10 10 48	+39 01	13.4	27.5	30	6499-7775		+6817	
NGC 3206 group									
UGC 5579	10 17 18	+57 28	15 5	27 5	52	503-1731			
anon.	10 19 06	+57 18	15.6	20.0	"	"			
NGC 3214	10 19 48	+57 18	15.2	27.5	44	"			
NGC 3329 group									
UGC 5854	10 41 36	+77 22	15.2	35.0	131	1033-2265			a
UGC 5926	10 46 30	+77 13	14 4	17.5	117	"			
NGC 3656 group									
NGC 3656	11 20 48	+54 07	13.4	22.5	44	2184-3425		+2828	
anon	11 19 32	+53 58		47.5	33	"			b
UGC 6446	11 23 48	+54 01	14.5	40.0	40	"	+643,+646		
NGC 4111 group									
UGC 7069	12 02 24	+43 25	15.7	40.0	53	168-1392			
NGC 4117	12 05 12	+43 24	14.3	17.5	44	"		+958	c
NGC 4725 group									
NGC 4712	12 47 06	+25 44	13.5	67.5	19	455-1682	+4376,+4429		
anon.	12 47 36	+25 17	15 4	55.0	21	"			d
anon.	12 50 42	+25 32	15.5	45.0	19	"			
NGC 5322 group									
NGC 5322	13 47 36	+60 26	11.3	37.5	42	1247-2481	+1902	+1804	
NGC 5342	13 49 48	+60 07	14.4	70 0	38	"		+2208	
NGC 5376	13 53 36	+59 45	12.9	97.5	30	"	+2077	+2064	e
NGC 5689 group									
NGC 5689	14 33 42	+48 57	12.7	40.0	29	1553-2790	+2160	+2163	f
NGC 5700	14 35 18	+48 25	15 2	22 5	36	"			g
NGC 5899 group									
anon.	15 11 36	+42 31	15.4	107.5	17	1886-3254			h
NGC 5893	15 11 42	+42 09	14.1	120 0	8	"	+5381	+5381	
NGC 5895/ 5896	15 12 00	+42 11	15.5	82.5	14	"			
Isolated galaxy									
UGC 10070	15 49 42	+47 23	13.6	77.5	19	1971-3211	+2618	+5958	
"	" " "	" "	"	45.0	28	5435-6702		"	
NGC 6340 group									
NGC 6340	17 11 18	+72 21	11.9	90 0	41	1456-2692	+1199,+1903		i
UGC 10713	17 05 24	+72 31	13.8	100.0	46	"			
UGC 10769	17 12 24	+72 27	14.7	40.0	76	"			
anon.	17 12 54	+72 39	15 3	27 5	"	"			
UGC 10791	17 15 30	+72 27	15.5	67.5	58	"			

a Possible detection at +1790 km s^{-1}
b α,δ measured from PSS
c NGC 4118 in the same beam ($\Delta\alpha\cos\delta$=1 ′1, $\Delta\delta$=1′)
d Possible detection at +1035 km s^{-1}
e 3σ flux density upper limit given by Knapp et al. (1977) is about 71 mJy
f Huchtmeier (1982) reports F_H=2.8 Jy km s^{-1} (velocity width 390 km s^{-1})
g Possible detection at +2284 km s^{-1}
h Possible detection at +2674 km s^{-1}
i UGC 10757, for which a velocity of +1193 km s^{-1} is given by Shostak et al. (1979), is in the same beam

Column (5) The 3σ flux density upper limit (mJy), where σ is the empirical rms fluctuation,

Column (6) The velocity range investigated (km s^{-1}),

Column (7) Velocities as given by HRBH and HDLT,

Column (8) Notes

Table II includes five primary galaxies, one isolated galaxy (which was observed in two velocity bands) and 25 companions

The groups for which results are reported in Tables I and II are discussed briefly below Each group is identified by its primary galaxy

NGC 2415 group

NGC 2415 is accompanied by a compact group of three companions about 22' north of the primary Besides in NGC 2415, HI line emission was detected in an observation centered on UGC 3937 Another (anonymous) companion was searched for but not detected With the beam centered on UGC 3937 there may be confusion with UGC 3934 ($\Delta\alpha\cos\delta = 1\,2$, $\Delta\delta = 3$) HI observations by Thuan et al (1979) with the 91-m Green Bank telescope centered on UGC 3934 yield an upper limit of 13 6 Jy km s^{-1}, taking the confusion with UGC 3937 into account and the fact that the profile width of UGC 3937 is 323 km s^{-1} (the observed velocity interval was -400 to +5800 km s^{-1}) This value is in agreement with the value given by Peterson (1979) and, within the errors, with the presently observed flux

The line profile of NGC 2415 is in good agreement with previously published profiles, except for the presence of a high velocity feature at about 4050 km s^{-1} with a velocity width of 200 km s^{-1} No confusion is possible with the companion galaxies The high velocity feature was excluded in calculating the results quoted in Table I Including it gives a systemic velocity of about 3874 km s^{-1} which is substantially higher than published values

NGC 2798 is the brightest galaxy in a group with at least nine members, three of which were searched for in HI Only the primary galaxy was detected This galaxy forms a close double system with NGC 2799 ($\Delta\alpha\cos\delta$ = 1'6, $\Delta\delta$ = 0'3) and is included in the Atlas of Peculiar Galaxies (Arp, 1966) It has been observed with the 91-m (Green Bank) radio telescope by Peterson and Shostak (1974, pointing about 3' South East of the center of interaction) and by Huchtmeier (1982) It has also been observed at Nançay by Bottinelli et al (1980, who also reported a detection at the position of NGC 2799 Bottinelli et al, 1982a, b) The shape of the line profiles of NGC 2798 published by these authors is in good agreement with the profile shown in Figure 1 Because of the small angular separation between NGC 2798 and NGC 2799 confusion is expected Moreover, the HI line profile may include a contribution from UGC 4904, 5 south from the primary galaxy In fact, at the optical velocity of NGC 2799 (+1882 km s^{-1}, HDLT) a signal at the 3σ level can be seen, both here and in previously published profiles The uncorrected HI flux at the position of NGC 2798, including this 3σ feature, is 4 7 Jy km s^{-1} which is less than half the value quoted elsewhere Correcting this flux in the standard way for an offset of 0'7 west from the optical center of NGC 2798 yields a value of 5 2 Jy km s^{-1}, which is still significantly lower than other published values This discrepancy could largely be explained if the gas associated with NGC 2798 were displaced in the direction of NGC 2799 (east of the primary) This system is clearly a good candidate for high resolution observations

NGC 3158 group

The NGC 3158 group includes ten companion galaxies within a radius of about 18', five of which have known optical velocities (CGCG) Because of the expected extensive confusion, only the primary galaxy has been observed, in order to resolve discordant reported velocities (HDLT +6817 km s^{-1}, CGCG +7024 km s^{-1}) However, no HI detection was made at either of these velocities, as might have been expected for a galaxy classified as elliptical

NGC 3206 group

NGC 3206 is surrounded by four companions within 17 of the primary All have been searched for in HI Other than the primary galaxy, only NGC 3220 was detected No previous HI observations of this galaxy have been reported The $[M_{HI}/L_B]$-value given in Table I agrees with values generally found for Sb galaxies The measured flux of NGC 3206 is in agreement with published values Outside the 17' radius there are five companions, four of which form a small sub-group

NGC 3329 group

UGC 5841 is one of the seven companions listed in the CGCG, all within 24' of NGC 3329 No references to previous HI observations could be found for this galaxy nor for any other galaxy in this group Because of the high declination (+77°) the observed flux in the 21-cm line is very uncertain UGC 5841 is located SE of NGC 3329 ($\Delta\alpha\cos\delta$ = 1'3, $\Delta\delta$ = 7'). When pointing at UGC 5841, the optical center of NGC 3329 falls close to the half-power ellipse of the Nançay beam Therefore, the observed line profile at the position of UGC 5841 may, in whole or in part, be attributed to NGC 3329 Moreover, the difference between the systemic velocity derived from the line profile of UGC 5841, shown in Figure 1, and the value for NGC 3329 given by Chincarini and Rood (1972), is only 77 km s^{-1} Because the position angle of NGC 3329 is 140°, a contribution to the observed line profile will mainly come from the SE part of this galaxy This might explain why we observed a single horned line profile at the position of UGC 5841, whereas a double horned profile could be expected for this inclined galaxy The attenuation at the NW extremity of the major axis of NGC 3329 (UGC diameter 2'1) is about 2 5 times that at the SE extremity Therefore we expect an uncorrected flux density from the NW side of about 45 mJy, as is actually observed at V = 1850 km s^{-1} The corrected $[M_{HI}/L_B]$-value for this Sb galaxy would then be 0 72. Two more members of this group were searched for but no emission was found

NGC 3656 group

The seven companion galaxies of NGC 3656 are located within 27' of the primary Two companions and the primary were searched for but not detected The flux density upper limit of NGC 3656 is 6 6 Jy km s^{-1} (assuming a velocity width of 150 km s^{-1}). The value

given by Hunter et al. (1982) is 10.5 Jy km s^{-1}; however no information regarding the velocity width and interval is given by these authors.

NGC 4111 group

The primary galaxy (classified SA(r)0^+: sp; 2RCBG) has been searched for by FT with the 91-m telescope at Green Bank, but no emission was found in the velocity range -400 to +3000 km s^{-1}. The observed 21-cm line flux in the Nançay observation implies an HI mass of 2.2×10^6 $M_\odot$ Mpc^{-2} (uncorrected), which is below the detection limit of the Green Bank observation assuming a velocity width of 327 km s^{-1}, but a preliminary examination of a recent WSRT observation does not appear to confirm this detection. NGC 4111 is accompanied by at least eight companions within 21' and, because of the relatively large beam of the Nançay telescope compared with the radius of this group, confusion with one or more of these companions must be considered. Possible candidates for confusion could be NGC 4109 (Sa?, 2RCBG; m_{pg} = 15.1, UGC) and a small anonymous galaxy about 4' south of NGC 4111. No observations have been reported for these galaxies. However, both galaxies appear too small to give such a wide signal. Moreover, the $[M_{HI}/L_B]$-value for the early type galaxy NGC 4109 would be very high. If the HI detected in the Nançay observation is in fact associated with NGC 4111, then the systemic velocity agrees well with the value of +791 km s^{-1} quoted by Sandage and Tammann (1981). The value for the HI mass to blue luminosity of this early type galaxy would be about 0.08. This is greater than the upper limit for the majority of S0 galaxies of 0.01 derived by Burstein and Krumm (1981) and falls near the low end of the range of values for early type spirals (Bottinelli et al., 1980; Huchtmeier, 1982). It is greater than the mean value of 0.04 for HI rich ellipticals (Gouguenheim, 1979; see also Knapp, 1983) and agrees with values found for HI rich lenticulars (van Woerden, 1983). Four more galaxies in this group were searched for, one of which (UGC 7089) was detected. Because no accurate position is available for this galaxy, the observed HI flux was corrected only for beam filling. This galaxy shows an optical extension to the north-east which may explain the asymmetrical shape of the observed line profile. The total HI flux is about 78% of the value measured (at the same position) by FT.

NGC 4725 group

This group includes four companions within 38 of the primary HI emission was detected from the primary galaxy and from NGC 4747 An anonymous galaxy, 29 south of the primary, was possibly detected NGC 4725 and NGC 4747 have recently been observed with the WSRT (Wevers et al , 1984) The integrated HI surface density map of NGC 4747, published by these authors, shows a long plume of HI which extends from the center of the galaxy toward the NE The HI distribution in NGC 4725 is dominated by a prominent outer arm, east of the center and an extended distribution of the gas toward the SW These features fall outside the half power ellipse of the Nançay telescope This may explain the difference in the profile shapes determined from the WSRT and Nançay observation The flux values listed in Table I (column 8) are therefore only lower limits, no corrections were applied

NGC 5322 group

This group consists of at least three faint companions within 44' of the primary One companion and the primary were searched for but not detected Outside this 44' region are two relatively bright galaxies One of these, NGC 5376, was searched for but no emission was found Note that the presently found upper limit to the HI flux (30 mJy) is lower than the value of 71 mJy, given by Knapp et al (1977)

NGC 5689 group

This group contains four companions within 19' of the primary Besides the primary, two companions were searched for NGC 5693 was the only galaxy detected in this group

NGC 5899 group

All galaxies in this group were searched for in HI Besides in NGC 5899, HI line emission was detected in an observation centered on NGC 5900 Because of the small angular separation between these galaxies (NGC 5900 is located 10' north of NGC 5899) confusion is expected and no definite conclusion with regard to the possible detection of NGC 5900 can be drawn from the present observations In fact, the flux observed at the position of

NGC 5900 is about the expected flux from NGC 5899, considering the beam attenuation factor of 0.55. Moreover, the major axis of NGC 5899 is nearly north-south, so that one might expect an asymmetrical line profile, as is actually observed at the position of NGC 5900. The peak at V = 2800 km s ^{1}, which is missing from the profile observed at the position of NGC 5900, would then originate in the southern part of NGC 5899. The observed velocity and profile width of NGC 5899 are in good agreement with Nançay observations made by Bottinelli et al. (1982a, b), with 91-m Green Bank observations made by Peterson (1979) and with Jodrell Bank (Mark I) observations made by McCutcheon et al. (1970). The HI flux obtained by Peterson (17.1 Jy km s^{-1}) is only slightly less than the Nançay values. This suggests that the contribution from NGC 5900 to the Nançay line profile of NGC 5899 is small (less than 3 Jy km s^{-1}), in contradiction with the flux of 26.6 Jy km s^{-1} for NGC 5900 reported by Bottinelli et al. (1982a, b). The remaining three companions were searched for and one was possibly detected.

NGC 6340 group

This group includes five companions within 28′ of NGC 6340. The primary galaxy, classified as S0/a (2RCBG), has been observed in the 21-cm line by several observers, using different telescopes. The results are contradictory : Bottinelli et al. (1970) and Bottinelli et al. (1976) reported from Nançay observations a systemic velocity of about 1900 km s^{-1}. Green Bank observations made by Balick et al. (1976) and Huchtmeier (1982), using the 43-m and 91-m telescope respectively, yield velocities of about 1200 km s^{-1}, in agreement with the optical velocity measured by Faber (see Balick et al., 1976). Shostak et al. (1979), using the high resolution of the WSRT, showed that the HI radiation at 1200 km s^{-1} is actually associated with IC 1251, a small Sc galaxy about 7′ north of NGC 6340. No emission was found associated with NGC 6340 in the velocity range +970 to +1400 km s^{-1}. From recent Nançay observations of NGC 6340 (where confusion with only IC 1251 is possible while at Green Bank IC 1254 is also in the beam), Balkowski et al. (1983) concluded, after careful inspection, that their detection of NGC 6340 at 1205 km s^{-1} is probably free from any confusion. No signal was measured from IC 1254 in the velocity range +700 to +1600 km s^{-1}. The HI fluxes measured by several observers at the position of NGC 6340 and at velocities around 1200 km s^{-1}, are in very good agreement (15.3 Jy km s^{-1}). If we attribute this flux to IC 1251 then, accounting for the attenuation by the different beams, we compute an $[M_{HI}/L_B]$ of about 0.76 from the 43-m and the Nançay observation, and about 1.8 from the 91-m Green Bank observation. Only the latter value is consistent with $[M_{HI}/L_B] > 1.4$, given by Shostak et al. (1979).

In view of the sparse data at higher velocities, an observation of this group was made in the velocity interval +1456 to +2692 km s^{-1}. All galaxies in the group were searched for but no emission was found. The HI flux upper limit for NGC 6340 of 12.3 Jy km s^{-1}, assuming a velocity width of 300 km s^{-1}, is marginally consistent with the detection made by Bottinelli et al. (1970) who report an observed flux of 12.02 Jy km s^{-1} but give no velocity width. The upper limit measured for UGC 10791 (5.8 Jy km s^{-1}) is between the values quoted by FT and Thuan et al. (1979), assuming a velocity width of 100 km s^{-1}.

Isolated galaxies

Three isolated galaxies from the list of Huchra and Thuan (1977) were observed in order to resolve discordant velocities reported in the literature or by private communication. NGC 2684 was marginally detected at a velocity which confirms the result reported in HDLT. NGC 6012 was strongly detected. The velocity and velocity width are in agreement with published values; the observed HI flux is 67% of the average of published values. UGC 10070 was not detected at either of the published velocities : +5958 km s^{-1} (HDLT) and +2618 km s^{-1} (Balkowski and Chamaraux, 1981, who reported an HI line flux marginally in contradiction with the present upper limit of 4.3 Jy km s^{-1}, using their velocity width of 228 km s^{-1}).

3 Conclusions

In total 43 galaxies located in 12 groups were examined in the 21-cm line of HI with the Nançay radio telescope. 12 galaxies were detected, 6 out of 11 primary galaxies and 6 out of 32 companions. In addition, four companion galaxies were possibly detected. During this period 41% of the total number of companions located in the 12 groups were actually examined. Four of the five undetected primary galaxies are of early morphological type. Several of the non-detected companions in this sample could have systemic velocities which lie outside the observed velocity range. These companions could be background galaxies, not gravitationally bound to the primary. An example is NGC 5893 (in the NGC 5899 group) whose systemic velocity, given in HDLT and HRBH, lies far beyond the presently observed velocity band (Table II). For two groups, NGC 5899 and NGC 6340, all members were searched for in HI. No emission was found for NGC 6340 or its companions; for the NGC 5899 group the primary galaxy was detected.

Confusion was often present because of the relatively small angular sizes of the groups, so that additional high resolution observations are generally required for a complete study.

Three new detections in HI are reported in section 2 : NGC 3220, NGC 4111 (doubtful) and UGC 5841 (which may be confused with NGC 3329). If the detection of NGC 4111 is correct then it is another example of a lenticular galaxy with a detectable amount of neutral hydrogen. For NGC 2684 (an isolated galaxy) new values for the HI line flux, profile width and systemic velocity are given, based on the detection at a velocity which is close to the optical result reported by HDLT but in disagreement with other reported velocities. At these velocities no HI signal could be found. The $[M_{HI}/L_B]$-values for the detected companion galaxies, which are all of late morphological type, range between 0.20 and 0.63 (except for UGC 5841). This range of values is not significantly different from previously reported values for late type field galaxies (Roberts, 1969; Shostak, 1978) and late type dwarf galaxies (Fisher and Tully, 1975).

Acknowledgements

The author is very grateful to the observers and technical staff of the Nançay Decimetric Radio Telescope, especially to Dr. I. Kazès and D. Aubry for their valuable help during the observations and reduction, to Prof. Dr. W.W. Shane, Dr. S. Shostak and an anonymous referee for critically reading the manuscript and constructive comments, and to Dr. N. Krumm for several useful remarks.

References

Arp, H.C. : 1966, Astrophys. J. Suppl. Ser. 14, 1

Bahcall, J.N., Tremaine, S.: 1981, Astrophys. J. 244, 805

Balick, B., Faber, S.M., Gallagher, J.S.: 1976, Astrophys. J. 209, 710

Balkowski, C., Chamaraux, P.: 1981, Astron. Astrophys. 97, 223

Balkowski, C., Chamaraux, P.: 1983, Astron. Astrophys. Suppl. Ser. 51, 331

Bottinelli, L., Chamaraux, P., Gouguenheim, L., Lauque, R.: 1970, Astron. Astrophys. 6, 453

Bottinelli, L.: 1971, Astron. Astrophys. 10, 437

Bottinelli, L., Chamaraux, P., Gouguenheim, L., Heidmann, J.: 1973, Astron. Astrophys. 29, 217

Bottinelli, L., Gouguenheim, L.: 1976, Astron. Astrophys. 47, 381

Bottinelli, L., Gouguenheim, L., Paturel, G.: 1980, Astron. Astrophys. 88, 32

Bottinelli, L., Gouguenheim, L., Paturel, G.: 1981, Astron. Astrophys. Suppl. Ser. 44, 217

Bottinelli, L., Gouguenheim, L., Paturel, G.: 1982a, Astron. Astrophys. Suppl. Ser. 47, 171

Bottinelli, L., Gouguenheim, L., Paturel, G.: 1982b, Astron. Astrophys. 113, 61

Burstein, D., Krumm, N.A.: 1981, Astrophys. J. 250, 517

Chamaraux, P., Balkowski, C., Gérard, E.: 1980, Astron. Astrophys. 83, 38

Chincarini, G., Rood, H.J.: 1972, Astron. J. 77, 4

Dressel, L., Condon, J.: 1976, Astrophys. J. Suppl. Ser. 31, 187

Fisher, J.R., Tully, R.B.: 1975, Astron. Astrophys. 44, 151

Fisher, J.R., Tully, R.B.: 1981, Astrophys. J. Suppl. Ser. 47, 139 (FT)

Fouqué, P.: 1983, Astron. Astrophys. 122, 273

Foy, F., Guelin, M., Weliachew, L.: 1968, Internal Report No. 23/68, (Radioastronomie, Observatory of Paris)

Gallouët, L., Heidmann, N., Dampierre, F.: 1973, Astron. Astrophys. Suppl. Ser. 12, 89

Gordon, D., Gottesman, S.T.: 1981, Astron. J. 86, 161

Gouguenheim, L.: 1979, in Photometry, Kinematics and Dynamics of Galaxies, ed. D.S. Evans (University of Texas Press) p. 201

Hewitt, J.N., Haynes, M.P., Giovanelli, R.: 1983, Astron. J. 88, 272

Huchra, J., Thuan, T.X.: 1977, Astrophys. J. 216, 694

Huchra, J., Davis, M., Latham, D., Tonry, J.: 1983, Astrophys. J. Suppl. Ser. 52, 89 (HDLT)

Huchtmeier, W.K.: 1982, Astron. Astrophys. 110, 121

Huchtmeier, W.K., Richter, O.G., Bohnenstengel, H.D., Hauschildt, M.: 1983, ESO preprint, No. 250 (HRBH)

Hunter, D.A., Gallagher, J.S., Rautenkranz, D.: 1982, Astrophys. J. Suppl. Ser. 49, 53

Knapp, G.R., Gallagher, J.S., Faber, S.M., Balick, B.: 1977, Astron. J. 82, 106

Knapp, G.R.: 1983, in Internal Kinematics and Dynamics of Galaxies (IAU Symp., No. 100), ed. E. Athanassoula (Reidel) p. 297

McCutcheon, W.H., Davies, R.D.: 1970, Monthly Notices Roy. Astron. Soc. 121, 531

Nilson, P.: Uppsala General Catalogue of Galaxies, Ann. Uppsala Astron. Obs. 6 (UGC)

Peterson, S.D., Shostak, G.S.: 1974, Astron. J. 79, 767

Peterson, S.D.: 1979, Astrophys. J. Suppl. Ser. 40, 527

Roberts, M.S.: 1969, Astron. J. 74, 859

Sandage, A., Tammann, G.: 1981, Revised Shapley-Ames Catalog of Bright Galaxies (Carnegie Institution of Washington Publication)

Shostak, G.S.: 1975, Astrophys. J. 198, 527

Shostak, G.S.: 1978, Astron. Astrophys. 68, 321

Shostak, G.S., van Woerden, H., Schwarz, U.J.: 1979, in Photometry, Kinematics and Dynamics of Galaxies, ed. D.S. Evans (University of Texas Press), p. 213

Thuan, T.X., Seitzer, P.O.: 1979, Astrophys. J. 231, 327

de Vaucouleurs, G., de Vaucouleurs, A., Corwin, H.G.: 1976, Second Reference Catalogue of Bright Galaxies (University of Texas Press) (2RCBG)

Wevers, B.M.H.R., Appelton, P.N., Davies, R.D., Hart, L.: 1984, Astron. Astrophys. 140, 125

van Woerden, H., van Driel, W., Schwarz, U.J.: 1983, in Internal Kinematics and Dynamics of Galaxies (IAU Symp., No. 100), ed. E. Athanassoula (Reidel) p. 99

Zwicky, F., Herzog, E., Wild, P., Kapowicz, M., Kowal, C.T.: 1961-1968, Catalogue of Galaxies and Clusters of Galaxies (California Institute of Technology) Vols I-VI (CGCG)

CHAPTER 6 THE MASS OF THE EARLY-TYPE GALAXY NGC 2859 INFERRED FROM HI OBSERVATIONS OF ITS COMPANIONS

Summary

We present 21-cm line HI observations of the early-type galaxy NGC 2859 and its late-type companions. Four of the companions appear to be rich in HI and have redshifts comparable to that of NGC 2859. This and the small crossing time of the group suggest that these companions are bound to NGC 2859 and that the total mass may be inferred from the radial velocities and projected distances from NGC 2859. Applying the so-called projected mass method of Bahcall and Tremaine (1981) yields $M_0 = 1.4\ 10^{12}\ h^{-1}\ M_\odot$ ($H_0 = 100$ h km s^{-1} Mpc^{-1}). The corresponding $[M/L_B]$-value of 56 h for this group is in agreement with values generally found in small groups of galaxies. The value of M_0 provides a measurement of the mass within a region centered on NGC 2859 and with an average deprojected radius of roughly seven times the Holmberg radius of the galaxy. Subtracting the luminosities and the estimated masses of the companions, we find, for the S0 galaxy alone, an $[M/L_B]$-value of about 60 h. This is three times the average value found within one Holmberg radius for early-type galaxies. The increase of M/L_B with galactocentric radius is less than that would be required for a flat rotation curve.

1 Introduction

Observations of neutral hydrogen in and around the barred lenticular galaxy NGC 2859 are presented and discussed in this paper. This galaxy is a representative of the class of single bright galaxies accompanied by several much fainter companions. High resolution HI observations by Shane and Krumm (1983) have shown that several of these companions are rich in HI and have systemic velocities close to that of NGC 2859. If this small group is bound, we can use the projected mass method proposed by Bahcall and Tremaine (1981) to estimate the mass of the dominating central galaxy, NGC 2859. These calculations are of particular interest because they provide the mass and, consequently, M/L_B out to several Holmberg radii, so that information can be obtained regarding the presence of a possible dark halo. This kind of data is available for only a very limited sample of lenticulars, and, as noted by Fall (1986), the results are not always free from ambiguity. Therefore, the projected mass method applied in this paper might provide important additional data on the distribution of mass around early-type galaxies.

Aside from the HI-rich companions, the high resolution HI observations made by Shane and Krumm (1983) indicated that gas might be present in two dark clouds and in the optical ring around NGC 2859. The gas surrounding NGC 2859 might play an important role in the future evolution of this galaxy. If it were captured by NGC 2859 it could turn it into a gas-rich S0. Such accretion events have been proposed for several other S0 galaxies, e.g. NGC 2685 (Shane, 1980) and NGC 1023 (Sancisi et al., 1984), and may account for the wide range in the HI content and distribution in galaxies of this morphological type. A more extensive review of the HI content in lenticular galaxies is given by van Woerden et al. (1983) and Wardle and Knapp (1986). However, several of the detections reported by Shane and Krumm were uncertain and required confirmation. Therefore, new and more sensitive observations with the Westerbork Synthesis Radio Telescope (WSRT) were made. Since three of the detections reported by Shane and Krumm were near the band-edge, the observed velocity interval in the new observations was increased to 1000 km s^{-1}. These new observations are presented in this paper.

In section 2 we describe the NGC 2859 group of galaxies. In section 3 the observations and reduction procedures are discussed and section 4 gives the results. In section 5 the projected mass method is applied and the resulting mass is discussed. Section 6 deals with the central galaxy.

2 The NGC 2859 group of galaxies

Figure 1 is a photograph of the NGC 2859 group of galaxies. This photograph is a reproduction of a 60 minute blue exposure with the 48 inch Palomar Schmidt made by H. Arp, on November 30th 1979 (see Arp, 1980). The brightest galaxy of the group is the early-type galaxy NGC 2859, which, according to de Vaucouleurs (1965), is a member of the Leo II cloud complex. The galaxy is barred and possesses a bright outer ring; the morphological type assigned by de Vaucouleurs et al. (1976, hereafter 2RCBG) is RSBO/*a*. Photoelectric UBV color measurements made by Gallagher and Wirth (1980) indicate a dominant old stellar population; obvious dust lanes or knots are absent. Photographs of the central part of the galaxy have been published by de Vaucouleurs (1959) and by Sandage (1961).

NGC 2859 is an example of the class of galaxies which are accompanied by several faint companions (van der Burg, 1985). Other members of this class recently investigated are NGC 1023 (Sancisi et al., 1984), NGC 3992 (Gottesmann et al., 1982), NGC 4111 (van der Burg, 1987) and NGC 4731 (Gottesmann et al., 1984). From Figure 1 it can be seen that the galaxy is apparently located at the center of a group of six faint galaxies within about 30' of the primary, of which the brightest is about 3.5 mag fainter than NGC 2859. These six galaxies are: UGC 4988, 5004, 5011, 5014, 5015 and 5020 (Nilson, 1973, hereafter UGC). Three of these companions, (UGC 4988, 5015 and 5020), are also catalogued by Zwicky et al. (1961 - 1968). According to Arp (1980) each of the companions UGC 4988, 5004, 5015 and 5020 is associated with an object of high redshift. In a study of a possible relationship, Arp measured the systemic velocities of these four companions. These values are generally consistent with the systemic velocities published by Shane and Krumm (1983) as determined from a previous WSRT observation. The velocities of these companions are all close to the optically derived systemic velocity of NGC 2859 of 1685 $\pm$ 14 km s^{-1}, obtained by Tonry and Davis (1981) (the velocities in this paper are heliocentric and calculated according to the conventional optical definition). Correcting this velocity for the solar motion with respect to the Local Group and adopting a linear Virgocentric flow model for the velocity field of the Local Supercluster (Aaronson et al., 1982, solution 3.1), yields a distance D of 21.5 h^{-1} Mpc, which will be used throughout this paper, where the Hubble constant is H_0 = 100 h km s^{-1} Mpc^{-1}. Optical data for NGC 2859 and its companions are summarized in Tables 1a and b respectively. For NGC 2859 the blue luminosity L_B was calculated from the total blue magnitude B_T^0 listed in 2RCBG. The magnitudes, optical dimensions and morphological types of the companions are taken from the UGC catalogue. Since the positions listed in this catalogue showed some deviation from the optical centers of the galaxies on the print reproduced in Figure 1, new

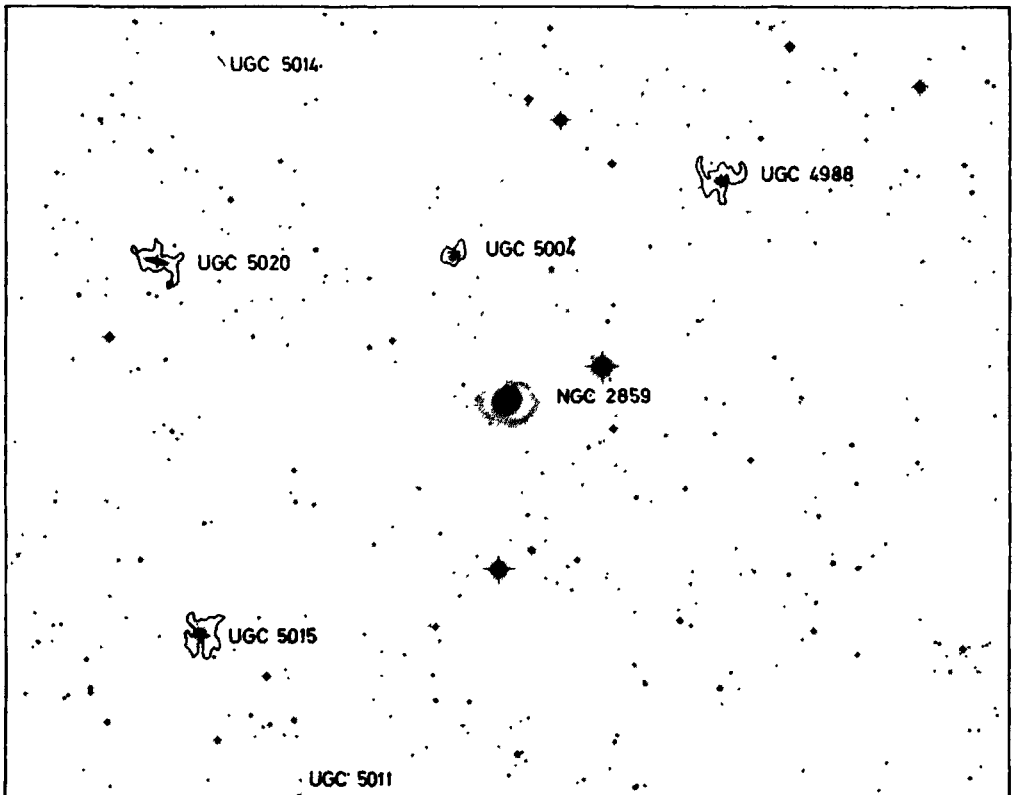

Figure 1. *Reproduction of the photograph by H. Arp showing the NGC 2859 group. On each companion the lowest contour of the HI distribution shown in Figure 4 is superimposed.*

Table 1a. Optical data for NGC 2859

		Ref.
α_{1950}	$09^h 21^m 15\overset{s}{.}9$	1
δ_{1950}	+34°43′41″	1
Type	RSBO/a	2
Optical dimensions	4′.7 × 4′.2	3
Holmberg radius	3′.3	3
m_{pg}	11.8	3
B_T^0	11.36	2
$(B-V)_{center}$	1.00	4
$(U-B)_{center}$	0.58	4
Inclination	30°	3
Position angle	85°:	3
Distance	21.5 h^{-1} Mpc	5
Blue luminosity	2.1 10^{10} h^{-2} $L_\odot$	2

1: Dressel and Condon (1976)
2: de Vaucouleurs et al. (1976)
3: Nilson (1973)
4: Gallagher and Wirth (1980)
5: This paper

positions were measured from this print (based on the positions of four AGK2 stars in the field of NGC 2859). The inclination, Holmberg radius and B_T^0 of the companions were derived using the precepts given by Fisher and Tully (1981). The absolute magnitude of the sun is taken to be 5.48 mag.

Table 1b Optical data for the companions of NGC 2859

	UGC 4988	UGC 5004	UGC 5011	UGC 5014	UGC 5015	UGC 5020	Ref
α_{1950}	$09^h\,20^m\,12^s$	$09^h\,21^m\,31^s$	$09^h\,22^m\,17^s$	$09^h\,22^m\,39^s$	$09^h\,22^m\,46^s$	$09^h\,22^m\,59^s$	1
δ_{1950}	+34°56 53″	+34°52 32′	+34°19′39	+34°52 14	+34°29′35″	+34°52 14′	1
Type	SAB m	AB m	SBc		SAB dm	Sc	2
Optical dimensions	1′1 × 0′9	1 4 × 1 1	1′2 × 0′9	1 1 × 0 1	2′0 × 1 8	2 3 × 0 5	2
Holmberg radius	1 2	1 1	1′0	1′0	1′6	1′8	2
m_{pg}	15 7	16 5	16 0	17 0	15 7	15 3	2
B_T^0	15 2	15 8	15 4	15 9	14 2	14 9	2
Inclination	34°	37°	40°	84°	25°	78°	2
Position angle	70°	130°	165°	38°	20°	79°	2
Separation from NGC 2859	18′6	9′3	29′2	31′8	23′3	22′8	1
Blue luminosity ($10^9\,h^{-2}\,L_\odot$)	0 6	0 4	0 5	0 3	1 5	0 8	2
Absolute magnitude (M_B)	-16 5	-15 9	-16 6	-15 8	-17 5	-16 8	2

1 This paper
2 Nilson (1973)

3 Observations and reduction

The NGC 2859 group of galaxies was observed with the WSRT during two 12-hour periods in July 1981. The two observations were made with different baseline configurations but were reduced as a single unit. The minimum and maximum baselines in the combined observation are 54 m and 1458 m respectively, so that with an increment

of 36 m, 40 different baselines were sampled. The half-power dimensions of the synthesized antenna pattern are 24″3 × 42″3 (α × δ). Orthogonal polarizations were recorded with the 5120-channel digital line backend (Bos et al., 1981). The total bandwidth of 5 MHz was divided into 63 frequency channels, centered at a velocity of 1670 km s^{-1}. Hanning smoothing in frequency yielded a velocity resolution (FWHM) of 33.4 km s^{-1}. A summary of the observational parameters is given in Table 2. After standard calibration

Table 2. Observational parameters

Observing dates	16 July 1981,	25 July 1981
Duration	12 hours;	12 hours
Baselines (min, max, increment)	90, 1458, 72 m,	54, 1422, 72 m
α field center (1950)	$09^h 21^m 12^s$	
δ field center (1950)	+34°44′	
Synthesized beam (α × δ)	24″3 × 42″3	
Primary beam (FWHM, α × δ)	36′	
First grating ring diameter (α × δ)	20′.2 × 35′.6	
Bandwidth	5 MHz	
Number of frequency channels	63	
Central velocity	1670 km s^{-1}	
Channel spacing	16.6 km s^{-1}	
Velocity resolution (FWHM)	33 4 km s^{-1}	
R m s. noise in channel maps	0.75 K	

and correction the continuum data were Fourier-transformed into a map of the intensity distribution in the observed field (Hogbom and Brouw, 1974). The strongest point sources were measured by fitting the antenna pattern to the data and then subtracted in the U-V domain before the transforms of the individual channel maps were made. None of the continuum sources appeared to be associated with NGC 2859 or any of the faint galaxies seen in Figure 1. The fluxes and positions of the continuum sources stronger than 10 mJy (after correction for primary beam attenuation) are listed in Table 3.

Table 3. Radio continuum sources in the field

α_{1950} h m s	δ_{1950} ° ′ ″	S_{1413} mJy
09 19 32.2	+34 22 48	27.6
09 19 38.7	+34 41 45	13.8
09 19 49.8	+35 12 32	58.1
09 20 01.0	+34 27 44	256*
09 20 38.6	+35 06 03	22.9
09 20 38.6	+34 30 44	27.3
09 20 40.5	+34 43 14	24.4
09 20 59.5	+35 09 14	28.2
09 21 06.8	+34 59 05	12.3
09 21 13.4	+34 20 35	22.5
09 22 33.5	+34 51 15	30.4
09 22 44.4	+34 14 33	115.0
09 23 03.7	+34 47 36	12.0
09 23 10.9	+35 00 19	184*
09 23 43.4	+34 35 17	27.4
09 23 49.1	+34 28 06	135.5

* Extended sources, flux determined by integrating over the source

Because of band-edge effects six of the channel maps (one at the lowest velocity and five at the highest velocities) were discarded. The remaining channel maps were examined for the presence of 21-cm line radiation. A continuum correction map was made by averaging 22 channels which were free from line radiation. These 22 channels were equally divided between the low and high velocity ends of the observed velocity interval. Residual continuum radiation was removed by subtracting this correction map from each channel map. In order to remove grating rings associated with HI line emission the continuum corrected channel maps were cleaned to a level of about two times the r.m.s. noise and restored using the central maximum of the synthesized antenna pattern. On these maps emission associated with UGC 4988, 5004, 5015 and 5020 can be seen. The signal-to-noise ratio of the channel maps was then increased by convolving to a resolution of 60″ × 60″ ($\alpha \times \delta$). The detections of NGC 2859, UGC 5011, UGC 5014 and

the two dark clouds reported by Shane and Krumm (1983) were not confirmed. These suspected detections may have resulted from low-level interference.

Using the 60 arcsec maps the velocity range of each companion was determined. For each companion a second correction map was constructed by averaging 20 channel maps, ten channels below and ten channels above the corresponding velocity interval. In order to correct for possible local baseline offsets within the 5 MHz wide frequency band, this second correction map was subtracted from the individual channel maps, resulting in a final set of full resolution channel maps for each companion. A representative set of these maps is shown in Figure 2. The maps have not been corrected for primary beam attenuation in the interest of maintaining a uniform noise level.

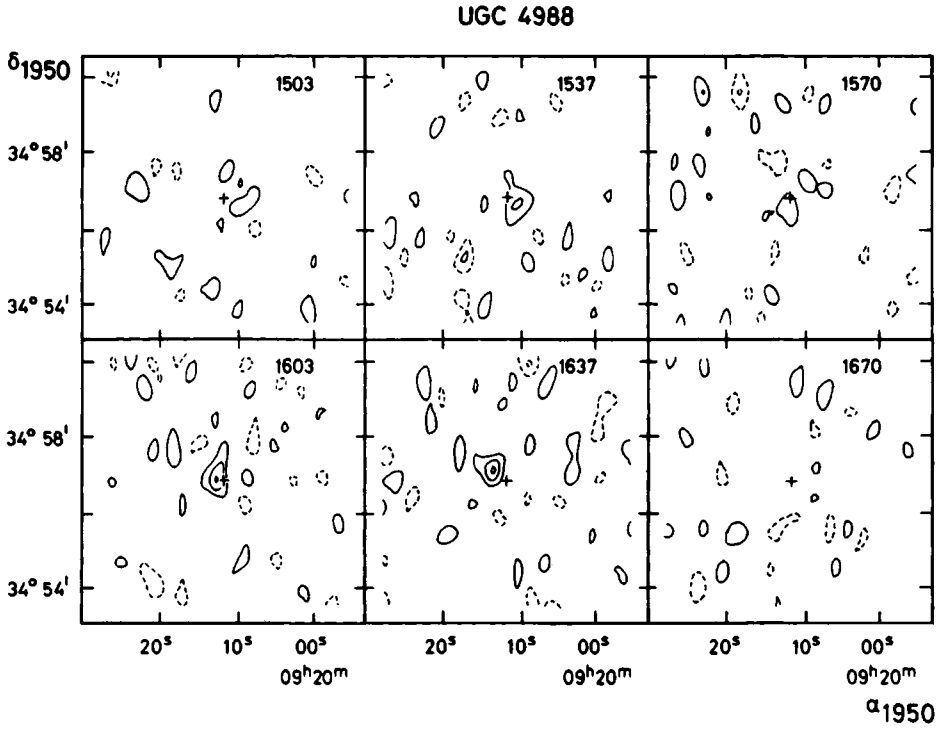

Figure 2a. Full resolution channel maps of the line emission from UGC 4988. The heliocentric velocity (in km s^{-1}) is given in the upper right-hand corner of each channel map. The cross marks the optical center. The first contour and contour intervals are 1.5 K. The zero-level contour is omitted and negative contours are dashed. The maps are not corrected for primary beam attenuation. In order to obtain true temperatures a correction factor, a, which depends on the position of each companion relative to the pointing center, must be applied. For UGC 4988: a = 2.02.

UGC 5004

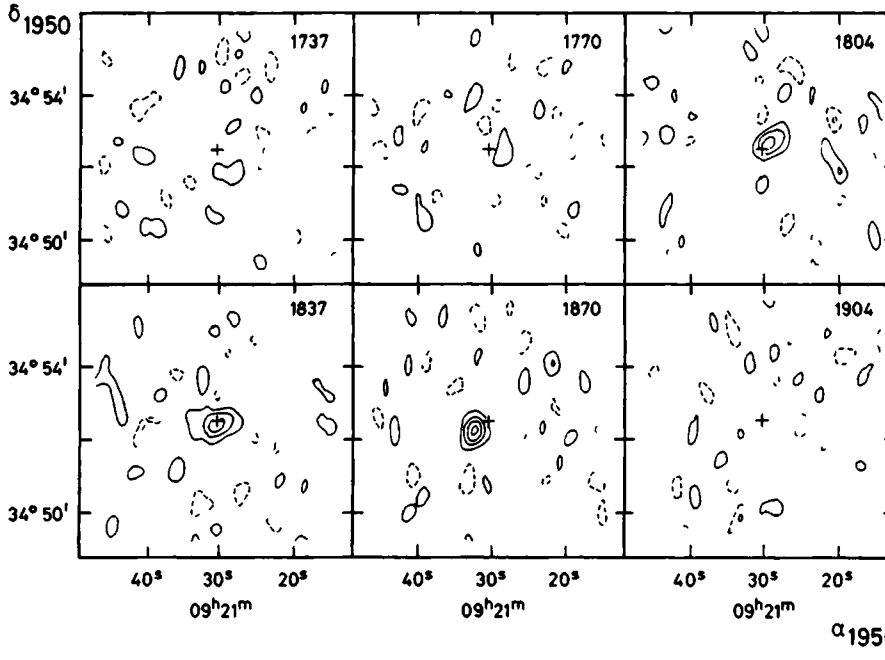

UGC 5015

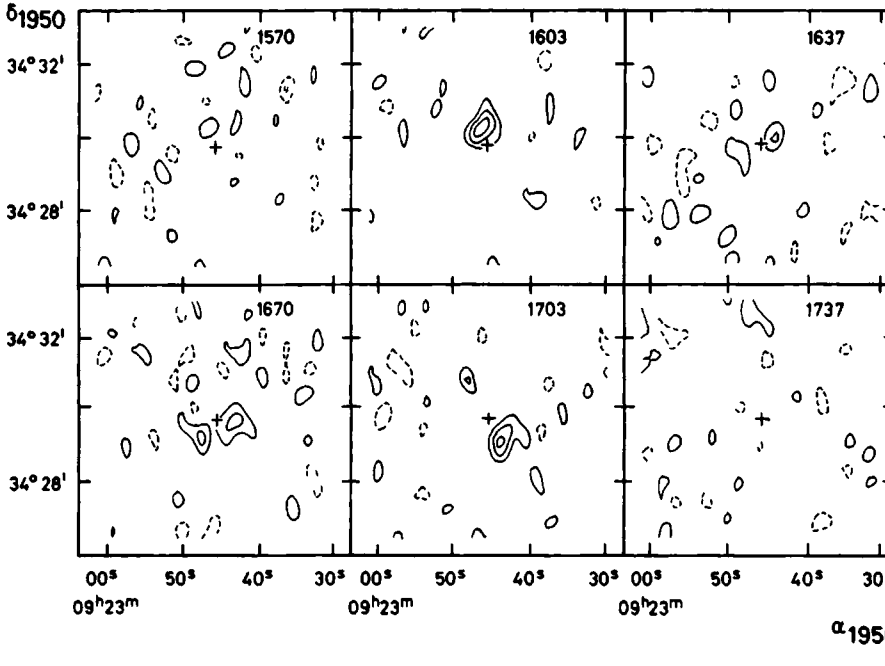

Figure 2b. Full resolution channel maps of the line emission from UGC 5004, plotted as in Figure 2a, a = 1 19

Figure 2c. Full resolution channel maps of the line emission from UGC 5015, plotted as in Figure 2a, a = 3 00

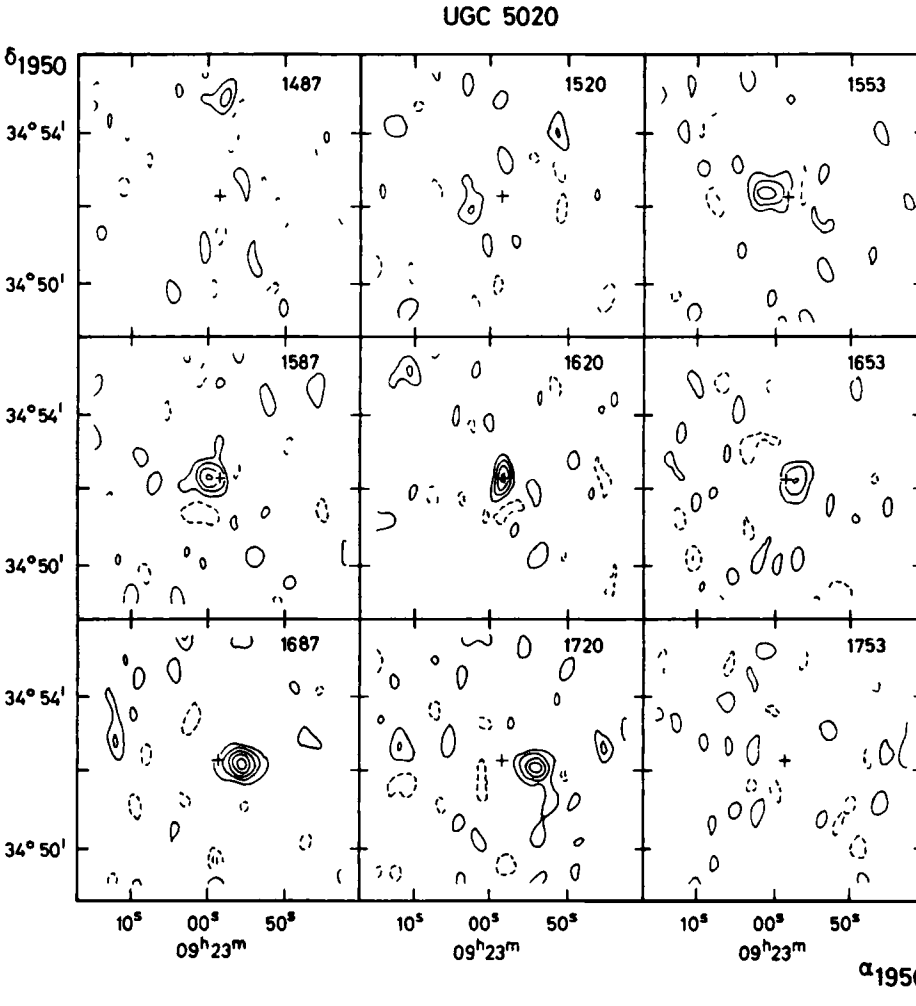

Figure 2d. Full resolution channel maps of the line emission from UGC 5020, plotted as in Figure 2a, a = 2 87

4.1 Global 21-cm line profiles

The global 21-cm line profiles of the companions were obtained using the full resolution channel maps corrected for attenuation by the primary beam. The total HI flux in each channel was derived by integration of the flux over a limited region. The size of this region was determined by the 2σ contour of the line emission in the 60 × 60 arcsec channel maps and care was taken that a single continuous series of velocities at each grid point was included. This masking procedure, which is described by Krumm and Shane (1982), was carried out for each companion separately.

Since NGC 2859 was not detected, only an upper limit to the HI flux could be derived. For this purpose, the full resolution channel maps were integrated over circles with radii up to 3 times the radius of the optical ring and centered on the optical center. From the line profiles a 3σ upper limit to the flux integral $\int SdV$ (in Jy km s^{-1}) was calculated from $\int SdV \leq 3\sigma\Delta V$, where σ is the r.m.s. fluctuation in the line profile (about 5 mJy) and ΔV = 170 km s^{-1} is the velocity width in HI reported by Bieging and Biermann (1977). This results in $\int SdV \leq 2.5$ Jy km s^{-1}. The upper limit to the total HI mass M_{HI}, assuming that the HI is optically thin, is $M_{HI} \leq 2.9\ 10^8\ h^{-2}\ M_\odot$ corresponding to $[M_{HI}/L_B] \leq 0.014$.

The flux integral derived for NGC 2859 can be compared with previous HI observations reported in literature. Assuming ΔV = 170 km s^{-1}, the non-detection by Knapp et al. (1977) with the NRAO 91 m telescope yields $\int SdV \leq 2.1$ Jy km s^{-1}. Bieging and Biermann (1977) marginally detected NGC 2859 with the Arecibo 300 m telescope. They find $\int SdV$ = 0.84 Jy km s^{-1}. A more recent Arecibo observation carried out by Giovanardi et al. (1983) shows a marginal line profile with a velocity width of 350 km s^{-1}. The flux integral calculated from this observation is 1.5 Jy km s^{-1} (which is comparable to the value given by Bieging and Biermann if we account for the different velocity widths). The line profile observed by Bieging and Biermann (1977) gives a systemic velocity of 1587 km s^{-1}, which is 98 km s^{-1} less than the optically measured value of 1685 km s^{-1} (Tonry and Davis, 1981), while the systemic velocity obtained by Giovanardi et al. (1983) is 1716 km s^{-1}. Since the diameter of the ring of NGC 2859 is slightly greater than the half-power diameter of the Arecibo beam (~3'), NGC 2859 may be marginally resolved by this telescope. Therefore, results obtained from different observations may be difficult to compare and may show significant differences, due, for example, to

detection of only the low or the high velocity peak of the profile. Confusion with one of the companions is improbable since the closest companion is at an angular distance from NGC 2859 of 9'.3 (see Table 1b).

The global HI line profiles of the detected companions are shown in Figure 3. The data listed in Table 4 were obtained from these line profiles. The systemic velocity is taken as the velocity half way between the 20% maximum power points of the profile; the velocity width of a profile is the velocity difference between these points.

If we compare the systemic velocities derived from the line profiles in Figure 3 with the optically derived velocities given by Arp (1980), we find that for UGC 4988, 5004 and 5020 the velocities agree within the accuracy of the optical measurements. For three of the companions the systemic velocities obtained from the WSRT observation made by Shane and Krumm (1983) are in excellent agreement with the presently derived values; only the velocity of UGC 4988 is discordant by 40 km s^{-1}. This difference and that in the reported velocity width can be explained by the uncertain detection of this galaxy by Shane and Krumm (1983). The width of the profiles of UGC 5015 and UGC 5020, reported by Shane and Krumm, is somewhat smaller than the presently derived values. Note that UGC 5004 fell partly outside their observed frequency band. The total HI masses of UGC 5004, 5015 and 5020, obtained by Shane and Krumm (1983) when adjusted to D = 21.5 h^{-1} Mpc, agree with the masses derived in this paper.

The $[M_{ind}/L_B]$-values, with the indicative mass M_{ind} calculated following Fisher and Tully (1981), range from 16 h to 71 h. These values are larger than the $[M_{ind}/L_B]$-values for dwarf galaxies as given by Fisher and Tully (1975) and by Gottesmann et al. (1984). Only the value for UGC 5020 lies in the range given by these authors. Note that this galaxy has a large inclination (see Table 1b). The other three galaxies have small inclinations and, as a result, the deprojection effect is large. Therefore, the $[M_{ind}/L_B]$-values for these three companions are very uncertain. Note that the inclination is calculated from the apparent axial ratio so that an underestimation of the intrinsic thickness of these dwarfs or the neglect of a warp, if present, would lead to an underestimation of their inclination and thus to an overestimation of the mass.

The distance-independent ratio of the HI-mass to blue-luminosity ($[M_{HI}/L_B]$) is obtained using the luminosities given in Table 1b. The resulting values, between 0.37 and 0.65, are typical for late-type spirals and irregulars (Shostak, 1978).

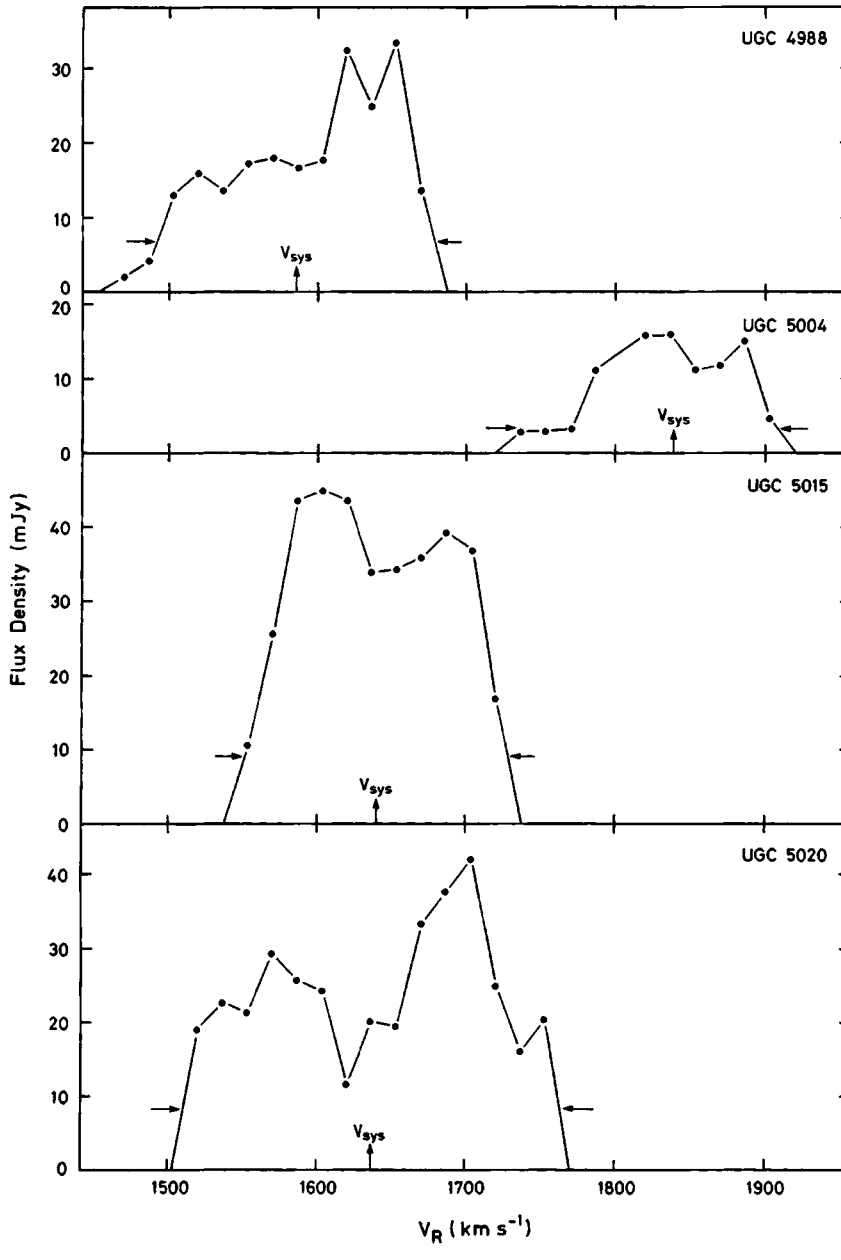

Figure 3. Global HI line profiles of UGC 4988, 5004, 5015 and 5020. The horizontal arrows indicate the 20% maximum power points; the systemic velocity is indicated by a vertical arrow.

Table 4. Derived global properties of the companions of NGC 2859

	UGC 4988	UGC 5004	UGC 5015	UGC 5020
Systemic velocity (km s^{-1})	1584	1838	1640	1636
Line profile width (km s^{-1})	187	136	178	249
M_{HI} (10^9 h^{-2} $M_\odot$)	0.41	0.20	0.67	0.67
$[M_{HI}/L_B]$	0.65	0.59:	0.45	0.37
M_{ind} (10^{10} h^{-1} $M_\odot$)	2.7:	2.5:	7.0:	2.9
$[M_{ind}/L_B]$	43 h:	71 h:	47 h:	16 h

4.2 The distribution of neutral hydrogen

Figure 4 shows the distribution of the integrated HI column density in each of the four companions, superimposed on enlargements from the photograph reproduced in Figure 1. The column density maps were obtained by adding the masked channel maps after correction for primary beam attenuation. Since the number of channels contributing to the total flux at each grid point varies, the noise level over the maps is nonuniform. The lowest contour levels plotted in Figure 4 are at approximately two times the r.m.s. noise. Because of the large beam relative to the dimensions of the companions, only the gross HI distribution can be studied.

UGC 4988: As shown in Figure 4a, the integrated HI surface density distribution of this galaxy is highly asymmetric. Most of the HI is found just outside the bright central part of the galaxy where it seems to form an incomplete ring. No HI is detected on the south-western side of the galaxy. For the peaks on the north and north-west side of the galaxy no obvious optical counterparts can be seen.

UGC 5004: The maximum of the centrally peaked HI distribution in this galaxy coincides with the bright optical center. On the north-west side a small extension of the HI beyond the optical image can be seen, which may be related to a spiral arm. Otherwise the distribution of the neutral hydrogen is nearly as structureless as the optical image.

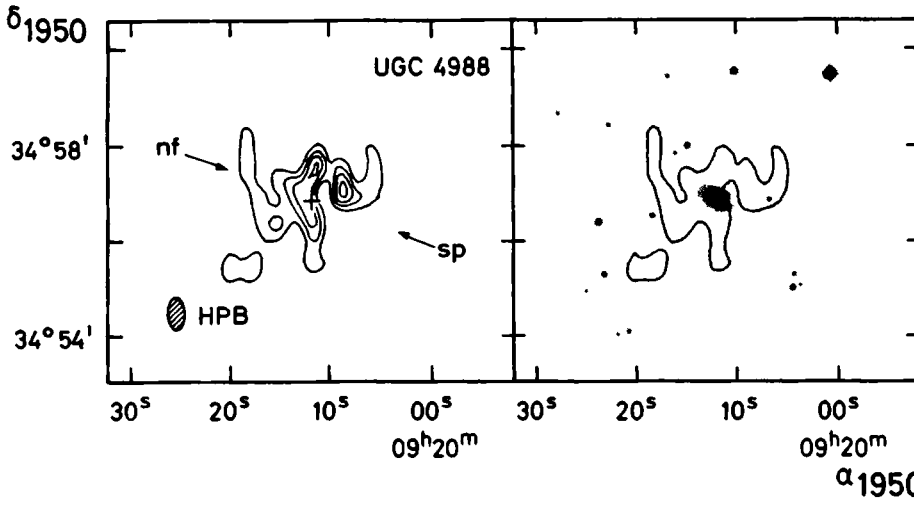

Figure 4a. Integrated HI surface density map of UGC 4988, corrected for primary beam attenuation The lowest contour level and contour interval are 1.9 10^{20} atoms cm^{-2}, assuming optically thin HI. The cross marks the optical center and the arrows indicate the direction along which the position-velocity maps shown in Figure 5 were made In the right panel the lowest contour is superimposed on an enlargement of a part of Figure 1

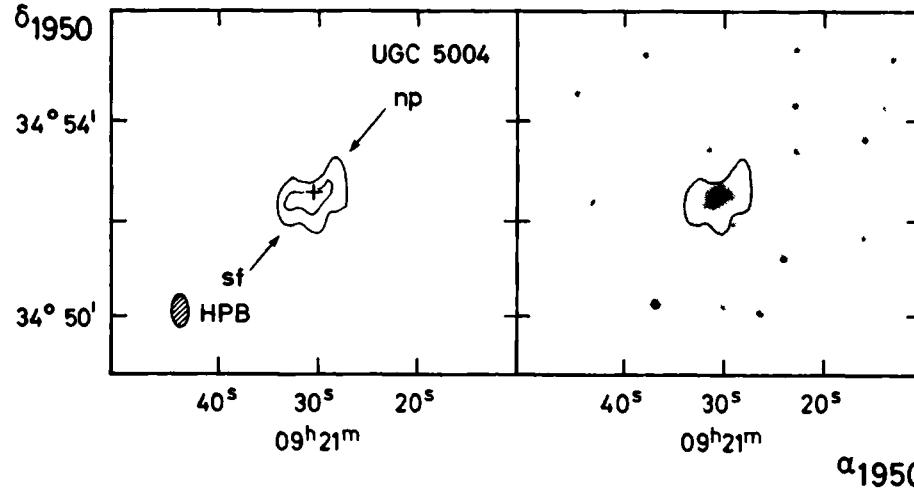

Figure 4b. Integrated HI surface density map of UGC 5004, plotted as in Figure 4a

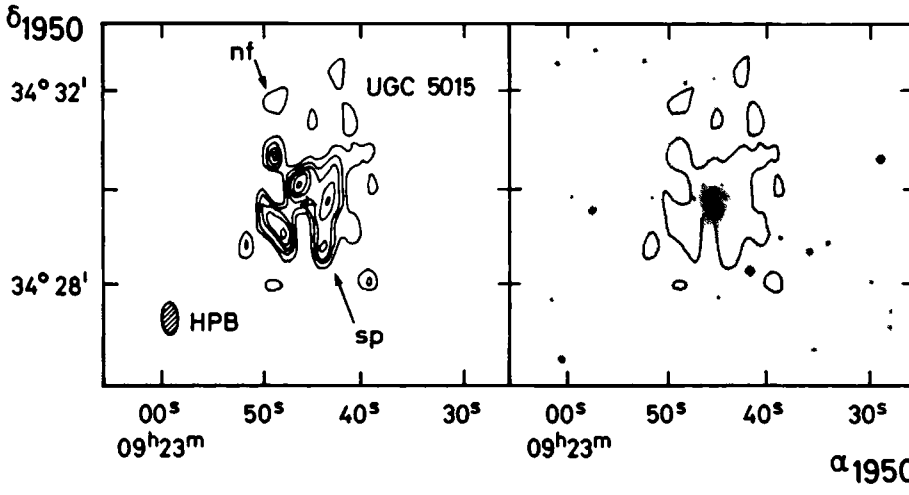

Figure 4c. Integrated HI surface density map of UGC 5015, plotted as in Figure 4a.

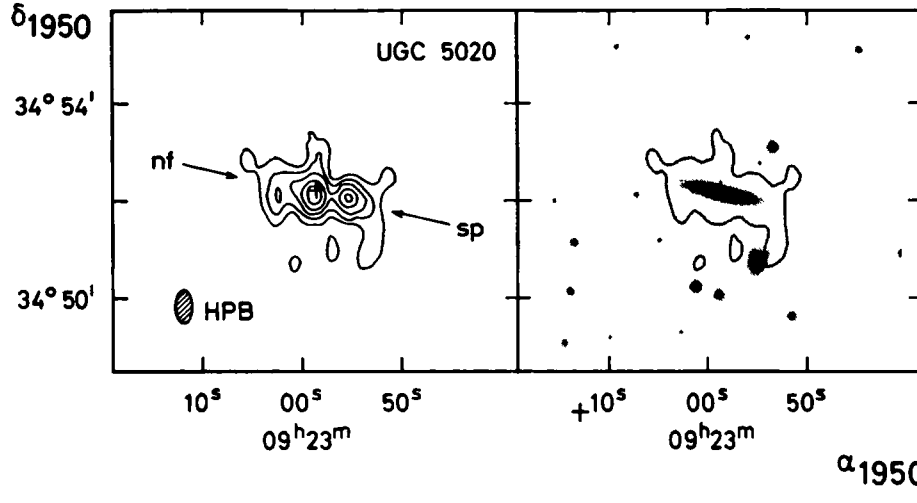

Figure 4d. Integrated HI surface density map of UGC 5020. The lowest contour level in both panels is 1.9 10^{20} *atoms* cm^{-2}, *the contour interval in the left panel is* 3.8 10^{20} *atoms* cm^{-2}.

UGC 5015: The peaks of the HI distribution lie near the outer edge of the optical disk, while the central part appears to be free from gas. The observed neutral hydrogen distribution seems to match the two armed spiral structure which can be distinguished on the photograph. One spiral arm may be associated with the northern and western peaks and the other with the HI peaks south-east and north-east of the galaxy.

UGC 5020: The distribution of HI in this galaxy, which is seen nearly edge-on, seems to be composed of an outer ring-like distribution along with a concentration of gas near the optical center. The latter component may be an unresolved inner ring or a small disk. As Figure 4d shows, the HI surface density in the outer component appears to be asymmetric with the larger concentration on the sp side. On this side, where optically a small warp is visible, a filament of gas in the direction of a small anonymous galaxy is seen. This filament originates from emission scattered over several velocity channels and must be considered as very doubtful. The radial velocity of UGC 5020 (1636 km s^{-1}) and of the anonymous galaxy located 1'.5 to the south-west (7442 km s^{-1}; Arp, 1980) differ strongly so that interaction between these galaxies seems very improbable.

We conclude that the four dwarf galaxies show variety in their HI distribution. In UGC 5004 the HI distribution is centrally peaked and no details can be distinguished. In this respect the galaxy resembles the situation encountered in UGC 7094, a dwarf companion of NGC 4111 (van der Burg, 1987), and the satellites of NGC 3992 and UGC 4731 mapped by Gottesmann et al. (1984). In the other three galaxies the HI distribution is clumpy and concentrated in the outer part of the visible system. The $[M_{HI}/L_B]$-values of the presently studied companions are slightly higher than the averages listed by Thuan and Seitzer (1979) for late-type dwarfs, but they are slightly less than the values listed by Gottesmann et al. (1984) for the satellites of NGC 3992 and NGC 4731. The HI column density maps of the companions of NGC 2859 reveal no sign of interaction with the primary or with the objects of high redshift noted by Arp (1980). An exception might be UGC 5020 which shows an asymmetric HI distribution (see Figure 4d) with a concentration of gas near its center. As noted by Soifer et al. (1984) interaction of galaxies with companions might enhance their infrared emission. However, none of the members of the NGC 2859 group is listed in the IRAS Point Source Catalogue (1985). This is consistent with the undisturbed HI distributions measured in the companions.

4.3 Kinematics

In Figure 5 the distribution of the surface brightness along the major axis as a function of velocity is shown for each of the detected companions. These position-velocity maps were made from the full resolution channel maps along lines through the optical centers of the companions with the position angles listed in the UGC. It is clear from Figure 4 that the kinematical information, especially in the position velocity maps of UGC 4988 and UGC 5015, is incomplete.

Therefore, the velocity fields of the four companions are also shown (Figure 6). These maps were made using the channel maps convolved to a resolution of 40″ × 40″. The velocity at each grid point was determined by fitting a Gauss function to the line profile at that position. A fit was attempted only at positions where the peak flux was larger than 1σ. Due to the small HI dimensions of the companions compared with the convolved beam, only large-scale structures are visible and effects of beam smearing are inevitable. Despite certain irregularities, the velocity fields of the companions are typical of differentially rotating systems. The position angles listed in the UGC are roughly consistent with the position angles of the kinematic major axes estimated from these velocity fields. Thus the limited kinematic data available from these observations gives no indication of interaction or other large-scale disturbances affecting the companions.

5 Dynamical interpretation

From the systemic velocities of the companions, derived in sub-section 4.1, the mass of NGC 2859 including a possible dark halo can be estimated using the projected mass method proposed by Bahcall and Tremaine (1981). In the following sub-section we will show that the conditions under which the use of this mass estimator is valid are fulfilled by the NGC 2859 group of galaxies. In sub-section 5.2 we will apply the projected mass method and discuss the results.

5.1 Discussion of the requirements

The projected mass method can be applied to a physical group of galaxies which is in virial equilibrium and isolated, and for which the companions can be treated as test-particles moving in a potential field dominated by the primary galaxy.

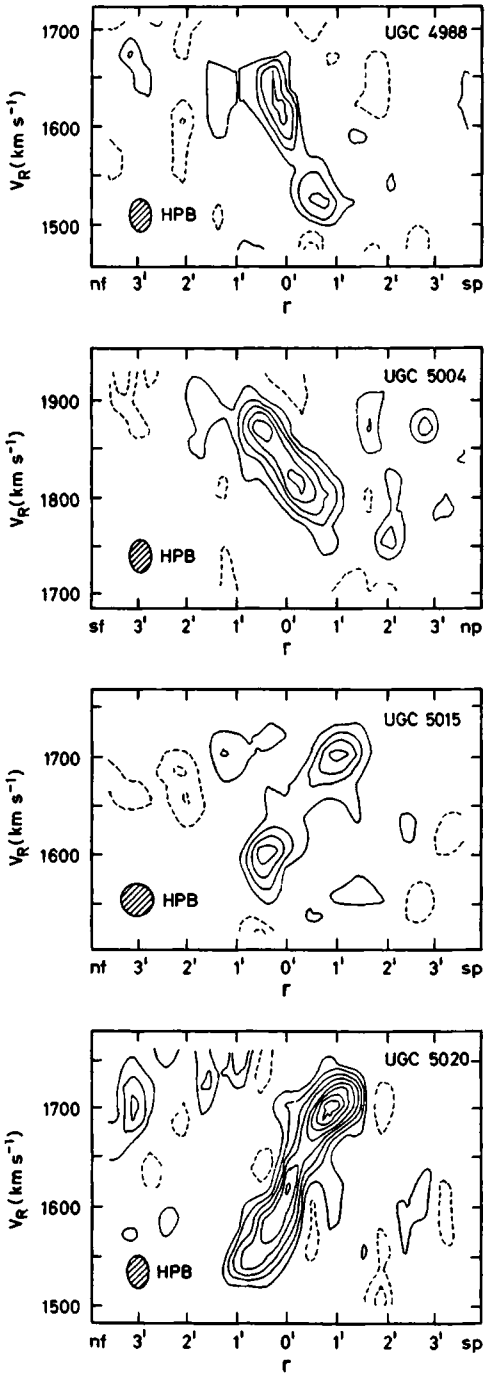

Figure 5. Maps of the HI brightness distribution in UGC 4988, 5004, 5015 and 5020 along the major axis as a function of heliocentric radial velocity V_R (in km s^{-1}) and distance r (in arcmin) from the optical center. The first contour and contour interval are 1.1 K. The maps are not corrected for primary beam attenuation (for the correction factors see Figure 2).

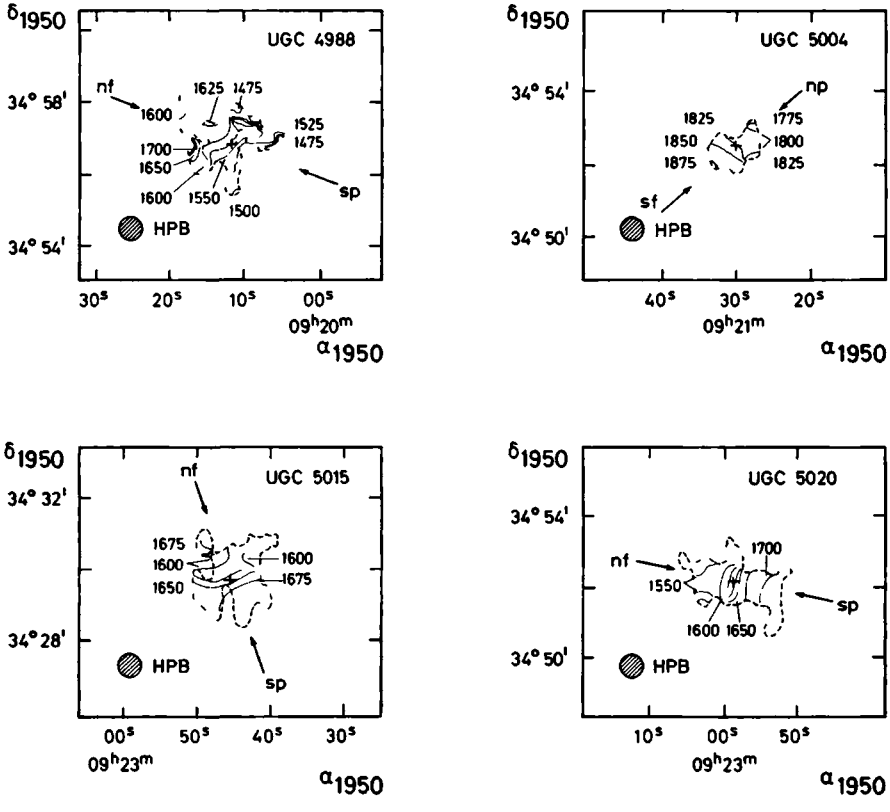

Figure 6. Isovelocity maps of the four detected companions The velocities are given in km s^{-1} and are plotted at intervals of 25 km s^{-1}, the broken contour corresponds to the lowest contour plotted in Figure 4 The contours are missing from some regions on account of the low intensities

An indication that NGC 2859 and the four detected galaxies constitute a real physical group, with all members at roughly the same distance, and that we are not dealing with galaxies accidently projected on the same area of the sky, is the similarity of the systemic velocities of the members. If we adopt 1685 km s^{-1} (Tonry and Davis, 1981) for the systemic velocity of NGC 2859 the maximum difference in radial velocity of any companion is 153 km s^{-1}. Moreover, the luminosity weighted average velocity of the four detected companions is 1646 km s^{-1}, which differs only slightly from the adopted systemic velocity of NGC 2859. The projected mass method requires that the group be bound and in virial equilibrium. In order to meet these requirements the characteristic time for a galaxy to transit the group must be sufficiently short, in any case less than a Hubble time. In the following sub-section we shall assume that the NGC 2859 group is virialized and calculate the mass according to the method of Bahcall and Tremaine (1981). We shall then use this mass determination to calculate the corresponding time scale and show that it is consistent with the assumption of virial equilibrium.

The method of Bahcall and Tremaine (1981) further requires that the group be isolated. Bright galaxies close to NGC 2859 are NGC 2793 and the double system NGC 2831/NGC 2832 (Zwicky et al., 1961-1968). The radial velocities of NGC 2831/NGC 2832 are 5155 and 6974 km s^{-1} implying that these galaxies are background objects. NGC 2793 has a radial velocity of 1674 km s^{-1}, close to that of NGC 2859. However, the projected separation between these galaxies is 7.5<R> (where <R> is the average of the projected distance between NGC 2859 and its companions) so that the interaction between NGC 2859 and its companions is about 50 times greater than the interaction of NGC 2793 with the companions. Moreover, NGC 2793 is about two magnitudes fainter than NGC 2859; assuming for NGC 2793 (classified as SB(s)m) an $[M/L_B]$-value of 4 (Faber and Gallagher, 1979) which is 5 times smaller than their average $[M/L_B]$-value for S0 galaxies, we estimate the mass of NGC 2859 to be 40 times the mass of NGC 2793. Therefore, the NGC 2859 group of galaxies is to a good approximation isolated.

Finally, the projected mass method of Bahcall and Tremaine (1981) also requires that the central galaxy be identified with the barycenter of the group. This assumption is justified since 80% of the luminosity of the group is concentrated in NGC 2859 (83% if we include only the four HI-rich companions in which case the center of luminosity is located only 3 arcmin east of the optical center of NGC 2859). Therefore, distances and velocities may be calculated with respect to NGC 2859. In the following sub-section, where the mass of NGC 2859 is calculated, it will be verified that the companions can be considered as test-particles.

5.2 Application of the projected mass method and discussion of the result

Since no information on the orbital eccentricities of the companions is available, we have used the mass estimator $M_0 = \frac{24}{\pi G n} \sum_{i=1}^{n} \Delta V_i^2 R_i$ recommended by Bahcall and Tremaine (1981). Here n is the number of companions included in the calculation, ΔV_i the difference in radial velocity between the primary and the i^{th} companion and R_i the corresponding projected distance. Application of this mass estimator, using data for the detected companions listed in Table 4 and assuming that the systemic velocity of NGC 2859 is 1685 km s^{-1}, yields $M_0 = 1.4\ 10^{12}\ h^{-1}\ M_\odot$. According to Bahcall and Tremaine the fractional standard deviation of M_0 is $1.4\ n^{-1/2}$. For n = 4 this is 70%, so that M_0 is expected to lie between 0.8 and $2.4\ 10^{12}\ h^{-1}\ M_\odot$. A lower limit M_{bound} to the mass can be calculated if we require that all companions be bound to NGC 2859, $M_{bound} = 1/(2G) \max_{i=1,n} \Delta V_i^2 R_i$. This results in $M_{bound} = 1.6\ 10^{11}\ h^{-1}\ M_\odot$ which is determined from the requirement that UGC 5004 be bound. The projected mass method estimates the mass inside a region with a deprojected radius $<r> = 4<R>/\pi$. For NGC 2859 with its four HI-detected companions <r> is 147 h^{-1} kpc. The corresponding mass-to-light ratio $[M/L_B]$ of the NGC 2859 group, using the blue luminosities listed in Table 1a and 1b, is 56 h. This value is in agreement with values generally found in small groups of galaxies (Faber and Gallagher, 1979).

The ratio M_{ind}/M_0 ranges between 0.02 and 0.05 (taking M_{ind} from Table 4 where, as noted above, the values are probably overestimated) showing that the companions can indeed be treated as test-particles (see the previous sub-section).

Using the above estimate M_0 for the mass within a radius <r> of NGC 2859, we can now verify that the crossing time T, defined as the time required for a companion to travel from one side of the group to the other, is small compared to a Hubble time so that, unless the group was recently formed, the virial assumption is valid. The crossing time on a circular orbit is $2.2\ 10^9\ h^{-1}$ years and on a linear orbit through the center of the group, assuming a mass distribution giving a flat rotation curve, $1.8\ 10^9\ h^{-1}$ years, compared to a Hubble time of $10^{10}\ h^{-1}$ years. The estimate according to the method of Rood and Dickel (1978) is $0.8\ 10^9\ h^{-1}$ years.

A source of uncertainty is the systemic velocity of NGC 2859 for which values between 1587 km s^{-1} (Bieging and Biermann, 1977) and 1716 km s^{-1} (Giovanardi et al., 1983) have been reported in the literature. The effect on the estimated mass M_0 of varying the systemic velocity is displayed in Figure 7. Aside from calculating new values of ΔV_i, the distance of the group derived from the systemic velocity of NGC 2859 (following Aaronson et al., 1982), was also adjusted, resulting in new values of R_i. We

see that, within the velocity range examined, M_0 varies by about a factor 2. The minimum value of M_0, 1.2 10^{12} h^{-1} $M_\odot$ found for V = 1645 km s^{-1}, is only slightly less than the mass calculated for V = 1685 km s^{-1}. In Figure 7, M_{bound} is also plotted as function of the assumed velocity of NGC 2859. It reaches a minimum near 1685 km s^{-1}.

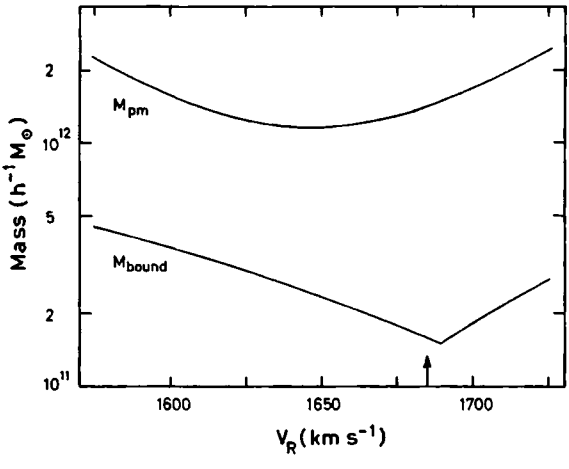

Figure 7. Mass estimates of NGC 2859 as a function of its systemic velocity. The estimates plotted are from the projected mass method (M_{pm}) and from the requirement that all companions be bound (M_{bound}). The systemic velocity of NGC 2859 which is adopted in this paper is indicated by an arrow.

In the mass estimation only the four detected companions are taken into account since for UGC 5011 and UGC 5014 no systemic velocities are available. The reasons for not detecting these galaxies may be that a) their systemic velocities lie within the observed velocity interval but their HI content is too small to be observed, b) their systemic velocities lie just outside the observed velocity interval ($|\Delta V| \geq 500$ km s^{-1}) or c) they are background galaxies. In the latter case they are not physical member of the group and are therefore of no importance for the mass calculations. In case b) their impact on M_0 would be considerable. Including both galaxies, assuming $|\Delta V| = 500$ km s^{-1}, yields M_0 = 2.9 10^{13} h^{-1} $M_\odot$. This value is at least an order of magnitude greater

than the masses of lenticular galaxies measured out to radii in excess of optical radii by Fabian et al. (1986). Using X-ray data these authors showed that the average binding mass of lenticular galaxies is at least 1 to 3.5 10^{12} h^{-1} $M_{\odot}$. Note that the large amount of additional mass (with respect to the mass calculated using the four detected companions) must be located between radii 147 h^{-1} and 179 h^{-1} kpc. This would imply a very unrealistic mass distribution so that the assumption $|\Delta V| = 500$ km s^{-1} for the undetected galaxies is probably wrong. Case a) is supported by considering the probable HI content of these galaxies, which appear to be late-type, and adopting hydrogen mass-to-light ratios given by Shostak (1978). The expected flux densities will then be less than 15 mJy (assuming a velocity width of 150 km s^{-1}). Together with their large angular distance from the field center (see Table 1b), which gives an attenuation by the primary beam of about 80%, they will be at best marginally detectable with the present sensitivity.

We conclude from the projected mass method that the most probable value for the mass of the NGC 2859 group is 1.4 10^{12} h^{-1} $M_{\odot}$ with an uncertainty of a factor 2 to 3.

6 The central galaxy NGC 2859

Using the projected mass method the mass distributed inside a volume with an average radius <r> of 147 h^{-1} kpc and centered on NGC 2859 has been determined. This radius corresponds to about seven Holmberg radii of NGC 2859. If we associate the calculated mass inside this region with NGC 2859, the corresponding mass-to-light ratio is 68 h. Note that Tonry and Davis (1981) list an $[M/L_B]$ of 15 h, based on measurements of the stellar velocity dispersion in NGC 2859. However, as noted by these authors, their $[M/L_B]$-values for S0 galaxies are less meaningful than the $[M/L_B]$-values derived for ellipticals, because the disk begins to violate the assumptions used in their calculations. The average value quoted by Faber and Gallagher (1979) for a small sample of S0 galaxies and measured within one Holmberg radius, is 20 h. Therefore, based on this average value there appears to be an increase in M/L_B of a factor three, which we attribute to dark matter associated with NGC 2859 outside the Holmberg radius. This increase of M/L_B with radius is less than would be required by a mass distribution which would lead to a flat rotation curve, as is often observed in the outer parts of late-type galaxies. Van der Burg (1987) has calculated the mass of the $S0^+$ galaxy NGC 4111 by means of the projected mass method. The corresponding $[M/L_B]$-value, 101 h within five Holmberg radii, roughly agrees with the increase of M/L_B with radius expected for a flat rotation curve. Although the uncertainty is great, the slower increase of M/L_B for NGC 2859 along with the presence of a bar in this galaxy suggests agreement with theoretical calculations, which

predict bar-like instabilities in disks of galaxies in the absence of a massive halo.

The suggestion that S0's can accrete HI from their surroundings has recently drawn attention (Silk and Norman, 1979; Wardle and Knapp, 1986). If we consider the possibility that one of the companions should be captured by NGC 2859, the increase of the HI mass would be roughly between 0.2 and 0.7 10^9 h^{-2} $M_\odot$ (see Table 4). This increase is much greater than the HI content calculated from the flux integral obtained by Bieging and Biermann (1977, see sub-section 4.1). However, it is in the same order as is measured in HI-rich lenticulars (Wardle and Knapp, 1986). The corresponding $[M_{HI}/L_B]$-values for NGC 2859 would than be between 0.01 and 0.03.

The amount of gas in NGC 2859, as detected by Bieging and Biermann (1977) and Giovanardi et al. (1983), is insufficient for detection with the sensitivity achieved with the WSRT. However, it would be important to map its distribution and to study its kinematics. This might offer the possibility of estimating the $[M/L_B]$-value within a smaller volume centered on NGC 2859, and comparing that value with the one obtained from the projected mass method.

Acknowledgements

We would like to thank Dr. H. Arp for kindly supplying the photograph reproduced in Figure 1. The Westerbork Synthesis Radio Telescope is operated by the Netherlands Foundation for Radio Astronomy, with the financial support of the Netherlands Foundation for the Advancement of Pure Research (Z.W.O.).

Aaronson, M., Huchra, J., Mould, J., Schechter, P.L., Tully, R.B.: 1982, Astrophys. J. 258, 64

Arp, H.: 1980, Astrophys. J. 240, 415

Bahcall, J.N., Tremaine, S.: 1981, Astrophys. J. 244, 805

Bieging, J.H., Biermann, P.: 1977, Astron. Astrophys. 60, 361

Bos, A., Raimond, E., van Someren Greve, H.W.: 1981, Astron. Astrophys. 98, 251

de Vaucouleurs, G.: 1959, Handbuch der Physik, Volume LIII Astrophysik: Sternsysteme, Flugge, S., Springer Verlag

de Vaucouleurs, G.: 1965, Stars and Stellar Systems Volume IX, Sandage, A., Sandage, M., Kristian, J., University of Chicago Press

de Vaucouleurs, G., de Vaucouleurs, A., Corwin, H.G.: 1976, Second Reference Catalogue of Bright Galaxies, University of Texas Press (2RCBG)

Dressel, L.L., Condon, J.J.: 1976, Astrophys. J. Suppl. 31, 187

Faber, S.M., Gallagher, J.S.: 1979, Ann. Rev. Astron. Astrophys. 17, 135

Fabian, A.C., Thomas, P.A., Fall, S.M., White III, R.E.: 1986, Space Telescope Science Institute, Preprint Series, 118

Fall, S.M.: 1986, Space Telescope Science Institute, Preprint Series, 149

Fisher, J.R., Tully, R.B.: 1975, Astron. Astrophys. 44, 151

Fisher, J.R., Tully, R.B.: 1981, Astrophys. J. Suppl. Ser. 47, 139

Gallagher, J.S., Wirth, A.: 1980, Astrophys. J. 241, 567

Giovanardi, C., Krumm, N., Salpeter, E.E.: 1983, Astron. J. 88, 1719

Gottesmann, S.T., Hunter, J.H. Jr.: 1982, Astrophys. J. 260, 65

Gottesmann, S.T., Ball, R., Hunter, J.H. Jr., Huntley, J.M.: 1984, Astrophys. J. 286, 471

Högbom, J.A., Brouw, W.N.: 1974, Astron. Astrophys. 33, 289

IRAS Point Source Catalogue: 1985, prep. by Joint IRAS Science Working Group, U.S. Government Printing Office, Washington D.C.

Knapp, G.R., Gallagher, J.S., Faber, S.M., Balick, B.: 1977, Astron. J. 82, 106

Krumm, N., Shane, W.W.: 1982, Astron. Astrophys. 116, 237

Nilson, P.: 1973, Uppsala General Catalogue of Galaxies, Uppsala Astron. Obs. Ann. 6 (UGC)

Rood, H.J., Dickel, J.R.: 1978, Astrophys. J. 224, 724

Sancisi, R., van Woerden, H., Davies, R.D., Hart, L.: 1984, Mon. Not. Roy. Astron. Soc. 210, 497

Sandage, A.: 1961, The Hubble Atlas of Galaxies, Carnegie Institution of Washington, Publication 618, 42

Shane, W.W.: 1980, Astron. Astrophys. 82, 314

Shane, W.W., Krumm, N.: 1983, Internal Kinematics and Dynamics of Galaxies, IAU symp. 100, ed. E. Athanassoula, Reidel Dordrecht, 105

Shostak, G.S.: 1978, Astron. Astrophys. 68, 321

Silk, J., Norman, C.: 1979, Astrophys.J. 234, 86

Soifer, B.T., Rowan-Robinson, M., Houck, J.R., de Jong, T., Neugebauer, G., Aumann, H.H., Beichman, C.A., Boggess, N., Clegg, P.E., Emerson, J.P., Gillet, F.C., Habing, H.J., Hauser, M.G., Low, F.J., Miley, G., Young, E.: 1984, Astrophys. J., 278, L71

Thuan, T.X., Seitzer, P.O.: 1979, Astrophys. J. 231, 680

Tonry, J.L., Davis, M.: 1981, Astrophys. J. 246, 666

van der Burg, G.: 1985, Astron. Astrophys. Suppl. Ser. 62, 147

van der Burg, G.: 1987, to be published

van Woerden, H., van Driel, W., Schwarz, U.J.: 1983 Internal Kinematics and Dynamics of Galaxies, IAU Symposium 100, ed. E. Athanassoula, Reidel, Dordrecht, 99

Wardle, M., Knapp, G.R.: 1986, Astron. J. 91, 23

Zwicky, F., Herzog, E., Wild, P., Karpowicz, M., Kowal, C.T.: 1961-1968, Catalogue of Galaxies and of Clusters of Galaxies, California Institute of Technology

CHAPTER 7 THE MASS OF THE EARLY-TYPE GALAXY NGC 4111 INFERRED FROM HI OBSERVATIONS OF ITS COMPANIONS

Summary

We present high resolution 21-cm line HI observations of the lenticular galaxy NGC 4111. This galaxy is accompanied by several faint companions, five of which appear to be rich in HI and to have systemic velocities close to that of NGC 4111. No HI was detected in NGC 4111 itself giving $[M_{HI}/L_B] < 0.04$. If the faint galaxies are bound to NGC 4111 the total mass within the region occupied by the companions can be estimated from their radial velocities and projected distances from NGC 4111. Using the method proposed by Bahcall and Tremaine (1981) the result is $M_0 = 3.2\ 10^{11}\ h^{-1}\ M_\odot$ for $H_0 = 100\ h$ km s^{-1} Mpc^{-1}, corresponding to a mass-to-light ratio of 101 h. These calculations provide a measurement of the mass-to-light ratio of a lenticular out to about five Holmberg radii. The resulting value is about a factor five greater than generally measured for lenticular galaxies within one Holmberg radius and agrees with the increase which would be required by a flat rotation curve. It is argued that there is sufficient neutral hydrogen in the immediate neighbourhood of NGC 4111 that, should it be captured, it could turn this galaxy in an HI-rich S0.

1 Introduction

In recent years it has become apparent that the results of dynamical mass determinations for galaxies strongly depend upon the extent of the region examined. Rotation curve measurements of individual galaxies provide information on the distribution of mass within the radius of the optical or HI disk. For most galaxies the total mass appears to increase significantly with radius, even at the outermost observed points. Double galaxy observations provide information on an intermediate scale (about 100 kpc), particularly relevant to the problem of the distribution of matter around galaxies.

A class of objects for which radial velocity observations can provide important additional data on about the same scale as do binary galaxy observations is that of single bright galaxies accompanied by several much less fainter and thus presumably less massive companions. Mass determinations of representatives of this class offer several advantages. If the companions are much less massive than the primary galaxy, they can be treated as test-particles. Because the individual masses do not enter the problem, an important source of uncertainty is eliminated. Moreover, the presence of several test particles will greatly increase the statistical significance of a single mass determination. The usefulness of this method depends upon the detectability of the faint companions. Optical velocity determinations of these faint galaxies can generally not be made with the accuracy required to obtain a reliable mass estimate. However, recent 21-cm line Nançay observations of faint companions in several groups (van der Burg, 1985), and high resolution HI observations of NGC 2859 (Shane and Krumm, 1983), NGC 3992 (Gottesman and Hunter, 1982) and NGC 1961 (Gottesman et al., 1983) have shown that in these cases several companions of the bright galaxies are rich in HI. If these examples of the detection of faint companions are typical, then a large sample of galaxies is available for this kind of investigation.

This paper presents HI line observations of one representative of the above described class of objects, viz. NGC 4111. Observations of the distribution of HI in and around this galaxy are of particular interest for the following reasons. Firstly, NGC 4111 is a lenticular galaxy and mass determinations out to large galactocentric radii are scarce for this kind of object (Faber and Gallagher, 1979; Fall, 1986). Secondly, NGC 4111 is an example of a lenticular galaxy in which HI has been reported (van der Burg, 1985). If this detection were real then we would have another example of an S0 galaxy with a detectable amount of HI, and it would be interesting to study the distribution of HI in the immediate vicinity of NGC 4111 where several companions are found. Such observations might shed light on the hypothesis that S0 galaxies accrete HI from their surroundings, as proposed for instance for NGC 2685 (Shane, 1980) and NGC 1023 (Sancisi et al., 1984).

In order to map the distribution of HI and study its kinematics in the NGC 4111 group of galaxies, we employed the high sensitivity and angular resolution of the Westerbork Synthesis Radio Telescope (WSRT). In Section 2 of this paper a description of the NGC 4111 group of galaxies is given. The observations and reduction procedure are described in section 3; the global results are presented in section 4. A discussion of the results and the conclusions are given in section 5.

2 The NGC 4111 group of galaxies

NGC 4111 is a bright, lenticular galaxy apparently located at the center of a small group of faint galaxies. In Figure 1 a reproduction of the blue plate of the Palomar Observatory Sky Survey of the region is shown with superposed the outermost contours of the observed HI distribution in the detected companions (see sub-section 4.2). The morphological type assigned to NGC 4111 by de Vaucouleurs et al. (1976, hereafter 2RCBG) is SA(r)0^+:sp. Photometric observations of the galaxy were made by van Houten (1961) who was able to determine the spatial distribution of light. Combining his photometry with unpublished radial velocity measurements of the inner parts made by Humason, van Houten calculated a mass to light ratio of 19 h (where $H_0 = 100$ h km s^{-1} Mpc^{-1}). More recent surface photometry of NGC 4111 is given by Tsikoudi (1980). The optically determined systemic velocity of NGC 4111, corrected for solar motion with respect to the Local Group, is 841 $\pm$ 14 km s^{-1} (2RCBG). This yields a distance D of 8.4 h^{-1} Mpc, which will be used throughout this paper. Radio observations of NGC 4111 were made by Hummel and Kotanyi (1985) in an attempt to detect continuum emission from the disk. However, no emission was detected, which, according to these authors, is in agreement with the low gas content as indicated by 21-cm line observations made by Fisher and Tully (1981). Recent single dish HI observations using the Nançay Decimetric Radio Telescope were made by van der Burg (1985). These observations yielded a doubtful detection corresponding to an HI mass of 1.9 10^8 h^{-2} $M_\odot$ and an HI-mass to blue-luminosity ratio $[M_{HI}/L_B]$ of 0.08. In Figure 1 at least nine faint galaxies can be distinguished within 30 arcmin of NGC 4111. Most of these galaxies are listed in the Catalogue of Galaxies and of Clusters of Galaxies (Zwicky et al., 1961 - 1968) and in the Uppsala General Catalogue of Galaxies (Nilson, 1973 hereafter UGC). Only three objects are anonymous; their positions were measured on the Palomar Observatory Sky Survey. A summary of the optical properties of NGC 4111 and of those companions detected in HI is given in Table 1. As can be seen from this table, the morphological types of the detected companions, where known, are lenticular or late-type spiral. The brightest

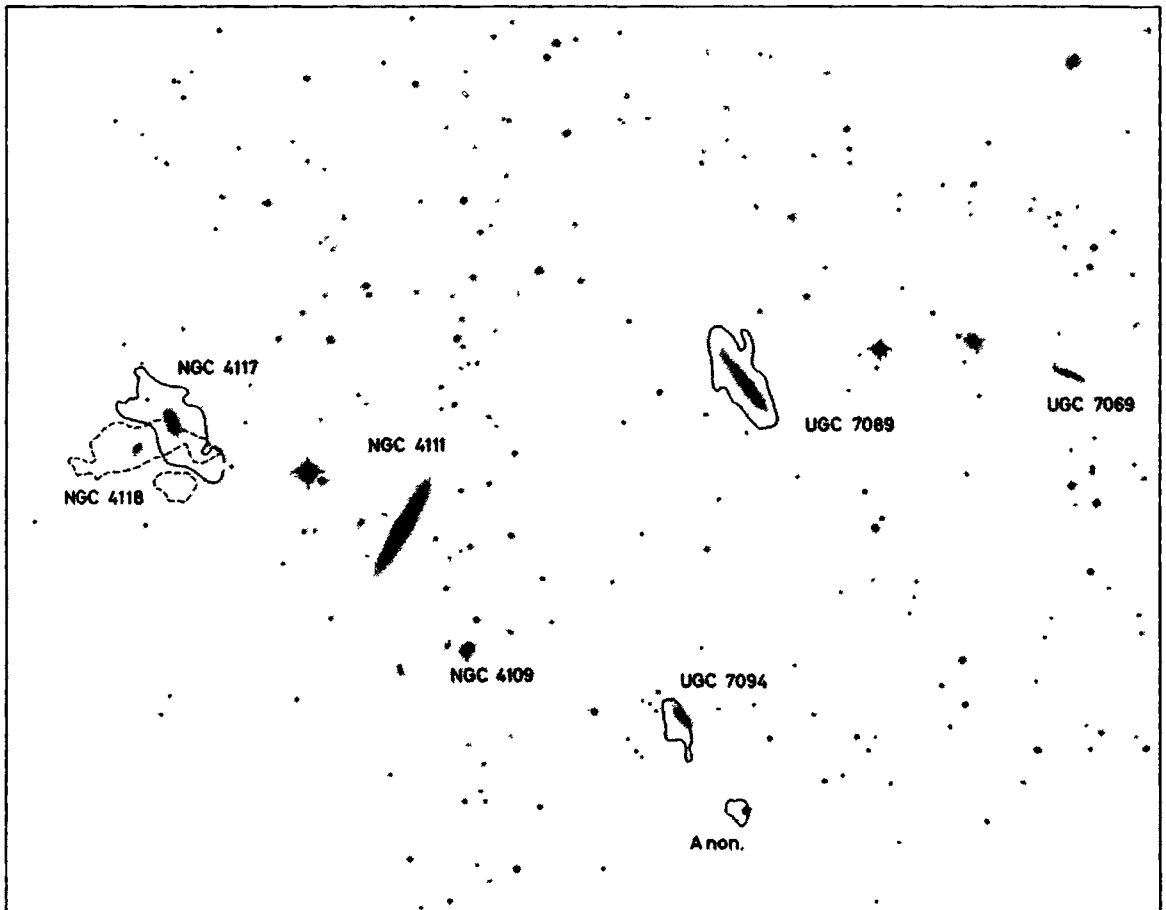

Figure 1. Reproduction of the blue print of the Palomar Observatory Sky Survey showing the NGC 4111 group of galaxies Superposed are the outermost contours of the integrated HI distributions of the detected companions as shown in Figure 4

Table 1. Optical data

	NGC 4111	UGC 7089	NGC 4117	NGC 4118	UGC 7094	Anon.	Ref.
α_{1950}	$12^h04^m31^s.6$	$12^h03^m24^s$	$12^h05^m14^s.4$	$12^h05^m21^s.0$	$12^h03^m36^s$	$12^h03^m27^s$	1,2,3*
δ_{1950}	+43°20'41"	+43°25'	+43°24'20"	+43°23'27"	+43°14'	+43°10'.8	1,2,3*
Type	SA(r)0$^+$:sp	dm-m	S0$^-$:	S0$^+$?	Sdm:		4,2*
Blue dimensions	4'.3 × 0'.8	3'.5 × 0'.9	2'.5 × 0'.9	0'.85 × 0'.47	1'.3: × 0'.5:	0'.3: × 0'.3:	2,3*
Holmberg diameter	6'.2	5'.0	4'.2	2'.0	2'.2		5
m_{pg}	11.4	14.8	14.3	15.7	15.6	>17	2
B_T^0	11.5	13.0	13.7	15.3	15.2		5
$L_B/L_\odot$	$2.8\ 10^9\ h^{-2}$	$6.9\ 10^8\ h^{-2}$	$3.5\ 10^8\ h^{-2}$	$8.6\ 10^7\ h^{-2}$	$9.1\ 10^7\ h^{-2}$	$<1.7\ 10^7\ h^{-2}$	3
Inclination	80°	75°	68°	67°	66°		5
Position angle	150°	36°	18°		40°		2
Separation from NGC 4111		12'.9	8'.7	9'.5	11'.7	15'.2	3

1: Gallouët et al. (1973); 2: UGC; 3: this paper; 4: 2RCBG;
5: UGC or 2RCBG, using the method of Fisher and Tully (1981)
* in order of preference

companion is NGC 4117 which is 2.9 magnitudes fainter than NGC 4111. Of the companions only UGC 7089 was known to be rich in HI (Fisher and Tully, 1981; van der Burg, 1985). It appeared to have a redshift close to the optically determined value for NGC 4111. The only other companion for which an accurate (optically determined) redshift is available, is NGC 4117 (Huchra et al., 1982). This galaxy was observed with the Nançay Decimetric Radio Telescope (van der Burg, 1985) but no HI emission was detected. According to Dahari (1985), NGC 4117 is a Seyfert galaxy with a small companion (NGC 4118) with a comparable redshift. The nearest bright neighbours of NGC 4111 with

comparable systemic velocities are NGC 4143 and NGC 4138, located at angular separations from NGC 4111 of 42.7 and 46.0 arcmin respectively. According to de Vaucouleurs (1975) NGC 4111 and NGC 4143 are probably members of the Canes Venatici II Cloud which consists of at least a dozen bright galaxies, mainly of late morphological type.

3 Observations and reduction

NGC 4111 and its companions were observed with the Westerbork Synthesis Radio Telescope (WSRT) on May 25 1982, using the 5120-channel digital line backend (Bos et al., 1981). In order to achieve optimal sensitivity a configuration with 20 interferometers was chosen, such that the baselines ranged between 90 m and 1458 m with an increment of 72 m. This resulted in a synthesized antenna pattern with half-power dimensions of 24.″3 × 32.″4 ($\alpha \times \delta$); the radius of the first grating ring was 10.′0 × 14.′6 ($\alpha \times \delta$). Because of uncertainty regarding the velocities of the galaxies, a 5 MHz wide frequency band was observed in which orthogonal polarizations were recorded. This band was centered on the systemic velocity of NGC 4111; the total velocity range covered by these observations was 314 to 1342 km s^{-1}. Unless otherwise stated all velocities in this paper are heliocentric. A summary of the observational parameters is given in Table 2.

Standard correction and calibration procedures were applied to the observations and, through Fourier transformation of the sum of the U-V data over all channels, a map of the distribution of the total emission in the observed field was obtained. The strongest continuum sources were identified on this map and subtracted from the U-V data before the transformations of the individual channel data were made. In Table 3 the fluxes (corrected for attenuation by the primary beam) and positions of these sources are given. This table includes nuclear point sources in NGC 4111, NGC 4117 and an anonymous galaxy 20.6 arcmin north west of NGC 4111. About 2.2 arcmin south east of the center of NGC 4111, coinciding with the outermost optical emission along the major axis of the galaxy, a second point source has been detected. This source was also detected by Hummel and Kotanyi (1985); the flux and position are in good agreement. A line-free map was made by averaging channels 2-11 and 50-59 (channels 1 and 60-63 were rejected because of band-edge effects). This continuum correction map was subtracted from the individual channel maps. In order to remove the grating rings associated with the HI line emission, the continuum corrected channel maps were cleaned and then restored using the central maximum of the synthesized antenna pattern. This resulted in the final set of full resolution maps which was used for the further data reduction. The final channel

Table 2. Parameters of the observation

Date of observation	25 May 1982
length of observation	12 hours
α(1950) field center	$12^h04^m30^s$
δ(1950) field center	+43°19'58".8
baselines	
(min, max, increment)	90, 1458, 72 m
synthesized beam ($\alpha \times \delta$)	24".3 × 32".4
FWHP primary beam	36'
radius first	
grating ring ($\alpha \times \delta$)	10'.0 ×14'.6
bandwidth	4.8 MHz
number of	
frequency channels	63
central velocity	+827 km s^{-1}
channel spacing	16.6 km s^{-1}
velocity resolution	
after Hanning smoothing	33.4 km s^{-1}
r.m.s. noise	
channel maps	0.9 K

maps of UGC 7089, UGC 7094 and the uncatalogued dwarf galaxy about 3.9 arcmin south west of UGC 7094 are shown in Figures 2a and 2b; the rms noise in these maps is about 0.9 K. In Figure 2c the line emission from NGC 4117 is shown on the maps convolved to a resolution of 40" × 40". Maps smoothed to 60" × 60" are displayed in Figure 2d showing the line emission associated with NGC 4118. For the other galaxies in the field shown in Figure 1 no HI emission was detected. NGC 4109 is classified Sa: (2RCBG) so that a low HI content is expected. Assuming for the remaining three undetected galaxies an HI line profile width of 150 km s^{-1}, m_{pg} = 15.2 (for the brightest of these three) and an HI-mass to blue-luminosity ratio of 0.6, the expected flux density is about 20 mJy, which would be just detectable with the present sensitivity. Furthermore, these three undetected galaxies lie outside the half-power primary beam of the Westerbork telescope so that their detection is not expected.

The 60 arcsec maps were used to determine, at each velocity and for each galaxy separately, the region in which HI was present. These regions defined masks which, if necessary, were broadened to obtain a single continuous series of velocities at each grid point. The resulting masks were used to derive the global line profiles and the integrated HI surface density distributions of the companions (see section 4).

Table 3. Radio continuum sources in the field

α_{1950} h m s	δ_{1950} ° ′ ″	S_{1416} mJy	Notes
12 02 30.4	+43 16 40	65.4	
12 02 42.9	+43 26 51	22.9	a
12 04 03.8	+42 58 17	17.9	
12 04 09.5	+43 24 50	16.9	
12 04 30.9	+43 20 39	11.7	b
12 04 36.8	+43 18 47	17.6	c
12 04 39.8	+42 52 56	24.6	
12 05 14.1	+43 24 19	5.2	d
12 05 26.5	+43 19 04	28.0	
12 05 28.5	+43 19 04	8.7	
12 05 28.7	+43 14 23	16.6	
12 05 41.5	+42 59 46	20.5	
12 05 49.1	+43 45 42	26.4	
12 05 50.3	+43 20 26	6.7	
12 05 55.1	+43 16 27	24.8	
12 06 11.0	+43 18 33	11.0	
12 06 42.0	+43 56 01	306.0	

Notes:

a = source associated with an anonymous galaxy 20.6 arcmin north west of NGC 4111

b = central continuum source of NGC 4111

c = continuum source on south east side of NGC 4111

d = central continuum source of NGC 4117

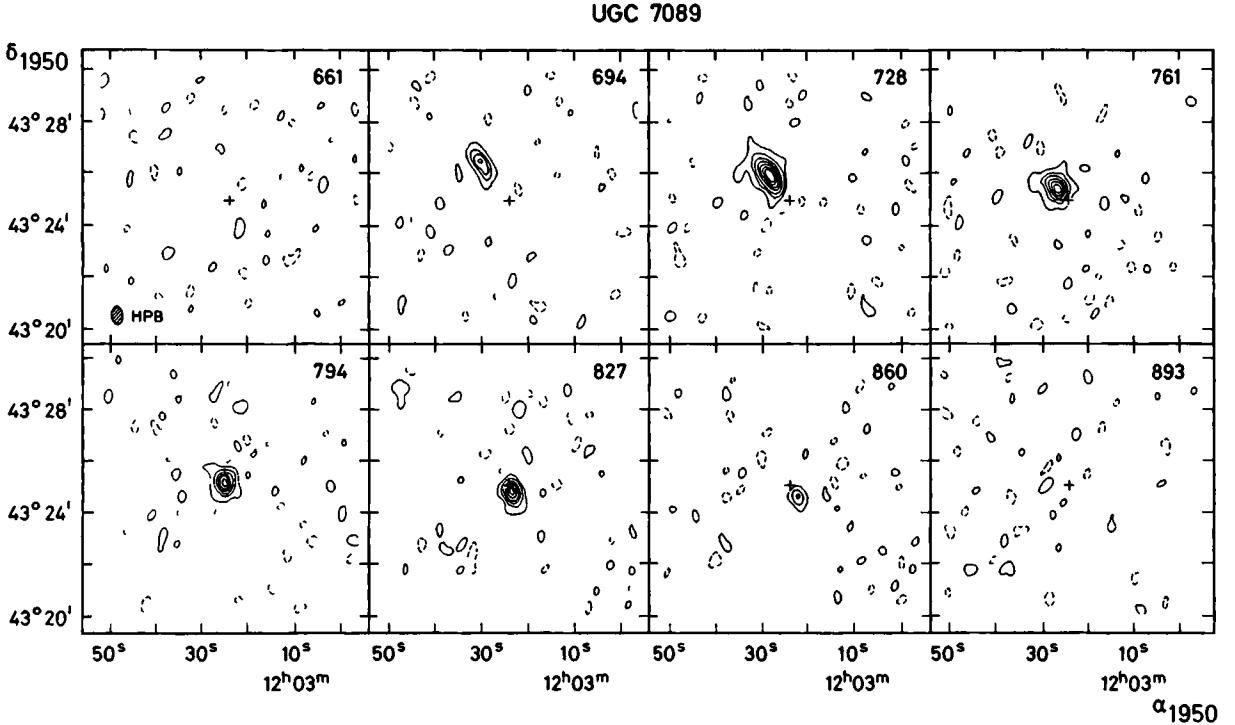

Figure 2a. Full resolution channel maps showing the line emission of the companion UGC 7089 In the upper right hand corner of each map the heliocentric radial velocity (in km s^{-1}) is given The first positive contour is plotted at 1 7 K, the contour interval is 3 4 K, negative contours are plotted as broken curves The cross in the center marks the position as listed in Table 1 The maps were not corrected for primary beam attenuation To obtain true temperatures a correction factor, a, which depends upon the distance of the companion from the field center, must be applied. For UGC 7089 a = 1 40

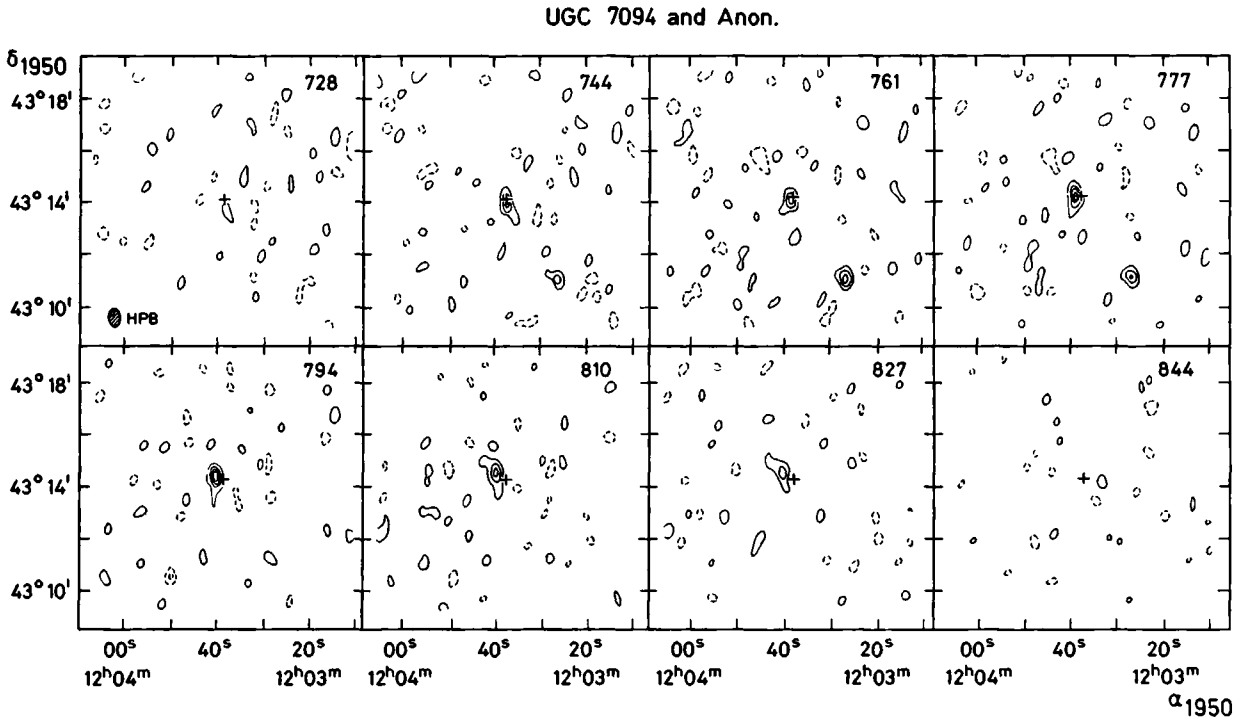

Figure 2b. *Full resolution channel maps of UGC 7094 and the anonymous galaxy 3.9 arcmin south west of UGC 7094, plotted as in Figure 2a but with a contour interval of 1.7 K, a = 1.32 and 1.60 for UGC 7094 and the anonymous galaxy respectively (the zero level contour has been omitted).*

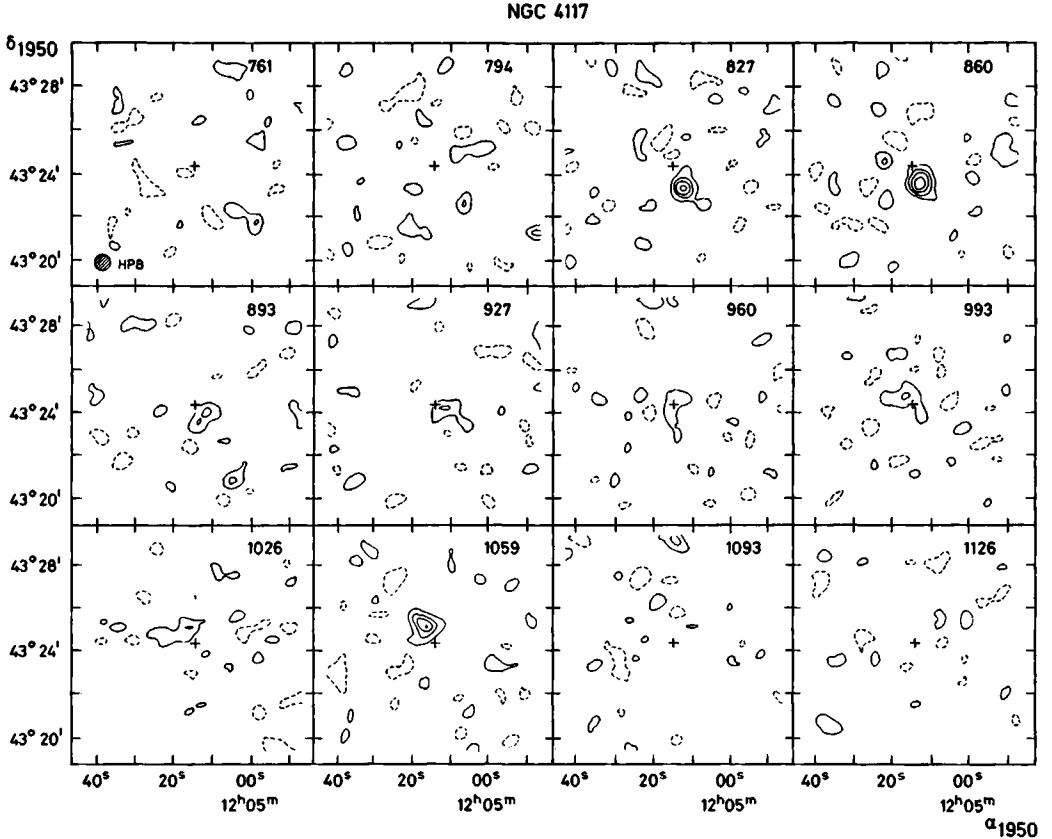

Figure 2c. Channel maps convolved to a resolution of 40" × 40", showing the line emission of NGC 4117, and plotted as in Figure 2a with a first contour and contour interval of 0.7 K, a = 1.16 (the zero level contour has been omitted).

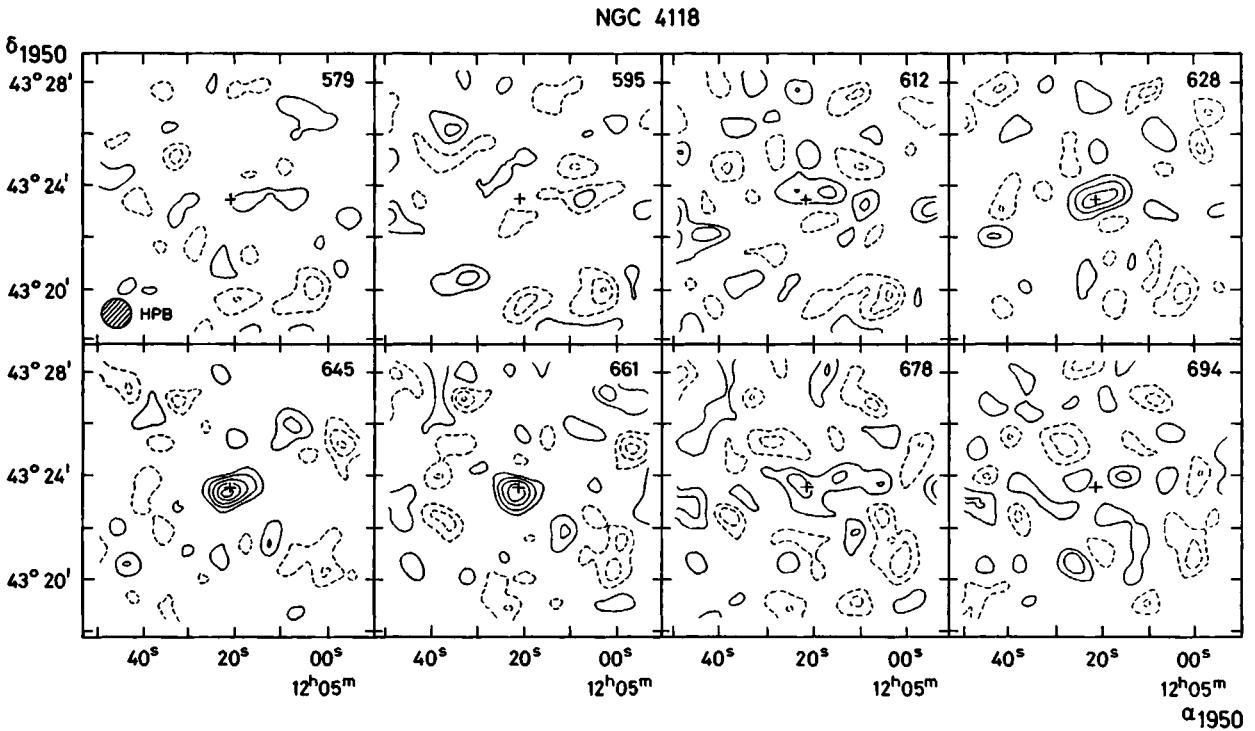

Figure 2d. Channel maps of NGC 4118 convolved to a resolution of 60" × 60" and plotted as in Figure 2a with a first contour and contour interval of 0.2 K, a = 1.20 (the zero level contour has been omitted).

4.1 Global 21-cm line profiles

For each detected galaxy the 21-cm line profile was obtained by integration of the masked channel maps after correction for attenuation by the primary beam. The resulting profiles, plotted on a common velocity axis, are shown in Figure 3; the systemic velocity V_{sys}, defined as the point halfway between the points at 20% of the peak flux, is indicated by an arrow. The parameters derived from the line profiles are listed in Table 4, where W_{20} is the profile width between the 20% points, uncorrected for inclination and instrumental resolution. Because of the low signal-to-noise ratio in the line profile of the anonymous dwarf the systemic velocity and velocity width of this galaxy are determined at the 50% peak level. The neutral hydrogen mass M_{HI} was calculated from $M_{HI} = 2.36\ 10^5\ D^2 \int SdV\ M_\odot$ assuming the HI to be optically thin, where D is the distance in Mpc and $\int SdV$ the 21-cm line flux in Jy km s^{-1}. The ratio of the HI-mass to blue-luminosity $[M_{HI}/L_B]$ in solar units is calculated using the luminosity given in Table 1. The indicative masses M_{ind} were obtained from the velocity widths of the line profiles using the method of Fisher and Tully (1981). The corresponding total-mass to blue-luminosity ratios $[M_{ind}/L_B]$ are also given in Table 4. Except for UGC 7089 these values are greater than the values listed by Faber and Gallagher (1979) for galaxies of corresponding morphological type and are also greater than the values listed by Thuan and Seitzer (1979) for a sample of Nilson and DDO dwarfs. Note that in order to calculate M_{ind} the projected rotational velocity must be corrected for the inclination angle i. The latter was calculated from the UGC diameters assuming an intrinsic axial ratio r_0 of 0.20 (Fisher and Tully, 1981). However, Thuan and Seitzer found that the dwarfs in their sample are not all highly flattened systems but that r_0 might vary between 0.25 and 1. Therefore, assuming $r_0 = 0.20$ for the companions of NGC 4111 may underestimate i, leading to an overestimation of M_{ind} and $[M_{ind}/L_B]$.

NGC 4111: The high resolution WSRT observation of NGC 4111 does not confirm the HI detection with the Nançay Decimetric Radio Telescope reported by van der Burg (1985). The 3σ flux density upper limit derived from the WSRT observation, obtained by integration of the channel maps over a rectangular region with dimensions equal to that of the half power beam of the Nançay telescope ($4' \times 22'$, $\alpha \times \delta$), is about 6 Jy km s^{-1} (assuming a velocity width W_{20} of 327 km s^{-1}; van der Burg, 1985). This is smaller than

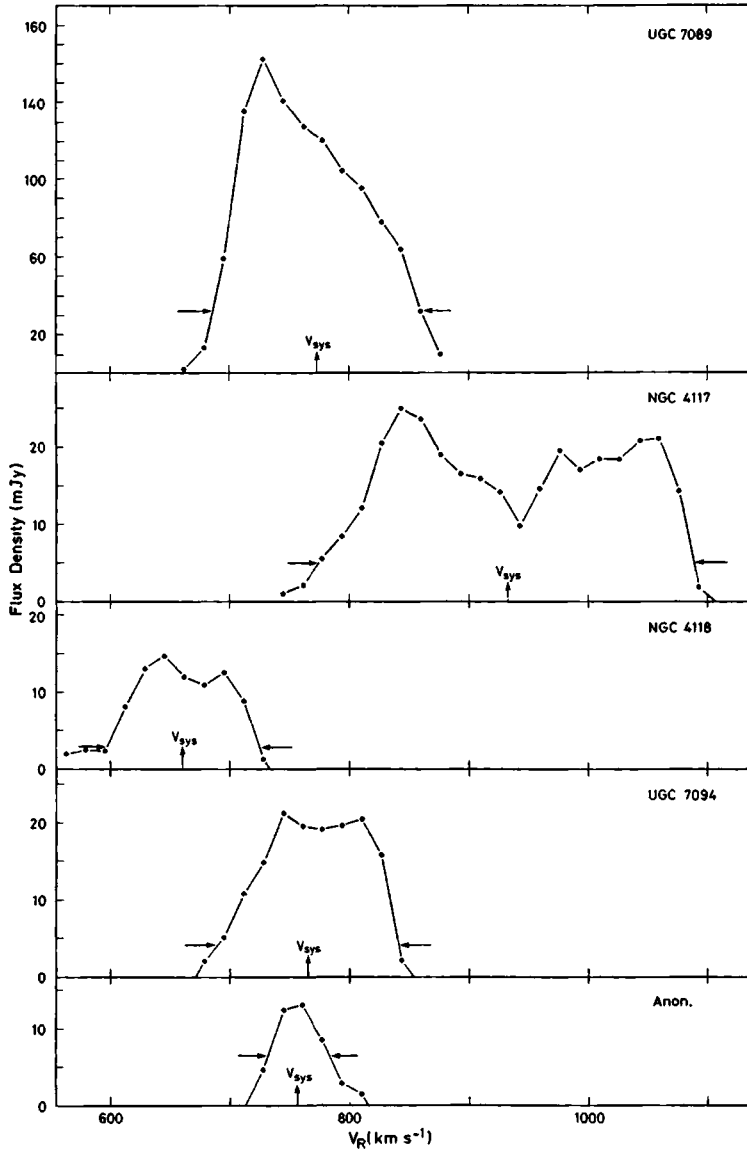

Figure 3. *Global 21-cm line profiles of UGC 7089, NGC 4117, NGC 4118, UGC 7094 and the anonymous dwarf galaxy. The horizontal arrows correspond to the 20% power points, except for the anonymous galaxy where they show the 50% power points. The vertical arrows indicate the systemic velocities.*

the upper limit of 29.4 Jy km s^{-1} reported by Fisher and Tully (1981, assuming W_{20} = 327 km s^{-1}) and is smaller than the Nançay flux of 11.6 Jy km s^{-1}. The corresponding upper limit to $[M_{HI}/L_B]$ is 0.04. Therefore, if the Nançay detection is real, the HI must be distributed over a region greater than that at which this WSRT observation loses sensitivity. It was noted by van der Burg (1985) that confusion in the Nançay observation with one or more companions of NGC 4111 could not be excluded. However, the present high resolution observations indicate that from the possible candidates for confusion (NGC 4109 and a small anonymous galaxy 4 arcmin south of NGC 4111) no significant contributions are to be expected.

UGC 7089: The bulk of the HI detected in the NGC 4111 group of galaxies (about 66%) is located in this companion. The $[M_{HI}/L_B]$-value of 0.45 is normal for a galaxy of type dm-m (Shostak, 1978). The shape of the line profile shown in Figure 3 agrees well with that measured with the Nançay Decimetric Radio Telescope (van der Burg, 1985). The peak at V = 727 km s^{-1} is caused by a concentration of gas on the north east side of the galaxy (see Figures 2a, 4 and 5). The total flux measured at Nançay is only 73% of the presently measured value (18.9 Jy km s^{-1}). UGC 7089 was also observed with the 91-m Green Bank radio telescope by Fisher and Tully (1981), and the flux reported by these authors (17.7 Jy km s^{-1}) agrees well with that measured with the WSRT. Note that the pointing center of the Nançay observation lies about 0.9 arcmin west of the concentration of gas at the north east side of UGC 7089 (see Figure 4). This might explain why the Nançay flux is less than the Green Bank and WSRT fluxes. Note that the radial velocity determinations from the three observations agree to within 6 km s^{-1}.

NGC 4117: The 21-cm line profile of this companion, classified as $S0^-$: (2RCBG) shows the classical double-horned profile characteristic of line emission from HI rotating in an annulus or in a disk with a flat rotation curve. The galaxy was observed at Nançay by van der Burg (1985) but only a 3σ upper limit, which was greater than the presently measured peak flux of about 25 mJy, could be determined. The $[M_{HI}/L_B]$-value of 0.25 is high for a galaxy classified S0; this might indicate that NGC 4117 is really of later morphological type. The systemic velocity listed in Table 4 is marginally consistent with the optically determined value of 958 ± 28 km s^{-1} quoted by Huchra et al. (1982).

NGC 4118: This faint galaxy (m_{pg} = 15.7, UGC) is clearly detected by the WSRT. The peak flux is about 15 mJy at V = 645 km s^{-1}. The total HI flux in the 21-cm line from this galaxy leads to an $[M_{HI}/L_B]$-value of 0.27 which is high for a galaxy classified as $S0^+$ (2RCBG). The line profile is symmetric and has a width of only 128 km s^{-1} (uncorrected for inclination). With a systemic velocity of 661 km s^{-1}, the radial velocity difference from NGC 4117 (located 1.3 arcmin north west) is 272 km s^{-1}. This value is much smaller than the velocity difference of 450 km s^{-1} quoted by Dahari (1985). However, the latter value is

described as quite uncertain.

UGC 7094: No previous HI or optical measurements have been reported for this galaxy. As in the case of NGC 4118, almost no central depression in the line profile is seen. As noted by Thonnard (1982) a centrally peaked HI surface density distribution along with a rotation curve which is gently rising with radius (a characteristic of low luminosity galaxies) may account for the absence of a central depression in the line profile.

Table 4. Global HI properties

	UGC 7089	NGC 4117	NGC 4118	UGC 7094	Anon.
systemic velocity V_{sys} (km s^{-1})	+772	+933	+661	+766	+756
line profile width W_{20} (km s^{-1})	176	314	128	153	50[a]
flux (Jy km s^{-1})	18.9	5.3	1.4	2.5	0.7:
$M_{HI}/M_{\odot}$*	3.1 10^{8} h^{-2}	8.8 10^{7} h^{-2}	2.3 10^{7} h^{-2}	4.2 10^{7} h^{-2}	1.2 10^{7} h^{-2}:
$[M_{HI}/L_B]$	0.45	0.25	0.27	0.42	> 0.7:
M_{ind}	8.2 10^{9} h^{-1}	2.4 10^{10} h^{-1}	1.9 10^{9} h^{-1}	3.0 10^{9} h^{-1}	< 2.2 10^{7} h^{-1}:[b]
$[M_{ind}/L_B]$	12 h	68 h	23 h	33 h	

* : $h = H_O/(100$ km s^{-1} $Mpc^{-1})$
a : profile width at 50% points
b : virial mass

Anonymous galaxy: The HI line profile of this irregular dwarf galaxy shows only a single peak at V = 756 km s^{-1}, with a maximum flux of about 13 mJy. The total HI flux in the 21-cm line is about 0.7 Jy km s^{-1}. Because no magnitude is known only a lower limit to $[M_{HI}/L_B]$ can be given; on the basis of catalogued comparison galaxies in the neighbourhood we estimate $m_{pg} > 17.0$ leading to $[M_{HI}/L_B] > 0.7$. As shown by the line profile in Figure 3, the emission from this galaxy extends over the velocity interval 728 to 794 km s^{-1}. The full width at half maximum is 50 km s^{-1}, which, after accounting for

instrumental broadening, yields an intrinsic velocity width of 38 km s^{-1}. This value is similar to the velocity widths of the dwarf irregulars detected by Lo and Sargent (1979). If the object is supported by random motions, as has also been suggested for the irregular dwarf M81 dwA studied by Sargent et al. (1983), the total mass can be calculated from the virial theorem: $M = \sigma^2 R/G$, with σ the velocity dispersion and R the HI radius. Because the galaxy is unresolved only an upper limit to R can be given. Using $R < 0.37\ h^{-1}$ kpc and $\sigma = 16$ km s^{-1} we calculate $M < 2.2\ 10^7\ h^{-1}\ M_\odot$. This means that at least 50% of the mass of this dwarf irregular must be in the form of neutral hydrogen.

4.2 The distribution of HI

The integrated HI surface density distribution of each detected galaxy has been obtained by adding the masked channel maps over the relevant velocity interval. The results, corrected for attenuation by the primary beam, are shown in the left panels of Figures 4a, b, c and d. In these figures the position angle at which the cross sections discussed in sub-section 4.3 were made are indicated. In the right panels a reproduction of the galaxy from the blue plate of the Palomar Observatory Sky Survey is shown with superposed the outermost contour of the HI distribution as shown in the left panel. These same contours are superposed on the reproduction of the NGC 4111 group shown in Figure 1. For UGC 7089, UGC 7094 and the irregular dwarf the full resolution maps are shown, for NGC 4117 the map convolved to a resolution of 40" and for NGC 4118 the 60" map. The different number of channels which contribute to the total flux at different grid points results in a nonuniform noise level in the maps. Due to the relatively large beam with respect to the dimensions of the companions, only the large-scale distribution of gas can be studied.

UGC 7089: The HI distribution in UGC 7089 is asymmetric, with a concentration of gas on the north east side. On this side the optical emission extends further out than on the south west side. The additional features in the immediate surroundings of UGC 7089 are probably noise; they have no apparent coherance in velocity. Perpendicular to the major axis, the HI is unresolved; its apparent width is almost completely determined by the width of the synthesized antenna pattern. No warp is visible; the position angle derived from the distribution of HI agrees with the optically determined value (Table 1).

NGC 4117: The bulk of the HI in NGC 4117 is concentrated in two clumps, and the optical center of NGC 4117 lies in between these clumps. The position angle defined by the centroids of the clumps agrees with the optically determined position angle listed in the

UGC. The position of the clumps on the major axis suggests that the gas is confined to an annulus. The HI diameter measured between the outermost contours along the major axis is almost equal to the optical diameter D_0 quoted in 2RCBG. However, the angular separation between the centroids of the clumps is only 0.6 D_0. The distribution of the HI perpendicular to the major axis is, at least in the outer parts, roughly a factor two broader than the length of the minor axis listed in the UGC. On either side of the nucleus and on opposite sides of the major axis, small extensions of HI are visible emerging from the clumps described above. As Figure 1 shows, the surface density distribution of NGC 4117 partly overlaps that of NGC 4118. However, because of the large difference in radial velocity (272 km s^{-1}, see Table 4 and Figure 3), no velocity confusion occurs and no difficulties arise in attributing the gas to the correct galaxy.

NGC 4118: The neutral hydrogen in NGC 4118 appears to be composed of several components. One component coincides with the optical image of the galaxy, and its reality is well established. This component has an extension to the west, partly overlapping NGC 4117. Inspection of the channel maps and the position-velocity map (Figure 5) shows that contributions to this extension come from channels with velocities between 610 and 700 km s^{-1}, with an interruption at velocity 661 km s^{-1}. The filaments beyond 1.5 arcmin from the center (on both sides of the galaxy) originate from weak emission scattered over several channels and must therefore be considered very doubtful. The emission 2.5 arcmin south west of NGC 4118 originates from emission in at least three consecutive channels. The major axis of the hydrogen distribution (position angle 110°) appears to be misaligned with respect to the major axis of the optical image (position angle about 150°).

UGC 7094: The HI distribution in UGC 7094 is centrally peaked and just barely resolved. It seems to be slightly shifted to the east with respect to the optical image. The optically determined position angle of the major axis agrees with the value derived from the HI distribution.

Anonymous galaxy: The integrated HI distribution of this dwarf is unresolved. No interaction with UGC 7094, located 3.9 arcmin north east, appears to be present.

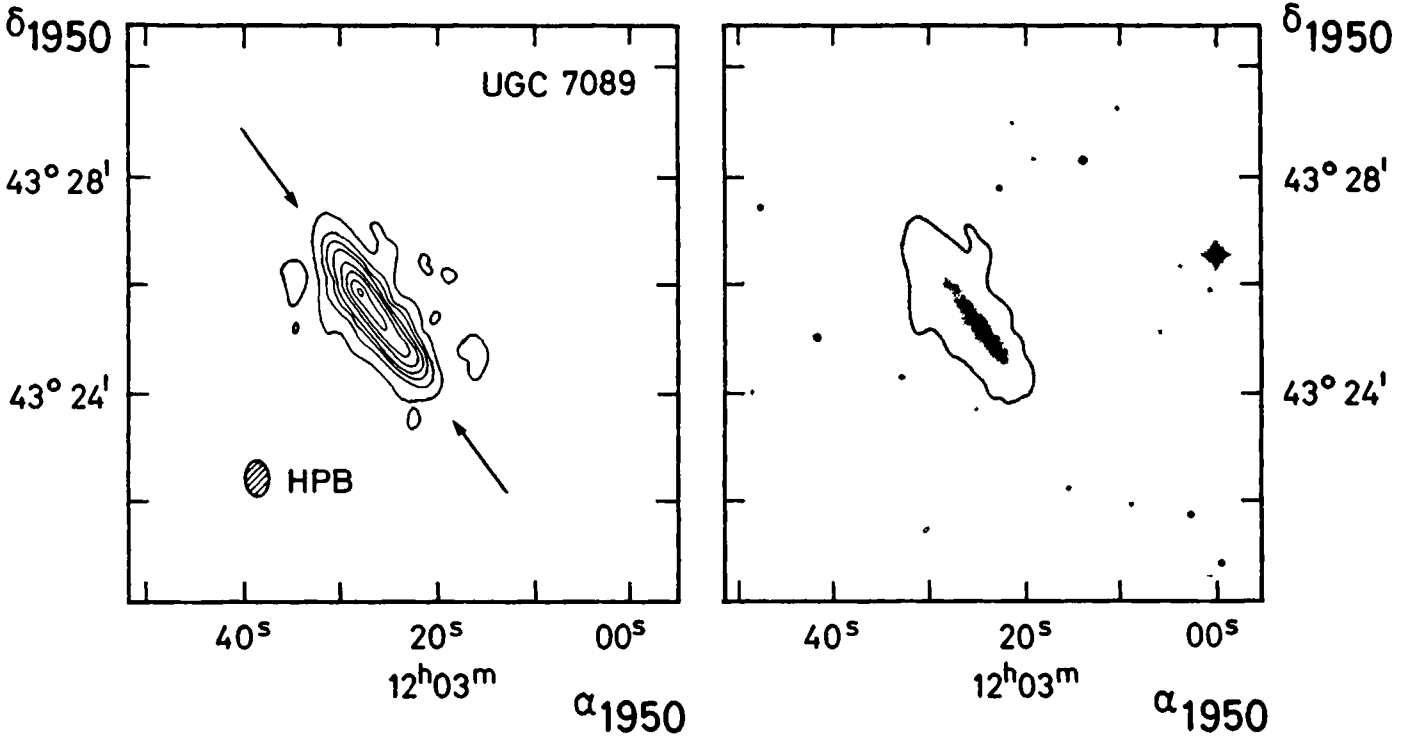

Figure 4a. Left panel Full resolution HI column density map of UGC 7089 after correction for primary beam attenuation The lowest contour is 2.3 10^{20} atoms cm^{-2}, the contour interval is 4.6 10^{20} atoms cm^{-2} The arrows indicate the direction along which the crosscut, plotted in Figure 5, is made Right panel Enlargement of the relevant part of Figure 1 with superposed the lowest contour as plotted in the left panel The cross within the optical emission corresponds with the position of the galaxy listed in Table 1

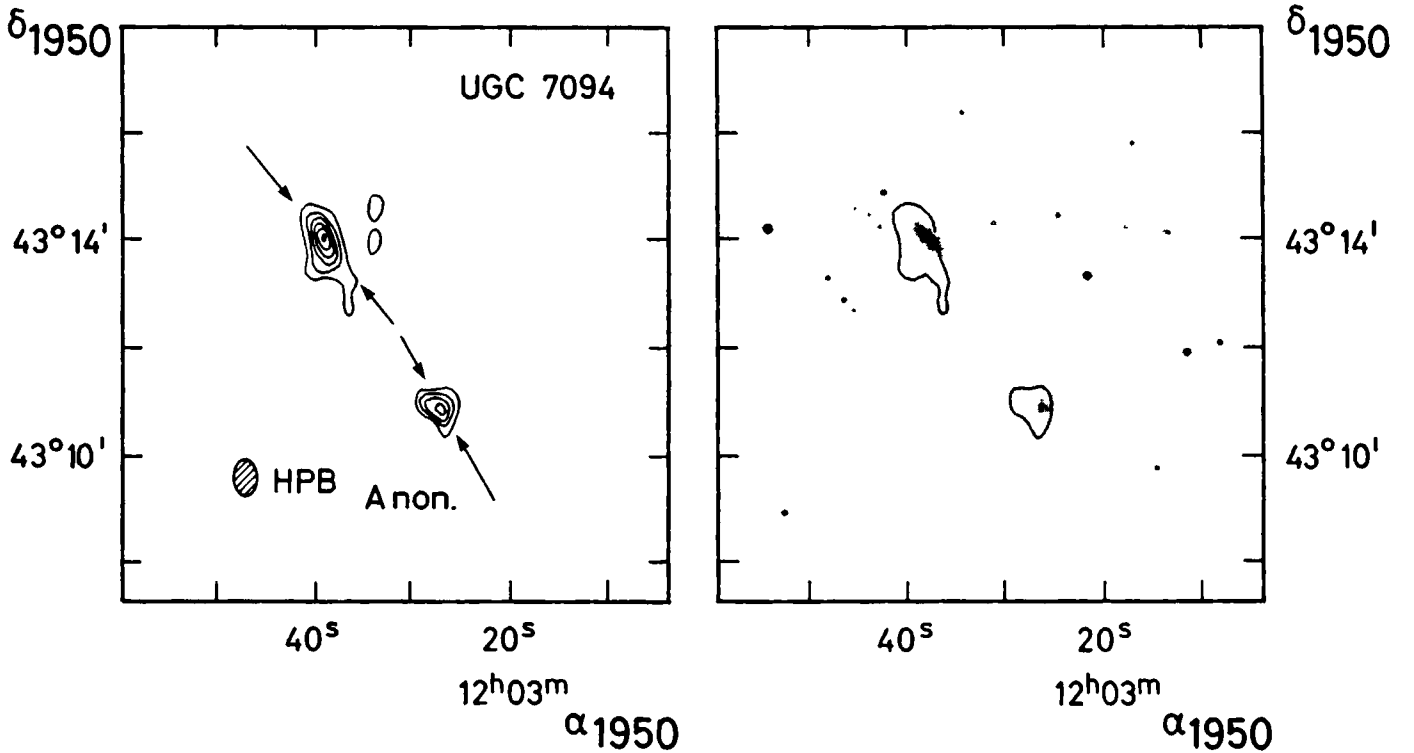

Figure 4b. HI column density map of UGC 7094 and the anonymous galaxy, plotted as in Figure 4a but with a contour interval of 2.3 10^{20} *atoms* cm^{-2}.

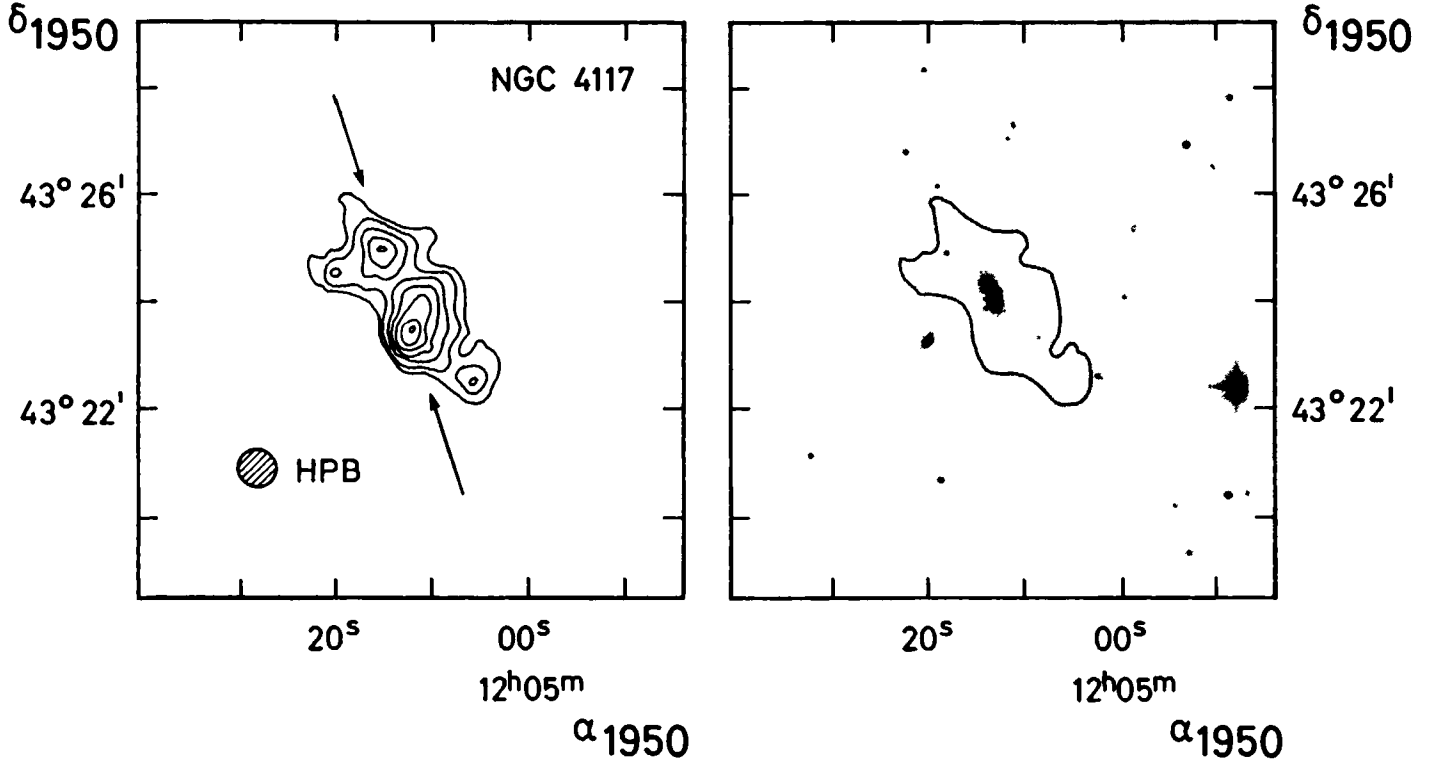

Figure 4c. HI column density map of NGC 4117 convolved to a resolution of 40" × 40" Except for the first contour and contour interval (which are 8 2 10^{19} atoms cm^{-2}) this figure is plotted as described for Figure 4a

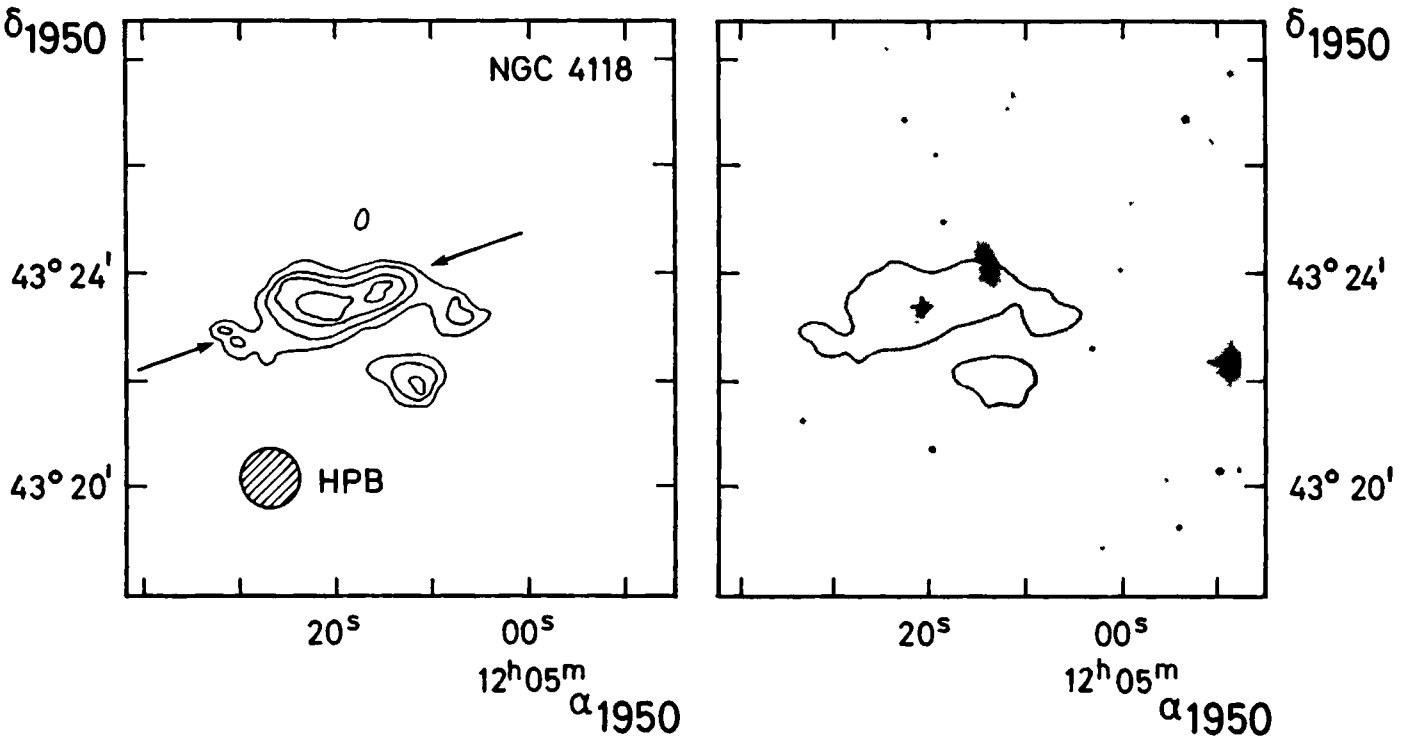

Figure 4d. HI column density map of NGC 4118 convolved to a resolution of 60″ × 60″ Except for the first contour and contour interval (which are 3.4 10^{19} atoms cm^{-2}) this figure is plotted as described for Figure 4a

For each of the five detected companions the brightness temperature as a function of velocity and position along the major axis is shown in Figure 5. The position angles, indicated in Figure 4, were taken from the UGC (for UGC 7089, NGC 4117 and UGC 7089) or determined from the distribution of HI (for NGC 4118 and the anonymous dwarf). For NGC 4117 and NGC 4118 the plots were made through the optical position given by Gallouët et al. (1973) which, for NGC 4117, agrees with the position of the nuclear continuum source (Table 3; for NGC 4118 no continuum emission was detected). For UGC 7089, UGC 7094 and the anonymous dwarf no accurate positions are available and the position-velocity map was made through the maximum in the total HI distribution. For the construction of the maps, the channel maps shown in Figure 2 were used. In Figure 6 the velocity fields of NGC 4117 and NGC 4118, which have rather extended HI distributions and are only moderately inclined to the line of sight, are shown. These maps were made by fitting a Gauss component to the spectrum measured at each grid point.

UGC 7089: On both sides of UGC 7089 the gas reaches its maximum rotation velocity within about 1 arcmin of the center; on the north east side the major axis rotation curve remains flat thereafter over the range of radii where it can be traced. The position-velocity map along with the distribution of HI (Figure 4a) suggest that the gas rotates in a disk rather than in a ring. This is confirmed by the absence of a central minimum in the line profile shown in Figure 3 (Thonnard, 1982).

NGC 4117: In the velocity field of NGC 4117 the central isovelocity contours (with velocities between 900 and 1025 km s^{-1}) are tilted with respect to the optical major axis. This could indicate that the gas possesses radial motions (Bosma, 1978). The position-velocity map confirms the conclusion in sub-section 4.2 that the gas in this galaxy is confined to an annulus.

NGC 4118: The position-velocity map of NGC 4118 is made at position angle 110°. This angle is determined by a line through the optical center and the two peaks of the total HI distribution shown in Figure 4d. From the resulting position-velocity map it is clear that the np peak with a velocity of about 690 km s^{-1}, corresponding to the extension of gas (Figure 4d), does not show coherance in velocity with the main feature associated with the optical emission visible on the Palomar Observatory Sky Survey. The very poorly defined velocity field shown in Figure 6 suggests that if their is any rotation, the kinematical major axis must be oriented almost north-south.

UGC 7094: The position-velocity map of UGC 7094 is quite symmetrical. The major axis rotation curve on both sides of the galaxy is constant or slightly declining with radius for r greater than about 0.5 arcmin.

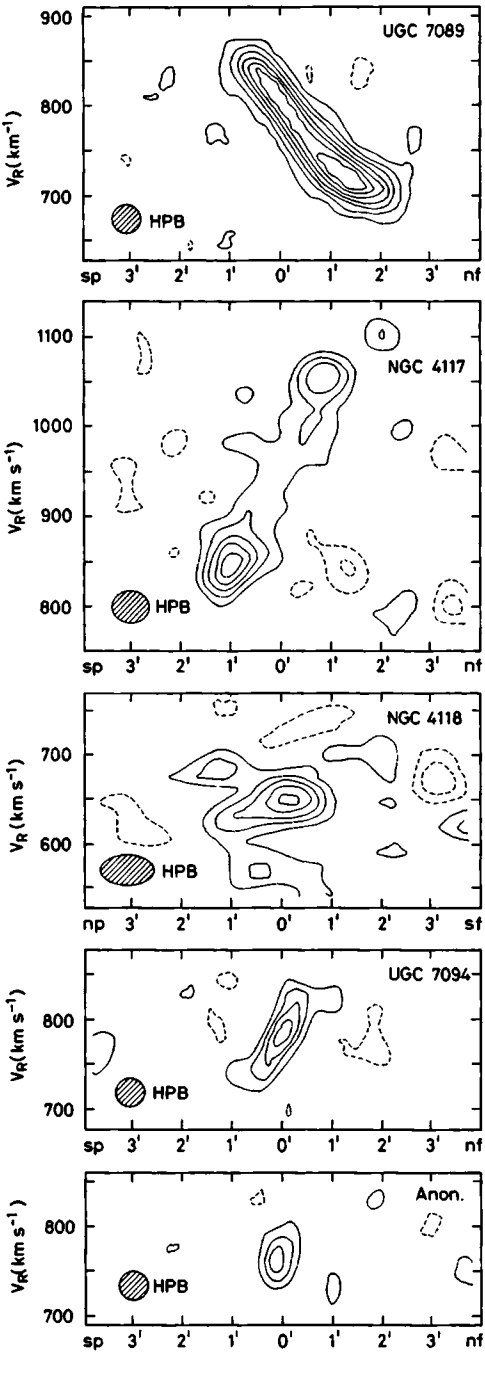

Figure 5. *Maps of the HI brightness distribution along the major axes as a function of radial velocity V_R and distance r from the positions listed in Table 1. Plots are shown for UGC 7089 (first contour 1.7 K and contour interval 3.4 K), NGC 4117 (first contour and contour interval 0.7 K), NGC 4118 (first contour and contour interval 0.2 K), UGC 7094 (first contour and contour interval 1.7 K) and the anonymous dwarf galaxy (first contour and contour interval 1.7 K). Negative contours are plotted as broken curves. The zero level contour is omitted. No correction for attenuation by the primary beam has been applied (see Figure 2 for the correction factors).*

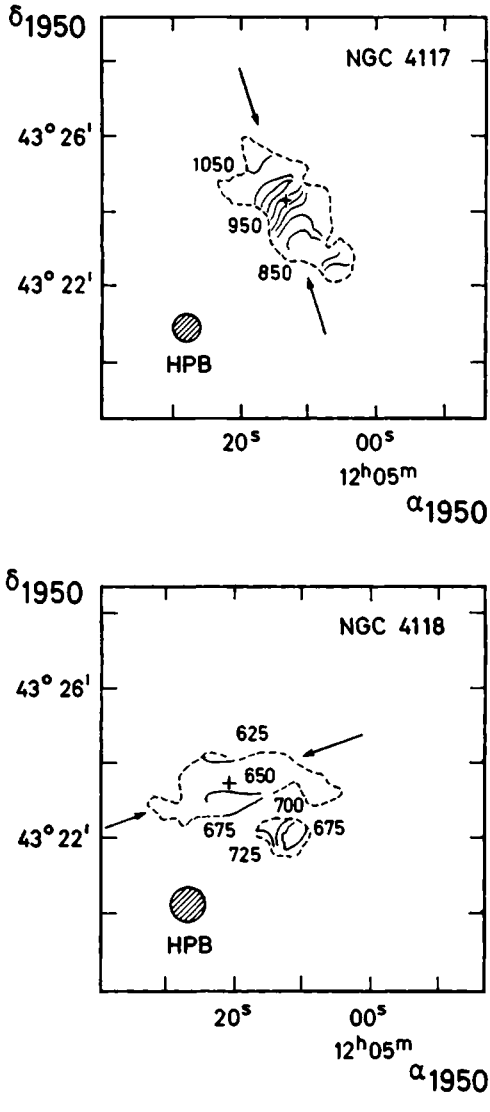

Figure 6. Isovelocity maps of NGC 4117 (upper panel) and NGC 4118 (lower panel) For both galaxies the outermost contour of the HI column density map, plotted in Figure 4, is shown as a broken curve The arrows indicate the direction along which the crosscuts of these galaxies, shown in Figure 5, were made The contour interval is 25 km s^{-1}

Anonymous galaxy: For the anonymous dwarf galaxy the position-velocity map is made at a position angle of 30°. Except for the slight elongation of the contours (which disappears at a position angle of 120°) no evidence for rotation is found, although this might be hidden by the poor spatial resolution.

5 Dynamical interpretation

Once the systemic velocities of the detected companions are known (see sub-section 4.1) we can employ the so-called projected mass method proposed by Bahcall and Tremaine (1981) to calculate the mass associated with the NGC 4111 group of galaxies. This method requires that the group be virialized and isolated, and that the mass of the companions be much smaller than the central mass. In the next sub-section we will comment on these requirements.

5.1 Discussion of the requirements

In section 2 it was noted that NGC 4111 is a bright galaxy apparently located at the center of a small group of faint galaxies. In section 4 it was shown that five members of this group contain detectable amounts of HI and that the systemic velocities of these galaxies lie in a fairly small velocity interval between 661 and 933 km s^{-1}. The luminosity weighted average systemic velocity of the group of faint galaxies (about 803 km s^{-1}) is very close to the optically determined systemic velocity of NGC 4111 quoted in 2RCBG (794 ± 14 km s^{-1}). This indicates that NGC 4111 and the group of faint companions are at the same distance. (Note that if the faint galaxies were background objects, the apparent central position of NGC 4111 would be very improbable). From the data on the detected companions listed in Table 1 we calculate an average projected radial separation $\langle R \rangle$ from the central galaxy of 28.3 h^{-1} kpc, which corresponds to a three-dimensional average radius $\langle r \rangle$ of about 36.1 h^{-1} kpc (since $\langle r \rangle = 4\langle R \rangle/\pi$). This implies that the five companions occupy a fairly small region centered near NGC 4111, so that they are probably physically associated and constitute a small group.

The method of Bahcall and Tremaine (1981) requires that, in addition to being bound, the group be in virial equilibrium. In order to satisfy this criterion the characteristic time required to traverse the group should be less than a Hubble time. A concept generally used in this respect is the crossing time. Several definitions have been given in the literature (see Faber and Gallagher, 1979, and references therein). If the gravitational

potential of the group is dominated by NGC 4111 (which is supported by the fact that about 70% of the total luminosity in the group comes from this galaxy) then the linear crossing time t_L defined by Rood and Dickel (1978) can be calculated from $t_L = 2<R>/(\pi<\Delta V>)$. Here $<\Delta V>$ is the average of the absolute values of the radial velocities with respect to the center of mass. The latter is assumed to coincide with the optical center of NGC 4111. Using the data listed in Table 4 gives $t_L = 2.4\ 10^8\ h^{-1}$ yr, which is significantly less than a Hubble time. However, the inclusion of galaxies which are not physical members of the group would tend to bias the crossing time toward small values. In this paper we will assume that the NGC 4111 group is virialized and calculate its mass using the projected mass method. We will then use the result of this mass determination to calculate the free fall time and to show that this characteristic time scale is not inconsistent with the assumption that virial equilibrium has been achieved. That the group is probably bound is already suggested by the small velocity range of the galaxies along with their small angular separations. If the group be not bound it must be very young which seems implausible, because otherwise it should have dispersed long ago.

The low luminosities of the companions (Table 1) along with their small indicative masses suggest that the satellites contribute only very little to the total mass of the group. Therefore we will consider the companions as test-particles orbiting in the gravitational field of the dominating galaxy, NGC 4111. This assumption will be verified in sub-section 5.2, after the total mass of the group has been calculated.

The projected mass method requires that the group be isolated. This requirement might be violated by the presence of NGC 4138 and NGC 4143, with about the same redshift as NGC 4111. However, their projected distances to NGC 4111 are $3.9<R>$ and $3.6<R>$ respectively, implying that the gravitational force exerted on the companions is at least an order of magnitude less than that exerted by NGC 4111. Moreover, both galaxies are fainter than NGC 4111 so that these systems, which are also of slightly later morphological type than NGC 4111 (see Sandage and Tammann, 1981), are probably less massive. However, note that the galaxies could have travelled the projected separation in about 4 t_L (assuming that the tangential velocity equals the radial velocity dispersion of 98 km s^{-1} derived for the NGC 4111 group of galaxies as described by Vennik, 1986). Therefore, if a gravitational encounter has taken place it might be doubtful whether virial equilibrium has been achieved.

5.2 Application of the projected mass method

In the previous sub-section it was argued that the NGC 4111 group of galaxies is probably bound and, to good approximation, isolated. Bahcall and Tremaine (1981) have shown that, under these conditions and in the absence of any information regarding the orbital eccentricities of the companions, the best estimate of the mass associated with the group is:

$$M_0 = \frac{24}{\pi G n} \sum_{i=1}^{n} \Delta V_i^2 R_i . \qquad (1)$$

Here n is the number of companions used in the calculation, R_i is the projected radial separation of a companion from the principal galaxy, and ΔV_i the difference in radial velocity. For each of the detected companions R and ΔV are listed in Table 5. Using these data, equation (1) yields $M_0 = 3.2\ 10^{11}\ h^{-1}\ M_\odot$ (for n = 5). Note that the indicative

Table 5. Parameters for the detected companions

Object	$\lvert\Delta V\rvert$ (km s^{-1})	R (kpc)	$\Delta V^2 R/2G$ ($10^{10}\ h^{-1}\ M_\odot$)
UGC 7089	22	31.5 h^{-1}	0.2
NGC 4117	139	21.3 h^{-1}	4.8
NGC 4118	133	23.2 h^{-1}	4.7
UGC 7094	28	28.6 h^{-1}	0.3
Anon.	38	37.1 h^{-1}	0.6

mass of the companions (which is probably overestimated; see sub-section 4.1) constitutes altogether only a fairly small fraction of M_0 (the largest contribution, about 7%, coming from NGC 4117: see Table 4). This supports the assumption that the companions may be considered as test-particles (see sub-section 5.1). According to Bahcall and Tremaine, the mass estimator M_0 has a fractional standard deviation of 63% for n = 5 so

that M_0 could be as high as 5.2 10^{11} h^{-1} $M_\odot$. The minimum possible mass is obtained from the requirement that all companions be bound to the group. As can be seen from column 4 of Table 5, this minimum mass, determined by NGC 4117, is 4.8 10^{10} h^{-1} $M_\odot$.

As argued is sub-section 5.1 the question arises whether this mass determination gives rise to characteristic time scales short enough that virial equilibrium could have been achieved. An indication can be obtained from the free fall time of a particle. Assuming a diameter two times the three-dimensional average radius <r> of the group, we derive a crossing time on a linear orbit $t = <r>/\sqrt{(2G\,\varrho_0)} = 4.6\ 10^8\ h^{-1}$ year for a mass distribution $M(r) \propto r$ with ϱ_0 given by $\varrho_0 = M(<r>)/(4\pi<r>)$. An alternative time scale is obtained from half the orbital time at r = <r>. This yields $t = 5.5\ 10^8\ h^{-1}$ year. These characteristic times are in the same order of magnitude as the crossing time calculated in sub-section 5.1. These small time scales justify the assumption that the group is virialized.

As pointed out by Bahcall and Tremaine (1981), there is a maximum variation of a factor three in mass between the extreme assumptions that the companions move in purely circular orbits (yielding a total mass of 1.4 10^{11} h^{-1} $M_\odot$) and in purely linear orbits (in which case M_0 is 4.2 10^{11} h^{-1} $M_\odot$).

Considering the group as a whole the mass-to-light ratio $[M_0/L_B]$ is about 80 h with $L_B = 4.0\ 10^9\ h^{-2}\ L_\odot$ the total luminosity of NGC 4111 and its detected companions. Accounting for the different values of H_0, this is in agreement with the range of M/L-values quoted by Faber and Gallagher (1979) for small groups. In sub-section 5.3 we will associate the mass M_0 with the brightest galaxy of the group, NGC 4111, and calculate its M/L.

Vennik (1986) calculated the virial masses of several nearby groups of galaxies. One of the selected groups is a group of twelve of which NGC 4111 is the brightest. The center of mass of this group is located about 42.7 arcmin north west of NGC 4111 and the mean projected separation between the group members is 473 h^{-1} kpc (adjusting H_0 to 100 h km s^{-1} Mpc^{-1}). The group encompasses the presently studied group of faint companions of NGC 4111. If we calculate the virial M/L for NGC 4111 and its faint companions (using the method of Vennik) we obtain $[M/L_B] = 73$ h. This is in good agreement with the value of 80 h obtained through application of the projected mass method but is about a factor two smaller than the virial M/L of 153 h obtained by Vennik for his extended NGC 4111 group. Because the latter value applies to a much larger region, it suggests that on scales greater than that of NGC 4111 and its faint companions the cumulative mass is still increasing with radius, indicating that dark matter is still being encountered.

One of the main uncertainties in the values of M_0 and $[M_0/L_B]$ arises from the presence of several galaxies which were undetected in HI, i.e. NGC 4109, UGC 7069 and two anonymous galaxies 20.8 and 27.9 arcmin respectively north-west of NGC 4111. As shown in section 3, the present observations cannot rule out the possibility that these galaxies are physical members of the group. Should the undetected galaxies have systemic velocities just outside the observed velocity interval ($|\Delta V| > 500$ km s^{-1}), the mass estimator M_0 would be strongly biased to small values. However, this assumption seems very improbable for those undetected galaxies which have large projected separations from NGC 4111 (20.8 arcmin and greater); for any plausible mass distribution one expects these galaxies to have the smallest velocity differences. The lower limit to M_0 which is derived after including (in addition to the five detected companions) the undetected galaxy closest to NGC 4111 (NGC 4109, 4.8 arcmin south), assuming $|\Delta V| =$ 500 km s^{-1}, is 1.1 10^{12} h^{-2} $M_\odot$. This lower limit falls within the range of lower limits to the total binding mass of lenticular galaxies given by Fabian et al. (1986) as derived from X-ray observations.

In order that the mutual gravitational forces between the companions not dominate that exerted by the central galaxy, it is important that the companions not be clustered. Note that the major contribution to M_0 comes from NGC 4117 and NGC 4118 (see Table 5). The angular separation of these galaxies is only 1.5 arcmin which, at a distance of 8.4 h^{-1} Mpc, corresponds to a projected separation of only 3.7 h^{-1} kpc. It was proposed by Dahari (1984) that gravitational interaction with NGC 4118 might have induced the Seyfert properties observed in NGC 4117. If we consider these galaxies as a bound isolated pair, the minimum orbital mass, assuming a parabolic orbit, is 3.1 10^{11} h^{-1} $M_\odot$. This minimum mass is about equal to the total mass M_0 of the group calculated for n = 5. The corresponding minimum $[M/L_B]$ is 70 h. This lower limit to $[M/L_B]$ is much greater than the corresponding average of 5.7 h given by Blackman and van Moorsel (1984) for a small sample of spiral galaxies. Note that NGC 4117 and NGC 4118 are both classified as early type (see Table 1), but, according to Faber and Gallagher (1979), the scarce $[M/L_B]$-values of S0 binaries are broadly similar to those of late-type spiral pairs. Therefore it seems unlikely that NGC 4117 and NGC 4118 form a physical pair. Another possible pair is formed by UGC 7094 and the anonymous dwarf galaxy which lies 3.9 arcmin south west. The minimum $[M/L_B]$, assuming that this pair is bound, is about 1 h so that the possibility that these galaxies constitute a physical pair cannot be ruled out. However, due to its small mass the anonymous galaxy will hardly influence the dynamics of UGC 7094 with respect to NGC 4111. Excluding the anonymous galaxy from the calculation of the projected mass (n = 4) yields $M_0 =$ 3.8 10^{11} h^{-1} $M_\odot$, which is only slightly higher than the value obtained for n = 5.

In the previous sub-section it was shown that the best estimate of the mass associated with the group, calculated from the projected mass method, is 3.2 10^{11} h^{-1} $M_{\odot}$. Note that the projected mass M_0 represents the mass within a volume with an average radius <r> of 36.1 h^{-1} kpc (see sub-section 5.1) centered on NGC 4111. Therefore, these observations provide a measure of the mass of the S0 galaxy NGC 4111 interior to a radius about five times its Holmberg radius. Using the blue luminosity of this galaxy listed in Table 1 and subtracting the small mass contributions of the companions (Table 4), the mass-to-light ratio is about 101 h. This large mass-to-light ratio strongly suggests that NGC 4111 is embedded in a massive nonluminous halo. In order to obtain information regarding the distribution of mass around NGC 4111, we must look for a radial trend in M/L. The only optical rotation curve data available for NGC 4111 are the measurements made by Humason and published by van Houten (1961). These measurements extend to a maximum galactocentric radius of 44 arcsec (1.8 h^{-1} kpc or 0.2 R_{Ho}), much smaller than the region examined in the present study. The corresponding $[M/L_B]$-value for this small region, accounting for the different distances assumed, is 19 h (van Houten). According to Faber and Gallagher (1979) the mean value of $[M/L_B]$ within one Holmberg radius calculated for a small sample of S0 galaxies from rotation curve data, is about 20 h. Therefore we may conclude that the $[M/L_B]$-value of NGC 4111 inside about five Holmberg radii exceeds the average $[M/L_B]$-value for S0 galaxies within one Holmberg radius by about a factor five. It is interesting to note that this behaviour of M/L_B agrees with that calculated under the assumption of a flat rotation curve, such as is often found in the outer parts of galaxies. Recently Shostak (1987) calculated the $[M/L_B]$-value for the HI-rich SB0/a galaxy NGC 2787. The resulting value of 67 h (adjusted to $H_0 = 100$ h km s^{-1} Mpc^{-1}) is calculated from the rotation curve measured out to five optical radii. This $[M/L_B]$-value is comparable to the value calculated for the barred S0 galaxy NGC 2859 (van der Burg et al., 1987), but is smaller than the corresponding value for NGC 4111.

The upper limit to $[M_{HI}/L_B]$ for NGC 4111 is smaller than the value calculated from the (doubtful) detection reported by van der Burg (1985), but is greater than the upper limit of 0.01 calculated for the majority of undetected lenticular galaxies (Burstein and Krumm, 1981). However, considerable amounts of gas are present in the direct neighbourhood of NGC 4111. This gas is associated with five companions, which are located within about five Holmberg radii of NGC 4111. In this respect the situation resembles that encountered in the S0 galaxies NGC 2859 (Shane and Krumm, 1983; van der Burg et al., 1987), NGC 1023 (Sancisi et al., 1984), NGC 4026 (Appleton, 1983) and NGC 5084 (Gottesman and

Hawarden, 1986), and in the late type spirals NGC 3992 and NGC 4731 studied by Gottesman et al. (1984). Aside from orbiting HI-rich companions, NGC 1023 is embedded in a cloud of HI which, according to Sancisi et al., might represent the original gas content of a small companion 3 arcmin east of NGC 1023 which is currently being accreted. Signs of accretion are completely absent in the presently studied group. Nevertheless, the HI-rich companions might play an important role in the evolution of the S0 galaxy NGC 4111. If in the future the HI should be removed from one or more of these companions and captured by NGC 4111, the resulting $[M_{HI}/L_B]$-value would lie somewhere in the range 0.004 (in case only the anonymous galaxy was consumed) to 0.17 (in case all companions were captured in a short time). Note that the center of this range of $[M_{HI}/L_B]$-values lies close to the mean value of 0.08 for a sample of 11 HI-rich S0 galaxies which, according to Wardle and Knapp (1986), are members of small groups rather than large clusters. From a statistical study of the neutral hydrogen content of S0 galaxies, Wardle and Knapp conclude that the form of the distribution of $[M_{HI}/L_B]$ suggests that the gas originates from sources completely outside the galaxies. The present observations, along with HI observations of NGC 1023, NGC 4026 and NGC 2859, show that these S0 galaxies have plenty of HI gas in their direct surroundings which, if captured, might turn these S0 galaxies into gas-rich systems.

A possible scenario for accretion has been proposed by Silk and Norman (1979). These authors suggested that gas from HI-rich dwarf companions is stripped through interaction with a gaseous halo or a galactic wind. If this mechanism were important in the NGC 4111 group, the small crossing time of the five HI-rich companions suggests that at least some gas should have been removed, which evidently has not occurred. That this mechanism seems to be ineffective in this group may be related to the fact that the dwarfs considered by Silk and Norman consist predominantly of hydrogen, with $[M_{HI}/L] > 1$ and $M > -10$. In the NGC 4111 group these criteria may be fulfilled only by the anonymous dwarf irregular. An alternative way for NGC 4111 to acquire gas would be through the passage of a massive galaxy (like NGC 4138 and NGC 4143). Such an encounter might force one or more of the HI-rich companions into orbits which could ultimately lead to merging with NGC 4111.

Among the detected galaxies are two members classified as lenticular (see Table 1). These two galaxies, NGC 4117 and NGC 4118, have $[M_{HI}/L_B]$-values much greater than is typically measured for early type galaxies. This suggests that they may be, in fact, of later morphological type. However, it is known that a small number of lenticulars have a very high HI content (cf. NGC 5084, an $S0^+$ galaxy studied by Gottesman and Hawarden, 1986, for which $[M_{HI}/L_B] = 0.35$). If NGC 4117 and NGC 4118 are indeed of early morphological type the question arises how these companions were able to retain there HI in contrast to

the lenticular NGC 4111. Stripping of gas in the latter galaxy through interaction with an intracluster medium seems implausible because this mechanism would be much more effective in the low-mass companions (including the two lenticulars). On the other hand, infall of gas into the companions also seems very unlikely due to their modest masses. The high gas content in NGC 4117 and NGC 4118 may be left over from their formation and still be present due to the low rate of star formation in these low-mass systems.

Acknowledgements

The Westerbork Synthesis Radio Telescope is operated by the Netherlands Foundation for Radio Astronomy (SRZM), with the financial support of the Netherlands Organization for the Advancement of Pure Research (Z.W.O.).

Appleton, P.N.: 1983, Mon. Not. R. Astron. Soc. 203, 533

Bahcall, J.N., Tremaine, S.: 1981, Astrophys. J. 244, 805

Blackman, C.P., van Moorsel, G.A.: 1984, Mon. Not. R. Astron. Soc. 208, 91

Bos, A., Raimond, E., van Someren Greve, H.W.: 1981, Astrophys. J. 98, 251

Bosma, A.: 1978, The Distribution and Kinematics of Neutral Hydrogen in Spiral Galaxies of various morphological Types, Dissertation, University of Groningen

Burstein, D, Krumm, N.: 1981, Astrophys. J. 250, 517

Dahari, O.: 1984, Astron. J. 89, 966

Dahari, O.: 1985, Astron. J. 90, 1772

de Vaucouleurs, G.: 1975, Stars and Stellar Systems Vol. IX, 557

de Vaucouleurs, G., de Vaucouleurs, A., Corwin, H.G.: 1976, Second Reference Catalogue of Bright Galaxies (University of Texas Press) (2RCBG)

Faber, S.M., Gallagher, J.S.: 1979, Ann. Rev. Astron. Astrophys. 17, 135

Fabian, A.C., Thomas, P.A., Fall, S.M., White, R.E.: 1986, Space Telescope Science Institute, Preprint Series 118

Fall, S.M.: 1986, Space Telescope Science Institute, Preprint Series 149

Fisher, J.R., Tully, R.B.: 1981, Astrophys. J. Suppl. Ser. 47, 139

Gallouët, L., Heidmann, N., Dampierre, F.: 1973, Astron. Astrophys. Suppl. Ser. 12, 89

Gottesman, S.T., Hunter, J.H.: 1982, Astrophys. J. 260, 65

Gottesman, S.T., Hunter, J.H., Shostak, G.S.: 1983, Mon. Not. R. Astron. Soc. 202, 21p

Gottesman, S.T., Ball, R., Hunter, J.H., Huntley, J.M.: 1984, Astrophys. J. 286, 471

Gottesman, S.T., Hawarden, T.G.: 1986, Mon. Not. R. Astron. Soc. 219, 759

Huchra, J.P., Wyatt, W.F., Davis, M.: 1982, Astron. J. 87, 1628

Hummel, E., Kotanyi, C.G.: 1985, Astron. Astrophys. 145, 475

Lo, K.Y., Sargent, W.L.W.: 1979, Astrophys. J. 227, 756

Nilson, P.: 1973, Uppsala General Catalogue of Galaxies, Ann. Uppsala Astron. Obs 6 (UGC)

Rood, H.J., Dickel, J.R.: 1978, Astrophys. J. 224, 724

Sancisi, R., van Woerden, H., Davies, R.D., Hart, L.: 1984, Mon. Not. Astron. R. Soc. 210, 497

Sandage, A., Tammann, G.A.: 1981, A Revised Shapley-Ames Catalog of Bright Galaxies, Carnegie Institution of Washington Publication 635

Sargent, W.L.W., Sancisi, R., Lo, K.Y.: 1983, Astrophys. J. 265, 711

Shane, W.W.: 1980, Astron. Astrophys. 82, 314

Shane, W.W., Krumm, N.: 1983, in Internal Kinematics and Dynamics of Galaxies, IAU Symp. 100, ed. E. Athanassoula, Reidel Dordrecht, 105

Shostak, G.S.: 1978, Astron. Astrophys. 68, 321

Shostak, G.S.: 1987, Astron. Astrophys. 175, 4

Silk, J., Norman, C.A.: 1979, Astrophys. J. 234, 86

Thonnard, N.: 1982, in Proceedings of the Workshop: The Comparative HI content of Normal Galaxies, Green Bank, West Virginia

Thuan, T.X., Seitzer, P.O.: 1979, Astrophys. J. 231, 680

Tsikoudi, V.: 1980, Astrophys. J. Suppl. Ser. 43, 365

van der Burg, G.: 1985, Astron. Astrophys. Suppl. Ser. 62, 147

van der Burg, G., Hoevers, H.F.C., Shane, W.W.: 1987, to be published

van Houten, C.J.: 1961, Bull. Astron. Inst. Netherland 16, 1

Vennik, J.: 1986, Astron. Nachr. 307, 157

Wardle, M., Knapp, G.R.: 1986, Astron. J. 91, 23

Zwicky, F., Herzog, E., Wild, P., Karpowicz, M., Kowal, C.T.: 1961 - 1968, Catalogue of Galaxies and of Clusters of Galaxies, California Institute of Technology

CHAPTER 8 NEUTRAL HYDROGEN OBSERVATIONS OF THE GALAXY PAIR NGC 5899/ 5900

Summary

In this paper HI synthesis observations of the SABc galaxy NGC 5899 and its late type companions are presented. Measurements of the systemic velocities of these companions can provide important data on the distribution of mass in and around NGC 5899. Besides NGC 5899, only one of its companions, NGC 5900, has been detected. The systemic velocity difference between these two galaxies derived from the 21-cm line profiles is 111 km s^{-1}, suggesting that they are a physical pair. The $[M_{HI}/L_B]$-values of NGC 5899 and NGC 5900 are 0.14 and 0.64 respectively. The total mass to blue luminosity ratio M/L_B for NGC 5899 is quite normal for its type whereas for NGC 5900 a value roughly twice as high as the average for Sb galaxies is found. The lower limit to the orbital mass, assuming parabolic orbits, is smaller than the sum of the individual masses of NGC 5899 and NGC 5900 as determined from their rotation. Therefore there appears to be no requirement for the presence of large amounts of dark matter outside the Holmberg radii of these galaxies. The distribution of HI in NGC 5899 suggests gravitational interaction with NGC 5900. The ratio of the 80 μm infrared to blue luminosity indicates that the encounter has induced a weak burst of star formation in the latter galaxy.

1 Introduction

NGC 5899 is a representative of the class of single bright galaxies accompanied by several faint companions. The Palomar Observatory Sky Survey shows that the galaxy is located on the south east side of a group of at least four faint companions. Radial velocity measurements of these companions can provide an estimate of the mass in and around the primary galaxy NGC 5899. This galaxy is identified as a Seyfert (uncertain; see Dahari, 1984), and possesses a prominent two-armed spiral structure with extended luminous regions; the morphological type of the galaxy is SAB(rs)c (de Vaucouleurs et al., 1976; hereafter 2RCBG). NGC 5893, which lies about 17.4 arcmin south west of the primary, and NGC 5899 were included in a list of binary systems by Peterson (1979). However, the radial velocity of NGC 5893 turned out to be so much larger (Peterson, 1979) than that of NGC 5899 that it must be considered a background galaxy, not gravitationally bound to the primary. The closest companion to NGC 5899 is NGC 5900, two magnitudes fainter and located 9.7 arcmin north of the primary. This system is seen edge-on and has an asymmetrical and irregular appearance with a dust lane crossing the optical image to the south east of the nucleus. It is classified as Sb:(sp) (2RCBG); no further optical measurements of NGC 5900 are reported in the literature. The other companion galaxies in the group are NGC 5895, which forms a close pair with NGC 5896, and an anonymous galaxy 25 arcmin north west of NGC 5899 which is included in the Catalogue of Galaxies and Clusters of Galaxies (Zwicky et al., 1961 - 1968). About 2.9 arcmin south west of NGC 5899 a fuzzy knot, best seen on the red print of the Palomar Observatory Sky Survey, can be distinguished. This object, probably a background galaxy, was included in the list of companions of Seyfert galaxies by Dahari (1984), but was too faint to be studied (Dahari, 1985). In Table 1 the optical properties of all of these galaxies are reported.

Because redshift observations of the companions can provide important data on the distribution of mass around NGC 5899, the group was observed in the 21-cm line of neutral hydrogen by van der Burg (1985) using the Nançay Decimetric Radio Telescope. Only the primary galaxy NGC 5899 was detected with certainty. Due to the small angular separation between NGC 5899 and NGC 5900, no definite conclusion with regard to the origin of the line emission detected in the observation centered on NGC 5900 could be drawn from this observation.

In this paper Westerbork Synthesis Radio Telescope (WSRT) observations of the group are presented. It is shown that, in addition to NGC 5899, HI is detected in NGC 5900, which appears to have a redshift comparable with that of NGC 5899. In the observed velocity interval no HI could be detected associated with the other galaxies in the field. If we consider NGC 5899 and NGC 5900 as a binary system a lower limit to the orbital mass

Table 1. Optical data on individual group members

	NGC 5899	NGC 5900	NGC 5893	NGC 5895/ 5896	Anon.	Ref.
α_{1950}	$15^h 13^m 14\overset{s}{.}6$	$15^h 13^m 16\overset{s}{.}4$	$15^h 11^m 45\overset{s}{.}2$	$15^h 12^m 00^s$	$15^h 11^m 36^s$	1,2*
δ_{1950}	+42°13'57"	+42°23'41"	+42° 8'39"	+42°11'	+42°31'	1,2*
separation		9'.7	17'.4	14'.1	25'.0	3
type	SAB(rs)c	Sb:sp	SB(r)b			4
B_T^p	12.0	14.0	13.6			5
inclination	64°	74°	21°			5
position angle	18°	131°				5
D(0)	2'.51	1'.29	1'.41			4
Holmberg radius R_H	2'.1	1'.2	1'.2			5
Blue luminosity	1.9 10^{10} h^{-2} $L_\odot$	0.3 10^{10} h^{-2} $L_\odot$	0.4 10^{10} h^{-2} $L_\odot$			3

1: Gallouët et al. (1973)
2: Zwicky et al. (1961 - 1968)
3: this paper
4: de Vaucouleurs et al. (1976)
5: Nilson (1973)

*: in order of preference

can be determined (cf. van Moorsel, 1982; Karachentsev, 1985). The high angular resolution of the WSRT is employed to study the distribution and kinematics of the gas in this double system. Comparison of the lower limit to the orbital mass (calculated from the relative velocity of the galaxies and their projected separation) with the sum of the individual masses determined from the rotational velocities provides information on the possible presence of a massive, non-luminous halo.

In section 2 the observations and the reduction procedure are outlined, and the resulting global properties are presented in section 3. In section 4 we derive the masses of the individual galaxies and compare the sum of these masses with the lower limit to the orbital mass assuming a parabolic orbit. It is argued that the distorted distribution of gas in NGC 5899 and the enhanced infrared excess of NGC 5900 are probably due to gravitational interaction between these galaxies.

2 Observations and reduction

The 21-cm line HI observations of NGC 5899 and its surrounding region were carried out with the Westerbork Synthesis Radio Telescope (WSRT) in June 1982. The minimum and maximum baselines were 54 and 1422 meters respectively, with an increment of 72 meters so that a total number of 20 different baselines were sampled. The length of the observation was 10.8 hours, giving 90% hour-angle sampling. The resulting synthesized antenna pattern has half-power dimensions of $24''.3 \times 36''.3$ ($\alpha \times \delta$). The 5120-channel digital line backend (Bos et al., 1981) was used to record orthogonal polarizations in 63 frequency channels in a 4.8 MHz frequency band centered on the systemic velocity of NGC 5899. The data from the individual channels (with a velocity separation of 16.6 km s^{-1}) were Hanning smoothed in frequency resulting in a velocity resolution (FWHM) of 33.4 km s^{-1}. A summary of the observational parameters is given in Table 2. After standard corrections and calibration (Högbom and Brouw, 1974), the sums of the data over all channels were Fourier transformed to a map of the intensity distribution. This map was searched for the presence of continuum sources and the strongest sources were excluded from the data in the U-V domain before the transformations of the individual channels were made. The detected continuum sources are listed in Table 3 where the fluxes (after correction for primary beam attenuation) and positions, determined by fitting the antenna pattern to the data, are given. (For NGC 5899 and NGC 5900 these parameters were determined using a map from which the line emission had been removed.) A discussion of the detected continuum sources is given in sub-section 3.1. The channel maps, after continuum source removal, were inspected for the presence of HI emission, and those free from any line radiation were averaged so as to construct a continuum correction map. This correction map is composed of 19 channels; five channels, one at the lowest velocity and four at the highest velocities, were discarded because of band-edge effects. This continuum correction map was then subtracted from all individual channel maps in order to remove residual continuum radiation. Due to the incomplete coverage of the U-V plane, the synthesized antenna pattern has sidelobes with a maximum negative amplitude

Table 2. Parameters of the observation

Date of observation	23 June 1982
length of observation	10.8 hours
α field center	$15^h 13^m 12^s$
δ field center	+42°14′
baselines	
(min, max, increment)	54, 1422, 72 m
synthesized beam ($\alpha \times \delta$)	24.″3 × 36.″3
FWHP primary beam	36′
radius first	
grating ring ($\alpha \times \delta$)	10.′0×14.′9
bandwidth	4.8 MHz
number of	
frequency channels	63
center velocity	+2549 km s^{-1}
channel spacing	16.6 km s^{-1}
velocity resolution	
after Hanning smoothing	33.4 km s^{-1}
r.m.s. noise	
channel maps	1.3 K

of 13% of the central peak. In order to remove the sidelobes and the grating response of strong line emission in the field, the channel maps were cleaned and were restored using the central maximum of the synthesized antenna pattern. HI line emission in these cleaned (full resolution) maps was found associated with NGC 5899 (velocity interval +2331 to +2885 km s^{-1}) and NGC 5900 (velocity interval +2247 to +2750 km s^{-1}). (Velocities in this paper are heliocentric and were calculated according to the conventional optical definition.) In order to increase the signal-to-noise ratio and to search for possible extended low-level HI emission in the field, the maps were convolved to a circular beam of 90″ × 90″. No HI line radiation could be found associated with other galaxies in the field (observed velocity interval +2047 to +3019 km s^{-1}) and the possible detection of the anonymous galaxy 25 arcmin north west of NGC 5899 at a velocity of +2674 km s^{-1}, reported by van der Burg (1985), was not confirmed. Representative sets of full resolution channel maps of NGC 5899 and NGC 5900 are shown in Figures 1 and 2 respectively. Alternate maps are omitted so that the velocity spacing between subsequent maps equals the resolution in velocity. The r.m.s. noise in these maps is about 1.3 K corresponding to a 3σ detection limit of the HI column density of 1.2 10^{20} atoms cm^{-2}; contours are plotted at intervals of 1.7 K (the zero level contour being omitted).

Table 3. Radio continuum sources in the field

α_{1950} h m s	δ_{1950} ° ′ ″	S_{1408} mJy	Notes
15 11 12.2	+42 24 41	73.1	
15 12 15.1	+41 46 49	171.9	
15 12 19.1	+42 18 00	25.3	
15 12 40.4	+41 54 44	65.8	
15 13 05.2	+42 11 52	213.4*	a
15 13 07.8	+41 54 32	53.3	
15 13 08.2	+41 52 17	56.8	
15 13 14.8	+42 14 04	38.7*	b
15 13 17.0	+42 23 38	53.1*	c
15 13 38.6	+42 25 12	12.8	
15 13 47.6	+42 06 04	34.1	
15 14 35.7	+42 13 52	14.2	
15 15 01.3	+42 08 33	132.2	
15 15 03.1	+42 08 36	34.0	
15 15 11.4	+42 10 35	179.1	
15 15 23.4	+42 11 05	29.3	

Notes: a = double source; b = NGC 5899; c = NGC 5900.
* : flux integrated over extended source

3 Results

3.1 Identification of radio continuum sources

The observed field of the NGC 5899 group contains several radio continuum sources, some of which are fairly strong (see Table 3). In Figure 3 a contour map of the distribution of continuum radiation in four sources in the central part of the observed field is shown. This map is corrected for the line emission associated with NGC 5899 and NGC 5900. In order to avoid crowding the contour levels have been chosen separately for each source. Besides the nuclear source in NGC 5899, whose position (given in Table 3) closely coincides with the optical positions listed by Dressel and Condon (1976) and Gallouët et al. (1973; see also Table 1), extended weak emission associated with the disk is visible. The flux of the nuclear point source, 21.2 mJy, is in good agreement with the

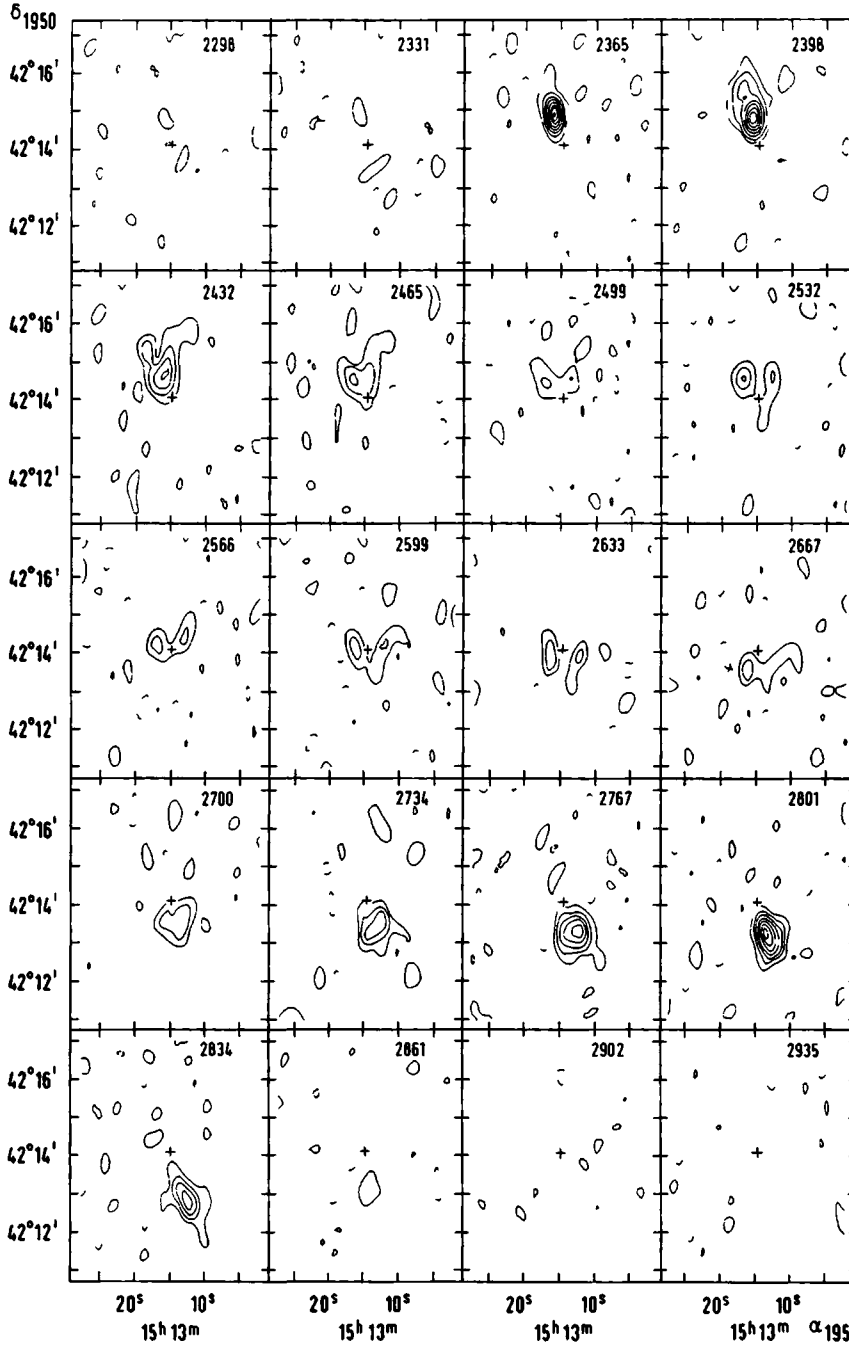
δ1950
42°16'
42°14'
42°12'
2298
2331
2365
2398
2432
2465
2499
2532
2566
2599
2633
2667
2700
2734
2767
2801
2834
2861
2902
2935
20s
10s
15h 13m
α1950

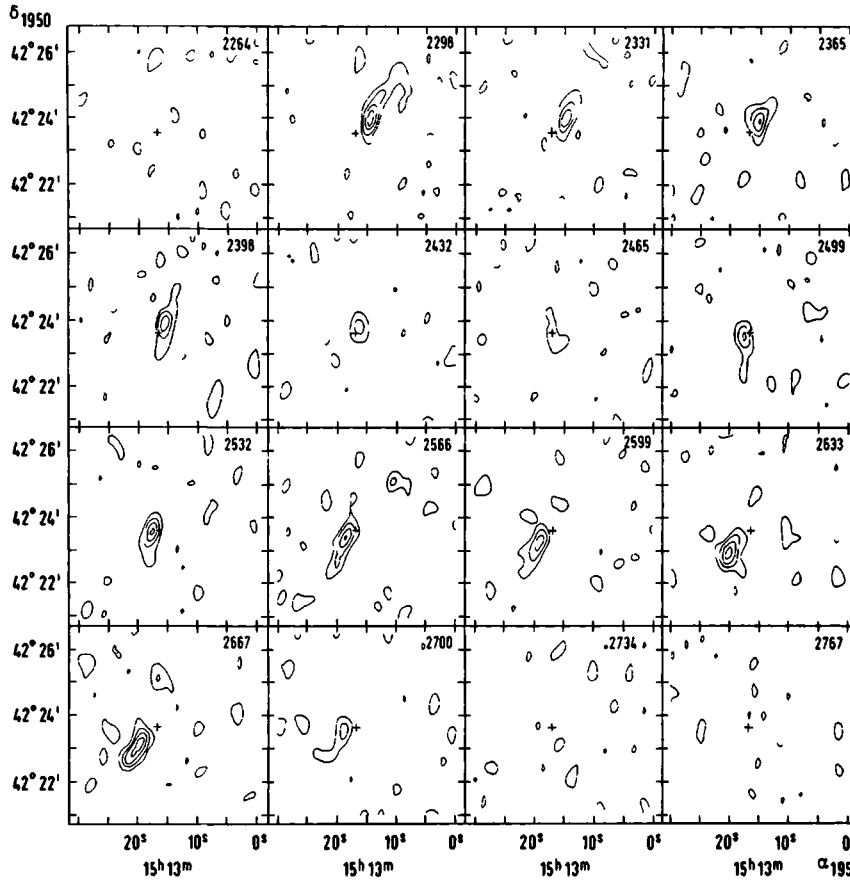

Figure 2. *Full resolution channel maps showing the line emission of NGC 5900, plotted as in Figure 1 The first contour and contour interval are 2 0 K*

Figure 1. *Full resolution channel maps showing the line emission of NGC 5899 The heliocentric radial velocity (in km s^{-1}) is indicated in the upper right hand corner of each map The first contour and contour interval are 1 7 K, negative contours are plotted as dashed curves, the zero contour has been omitted The cross in the center marks the position of the central continuum source*

value measured by Hummel (1980) After removal of this nuclear source the flux integrated over the disk is about 17 5 mJy The total flux (38 7 mJy) is in agreement with the upper limit of 50 mJy listed by Hummel (1980)

The position of the nuclear point source in the companion NGC 5900 also agrees with the optical positions listed in the above mentioned catalogues As shown by the lowest contours of the map in Figure 3, weak extended continuum emission is associated with

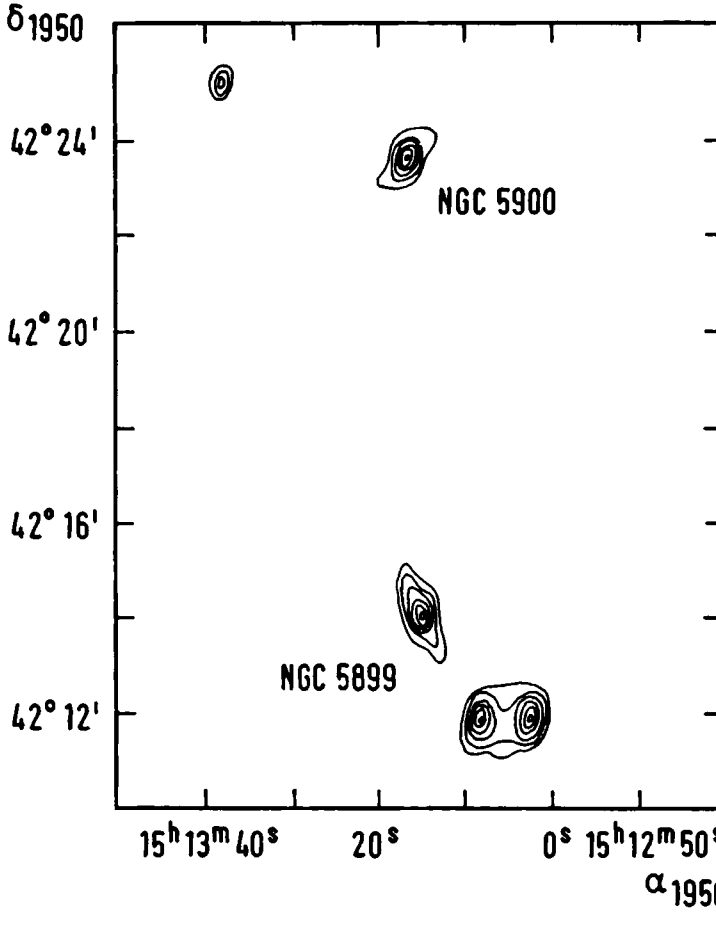

Figure 3. The distribution of radio continuum emission in the central part of the observed field This map shows the emission associated with NGC 5899 (first contour and contour interval 2 1 K), NGC 5900 (first contour 2 1 K, contour interval 6 3 K), the anonymous double source (contour levels 4 2, 8 4, 16 8, 25 2, 33 6 and 42 0 K) and an anonymous point source (contour levels 2 1, 4 2 and 6 3 K)

the optical image of the galaxy. After subtraction of a point source (flux = 47.1 mJy) the total flux of the remaining emission is about 6.0 mJy.

Among the detected continuum sources is a fairly strong, symmetric double source. This source, which is not listed in the standard catalogues, appears to be associated with the faint object 2.7 arcmin south west of NGC 5899. A reference to this faint object was made by Dahari (1984) who considered it as a candidate companion of the possible Seyfert NGC 5899. However, it is probably a background source in view of its position in between the lobes of the double source. The peak flux in each lobe is about 61 mJy and the total angular size of the double source is about 100 arcsec.

3.2 Global 21-cm line profiles

The global 21-cm line profile for each galaxy was obtained using the full resolution channel maps after correction for attenuation due to the primary beam. The total flux in each channel was determined by integration over a region whose size was defined by the 1.5σ contour of the line emission in the maps convolved to a resolution of 90″ × 90″. If necessary, this region was extended in order to obtain a single continuous series of velocities at each grid point (for a description of this masking procedure see Krumm and Shane, 1982). In Figure 4 the resulting line profiles of NGC 5899 and NGC 5900 are shown on a common velocity axis; the global properties derived from these line profiles are listed in Table 4. NGC 5899 has been observed in the 21-cm line of neutral hydrogen using single dish radio telescopes (McCutcheon, 1970; Peterson, 1979; Bottinelli et al., 1982a, b; van der Burg 1985, where a discussion of all previous results is given). Note that the small angular separation of 9.7 arcmin between NGC 5900 and NGC 5899 leads to confusion in the Nançay observations of these galaxies (the HPBW of the Nançay Telescope in declination is greater than 22′). This may explain the absence of the peak at about +2600 km s^{-1} in the line profiles of NGC 5899 measured with the WSRT and the Green Bank Radio Telescope (HPBW about 10.8 arcmin) as compared with the Nançay profiles measured by Bottinelli (1982a, b) and van der Burg (1985). It also explains why the fluxes of NGC 5899 measured at Nançay are higher than the total WSRT and Green Bank fluxes (14.4 and 16.5 Jy km s^{-1} respectively). The agreement between the latter two fluxes suggests that little or no HI flux was missed by the WSRT observations. The heliocentric velocities listed in Table 4 are the velocities of the midpoints between the points at 20% of the maximum flux, as indicated in Figure 4. Because of the small difference in radial velocity (ΔV = 111 km s^{-1}) the HI masses listed in Table 4 are based on a common distance of 27.6 h^{-1} Mpc. This distance is calculated from the systemic

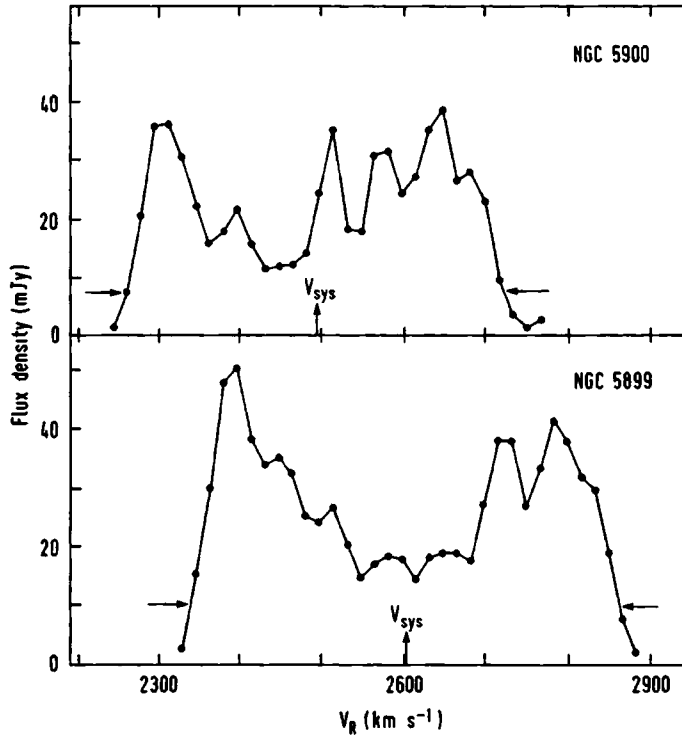

Figure 4. Global HI line profiles of NGC 5899 and NGC 5900. The horizontal arrows indicate the points at 20% of the peak flux, the vertical arrows mark the systemic velocities V_{sys}.

velocity of NGC 5899 corrected for solar motion with respect to the Local Group (2RCBG). A Hubble constant $H_0 = 100$ h km s^{-1} Mpc^{-1} is adopted.

The HI mass to blue luminosity ratio, $[M_{HI}/L_B]$ (see Table 4), is calculated from the magnitude given in the Uppsala General Catalogue (Nilson, 1973; hereafter UGC) transformed to the total blue apparent magnitude B_T^0 (corrected for internal and galactic absorption) using the relations provided by Fisher and Tully (1981) and assuming $M_B(\text{Sun}) = +5.48$. For NGC 5900 the resulting $[M_{HI}/L_B]$-value of 0.64 is greater than values generally found for Sb spirals; for NGC 5899 the value is 0.14, which is rather low

for a galaxy classified SABc (Roberts, 1969; Shostak, 1978; Bottinelli et al., 1982b). The line profile width of NGC 5899 (corrected for inclination: see Table 4) is greater than the average value given by Bottinelli et al. (1982b) for galaxies of this morphological type; for NGC 5900 the velocity width is normal for its type.

Table 4. Global HI properties

	NGC 5899	NGC 5900
systemic velocity V_{sys} (km s^{-1})	+2603	+2492
line profile width (km s^{-1}) (20% points)	582	474
flux (Jy km s^{-1})	14.4	10.7
$M_{HI}/M_{\odot}$*	2.6 10^9 h^{-2}	1.9 10^9 h^{-2}
$[M_{HI}/L_B]$	0.14	0.64
$\Theta_c(R_H)$ (km s^{-1})	256	208
I	0.07	0.19

* $h = H_0/(100 \text{ km s}^{-1} \text{ Mpc}^{-1})$

3.3 The distribution of neutral hydrogen

The integrated surface density distribution of neutral hydrogen in each galaxy has been obtained by adding all channel maps which show HI line emission associated with the galaxy. In order to prevent unnecessary noise being added, we used the masked channel maps for this integration. Therefore the number of channels which contribute to the total flux at a grid point varies over the map, resulting in a non-uniform noise level. In Figure 5a the total HI distribution (after correction for attenuation by the primary beam) in NGC 5899 and NGC 5900 is shown. In Figure 5b a reproduction of the blue print of the Palomar Observatory Sky Survey of this field can be found with superposed some contours from Figure 5a. Due to the small sizes of the galaxies relative to the beam only

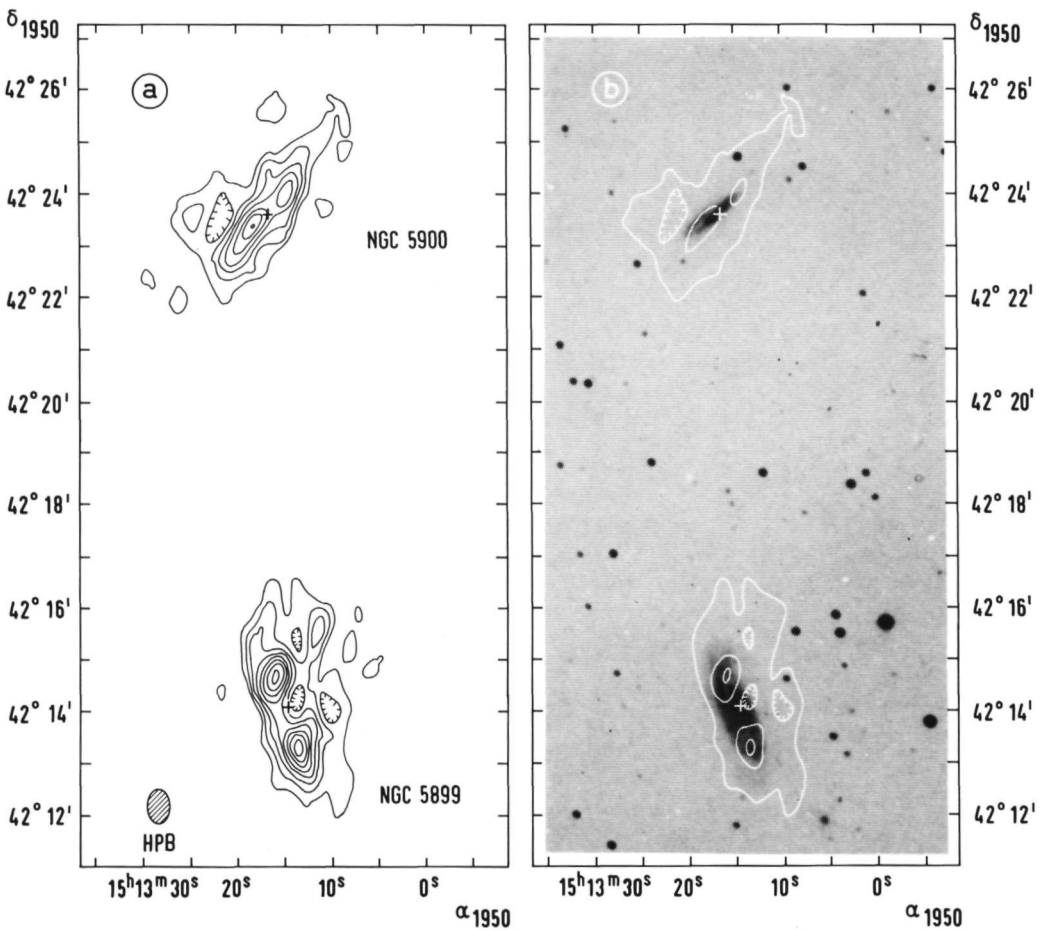

Figure 5.
a: *Integrated HI surface density maps of NGC 5899 and NGC 5900 after correction for primary beam attenuation. The first contour level is* $1.85\ 10^{20}$ *at* cm^{-2}*; the contour interval is* $3.70\ 10^{20}$ *at* cm^{-2}*. The crosses mark the positions of the nuclear continuum sources.* ***b:*** *Reproduction of the blue plate of the Palomar Observatory Sky Survey of the field. Superposed are some contours from the integrated HI surface density maps shown in Figure 5a.*

large scale features can be distinguished. The bulk of the HI in NGC 5899 is concentrated in two pronounced, unresolved peaks, which suggests a ring-like distribution. These peaks coincide with the optical emission at both ends of the major axis. On the south east edge the neutral hydrogen is sharply bounded and the contours follow the optical image closely. However, on the north and north west side (facing NGC 5900) extensions of gas far beyond the optical image can be seen. Inspection of the individual channel maps reveals that these extensions originate from emission with velocities roughly between +2365 and +2482 km s^{-1}.

The HI in the companion, NGC 5900, is concentrated at the north west and south east ends of the major axis. The clump of gas at the south east end coincides with the disturbed looking dust lane and is more elongated than the peak at the north west end. Over the whole galaxy the gas distribution is much wider than the optical image (only part of this widening being due to the beam size). The position angle derived from the peaks in the total HI map agrees with the optically determined position angle of +131° listed in the UGC. However, at radii in excess of the optical dimension the neutral hydrogen appears to turn off the major axis in opposite directions on either side of the nucleus, indicating a warp. An alternative explanation for the observed bending is that NGC 5900 is actually an inclined, barred spiral with HI arms emerging from the extreme ends of the optically visible system. Note that on the south east side the HI turns off the major axis in a direction opposite to that of the weak optical emission emerging from the main optical body east of the dust lane. The clump of gas east of the center (without an optical counterpart) originates from weak emission scattered over several velocity channels and must therefore be considered doubtful (the main contribution comes from line channels with velocities between +2633 and +2667 km s^{-1}). If disregarded, no sign of extensions, such as are observed in the distribution of gas in NGC 5899, is seen. The integrated HI surface density distribution in NGC 5900 is slightly asymmetric with respect to the minor axis. This is also reflected in the asymmetry index I listed in Table 4. This index is defined as the absolute value of the ratio of the difference to the sum of the total amounts of gas on either side of the minor axis. (For no asymmetry this index is 0. Note that this definition is different from that given by Krumm and Shane, 1982). For NGC 5900 I is 0.19, with the larger concentration facing NGC 5899.

In order to construct the velocity fields of the HI in NGC 5899 and NGC 5900 a Gauss analysis was performed using the unmasked channel maps. The velocity at each grid point was obtained by fitting a single Gauss component to the spectrum measured at that position, provided that the maximum intensity exceeded a specified threshold value. Due to the small number of synthesized beams within the HI image, effects of beam smearing in the derived velocity fields will be inevitable. Because of its high inclination (see Table 1) the kinematical information on NGC 5900 could be almost completely described by a map of the HI brightness distribution along the major axis as a function of velocity (a position-velocity map) provided that all of the HI lay in a plane. However, the plot of the HI column density displayed in Figure 5 indicates that this condition is probably not fulfilled. Because beam smearing is expected to be less important in the outer parts of the disk and because the velocity distribution may contain information on the presence of a warp (Bosma, 1978) we present in Figure 6 the velocity fields of both NGC 5899 and NGC 5900. In order to eliminate effects due to the elongated shape of the synthesized antenna pattern, the Gauss analysis was carried out using the channel maps convolved to a circular beam of 37 arcsec (FWHM). The position-velocity maps of both galaxies are shown in Figure 7. These maps were constructed from the full resolution channel maps along lines through the positions of the central continuum sources (see Table 3) and with the position angles listed in Table 1.

The overall picture of the isovelocity map of NGC 5899 is that of a moderately inclined, differentially rotating galaxy. It is obvious from this figure that there is a lack of symmetry between the north and the south sides of the galaxy. The isovelocity contours on the northern side of the galaxy are almost closed, indicating a decreasing rotation curve there; on the southern side, however, the contours are open and the rotational velocities rising with radius. This also is clearly seen in the position-velocity map shown in Figure 7. On both sides of the galaxy the neutral hydrogen extends out to a maximum radius of about 2′ along the major axis. On the north the gas attains its maximum velocity of 250 km s^{-1} at r = 0′.8 and declines to about 200 km s^{-1} at $r \approx 2'$. (These velocities are calculated with respect to the systemic velocity listed in Table 4.) On the south the maximum velocity is reached at r = 2′; the bulk of the HI on this side rotates with a velocity of about 210 km s^{-1} at r = 0′.8. At the Holmberg radius R_H listed in Table 1 and calculated from the UGC diameter according to the precepts given by Fisher and Tully (1981), the rotational velocity Θ_c (corrected for inclination and averaged over both sides) is about 256 km s^{-1}. No clear signs of an oval distortion or a kinematical warp are visible in the isovelocity plot of this galaxy.

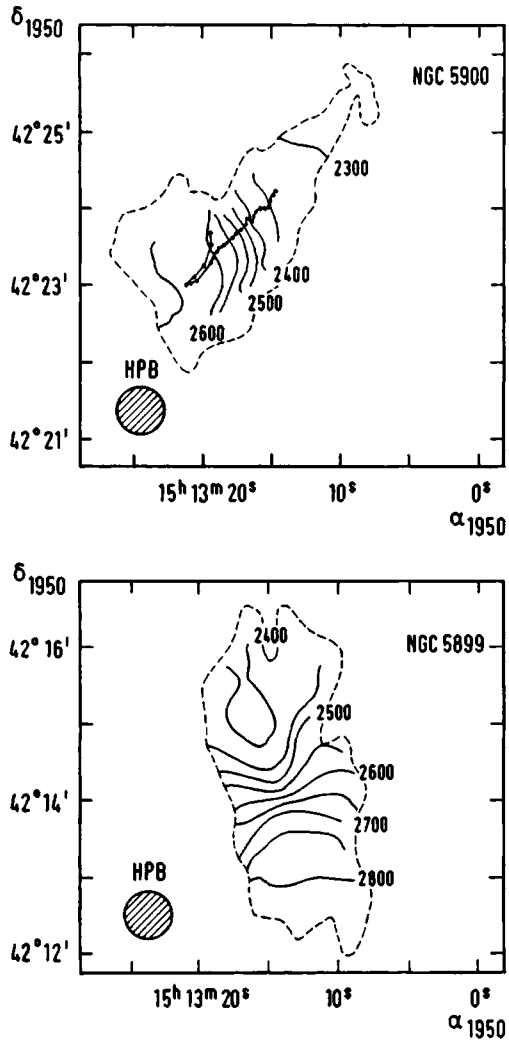

Figure 6. Isovelocity maps of NGC 5899 (lower panel) and of NGC 5900 (upper panel) For both galaxies the outermost contour of the integrated HI surface density map, plotted in Figure 5a, is shown as a broken curve. The connected dots in the velocity field of NGC 5900 indicate the centroids of HI emission in subsequent channel maps starting on the north west side with a velocity of 2264 km s^{-1} and continuing to 2717 km s^{-1} with an increment of 16.6 km s^{-1}.

As noted above, the isovelocity map of the HI in NGC 5900 is, at least in its central parts, strongly affected by beam smearing. Due to the lack of resolution the contours show no small scale structure. To the north west the kinematical major axis changes its position angle in the same sense as that of the total HI but in the south east the change appears to be in opposite direction. A careful inspection of the individual channel maps on the high velocity side of NGC 5900 reveals that the centroid of the HI emission in subsequent channels moves continuously outward with increasing velocity up to +2633 km s^{-1}. At higher velocities the centroid moves inward again and, at V = +2683 km s^{-1}, turns off the major axis in the direction of the weak optical emission east of the dust lane. This behaviour of the velocity of the centroid of HI emission is shown in Figure 6 and is reflected in the position-velocity map at r ≈ 0'.5 on the south east side of the galaxy (see Figure 7). In this region the velocity profiles are double peaked. Therefore the isovelocity field in this part of NGC 5900 is unreliable. Only the component with the greater amplitude has been found by the Gauss fitting procedure. Averaged over both sides we find a rotational velocity Θ_c at the Holmberg radius of 208 km s^{-1} (corrected for inclination).

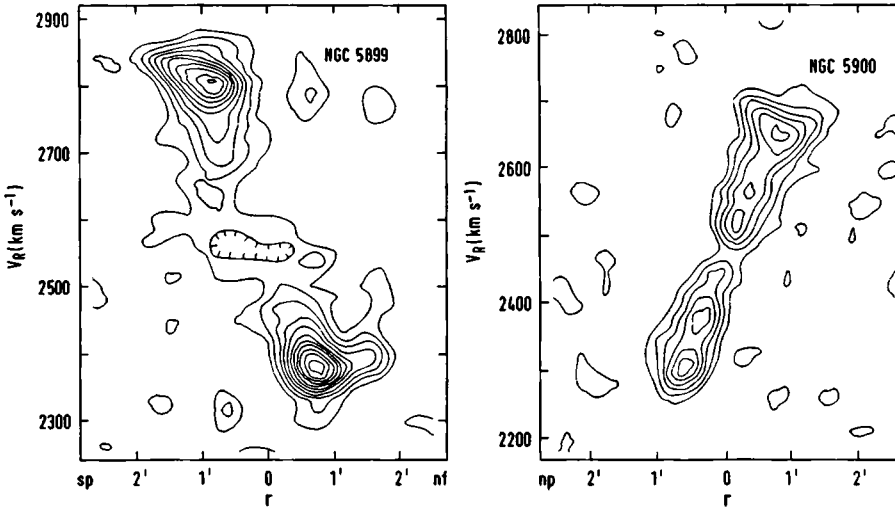

Figure 7. Maps of the HI brightness distributions in NGC 5899 and NGC 5900 along the major axes as a function of heliocentric radial velocity V_R (in km s^{-1}) and distance r (in arcmin) from the position of the nuclear continuum source For NGC 5899 the first contour and contour interval are 1 3 K, the first contour and contour interval for NGC 5900 are 1.6 K.

4 Discussion

4 1 Mass determination

As described in the previous sections, the gas patterns and the associated velocity fields in both galaxies are asymmetric Due to these asymmetries and because of the small radii involved, a detailed calculation of the mass distributions from the rotation curves seems inappropriate Instead, we simply assume that the mass is distributed in a thin disk and reduce the Keplerian mass within the Holmberg radius R_H, calculated from the rotational velocity $\Theta_c(R_H)$ (averaged over both sides) by 35% (Faber and Gallagher, 1979) Using the parameters listed in Tables 1 and 4, this yields $1\,6\,10^{11}\,h^{-1}$ and $6\,5\,10^{10}\,h^{-1}\,M_\odot$ for NGC 5899 and NGC 5900 respectively The corresponding total mass to blue luminosity ratios, $[M/L_B]$, are 9 h and 22 h The $[M/L_B]$-value for NGC 5900, converted to the spherical mass distribution adopted by Faber and Gallagher (1979) and accounting for the different values of H_0, is about twice the average of $[M/L_B]$-values (13 ±1) for galaxies of type Sab to Sbc listed by these authors For NGC 5899 $[M/L_B]$ is normal for its morphological type

The small angular separation of 9 7 arcmin (which corresponds to a projected separation r_p of $77\,9\,h^{-1}$ kpc) together with the small velocity difference between the galaxies suggest that they are physically associated This is confirmed by the presence of filaments in the distribution of HI in NGC 5899 (see Figure 5) which may well have resulted from gravitational interaction between the two galaxies (see sub-section 4 2) If these galaxies form an isolated physical pair, then the minimum orbital mass M_{min}, assuming a parabolic orbit, can be calculated from $M_{min} = r_p \Delta V^2/2G$ Using ΔV = 111 km s^{-1} and r_p = $77\,9\,h^{-1}$ kpc yields $M_{min} = 1\,1\,10^{11}\,h^{-1}\,M_\odot$ corresponding to a ratio of minimum mass to blue luminosity of 5 0 h The latter value is in good agreement with the mean minimum M/L of 5 7 for a sample of 13 pairs, quoted by Blackman and van Moorsel (1984) Comparison of M_{min} with the sum of the individual masses of NGC 5899 and NGC 5900 provides information on the possible presence of (dark) matter outside the Holmberg radii From the present data the sum of the individual masses ($2\,3\,10^{11}\,h^{-1}\,M_\odot$) is a factor 2 1 greater than the lower limit to the orbital mass M_{min} If we increase the individual masses by 35% (corresponding to a spherical mass distribution) this factor is 3 2 Therefore, other than the rising rotation curve at the south end of NGC 5899, there appears to be no indication for large amounts of matter outside the Holmberg radii of these galaxies Note that the absence of a massive, stabilizing halo might be related to the presence of a (weak) bar-like structure in the disk of NGC 5899

The presence of additional nearby galaxies might influence the dynamics of the pair NGC 5899/5900. It was noted in section 1 that NGC 5900 is a member of a small apparent group of galaxies, one of which (NGC 5893) is presumably a background galaxy. The companions for which no systemic velocity is known are all of low apparent luminosity. Combined with their large projected separation from the primary (compared with r_p for NGC 5900) this indicates that if they are gravitationally associated with NGC 5899, their influence on the dynamics of the close pair NGC 5899/5900 will be negligible. In fact, if they were members of the group with the expected flux densities based on $[M_{HI}/L] = 0.60$ for late type dwarf galaxies, with $m_{pg} = 15.5$ and with HI line profile widths of 150 km s^{-1}, they should have been detected in the present WSRT observation. This suggests that these galaxies are background objects.

4.2 Relation between NGC 5899 and NGC 5900

The 21-cm line HI observations presented in the previous sections give evidence of irregularities and asymmetries in the HI surface density distribution and the kinematics of both NGC 5899 and NGC 5900. According to Bosma (1978) such asymmetries are not unusual in spiral galaxies; they can be internally generated and sustained (Baldwin et al., 1980). This is most clearly illustrated by WSRT observations of two extremely isolated galaxies (NGC 5301 and NGC 2712), described by Krumm and Shane (1982). These authors showed that the HI disk of NGC 5301 is warped, while a pronounced asymmetry is observed in the distribution of neutral hydrogen in NGC 2712. The asymmetry index I of NGC 2712, calculated from the data listed by Krumm and Shane (1982) according to the definition given in section 3.3, is 0.37. This shows that an asymmetry index even greater than that for NGC 5900 (see Table 4) need not necessarily imply interaction with companions. Nevertheless, the small difference between the systemic velocities of NGC 5899 and NGC 5900 and the small projected separation leave open the possibility that some of the observed features reflect the effects of a tidal encounter. Most suggestive in this respect are the filaments in the distribution of HI in NGC 5899 (Figure 5) and the Seyfert properties of this galaxy, which might result from the presence of a companion of comparable size, as suggested by Dahari (1985). The total amount of gas associated with the filaments is about $8\ 10^8\ h^{-2}\ M_\odot$ (or 30% of the total HI mass). That the velocity field of the filaments seems to be a simple extension of that measured in the main body (Figure 6) suggests that this feature originates within NGC 5899 and argues against an accretion event. Toomre and Toomre (1972) have shown that gravitational interaction could well explain relatively mild distortions in the HI distribution, such as is observed in

the present pair. Their calculations indicate that filaments might result from a retrograde passage or, alternatively, reflect the initial response of the outermost loosely bound gas to an approaching companion. This latter possibility seems implausible in view of the difference by a factor of about 2.5 in mass, which makes it unlikely that at the present observed minimum distance of 77.9 h^{-1} kpc the companion has been able to pull out gas to (projected) radii in excess of 16 h^{-1} kpc (or 37 h^{-1} kpc if the filaments are in the principal plane of the galaxy). Moreover, Toomre and Toomre (1972) note that after a retrograde parabolic passage of a companion with equal mass the outermost gas partly interpenetrates the gas at smaller radii and starts to oscillate (see their Figure 1). This would offer an explanation for the observed sharp boundary opposite the filaments, to the south east of NGC 5899. An upper limit to the time elapsed since the passage may be obtained from an estimate of the maximum life time of the filaments: due to differential rotation these filaments would have been smeared out in a relatively short time, about 6 10^8 h^{-1} yr (Baldwin et al., 1980).

An alternative explanation of the observed features in the distribution of gas in NGC 5899 is that HI is being stripped as a result of interaction with an intergalactic medium. Stripping of gas has been proposed by Shostak et al. (1982) as a mechanism to explain the peculiar distribution of gas in the super-massive spiral NGC 1961. The HI in this galaxy exhibits a wing on one side and a sharp boundary on the opposite side. This morphology bears some resemblance to that found in NGC 5899 (see Figure 5). However, if NGC 5899 and NGC 5900 form a physical pair we would expect to observe a similar morphology in the companion as well, which, except perhaps the clump of gas east of the nucleus, seems not to be the case (see Figure 5). (Note, however, that if the component of the relative velocity of NGC 5900 with respect to an intergalactic medium is perpendicular to the plane of the sky such an effect would not be observable). Moreover, no sign of a ridge of enhanced radio continuum radiation, as in NGC 1961, is detected. Therefore stripping of gas seems unlikely as an explanation of the observed filaments in NGC 5899.

Soifer et al. (1984) have noted that interaction of a galaxy with its neighbour might be important in triggering a burst of star formation. Models of rapid star formation result in burst lifetimes of about 10^8 years (Joseph et al., 1984). Given the short lifetime of the extensions in NGC 5899, a possible encounter could have occurred no more than about 6 10^8 h^{-1} yr ago. Therefore, if interaction were important, enhanced star formation might still be observed. A distance-independent measure of the star formation rate is given by the ratio of the 80 μm infrared luminosity to the blue luminosity L_{IR}/L_B. For the companion, NGC 5900, the 80 μm infrared luminosity derived from the IRAS fluxes measured at 60 and 100 μm (Lonsdale et al., 1985) and calculated according to the

precepts given by Fairclough (1985), is about 1.5 10^{10} h^{-2} $L_{\odot}$ which, with the total blue luminosity L_B listed in Table 1, gives L_{IR}/L_B = 5.1. According to de Jong (1986) this value characterizes NGC 5900 as a weak starburst galaxy. For NGC 5899 we calculate L_{IR}/L_B = 0.6 from L_{IR} = 9.9 10^9 h^{-2} $L_{\odot}$ and L_B from Table 1. This value is in agreement with the mean value of 0.5 for a sample of 496 field galaxies given by Fairclough (1985). Therefore, the present star formation rate in NGC 5899 appears to be quite normal. As noted in subsection 3.2, the $[M_{HI}/L_B]$-value for NGC 5899 is somewhat low for a galaxy of type SABc; it more closely resembles that of an Sb. This suggests either that NGC 5899 is in fact of earlier morphological type or that gas has been depleted during a period of enhanced star formation in the past.

5 Conclusions

We have shown from high resolution WSRT observations that, within the examined velocity interval, two members of the NGC 5899 group of galaxies (NGC 5899 and NGC 5900) contain detectable amounts of neutral hydrogen. It is argued that the remaining galaxies in the observed field are probably background objects. The global HI properties of the two detected galaxies are listed in Table 4. The small difference between the systemic velocities along with the small angular separation suggest that these galaxies form a physical pair. If the galaxies are bound, the minimum orbital mass required for stability is smaller than the sum of the individual masses so that no evidence requiring the presence of a massive dark halo is found. The HI density and velocity distribution in both galaxies show irregularities which could have resulted from gravitational interaction. It is argued that the filaments in the distribution of neutral hydrogen in NGC 5899 along with the sharp boundary on the opposite side suggest a retrograde passage of NGC 5900. The distribution of gas in the latter galaxy appears to be less disturbed but the lack of sufficient spatial resolution combined with an unfavourable inclination angle might prevent irregularities of the kind observed in NGC 5899 being discovered. The presence of nuclear continuum sources in both galaxies is consistent with Hummel's (1981) finding that nuclear activity seems to be related to gravitational interaction. Balick and Heckman (1982) and Kennicutt and Keel (1984) have argued that gravitational interaction might also trigger the nuclear activity which characterizes Seyfert galaxies. This has recently been investigated by Dahari (1984, 1985) who concluded that, although Seyferts have a statistically significant excess of close companions, no correlation is found between the emitted power and pair parameters such as separation, size and redshift difference. In the case of the Seyfert NGC 5899, Dahari considered the anonymous object, identified in the

present study with a double radio source, as a candidate perturber. However, if gravitational interaction is the major cause of nuclear activity in NGC 5899, the presence of NGC 5900 seems to be more relevant. It was shown from the infrared properties, derived from the measured IRAS fluxes, that the effect of the proposed encounter on the star formation rate in the two galaxies was different. The passage induced a weak burst of star formation in NGC 5900 whereas no significant increase in the star formation rate in NGC 5899 appears to be present. The behaviour of the star formation rate in interacting galaxies has recently been studied by Noguchi et al. (1986). These authors carried out numerical simulations of close encounters between galaxies and showed that, in case of a retrograde passage with a perturber of equal mass, no significant increase in the star formation rate is to be expected. This is consistent with the situation encountered in NGC 5899 for which the perturber (i.e. NGC 5900) is 2.5 times less massive. The observed increase of the star formation rate in NGC 5900 might then be explained by the enhanced tidal forces exerted on this galaxy by the passage of the more massive perturber NGC 5899.

Acknowledgements

I would like to thank Drs. W.W. Shane and W.B. Burton for critically reading the manuscript and many useful comments. The Westerbork Synthesis Radio Telescope is operated by the Netherlands Foundation for Radio Astronomy (SRZM), with the financial support of the Netherlands Organization for the Advancement of Pure Research (Z.W.O.).

Allen, D.A., Roche, P.F., Norris, R.P.: 1985, Mon. Not. R. Astron. Soc. 213, 67p

Baldwin, J.E., Lynden-Bell, D., Sancisi, R.: 1980, Mon. Not. R. Astron. Soc. 193, 313

Balick, B., Heckman, T.M.: 1982, Ann. Rev. Astron. Astrophys. 20, 431

Blackman, C.P., van Moorsel, G.A.: 1984, Mon. Not. R. Astron. Soc. 208, 91

Bos, A., Raimond, E., van Someren Greve, H.: 1981, Astron. Astrophys. 98, 251

Bosma, A.: 1978, The Distribution and Kinematics of Neutral Hydrogen in Spiral Galaxies of various morphological Types, Dissertation, University of Groningen

Bottinelli, L., Gouguenheim, L., Paturel, G.: 1982a, Astron. Astrophys. Suppl. Ser. 47, 171

Bottinelli, L., Gouguenheim, L., Paturel, G.: 1982b, Astron. Astrophys. 113, 61

Burg, G. van der : 1985, Astron. Astrophys. Suppl. Ser. 62, 147

Dahari, O.: 1984, Astron. J. 89, 966

Dahari, O.: 1985, Astron. J. 90, 1772

Dressel, L., Condon, J.: 1976, Astrophys. J. Suppl. Ser. 31, 187

de Jong, T., Clegg, P.E., Soifer, B.T., Rowan-Robinson, M., Habing, H.J., Houck, J.R., Aumann, H.H., and Raimond, E.: 1984, Astrophys. J. Letters 278, L67

de Jong, T.: 1985, preprint

Faber, S.M., Gallagher, J.S.: 1979, Ann. Rev. Astron. Astrophys. 17, 135

Fairclough, J.H.: 1985, Extragalactic Infrared Astronomy, Rutherford Appleton Laboratory Workshop on Astronomy and Astrophysics, ed. P.M. Gondhalekar, p.32

Fisher, J.R., Tully, R.B.: 1981, Astrophys. J. Suppl. Ser. 47, 139

Gallouët, L., Heidmann, N., Dampierre, F.: 1973, Astron. Astrophys. Suppl. Ser. 12, 89

Högbom, J.A., Brouw, W.N.: 1974, Astron. Astrophys. 33, 289

Hummel, E.: 1980, Astron. Astrophys. Suppl. 41, 151

Hummel, E.: 1981, Astron. Astrophys. 96, 111

Joseph, R.D., Wright, G.S.: 1985, Mon. Not. R. Astron. Soc. 214, 87

Karachentsev, I.D.: 1985, Soviet Astron. 39, 243

Kennicutt, R.C., Keel, W.C.: 1984, Astrophys. J. Letters 279, L5

Krumm, N.K., Shane, W.W.: 1982, Astron. Astrophys. 116, 237

Lonsdale, C.J., Helou, G., Good, J.C., Rice, W.: 1985, Cataloged Galaxies and Quasars Observed in the IRAS Survey, Jet Propulsion Laboratory

McCutcheon, W.H., Davies, R.D.: 1970, Mon. Not. R. Astron. Soc. 121, 531

van Moorsel, G.A.: 1982, Astron. Astrophys. 107, 66

Noguchi, M., Ishibashi, S.: 1986, Mon. Not. R. Astron. Soc. 219, 305

Nilson, P.: 1973, Uppsala General Catalogue of Galaxies, Ann. Uppsala Astron. Obs. 6 (UGC)

Peterson, S.D.: 1979, Astrophys. J. Suppl. Ser. 40, 527

Roberts, M.S.: 1969, Astron. J. 74, 859

Sandage, A., Tammann, G.A.: 1981, A Revised Shapley-Ames Catalog of Bright Galaxies, Carnegie Institution of Washington Publication 635

Shostak, G.S.: 1978, Astron. Astrophys. 68, 321

Shostak, G.S., Hummel, E., Shaver, P.A., van der Hulst, J.M., van der Kruit, P.C.: 1982, Astron. Astrophys. 115, 293

Soifer, B.T., Rowan-Robinson, M., Houck, J.R., de Jong, T., Neugebauer, G., Aumann, H.H., Beichman, C.A., Boggess, N., Clegg, P.E., Emerson, J.P., Gillett, F.C., Habing, H.J., Hauser, M.G., Low, F.J., Miley, G., Young, E.: 1984, Astrophys. J. Letters 278 , L71

Toomre, A., Toomre, J.: 1972, Astrophys. J. 178, 623

de Vaucouleurs, G., de Vaucouleurs, A., Corwin, H.: 1976, Second Reference Catalogue of Bright Galaxies, Univ. of Texas Press, (2RCBG)

Zwicky, F., Herzog, E., Wild, P., Kapowicz, M., Kowal, C.T.: 1961- 1968, Catalogue of Galaxies and Clusters of Galaxies, California Institute of Technology

The aim of this dissertation is to contribute to the study of the distribution of mass of galaxies over different length scales. For this purpose high resolution observations in the 21-cm line of neutral hydrogen were made with the Westerbork Synthesis Radio Telescope (WSRT).

In the first chapter the present status of our knowledge of the mass distribution in and around galaxies is reviewed and an outline of the subsequent chapters is given.

In chapters 2 and 3 we present the results of a study of the internal mass distribution of NGC 4594 as inferred from WSRT observations of the distribution and kinematics of neutral hydrogen in the disk. The galaxy contains only a small amount of neutral hydrogen, with $[M_{HI}/L_B] = 0.010$. This gas is located in two rings within which it rotates at a velocity of about 370 km s^{-1} (constant with radius). A method is proposed which employs the dispersion relation from the density wave theory for tightly wound spirals to calculate the local surface density in the disk ($45 \pm 5\ M_\odot\, pc^{-2}$ at a galactocentric distance of 15 kpc). Using published surface photometry and assuming that the mass-to-light ratio in the disk is independent of radius, a mass model for the disk is derived. Due to the presence of dust in the disk only a lower limit to its luminosity could be derived. The corresponding upper limit to $[M/L_B]$ in the disk is 10, whereas the actual value is probably a factor two smaller. Subtracting the contribution of the disk from the observed rotation curve of the HI, the distribution of mass in the halo is calculated. The $[M/L_B]$-value increases only slightly, from about 5 (at $r = 10$ kpc) to about 6 (at $r = 20$ kpc), and is comparable to the value in the disk. It is concluded that the disk of NGC 4594 resembles in most of its global properties those in later type spirals, whereas the halo is much different from the haloes of late-type spirals.

The method used to derive the mass model of NGC 4594 can also be applied to other spiral galaxies. The condition is that a) the galaxy possesses a tightly wound spiral pattern (so that early-type spirals are most suitable), b) the shape of the spiral pattern along with

its pattern speed can be determined, and c) the rotation curve can be measured. If these conditions are fulfilled one obtains a) a disk model which is consistent with the dispersion relation for tightly wound spirals (i.e. it is constructed so as to sustain a spiral of the observed shape) without adopting M/L in advance, and b) the halo mass (within the maximum radius of the HI disk) without having to make ad hoc assumptions regarding the mass distribution. In addition, for those spirals for which the stellar velocity dispersion in the disk can be determined, Toomre's stability factor Q might be calculated. However, stellar velocity dispersions in disks of galaxies are difficult to obtain and are available for only a limited sample (see van der Kruit and Freeman, 1986).

A detailed analysis of the mass distribution in NGC 3593 and NGC 4281, two galaxies which show much morphological resemblance to NGC 4594, was not possible. The WSRT observations of these galaxies, presented in chapter 4, show that NGC 3593 contains only a very small amount of gas (with $[M_{HI}/L_B] = 0.02$), largely concentrated in two clumps, whereas NGC 4281 remained undetected.

Whether or not the properties of the disk and halo of NGC 4594 are characteristic of the class of early-type spirals as a whole remains unclear. Note in this respect that in NGC 7814, classified as Sab, only 2% of the mass resides in the disk (compared to 20 to 25% in NGC 4594) and that the mass-to-light ratio in the halo increases strongly with radius (van der Kruit and Searle, 1982). An obvious suggestion for future work is to enlarge the sample of galaxies studied, using the method introduced in chapter 3. At present such a study is underway at the Astronomical Institute of the University of Nijmegen.

The following chapters are devoted to the study of the distribution of mass in galaxies out to large galactocentric distances, i.e. several Holmberg radii. For this purpose WSRT observations of small groups of galaxies composed of a single massive system surrounded by several much less massive companions were obtained. The mass inside the region occupied by the companions is estimated from their radial velocities (determined from their 21-cm line profiles) and projected distances from the primary galaxy. In order to examine the detectability of these faint companions, observations with the Nançay Decimetric Radio Telescope were made. The results of these observations are given in chapter 5. In the following three chapters WSRT observations of three groups are discussed in detail.

Chapters 6 and 7 deal with two groups for which the primary galaxies are classified as lenticular, i.e. NGC 2859 and NGC 4111. The primary galaxies were not detected in HI but each is surrounded by several gas-rich companions. Both appear to be embedded in extended dark haloes. However, the halo of NGC 2859 seems to be less massive than that of NGC 4111. The $[M/L_B]$-value within about seven Holmberg radii from the center of NGC 2859 is 60 h ($H_0 = 100$ h km s^{-1} Mpc^{-1}), or three times the average value found for S0

galaxies within one Holmberg radius. For NGC 4111 [M/L_B] is 101 h within about five Holmberg radii, and agrees with the value which would be required for a flat rotation curve. In the HI observations of the companions, no sign of interaction with the primary galaxies is found. It is suggested that the gas content of one or more of the companions, they should be captured by NGC 2859 or NGC 4111, would be sufficient to turn these galaxies in HI-rich lenticulars.

Finally, in chapter 8, WSRT measurements of the NGC 5899 group are discussed. NGC 5899 and one of its companions (NGC 5900) were detected. Considered as a binary system, the lower limit to the orbital mass required to bind this pair is about a factor two less than the sum of the individual masses within one Holmberg radius. The minimum mass to blue luminosity ratio of the pair is 5.0 h. It is concluded that no large amount of dark matter is required to account for the dynamics of this double system. The observed distribution and kinematics of the HI in both NGC 5899 and NGC 5900 show asymmetries and irregularities such as might result from gravitational interaction. The ratio of the 80 μm infrared to blue luminosity of NGC 5900 indicates that the effect of this gravitational interaction was to induce enhanced star formation.

In the literature only a few galaxies are reported which have a sufficient number of orbiting companions for which the radial velocities are known to permit a mass calculation as discussed in chapters 6 and 7. These galaxies are NGC 3992, NGC 1961, NGC 1023 and NGC 4026. The first two were studied by Gottesman and Hunter (1982) and Gottesman et al. (1983) respectively. From the motions of its satellites Gottesman and Hunter conclude that NGC 3992 does not appear to have a massive halo, in contrast to what is suggested by the flat rotation curve. Gottesman et al. (1983) argue that NGC 1961 probably has a very pronounced dark halo with a mass exceeding that of the disk by about a factor 10. The NGC 4026 and NGC 1023 groups were studied in HI by Appleton (1983) and Sancisi et al. (1984) respectively. Both galaxies are classified as lenticular and are accompanied by several faint companions for which the radial velocities are known. However, the presence of a bright galaxy close to NGC 4026 and with a comparable velocity makes this group unsuitable for a mass determination of the kind discussed in chapters 6 and 7. For the NGC 1023 group the situation is less clear. Aside from four faint companions within about 20 arcmin of NGC 1023, a relatively bright galaxy (IC 239) is visible 48 arcmin west of the primary. This galaxy is about 2 magnitudes fainter than NGC 1023 but much brighter than the other companions. If it is bound to NGC 1023 then using the data given by Sancisi et al. (1984), the mass-to-light ratio of the group is 347 h. This large value is heavily influenced by IC 239. If the latter galaxy is not bound to the group and we exclude it from the calculation, the mass-to-light ratio is reduced to 134 h. However, it is very doubtful whether the group may still be considered as isolated. From

the above it is evident that the result of a mass determination using the motions of the orbiting companions is very sensitive to the inclusion of galaxies which are in fact not bound. Therefore, one has to be very cautious in selecting suitable groups.

It has been shown that in the inner parts of the halo of NGC 4594 no significant increase of M/L is measured. An increase as is established for NGC 2859 and NGC 4111 might possibly set in at radii greater than that of the HI disk. In order to gain more insight in the increase of M/L with radius in galaxies of different morphological classifications, the mass distribution on large and small scales must be studied. In this dissertation it is shown that both the method introduced in chapter 3 (for small length scales) and measurements of small groups (for larger length scales) can contribute significantly to this study.

References

Appleton, P.N.: 1983, Mon. Not. R. Astron. Soc. 203, 533

Gottesman, S.T., Hunter, J.H.: 1982, Astrophys. J. 260, 65

Gottesman, S.T., Hunter, J.H., Shostak, G.S.: 1983, Mon. Not. R. Astron. Soc. 202, 21p

Sancisi, R., van Woerden, H., Davies, R.D., Hart ,L.: 1984, Mon. Not. R. Astron. Soc. 210, 497

van der Kruit, P.C., Searle, L.: 1982, Astron. Astrophys. 110, 79

van der Kruit, P.C., Freeman, K.C.: 1986, Astrophys. J. 303, 556

In dit proefschrift worden de resultaten besproken van een onderzoek naar de verdeling van massa in en rondom melkwegstelsels. Veel waarnemingen van melkwegstelsels wijzen op het voorkomen van onzichtbare materie, mogelijk in de vorm van massieve halo's. Metingen van rotatiekromme's van melkwegstelsels leveren informatie over de massaverdeling binnen een gebied ter grootte van het waarneembare deel van de schijf. Informatie over een veel uitgebreider gebied, inclusief een halo, wordt geleverd o.a. door waarnemingen van dubbelstelsels.

In dit onderzoek wordt voor een beperkte klasse objecten met uitgesproken zichtbare halo's de interne massaverdeling bestudeerd door metingen van de verdeling en kinematica van neutraal waterstof (HI) in de schijf. Daarnaast wordt een studie gemaakt van de massaverdeling rondom stelsels die omgeven zijn door meerdere kleine begeleiders. Deze begeleiders kunnen dienen als een verzameling testdeeltjes die zich bewegen in het gravitatieveld van het centrale stelsel. Metingen van de snelheden van deze begeleiders leveren informatie over de massaverdeling in de directe omgeving van het centrale stelsel. Door het onderzoek te beperken tot groepen waarin de massa van de begeleiders verwaarloosd mag worden ten opzichte van die van het hoofdstelsel, wordt een belangrijke bron van onzekerheid in de massabepaling vermeden. De statistiek wordt verbeterd door de keus te laten vallen op stelsels met meerdere begeleiders.

In hoofdstuk 1 wordt een inleiding gegeven waarin de problematiek zoals hierboven is samengevat, in perspectief wordt geplaatst. Daarnaast wordt de gevolgde werkwijze toegelicht en de opzet van het proefschrift besproken.

In hoofdstuk 2 worden metingen met de Westerbork Synthese Radio Telescoop (WSRT) aan NGC 4594 (de Sombrero nevel) beschreven. Dit stelsel bezit een zeer uitgebreide halo waarvan het licht (in tegenstelling tot de halo's van de meeste andere stelsels) tot op zeer grote afstand van het centrum te meten is. De zeer geringe hoeveelheid waterstof in dit stelsel bevindt zich in een dunne schijf welke is ingebed in de

halo. Uit modelaanpassingen blijkt dat de gemeten HI verdeling is te reproduceren door middel van twee ringen waarin het gas cirkelbanen beschrijft met een snelheid van 370 km s^{-1}. Het ontbreken van gas in zowel het centrale als het buitenste deel van de schijf kan misschien worden verklaard door wisselwerking met materie, uitgestoten door oude sterren in de veel langzamer roterende halo.

Vervolgens wordt in hoofdstuk 3 de gemeten HI-verdeling geïnterpreteerd als nauw gewonden spiraalarmen in de schijf van de Sombrero. Uitgaande van de kennis van de vorm van het spiraalpatroon en metingen van de rotatiekromme, bleek het mogelijk zowel de massa van de schijf als die in het centrale deel van de halo te berekenen. De hier geïntroduceerde methode kan in principe ook op andere stelsels worden toegepast. Deze methode maakt het mogelijk de bijdrage van de halo te berekenen zonder a priori aannamen omtrent de massa van de schijf. Geconcludeerd wordt dat de schijf van de Sombrero, ondanks de aanwezigheid van een zeer opvallende halo, in veel opzichten lijkt op de schijf van stelsels waar een dergelijke relatief heldere halo ontbreekt. Ten opzichte van deze stelsels onderscheidt de halo van de Sombrero zich niet zozeer door zijn massa als door zijn helderheid.

In hoofdstuk 4 worden WSRT metingen aan NGC 3593 en NGC 4281 besproken. Beide stelsels vertonen optisch veel gelijkenis met de Sombrero, zij het dat de schijf van beide stelsels iets minder geprononceerd is. Een gedetailleerde analyse van de massaverdeling binnen deze stelsels, zoals uitgevoerd voor de Sombrero, bleek hier echter niet mogelijk. Alhoewel NGC 3593, net als de Sombrero, slechts een kleine hoeveelheid HI in de schijf bezit moet geconcludeerd worden dat, binnen de onzekerheden opgelegd door de waarneemomstandigheden, de verdeling van dit schijfgas in hoge mate verschilt met die gemeten in de schijf van de Sombrero. In NGC 3593 bevindt het gas zich op uitzonderlijk kleine afstand van het centrum en is er van enige correlatie tussen de verdelingen van gas en stof nauwelijks sprake. In NGC 4281 is met de WSRT geen detecteerbare hoeveelheid gas aangetroffen, in tegenstelling tot hetgeen single dish metingen van dit stelsel suggereren. Wel blijkt uit de metingen dat zich in de directe omgeving van NGC 4281 een HI-rijk stelsel bevindt dat wellicht de oorzaak van deze tegenstrijdige resultaten is.

In de vorige hoofdstukken is getracht door middel van bestudering van de verdeling en beweging van HI binnen het zichtbare deel van een stelsel informatie over de massaverdeling tot op betrekkelijk kleine afstanden van het centrum te verkrijgen. In de volgende hoofdstukken wordt voor een drietal stelsels geprobeerd het te bestuderen gebied te vergroten door de beweging van HI-rijke begeleiders rondom deze stelsels te beschouwen. Een probleem bij deze methode kan de beperkte detecteerbaarheid van deze begeleiders zijn. Om dit te onderzoeken zijn enkele stelsels en hun begeleiders waargenomen met de radio telescoop te Nançay. De resultaten van deze verkennende

metingen zijn samengevat in hoofdstuk 5.

In hoofdstuk 6 worden de resultaten besproken van WSRT metingen aan de NGC 2859 groep. NGC 2859 is een helder stelsel omgeven door 4 HI-rijke begeleiders. In NGC 2859 zelf is geen detecteerbare hoeveelheid HI aangetroffen. Uit de beweging van de begeleiders ten opzichte van NGC 2859 is informatie over de massa binnen een gebied met een diameter ongeveer 7 × de optische diameter van NGC 2859 verkregen. De verhouding tussen de massa en de lichtkracht (M/L) in dit gebied is een factor 3 groter dan de waarde welke in het algemeen gemeten wordt in het zichtbare deel van stelsels van hetzelfde morphologisch type.

In hoofdstuk 7 worden HI metingen aan de NGC 4111 groep beschreven. De WSRT metingen wijzen uit dat NGC 4111 is omgeven door vijf gas-rijke begeleiders. In tegenstelling tot eerdere metingen is geen detecteerbare hoeveelheid HI in NGC 4111 zelf aangetroffen. Ook hier is een toename naar buiten van M/L waargenomen. Deze toename stemt overeen met de toename die we berekenen als we veronderstellen dat NGC 4111 een donkere halo bezit met een massaverdeling die een vlakke rotatiekromme zou veroorzaken zoals van veel stelsels is gemeten.

NGC 2859 en NGC 4111 zijn van een morphologische klasse waarvan bekend is dat de HI inhoud tussen de verschillende representanten sterk uiteenloopt. Beargumenteerd wordt dat rondom NGC 2859 en NGC 4111 voldoende HI aanwezig is om, wanneer het kan worden ingevangen, deze stelsels in HI-rijke objecten te veranderen.

In hoofdstuk 8 wordt de verdeling van gas in en rondom het spiraalstelsel NGC 5899 besproken. Dit stelsel is omgeven door drie begeleiders. Een ervan, NGC 5900, is gedetecteerd in HI. Als dubbelstelsel opgevat kan de minimum massa die aanwezig moet zijn om NGC 5900 te binden worden afgeleid uit het waargenomen snelheidsverschil. Geconcludeerd wordt dat er geen strikt bewijs bestaat dat er grote hoeveelheden donkere materie aanwezig moeten zijn. Uit IRAS infrarood metingen is af te leiden dat NGC 5900 een (zwakke) uitbarsting van sterformatie ondergaat. Deze uitbarsting wordt toegeschreven aan de gravitationele wisselwerking als gevolg van een ontmoeting van NGC 5900 met NGC 5899. Deze verklaring is in overeenstemming met de verdeling van het gas in met name NGC 5899 waarin duidelijk sporen van interactie zijn terug te vinden.

Tenslotte worden in hoofdstuk 9 de resultaten van het onderzoek samengevat. Tevens worden enkele suggesties gedaan voor mogelijk toekomstig werk. Geconstateerd is dat in het binnendeel van de halo van de Sombrero geen sprake is van een significante toename van M/L met de afstand tot het centrum. Een toename, zoals geconstateerd voor de 2 groepjes, zet mogelijk pas in op afstanden groter dan de straal van de HI schijf. De M/L waarde die in de literatuur voor het NGC 3992 groepje van stelsels wordt vermeld is veel kleiner dan de corresponderende waarde voor met name het NGC 4111 groepje. Deze

kleinere M/L waarde voor zowel NGC 2859 als NGC 3992 suggereert dat deze stelsels minder massieve halo's bezitten. De M/L waarden van de NGC 4111 en de NGC 2859 groepjes liggen binnen het brede gebied van waarden gemeten voor kleine clusters, maar zijn wat groter dan die gemeten in dubbelstelsels.

Om een beter beeld van het verloop van M/L in stelsels van diverse morphologische klassificatie te krijgen is het van belang zowel de massaverdeling op grote als kleine schaal te kennen. Uit het huidige onderzoek blijkt dat zowel de methode geïntroduceerd in hoofdstuk 3 als metingen van groepjes aan deze studie een belangrijke bijdrage kunnen leveren.

Op 5 mei 1954 ben ik in De Steeg geboren. Aan de Da Costa ULO te Dieren behaalde ik in 1970 het Mulo-b diploma en in hetzelfde jaar werd met goed gevolg toelatingsexamen tot het Baudartius College te Zutphen afgelegd. Na het behalen van het HBS-b examen volgde in 1972 de studie natuur- en sterrenkunde aan de Rijksuniversiteit te Utrecht. Het kandidaatsexamen natuurkunde en sterrenkunde met bijvak wiskunde werd in 1976 behaald. Tijdens de doctoraalfase heb ik meegewerkt aan de verwerking van metingen met de Astronomische Nederlandse Satelliet (ANS) van röntgenstraling afkomstig van supernovarestanten (Laboratorium voor Ruimteonderzoek). Daarnaast verrichtte ik onderzoek naar de eigenschappen van amorf metaal (vakgroep Technische Natuurkunde). Mijn afstudeeronderzoek, verricht onder leiding van Dr. A. Kattenberg (Sterrenkundig Instituut), betrof de reductie en analyse van digitaal geregistreerde Type-I radio stoten van de zon. In 1980 behaalde ik het doctoraalexamen algemene sterrenkunde met groot bijvak natuurkunde. Tijdens het daaropvolgend promotie onderzoek aan het Sterrenkundig Instituut van de Katholieke Universiteit te Nijmegen werkte ik onder leiding van Prof. Dr. W.W. Shane aan het onderzoek dat leidde tot het verschijnen van dit proefschrift. Naast dit onderzoek verleende ik medewerking aan diverse werkcolleges in de natuur- en sterrenkunde. Sinds april 1987 ben ik werkzaam bij de afdeling Remote Sensing van het Nationaal Lucht- en Ruimtevaartlaboratorium.

STELLINGEN

behorende bij het proefschrift

MASS IN AND AROUND GALAXIES AS INFERRED FROM OBSERVATIONS OF NEUTRAL HYDROGEN

I

De bepalingen van Hacke et al. van de dikten van de stoflagen in extragalactische sterrenstelsels zijn, ten onrechte, niet gecorrigeerd voor bijdragen afkomstig van de projectie van het oppervlak van de stofschijf bij stelsels die niet precies edge-on worden gezien.

Hacke, G., Schielicke, R., Schmidt, K.H.: 1982, Astron. Nachr. **303**, 245
Dit proefschrift, hoofdstuk 3

II

Door het bevatten van veel sterrenstelsels zwakker dan magnitude 14.5 is de Uppsala General Catalogue of Galaxies geschikt voor een geautomatiseerde selectie van stelsels omgeven door meerdere, veel minder heldere, begeleiders.

Nilson, P.: 1973, Uppsala General Catalogue of Galaxies, Uppsala Astron. Obs. Ann. **6**

III

Bij het vergelijken van verschillende bepalingen van de massa-lichtkracht verhouding van sterrenstelsels wordt er veelal onvoldoende rekening mee gehouden dat het resultaat van een dynamische massabepaling afhankelijk kan zijn van de grootte van het beschouwde gebied.

IV

In hun modelberekeningen voor de bulge van NGC 7814 hebben Jarvis en Freeman onvoldoende rekening gehouden met de conclusies van van der Kruit en Searle dat de massa-lichtkracht verhouding toeneemt met de afstand tot het centrum van het stelsel en dat er zich slechts een zeer gering deel van de totale massa in de schijf bevindt.

Jarvis, J., Freeman, K.C.: 1985, Astrophys. J. **295**, 324
van der Kruit, P.C., Searle, L.: 1982, Astron. Astrophys. **110**, 79

V

Het verdient aanbeveling om voor sterrenstelsels, naast de verhouding van de totale massa van het neutrale waterstofgas (M_{HI}) tot de optische lichtkracht, waar mogelijk ook de verhouding van M_{HI} tot de optische lichtkracht beperkt tot het gebied waar de waterstof wordt aangetroffen, te berekenen.

Dit proefschrift, hoofdstuk 3

VI

De mate van succes van het operationeel maken van radar remote sensing, in het bijzonder met behulp van synthetische apertuur radar, zal meer nog dan voor optische remote sensing afhangen van de kwaliteit van de informatievoorziening ten behoeve van de gebruiker.

VII

Bosma merkt op dat er aan het resultaat van een massabepaling van een groot sterrenstelsel, verkregen door toepassing van de geprojekteerde massamethode, meestal geringe waarde wordt toegekend indien er weinig ruimte blijkt te zijn voor een uitgebreide massieve halo. Aldus gesteld kan deze opmerking ten onrechte de indruk wekken dat astronomen bevooroordeeld zijn.

Bosma, A.: 1983, Struktuur van Melkwegstelsels, Repro Huygens Laboratorium Rijksuniversiteit Leiden, No. 117

VIII

Redacties van tijdschriften dienen auteurs te verplichten de gebruikte waarde van de Hubble constante op een vastgestelde plaats in de publicatie op te nemen.

IX

De huidige keuze van de achtergrondmuziek bij populair wetenschappelijke televisieprogramma's over onderwerpen uit de sterrenkunde kan voor de gemiddelde kijker tot een verdere mystificatie van deze wetenschap leiden.

X

Curran beschrijft hoe hij meent dat de mens door toepassing van moderne remote sensing technieken de tijd-, afstand- en golflengteschaal waarbinnen zijn leefwereld kan worden waargenomen heeft weten te verruimen. Bij deze beschrijving wordt geen rekening gehouden met de schalen bestreken door de sterrenkunde.

Curran, Paul J.: 1985, Principles of Remote Sensing, p. 243, Longman Group Limited (Harlow Essex, England)

XI

De nu en dan gehoorde suggestie een tijdschrift op te richten genaamd "Astronomical Failures" verdient serieuze aandacht.

XII

Door de benaming "Millimeter Telescope" wordt dit instrument ten onrechte in het nadeel gesteld ten opzichte van de "Very Large Telescope".

XIII

Natuurreservaten dienen direct na de opening weer te worden gesloten.

G. van der Burg

Nijmegen, 17 september 1987